Universitat de Girona

Rhodium-catalyzed cyclization reactions of 1,5-bisallenes involving alkenes and alkynes: experimental and theoretical studies

Jordi Vila Vadrí

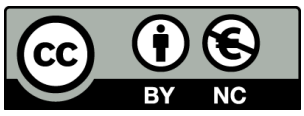

Universitat de Girona

Doctoral thesis

RHODIUM-CATALYZED CYCLIZATION REACTIONS OF 1,5-BISALLENES INVOLVING ALKENES AND ALKYNES: EXPERIMENTAL AND THEORETICAL STUDIES.

Jordi Vila Vadrí

2022

Universitat de Girona

Doctoral thesis

RHODIUM-CATALYZED CYCLIZATION REACTIONS OF 1,5-BISALLENES INVOLVING ALKENES AND ALKYNES: EXPERIMENTAL AND THEORETICAL STUDIES.

Jordi Vila Vadrí

2022

DOCTORAL PROGRAMME IN CHEMISTRY

Supervised by:

Prof. Anna Roglans Ribas

Dr. Anna Pla-Quintana

Tutor:

Prof. Anna Roglans Ribas

Presented to obtain the degree of PhD at the Universitat de Girona.

Universitat de Girona

Prof. Anna Roglans Ribas and Dr. Anna Pla-Quintana, from the Universitat de Girona,

WE DECLARE:

That this thesis entitled '**Rhodium-catalyzed cyclization reactions of 1,5-bisallenes involving alkenes and alkynes: experimental and theoretical studies**' presented by **Jordi Vila Vadrí** to obtain the doctoral degree has been completed under our supervision and meets the requirements to opt for an International Doctorate.

For all intents and purposes, we hereby sign this document

Prof. Anna Roglans Dr. Anna Pla-Quintana

Girona, February 24th of 2023.

Full list of publications

This doctoral thesis resulted in the following publications:

Chapter 3

Artigas, A.; Vila, J.; Lledó, A.; Solà, M.; Pla-Quintana, A.; Roglans, A. A Rh-Catalyzed Cycloisomerization/Diels–Alder Cascade Reaction of 1,5-Bisallenes for the Synthesis of Polycyclic Heterocycles. *Org. Lett.* **2019**, *21*, 6608.

(IF: 6.09; JCR Ranking: 4/57 (2019); 1st quartile Organic Chemistry)

Contribution: *J. V. V. participated in the optimization of the reaction conditions and examined the scope of the reaction.*

Chapter 4

Vila, J.; Solà, M.; Pla-Quintana, A.; Roglans, A. Highly Selective Synthesis of Seven-Membered Azaspiro Compounds by a Rh(I)-Catalyzed Cycloisomerization/Diels–Alder Cascade of 1,5-Bisallenes. *J. Org. Chem.* **2022**, *87*, 5279.

(IF: 4.20; JCR Ranking: 12/56 (2021); 1st quartile Organic Chemistry)

Contribution: *J. V. V. participated in the design of the project, performed all the experiments and calculations, contributed to the analysis of the results, and co-wrote the manuscript.*

Chapter 5

Vila, J.; Vinardell, R.; Solà, M.; Pla-Quintana, A.; Roglans, A. A Rh(I)-catalyzed cascade cyclization of 1,5-bisallenes and alkynes for the formation of cis-3,4-arylvinyl pyrrolidines and cyclopentanes. *Adv. Synth. Catal.* **2022**, *364*, 206.

(IF: 5.98; JCR Ranking: 13/72 (2021); 1st quartile Applied Chemistry)

Contribution: *J. V. V. participated in the design of the project, performed all the experiments and calculations, contributed to the analysis of the results, and co-wrote the manuscript.*

Chapter 6

Vila, J.; Solà, M.; Achard, T.; Bellemin-Laponnaz, S.; Pla-Quintana, A.; Roglans, A. Rh(I) Complexes with Hemilabile Thioether-Functionalized NHC Ligands as Catalysts for [2 + 2 + 2] Cycloaddition of 1,5-Bisallenes and Alkynes. *ACS Catal.* **2023**, *13*, 3201.

(IF: 13.7; JCR Ranking: 19/165 (2021); 1st quartile Physical Chemistry)

Contribution: *J. V. V. participated in the design of the project, performed all the experiments and calculations, contributed to the analysis of the results, and co-wrote the manuscript.*

Glossary of abbreviations

General abbreviations

°C	Degrees Celsius
1D	Monodimensional
2D	Bidimensional
Å	Angstrom
Ac	Acetyl
acac	Acetylacetone
AcOEt	Ethyl acetate
AcOH	Acetic acid
ACS	American Chemical Society
aq	Aqueous solution
Ar	Aryl
atm	atmosphere
ATR	Attenuated total reflectance
B3LYP	Becke, three parameter, Lee-Yang-Parr
B3LYP-D3	B3LYP functional with D3 Grimme's dispersion
BHT	Butylated hydroxytoluene
BINAP	2,2′-Bis(diphenylphosphino)-1,1′-binaphthalene
BIPHEP	2,2'-Bis(diphenylphosphino)biphenyl
Bn	Benzyl
BQ	Benzoquinone
Bu	Butyl
Bz	Benzoyl
Cbz	Benzyloxycarbonyl
cc-pVNZ	Correlation consistent-polarized basis sets by Dunning (N = D, T, Q, 5, 6, 7)
cc-pVNZ-PP	cc-pVNZ including pseudopotential (N = D, T, Q, 5, 6, 7)
cod	1,5-cyclooctadiene
Cp	Cyclopentadienyl
D3	D3 Grimme's dispersion model
DA	Diels–Alder
dba	Dibenzylideneacetone
DCE	1,2-Dichloroethane
DCM	Dichloromethane
DFT	Density Functional Theory
DMAD	Dimethyl acetylenedicarboxylate
DMF	*N*,*N*-Dimethylformamide
DM-Segphos	[(4,4′-Bi-1,3-benzodioxole)-5,5′-diyl]bis[bis(3,5-dimethylphenyl)phosphine]
DMSO	Dimethyl sulfoxide

DPEphos	(Oxydi-2,1-phenylene)bis(diphenylphosphine)
dppe	1,2-Bis(diphenylphosphino)ethane
dppp	1,3-Bis(diphenylphosphino)propane
d.r.	Diastereomeric ratio
DTBM-Segphos	[(4,4′-bi-1,3-benzodioxole)-5,5′-diyl]bis[bis(3,5-di-tert-butyl-4-methoxyphenyl)phosphine]
E	Electronic energy
e^-	Electron
ED	Electron-donating
ee	Enantiomeric excess
Eq.	Equation
eq.	Equivalent/s
ESI	Electrospray ionization
Et	Ethyl
et al.	from latin ‘et alia’, which means 'and others'
EW	Electron-withdrawing
f_k^-	Condensed Fukui function of the atom k removing 1 e^-
f_k^+	Condensed Fukui function of the atom k adding 1 e^-
G	Gibbs energy
g	grams
H	Enthalpy
h	hours
H_8-BINAP	2,2′-Bis(diphenylphospino)-5,5′,6,6′,7,7′,8,8′-octahydro-1,1′-binaphthyl
HOMO	Highest Occupied Molecular Orbital
HPLC	High-performance liquid chromatography
IMes	1,3-bis(2,4,6-trimethylphenyl)imidazol-2-ylidene
IPr	1,3-bis(2,6-diisopropylphenyl)imidazole-2-ylidene
*i*Pr	Isopropyl
IRC	Intrinsic reaction coordinate
K	Degrees Kelvin
k_i	Kinetic constant for the substance *i*
kcal	Kilocalory
L	Ligand
LUMO	Lowest Unoccupied Molecular Orbital
M	Molar (unless otherwise noted)
m-	Meta-
M06L	Minessota meta-GGA local functional including 0% HF exchange
m-CPBA	Metachloroperbenzoic acid
Me	Methyl
mg	Miligram/s

mL	Mililiter/s
mM	Milimolar
mol %	Molar percentage
Monophos	(3,5-Dioxa-4-phosphacyclohepta[2,1-a;3,4- a′]dinaphthalen-4-yl)dimethylamine
MS	Mas Spectrometry
MW	Microwave
NaBArF	Sodium tetrakis[3,5-bis(trifluoromethyl)phenyl]borate
NHC	*N*-Heterocyclic carbene
NMR	Nuclear Magnetic Resonance
NPA	Natural population analysis
o-	Ortho-
p-	Para-
PA	Phosphinous Acid
PES	Potential energy surface
Ph	Phenyl
PPh_3	Triphenylphosphine
$P(o\text{-}tol)_3$	Tri(o-tolyl)phosphine
$P(O\text{-}o\text{-}tol)_3$	Tri(o-tolyl)phosphite
$q_{k(N)}$	Natural charge of the atom *k* with N electrons (units are electrons)
quant.	Quantitative
RSC	Royal Society of Chemistry
r.t.	Room temperature
rx	reaction
S	Enthropy
Segphos	(4,4′-bi-1,3-benzodioxole)-5,5′-diyl]bis[diphenylphosphine]
SCRF	Self-consistent reaction field
SMD	Continuum model based on density
SPE	Single-point energy
SPO	Secondary phosphine oxide
T	Temperature
*t*Bu	Tert-butyl
TDI	TOF determining intermediate
TDTS	TOF determining transition state
TEMPO	2,2,6,6-Tetramethyl-1-piperidinyloxy, free radical
THF	Tetrahydrofuran
TLC	Thin layer chromatography
TM	Transition metal
TOF	Turnover frequency
Tol	Tolyl
TS	Transition state
Ts	Tosyl

UB3LYP	Unrestricted B3LYP functional
UB3LYP-D3	Unrestricted B3LYP functional with D3 Grimme's dispersion
ωB97X-D	Head-Gordon long range corrected hybrid density functional with damped atom-
Xantphos	4,5-Bis(diphenylphosphino)-9,9-dimethylxanthene
XPhos	2-Dicyclohexylphosphino-2′,4′,6′-triisopropylbiphenyl
ZPE	Zero-point Energy

Compound characterization

^{13}C NMR	Carbon nuclear magnetic resonance
^{1}H NMR	Proton nuclear magnetic resonance
$CDCl_3$	Deuterated chloroform
cm^{-1}	Reciprocal centimeters
COSY	Proton-proton correlation spectroscopy
d	Doublet
ddd	Doublet of doublets of doublets
dt	Double triplet
E.A.	Elemental analysis
ESI-HRMS	Electrospray ionization high resolution mass spectrometry
HMBC	Heteronuclear multiple-bond correlation spectroscopy
HSQC	Heteronuclear single-quantum correlation spectroscopy
Hz	Hertz
IR (ATR)	Infrared spectroscopy (attenuated total reflectance)
^{n}J	n bonds coupling constant (n = 1, 2, 3, 4, 5)
m	Multiplet
M.P.	Melting point
m/z	Mass to charge ratio
MHz	Mega-hertz
MW	Molecular weight
ppm	Parts per milion
q	Quadruplet
quint	Quintuplet
Rf	Retention factor
s	Singlet
sept	Heptuplet
t	Triplet
THF-d_8	Deuterated tetrahydrofuran
δ	Chemical shift
λ	Wavelength
ν	Frequency

Acknowledgements

This thesis would not have been possible without the cooperative effort of many people. I would like to thank them for their contribution and support during the realization of this work.

- My supervisors Prof. Anna Roglans Ribas and Dr. Anna Pla-Quintana, for their confidence and the opportunity to participate in the projects developed in this thesis. They have provided tons of teaching, support, and advice during this incredible journey. Thanks to them I have attained most of the fundamental knowledge to become a researcher in organic chemistry. My thankfulness to them is incommensurate. In addition, I should mention contribution of Prof. Miquel Solà. His teachings and revisions of all the computational work performed are equally valuable.
- Dr. Thierry Achard and Dr. Stéphane Bellemin-Laponnaz, to host me in their laboratories at the Institut de physique et de chimie des Matériaux de Strasbourg (IPCMS). I really appreciated our discussions about chemistry and the knowledge I could get from them.
- Dr. Sergio Braulio, Dr. Lluisa Matas, Anna Costa, Dr. Laura Rodríguez, Dr. Àngel Oliveras and Xavier Fontrodona from the *'Serveis Tècnics de Recerca'* at the Universitat de Girona for NMR, HPLC, MS and XRD analyses.
- All my colleagues at the METSO group who have coincided with me during these four years. First of all, the ones I shared most of the time, with whom I build a special friendship: Alex Diaz, Ricard López, Rubén Álvarez, Dr. Albert Artigas and Cristina Castanyer. Also, all the undergraduate students I had opportunity to mentor or help at some point in their time at the laboratory: Roger Vinardell, Nil Roig, Joan Vall-llosera, Leonie van Hijfte, Maria Eugènia López and Alba Sors. They have helped me to develop my abilities as a mentor.
- Prof. Xavier Ariza Piquer from the Universitat de Barcelona, who was my supervisor when I was a MSc student. He was an excellent mentor and drove my first steps in the organic chemistry research. Also, Prof. Jordi García Gómez, who along with Prof. Xavier Ariza Piquer, gave me great support and advice during and after my stance in their group.
- Bena Clapés Herrero, who introduced the seed of chemistry much before I already knew. She was for me a wonderful teacher and provided me infinite support and confidence during my last years in the school.
- My friends and family for their support and interest in the progress of this journey, with special mention to my parents.
- My love Cristina. She is, and has been, my support for many years. I feel so fortunate to be with her and share our lives day after day.

Lastly, I would like to mention the entities that provided financial support. The Spanish Ministry of Economy and Competitivity (Projects: CTQ2017-85341P, PID2020-113711GB-I00), the Generalitat de Catalunya (Project 2017SGR39), and the Universitat de Girona (IFUdG2018 predoctoral grant).

Table of contents

List of Figures

Supplementary material

List of Schemes

Supplementary material

List of Tables

Supplementary material

Summary

The development of novel catalytic methodologies involving the formation of carbon – carbon/heteroatom bonds to produce cyclic systems constitutes a field of great interest in the modern synthetic organic chemistry. Over the last 30 years, the combined use of transition metals with allenes allowed considerable progress in this field. Allenes are cumulated dienes, constituted by two perpendicular double bonds. The unsaturation spread over three contiguous carbons gives allenes additional versatility in cyclization reactions compared to other unsaturations, such as alkenes or alkynes, although the control of the selectivity becomes more challenging when allenes are used.

One paradigmatic process to produce cyclic systems is the *transition metal-catalyzed [2+2+2] cycloaddition* reaction, which enable the simultaneous formation of several bonds and/or stereogenic centers in a single step to produce six-membered rings in perfect atom economy. Our group has developed several rhodium-catalyzed [2+2+2] cycloaddition reactions and has made great mechanistic contributions employing DFT calculations and experimental techniques. Regarding the use of allenes, our group studied the rhodium(I)-catalyzed intramolecular [2+2+2] cycloaddition of linear substrates accommodating allenes and alkynes and/or alkenes. However, [2+2+2] cycloadditions involving two allenes with another unsaturated carbon – carbon bond remain scarce. Considering this, and as part of our continuous interest in the use of allenes, we envisaged the development of partially intramolecular [2+2+2] cycloaddition reactions of 1,5-bisallenes with alkenes and alkynes. Although 1,5-bisallenes exhibited rich chemistry with transition metals, very few examples were reported involving the incorporation of a third unsaturated partner in a cycloaddition reaction.

The main goal set within the context of this thesis was to develop new rhodium(I)-catalyzed cycloaddition reactions of 1,5-bisallenes with alkenes and alkynes. As reported in chapter 3, we have succeeded in reacting 1,5-bisallenes with a series of alkenes employing rhodium(I) catalysis. The reaction provided a series of polycyclic dihydroazepine and dihydrooxepine derivatives in a single step and perfect atom economy. The results obtained in chapter 3 allowed us to develop an homodimerization process of 1,5-bisallenes to obtain spirocyclic derivatives featuring six- and seven- membered rings in the spiro carbon (chapter 4). The process was found to be highly chemo- and regioselective, affording a single isomer out of six possible adducts. Moving forward to the use of alkynes, in chapter 5 and 6 we accomplished the proposed objectives by reacting 1,5-bisallenes and alkynes to form *cis*-3,4-arylvinyl pyrrolidines and cyclopentanes (chapter 5), and bicyclic *trans*-fused 3,6-dimethylenecyclohex-1-ene derivatives (chapter 6) from 1,5-bisallenes and alkynes using rhodium(I) as a catalyst. Additionally, the mechanism of the reaction was studied in all the developed protocols by means of DFT calculations and experimental techniques that allowed justify the selectivities observed.

Resum

El desenvolupament de noves metodologies catalítiques per generar sistemes cíclics involucrant la formació d'enllaços carboni – carboni/heteroàtom és de gran interès en l'àmbit de la química orgànica sintètica moderna. L'ús combinat d'al·lens i metalls de transició ha permès considerables progressos en aquest àmbit durant els últims 30 anys. Els al·lens son diens acumulats, formats per dos dobles enllaços perpendiculars. Al tenir dues insaturacions repartides en tres carbonis, els al·lens presenten una versatilitat addicional en reaccions de ciclació quan els comparem amb altres insaturacions, com els alquens o els alquins. No obstant, el control de la selectivitat resulta més complicat quan utilitzem al·lens.

Un procés exemplar per generar sistemes cíclics és la cicloaddició [2+2+2] catalitzada per metalls de transició, que permet la formació simultània de varis enllaços i/o centres estereogènics en una sola etapa per produir anells de sis baules amb economia atòmica perfecta. El nostre grup ha desenvolupat diverses cicloaddicions [2+2+2] catalitzades per rodi i ha fet importants contribucions a l'estudi del mecanisme de la reacció emparant càlculs DFT i tècniques experimentals. Pel que fa a l'ús d'al·lens, el grup ha estudiat la cicloaddició [2+2+2] intramolecular de substrats lineals incorporant al·lens i alquens i/o alquins. No obstant, els exemples de reaccions de cicloaddició [2+2+2] involucrant dos al·lens amb una tercera insaturació son escassos. Considerant aquest fet, i el nostre interès en l'ús d'al·lens, vam concebre el desenvolupament de reaccions de cicloaddició [2+2+2] parcialment intramoleculars entre 1,5-bisal·lens incorporant alquens o alquins. Tot i que els 1,5-bisal·lens han demostrat tenir una química rica quan es combinen amb metalls de transició, son molt pocs els exemples de cicloaddicions on s'hi incorpori una tercera insaturació.

El principal objectiu d'aquesta tesi va ser desenvolupar noves cicloaddicions catalitzades per rodi d'1,5-bisal·lens amb alquens i alquins. Al capítol 3, es va fer reaccionar satisfactòriament els 1,5-bisal·lens amb diversos alquens emparant rodi(I) com a catalitzador. La reacció forní derivats policíclics de dihidroazepina i dihidrooxapina en una sola etapa i economia atòmica perfecta. Els resultats obtinguts d'aquest capítol, ens van permetre desenvolupar un procés d'homodimerització de diferents 1,5-bisal·lens per generar compostos espirocíclics, exhibint anells de sis i set baules al carboni espiránic (capítol 4). El procés va resultar ser completament quimio- i regioselectiu, obtenint només un isòmer dels sis possibles. Avançant cap a l'ús d'alquins, als capítols 5 i 6 vam aconseguir els objectius marcats fent reaccionar els 1,5-bisal·lens amb alquins per formar, en un cas, *cis*-3,4-arilvinil pirrolidines i ciclopentans (capítol 5), i en l'altre, derivats bicicle en fusió *trans* de 3,6-dimetilenciclohex-1-ens (capítol 6). Altrament, els mecanismes de les reaccions van ser estudiats en tots els processos utilitzant càlculs computacionals DFT i tècniques experimentals que en van permetre explicar les diferents selectivitats observades.

Resumen

El desarrollo de nuevas metodologías catalíticas para generar sistemas cíclicos involucrando la formación de enlaces carbono – carbono/heteroátomo es de gran interés en el ámbito de la química orgánica sintética moderna. El uso combinado de alenos y metales de transición ha permitido considerables progresos en este ámbito durante los últimos 30 años. Los alenos son dienos acumulados, formados por dos dobles enlaces perpendiculares. Al tener dos insaturaciones repartidas en tres carbonos, los alenos presentan una versatilidad adicional en reacciones de ciclación cuando los comparamos con otras insaturaciones, como los alquenos o los alquinos. No obstante, el control de la selectividad resulta más complicado cuando utilizamos alenos.

Un proceso ejemplar para generar sistemas cíclicos es la cicloadición [2+2+2] catalizada por metales de transición, que permite la formación simultánea de varios enlaces y/o centros estereogénicos en una sola etapa para producir anillos de seis eslabones con economía atómica perfecta. Nuestro grupo ha desarrollado varias cicloadiciones [2+2+2] catalizadas por rodio y ha hecho importantes contribuciones al estudio del mecanismo de la reacción utilizando cálculos DFT y técnicas experimentales. En cuanto al uso de alenos, el grupo ha estudiado la cicloadición [2+2+2] intramolecular de sustratos lineales incorporando alenos y alquenos y/o alquinos. No obstante, los ejemplos de reacciones de cicloadición [2+2+2] involucrando dos alenos con una tercera insaturación son escasos. Considerando este hecho, y nuestro interés en el uso de alenos, concebimos el desarrollo de reacciones de cicloadición [2+2+2] parcialmente intramoleculares entre 1,5-bisalenos incorporando alquenos o alquinos. A pesar de que los 1,5-bisalenos han demostrado tener una química rica cuando se combinan con metales de transición, son muy pocos los ejemplos donde se incorpore una tercera insaturación en una cicloadición.

El principal objetivo marcado de esta tesis fue desarrollar nuevas cicloadiciones catalizadas por rodio de 1,5-bisalenos con alquenos y alquinos. En el capítulo 3, hicimos reaccionar satisfactoriamente los 1,5-bisal·lens con varios alquenos utilizando rodio(I) como catalizador. La reacción permitió la obtención de derivados policíclicos de dihidroazepina y dihidrooxapina en una sola etapa y economía atómica perfecta. Los resultados obtenidos en este capítulo nos permitieron desarrollar un proceso de homodimerización de varios 1,5-bisalenos para generar compuestos espirocíclicos, exhibiendo anillos de seis y siete eslabones en el carbono espiránico (capítulo 4). El proceso resultó ser completamente quimio- y regioselectivo, obteniendo soloamente un isómero de los seis posibles. Avanzando hacia el uso de alquinos, en los capítulos 5 y 6 conseguimos los objetivos marcados haciendo reaccionar los 1,5-bisalenos con alquinos para formar, en un caso, *cis*-3,4-arilvinil pirrolidinas y ciclopentanos (capítulo 5), y en el otro, derivados biciclo con fusión *trans* de 3,6-dimetilenciclohex-1-eno (capítulo 6). Además, los mecanismos de las reacciones fueron estudiados en todos los procesos utilizando cálculos computacionales DFT y técnicas experimentales que permitieron explicar las distintas selectividades observadas.

Chapter 1. Introduction

1.1. Allenes

1.1.1. History of allenes

The structure and the stereochemistry of allenes was predicted in 1875 by Van't Hoff[1] — along with the tetrahedral geometry of alkanes — but the lack of analytical tools in that time and the wrong thinking that the cumulated dienes would be unstable, kept them as mere curiosities for decades. The first synthesis of an allene was reported by Burton and von Pechmann[2] in 1887, but the structure could not be characterized until 1954 with the introduction of IR and Raman spectroscopy.[3] For other allene-containing natural products, the characterization of their structure also took place decades after their isolation.[4,5]

From that point, allenes became increasingly popular and went from just chemical curiosities to be considered an important synthetic motif in modern organic chemistry.[6] They can be found in more than 200 natural products[7] and in a wide variety of pharmacologically active substances. Depending on their location in the structure they can be classified as linear, exocyclic or endocyclic and have been found to be present in hydrocarbons,[8] fatty acids,[9] aminoacids,[10] terpenoids,[11] steroids[12] or nucleosides[13] among other classes of organic compounds (**Figure 1.1**).

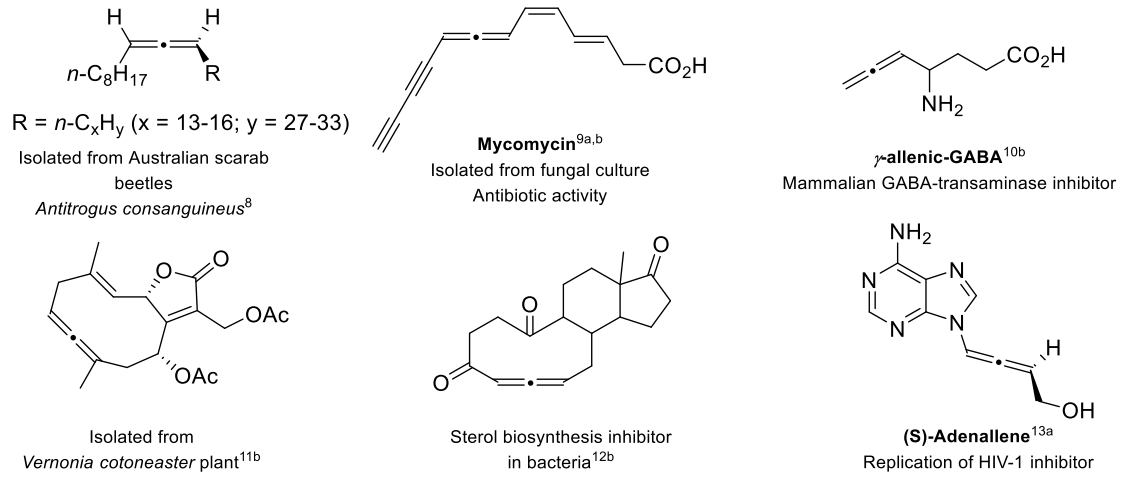

Figure 1.1. Selected examples of allene containing natural products and pharmacologically active molecules

1.1.2. Structure and stereochemistry of allenes

Allenes are cumulated dienes, and their bonding configuration involves two perpendicular double bonds. They present a linear geometry, which can be rationalized by looking at the *p* orbitals and the hybridization of each carbon atom. The external carbon atoms of allenes are sp^2 hybridized and their remaining *p* orbital is used to make the π–bond with the central carbon atom. As a singly occupied *p* orbital cannot make two consecutive double bonds in the same plane, the unhybridized p_z and p_y orbitals of the central carbon atom are used to make the corresponding orthogonal π–bonds with the external carbon atoms, being then the central carbon atom *sp* hybridized, and thus, linear (**Figure 1.2a**).

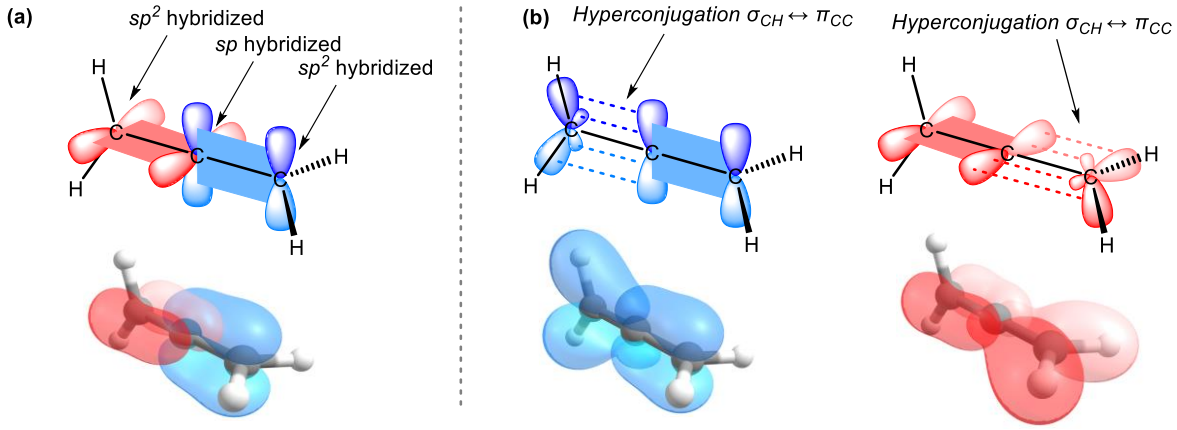

Figure 1.2. Representation of (a) perpendicular π-bonds and (b) $\sigma_{CH} \leftrightarrow \pi_{CC}$ hyperconjugation in allenes. Orbitals rendered with Chemcraft at 0.11 isosurface value.

On the other hand, the distance between the carbon atoms in the double bonds of 1,3-propadiene is slightly shorter (1.31 Å) than the one in ethylene (1.34 Å), which is caused by the $\sigma_{CH} \leftrightarrow \pi_{CC}$ hyperconjugation (σ_{CH} – π_{CC} overlap).[14] This overlap is particularly favorable in allenes as the σ_{CH} bonds in one of the double bonds of the allene are coplanar with the π_{CC} bonds in the second one (**Figure 1.2b**). For that reason, allenes have often been considered like hybrids of alkenes and alkynes since the hyperconjugation $\sigma_{CH} \leftrightarrow \pi_{CC}$ can be interpreted as a partial triple bond. This bonding particularity confers them unique reactivity, for example, in cycloaddition reactions, which resides between that of alkenes and alkynes.

As predicted by Van't Hoff,[1] such structure and bond configuration in allenes has stereochemical consequences. The orthogonal arrangement of the substituents in each side of the allene can be interpreted as an elongated tetrahedron, which has an orthogonal symmetry plane for each terminus when their substituents are equal, A = B and/or A' = B' in **Figure 1.3**. Otherwise, if the substituents are not equivalent (A ≠ B and A' ≠ B'), the allene become dissymmetric and a chirality axis across the three lined carbon atoms is generated (**Figure 1.3**). These structural and stereochemical properties provide additional interest to allenes. For instance, their inherent axial chirality has been widely used for the development of chirality transfer reactions.[15]

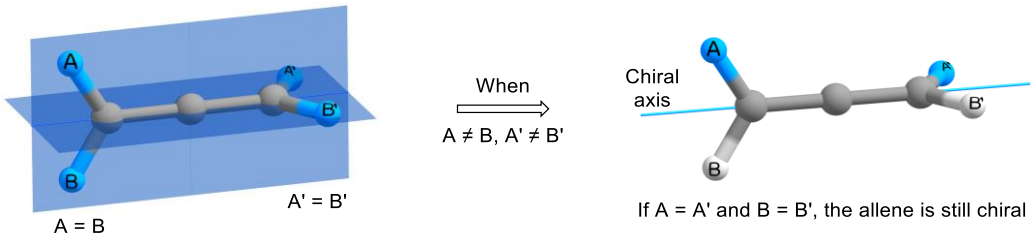

Figure 1.3. Symmetry planes and chiral axis in allenes.

1.1.3. Allenes as versatile substrates for TM-catalyzed cyclization reactions

Modern synthetic organic chemistry looks for rapid and efficient ways to increase complexity in molecules while minimizing reaction steps. Within this context, the development of catalytic methodologies involving the formation of carbon – carbon/heteroatom bonds to access cyclic systems constitutes a field of great relevance. Since the early 1990s, the combined use of transition metals with allenes allowed considerable progress in this field by exploiting the cumulated system. The unsaturation spread over three contiguous carbon atoms gives allenes additional versatility in cyclization reactions compared to alkenes or alkynes. However, as depicted in **Figure 1.4**, the control of selectivity is much more challenging when allenes are used, since two different double bonds or both of them are susceptible to be involved in the reaction (chemoselectivity). In addition, each double bond of the allene has two faces to react (stereoselectivity), and in the case of cycloaddition reactions two orientations are possible for each face on both double bonds (regioselectivity).

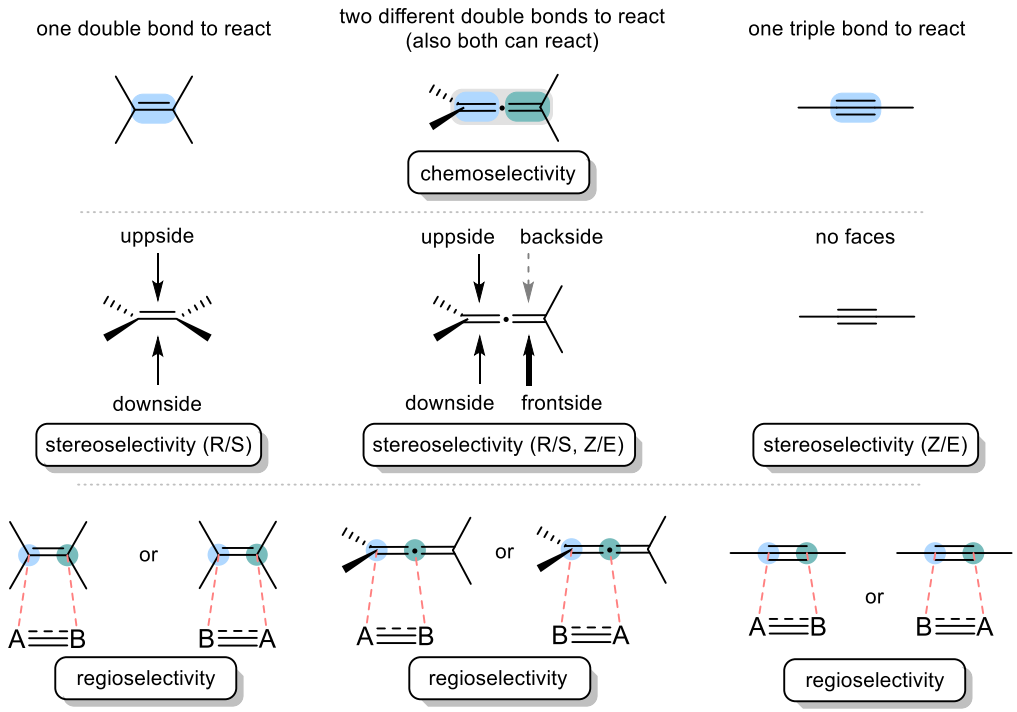

Figure 1.4. Chemo-, stereo- and regioselectivity in allenes compared to alkenes and alkynes.

Progress has been made over the years to achieve good selectivities by modifying the substitution pattern of the allenes and the nature of the transition metal, as well as the ligands employed in the catalytic system. It is also important to note that in most cases, at least one new sp^3-hybridized carbon atom will be generated from an allene cyclization, and an endo- or exocyclic double bond will remain in the product for further functionalization.

A particular case of interest are the cyclization reactions on substrates featuring allenes linked to other unsaturated carbon – carbon/heteroatom moieties. The high unsaturation degree of these substrates confers them unique reactivity and excellent opportunities to tune the selectivity. The use of these substrates in

transition metal-catalyzed cycloisomerizations and cycloaddition reactions allowed the construction of carbo- and heterocyclic compounds in a single step with perfect atom economy.[16] Most of these transformations have high levels of chemo- and regioselectivity, but more interestingly small adjustments in the starting material or the catalyst can lead to diverging pathways or even completely different mechanisms, opening the door to perfectly tunable systems. For instance, in 2003 Itoh *et al.*[17] developed a rhodium-catalyzed ligand-controlled cycloisomerization of allenenes. An *exo*-cyclization was found to occur in the presence of the neutral rhodium complex $[Rh(cod)Cl]_2$ employing triaryl phosphites as ligands to get 5-membered carbo- and heterocycles. In striking contrast, an *endo*-cyclization pattern was observed when the Wilkinson's complex $[Rh(PPh_3)_3Cl]$ was used, in a process that could be further optimized with $[Rh(CO)_2Cl]_2$ under carbon monoxide atmosphere (**Scheme 1.1a**). The authors postulated that a rhodametallacycle pathway takes place with triaryl phosphites, while an allylic C-H activation is involved for the generation of the 7-membered scaffold. More recently, the group of Breit observed a different cycloisomerization pattern on closely related terminal allenenes with the same neutral $[Rh(CO)_2Cl]_2$ complex but using the biphosphine DPEphos as ligand. 6-Membered rings with two exocyclic double bonds were obtained in a process involving a rhodametallacycle intermediate (**Scheme 1.1b**).[18]

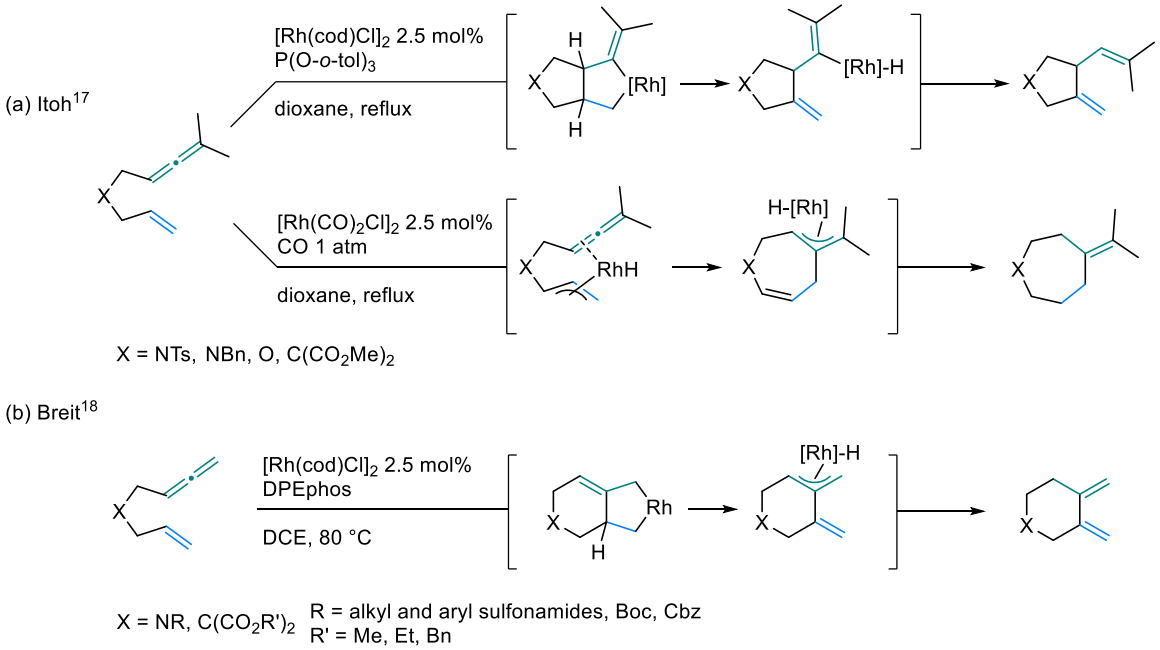

Scheme 1.1. Ligand-controlled cycloisomerization of allenenes leading to 5-, 6- or 7-membered rings.

In another example, Malacria *et al.*[19] reported a platinum-catalyzed cycloisomerization of allenynes, which could lead to either indene scaffolds, alder-ene adducts or vinylallenes by just changing the temperature or adding a methyl group in the terminal alkyne moiety (**Scheme 1.2**).

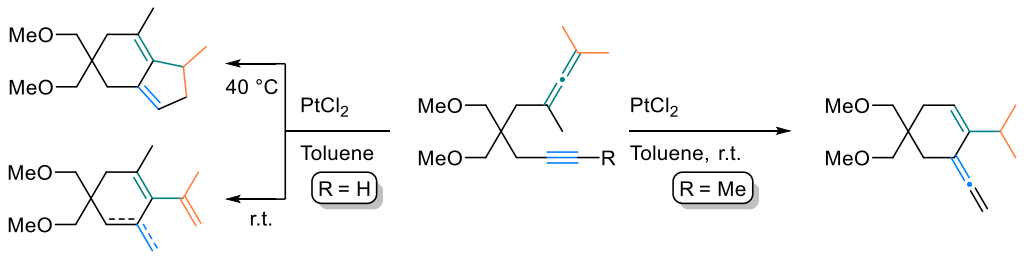

Scheme 1.2. Divergent cyclization patterns of 1,6-allenynes observed

Different studies between 2008 and 2010 highlighted the ability of allenes to behave as two- or three-carbon partners. Mascareñas, Lopez *et al.*[20] firstly reported the platinum- and NHC-gold-catalyzed [4+3] cycloaddition of allenedienes to form cycloheptadiene fused systems in a completely diastereoselective manner. In further studies[21] they observed that a preference for a [4+2] cycloaddition could be reached by using highly electrophilic phosphite-based ligands. Almost simultaneously, the group of Toste[22] observed the same ligand-governed selectivity in these cycloadditions. Experimental and computational studies showed that both mechanisms leading to [4+3] and [4+2] cycloadducts start with a concerted [4+3] cycloaddition between the allylic cation-metal complex and the diene moiety, giving rise to cycloheptenyl carbene. From this point, strong σ-donor ligands favor the subsequent 1,2-H migration to give the seven-membered rings. In contrast, with bulky π-acceptor phosphite ligands, a ring contraction via internal 1,2-alkyl migration is preferred to give the formal [4+2] adduct (**Scheme 1.3**).

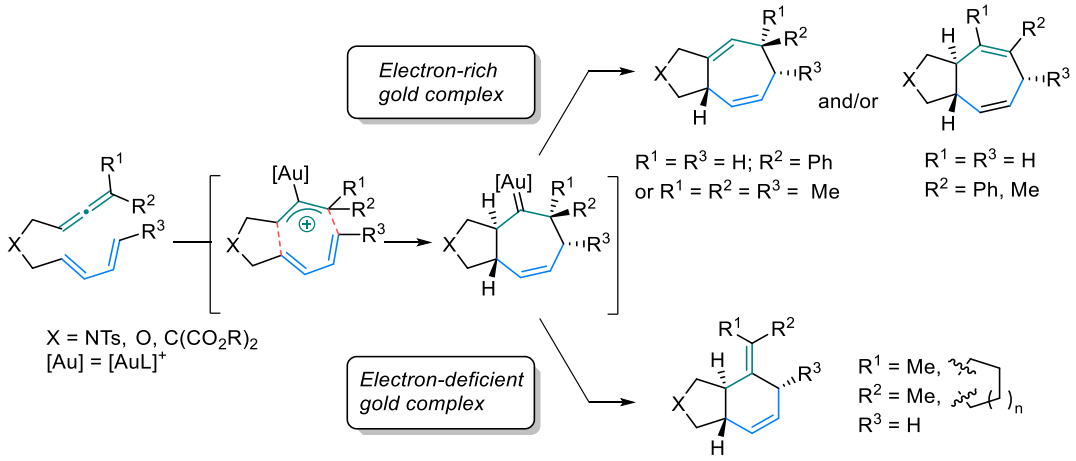

Scheme 1.3. Ligand-dependent diverging pathways leading to [4+3] or [4+2] cycloadducts of allenedienes.

Later studies in this line showed that steric factors also play an important role. Toste, Sigman *et al.*[23] used the gold – chloride bond distance as an indicator of both steric hindrance and net σ-donation of various ligands to explain and predict the selectivity of the allenediene towards the [4+3] or the [4+2] cycloaddition.

The versatility of allenes is further manifested in substrates that have two other unsaturations involved in the reaction. Mukai *et al.*[24] reported a tether-controlled cycloisomerization of allene – yne – ene derivatives to get either tricyclic scaffolds or fused 5/8-membered rings depending on the length of the tether when treated with the neutral $[Rh(CO)_2Cl]_2$ complex. The reaction is postulated to proceed via oxidative cyclometalation of the

allene and alkyne moieties, followed by alkene insertion and *β*-hydride elimination. The authors concluded that the key fused 6/8-membered intermediate (n=2) is formed by an alkene insertion into the Rh-H bond generated in the *β*-hydride elimination (with reverse regioselectivity) and reductive elimination to get the tricyclic scaffolds. As opposite to this, in the smaller-sized 5/8-membered intermediate (n=1) the hydride may not be able to approach successfully to the double bond due to the more rigid structure, therefore a reductive elimination would preferentially occur to produce the fused 5/8-membered product (**Scheme 1.4**).

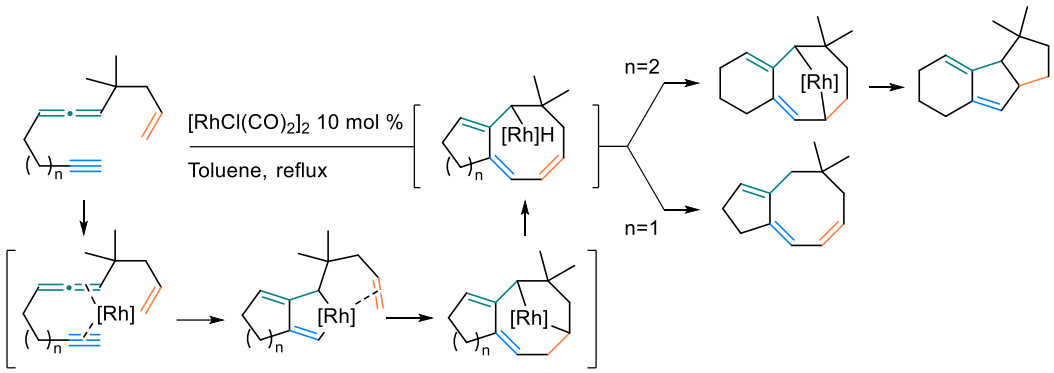

Scheme 1.4. Tether-controlled cycloisomerization of allen-yne-enes leading fused 5/6-membered products or tricyclic scaffolds.

As a final example, Alexanian *et al.*[25] reported a ligand-controlled partially intramolecular nickel-catalyzed stereoselective cyclization of allenenes with alkenes, getting multiple outcomes when triaryl phosphites, alkyl phosphines or biphosphines were used as ligands. With electron-rich PBu_3, a *β*-hydride elimination in a late-stage of the mechanism followed by a reductive elimination leads to the alkenylative cyclization product. Instead of the *β*-hydride elimination, a reductive elimination is preferred for the bulkier P(*o*-Tol)$_3$, leading to the [2+2+2] cycloaddition product. Alternatively, with the large bite angle biphosphine Xantphos, a reductive elimination occurs, before the alkene insertion takes place, to produce the intramolecular [2+2] cycloadduct (**Scheme 1.5**).

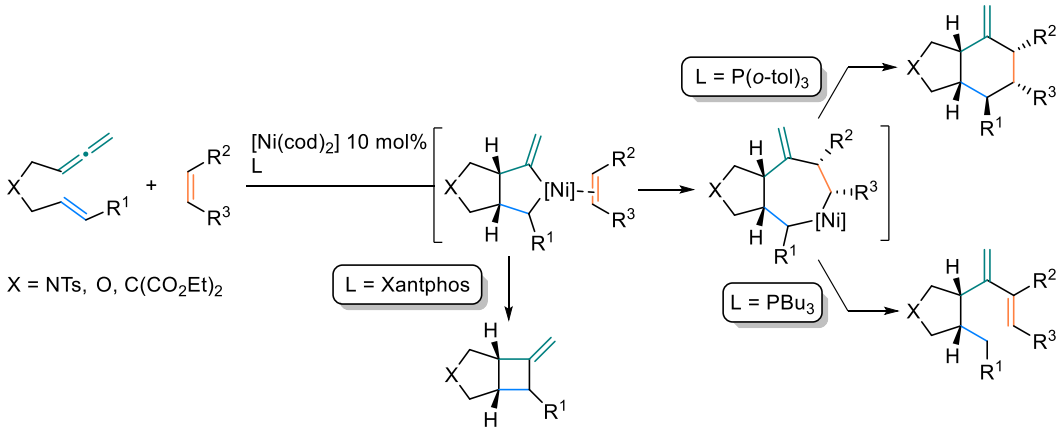

Scheme 1.5. Ligand-controlled partially intramolecular cyclization of allenenes with alkenes.

1.2. Transition metal-catalyzed [2+2+2] cycloaddition reaction

1.2.1. General aspects

The development of cyclization reactions that enable the simultaneous formation of several bonds and/or stereogenic centers in a single step is of great interest for greener and more efficient synthetic organic chemistry. One paradigmatic process to accomplish these goals is the *transition metal-catalyzed [2+2+2] cycloaddition* reaction, since it enables the efficient formation of a large scope of highly functionalized 6-membered carbo- and heterocyclic scaffolds in a single step with perfect atom economy and extraordinary functional group tolerance.

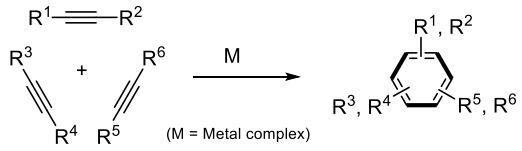

Scheme 1.6. Transition metal-catalyzed [2+2+2] cycloaddition of alkynes. Newly formed bonds are highlighted in bold.

In the field of synthetic organic chemistry, newly discovered methodologies often require a certain span of time to evolve into commonly used processes, and the [2+2+2] cycloaddition is no exception. Berthelot *et al.*[26] discovered the thermal cyclotrimerization of acetylene to produce benzene back in 1866 but it was not until 1948 when Reppe, Schweckendiek *et al.*[27] reported the first transition metal-catalyzed [2+2+2] cycloaddition of acetylenes using the nickel complex $[Ni(PPh_3)_2CO_2]$. Later in 1993, the first regioselective process which led to 1,3,5- or 1,2,4-trisubstituted benzenes was developed by Rothwell *et al.*[28] From that point, the reaction has been widely studied and nowadays the transition metal-catalyzed [2+2+2] cycloaddition is an established instrument of the synthetic toolbox. The participation of different unsaturations, like alkynes, alkenes, allenes, nitriles, ketones, aldehydes, imines, isocyanates and isothiocyanates allows the formation of a huge range of cyclic substrates difficult to obtain by other means. It has been proven that many metals are capable to perform this reaction, such as Ni, Co, Pd, Rh, Ru, Ir, Fe, Ti, Zr, Nb or Ta. The reaction proceeds efficiently in its intermolecular version when three disconnected unsaturated motifs are used, although the regio- and the chemoselectivity must be controlled since the number of possible products dramatically increases when different or non-symmetrical unsaturated motifs are involved. Certainly, the control of the regio- and chemoselectivity become less complicated in the reactions involving linked di- (partially intramolecular) or tri-unsaturated (intramolecular) substrates (**Scheme 1.7**).

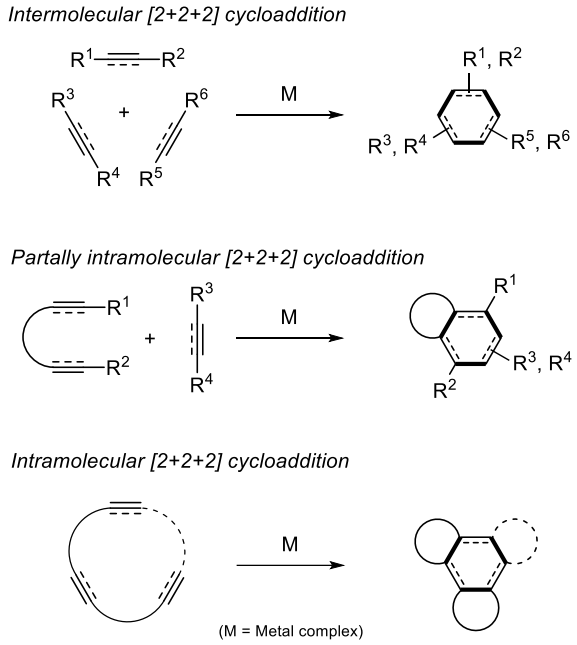

Scheme 1.7. Tethered and non-tethered [2+2+2] cycloaddition reactions. Newly formed bonds out lighted in bold.

In addition, it is important to note that stereochemistry needs to be considered when central, axial, planar or helical chirality is formed. Significant progress has been made in the field after the pioneering works of Mori,[29] Stará and Starý[30] and Shibata,[31] who achieved, respectively, central chirality by desymmetrization of diynes, helical chirality using triynes, and central chirality with enynes in an enantioselective manner.

The large number of reviews published in the past two decades, covering general aspects of the transition metal-catalyzed [2+2+2] cycloaddition,[32] the involvement of unsaturations other than alkynes,[33] stereoselective versions,[34] and applicability of the reaction in the synthesis of relevant organic molecules,[35] clearly exemplifies the importance of the reaction. The endeavours of our group in the development of efficient [2+2+2] cycloaddition reactions catalyzed by rhodium have been recently summarized in a personal account.[36] In line with the methodologies developed in this thesis, this section makes an overview of the [2+2+2] cycloaddition reaction involving allenes. However, the use of allenes in [2+2+2] cycloadditions with hetero-unsaturated multiple bonds[37] will not be covered.

1.2.2. Mechanism

Many advances were achieved in the mechanistic understanding of the transition metal-catalyzed [2+2+2] cycloaddition by synergic experimental and computational studies. Although the mechanism particularities strongly depend on the whole system (metal, ligand, substrate, and solvent), over the years a consensus has been reached for the general mechanism of the transition metal-catalyzed cyclotrimerization of alkynes (**Scheme 1.8**). The reaction starts with the coordination of two alkyne units followed by an oxidative cyclometalation to furnish the metallacyclopentadiene **IIa** or the biscarbene type metallacyclopentatriene **IIb** (with Ru as a metal), increasing the oxidation state of the metal by two units. The generation of **IIa** or **IIb** during the reaction has been confirmed in many occasions.[38] In most cases, the oxidative cyclometalation was

found to be the rate-determining step of the process.[39] Coordination of the third alkene generating **III** is followed by either: (a) alkyne insertion via Schore's mechanism[40] leading to cycloheptatriene **IVa**; (b) [4+2] cycloaddition to form the metallanorbornadiene **IVb** or (c) [2+2] cycloaddition to give metallabicyclic species **IVc**. From this point, reductive elimination and subsequent release of the metal complex furnishes the arene **V** and closes the catalytic cycle. The energy barriers for the transition metal-catalyzed [2+2+2] cycloadditions are relatively low, which correlates with the experimental occurrence of these processes under mild conditions. In addition, the process is highly exothermic with the thermodynamic driving force provided by the formation of three new σ-bonds and the gained aromaticity.

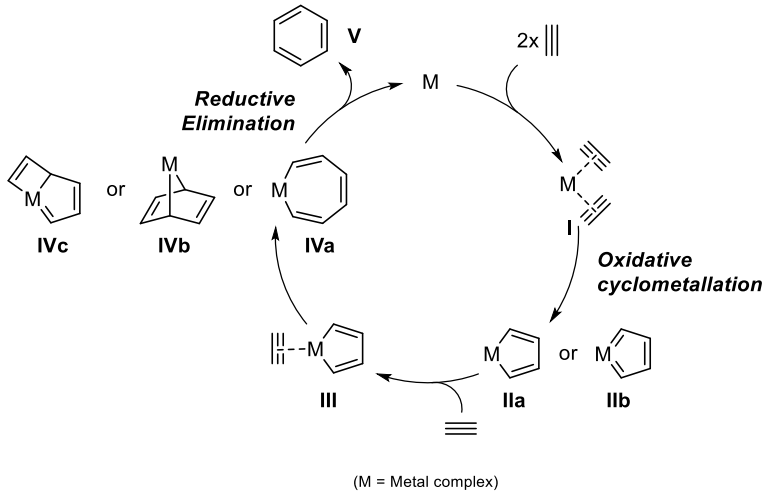

Scheme 1.8. Generally accepted mechanism of the transition metal-catalyzed [2+2+2] cycloaddition of three alkynes

The first computational study of the Rh-catalyzed [2+2+2] cycloaddition reaction was reported by Bickelhaupt *et al.*[39d] in 2007, in which the cyclotrimerization of acetylene to produce benzene was studied. The authors concluded that the reaction proceed via initial oxidative cyclometalation of two acetylene molecules giving intermediate **IIa**, as the rate-determining step of the process. The coordination of the third alkyne unit is then followed by a [4+2] cycloaddition, to generate intermediate **IVb** which evolves to an η^4-benzene-Rh complex in a barrierless reductive elimination process. Finally, the benzene is released to complete the catalytic cycle. Our group[39b] also studied computationally the acetylene [2+2+2] cyclotrimerization using the Wilkinson's catalyst [$RhCl(PPh_3)_3$]. The mechanism was found to be closely related to the one described by Bickelhaupt, but more importantly, this study demonstrated that using the simplified PH_3 ligand instead of the PPh_3, the thermodynamics and kinetics of the process were not significantly altered. These means to reduce computational costs, were later used in 2014 by our group to study the pyridine formation through the [2+2+2] cycloaddition of two acetylene molecules and hydrogen cyanide.[41] In addition, our group has recently published an extensive review, from the seminal studies until 2021, of the key mechanistic aspects that influence the reactivity and selectivity of the reaction.[42]

1.2.3. Allenes in transition metal-catalyzed [2+2+2] cycloadditions

Replacing *sp*-hybridized substrates by sp^2-hybridized ones in the transition metal-catalyzed [2+2+2] cycloaddition, allows the eventual introduction of a stereocenter in the newly formed 6-membered ring (**Scheme 1.9**). However, the use of alkenes generally results in decreased reactivity, therefore, chemoselectivity becomes difficult to control given the high reactivity of alkynes in this reaction. An excellent alternative is to use allenes, since stereocomplexity can be achieved while maintaining high reactivity.

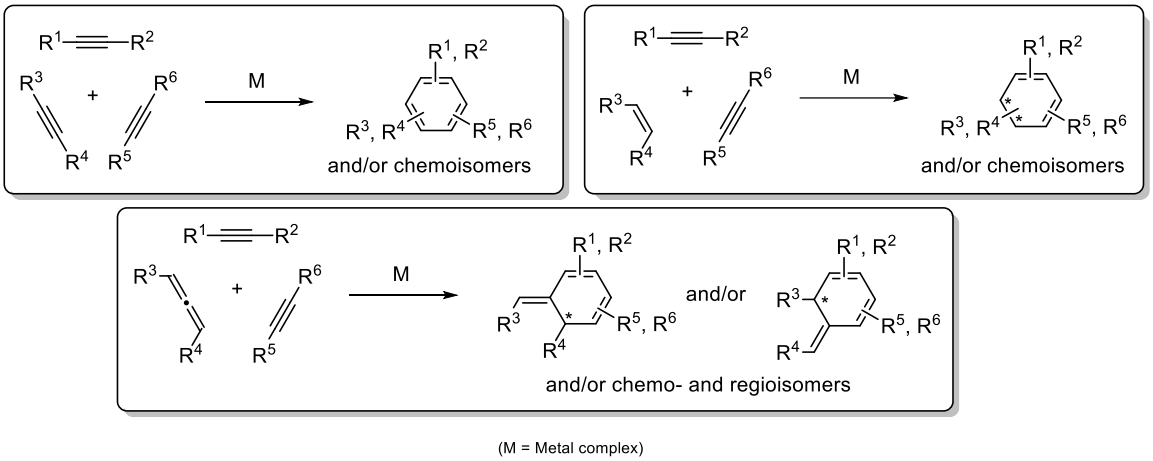

Scheme 1.9. General [2+2+2] cycloadducts that are obtained from three alkynes or two alkynes with either an alkene or allene.

Pioneering studies into the use of the allenes in the transition metal-catalyzed [2+2+2] cycloaddition were performed by Benson and Lyndsey *et al.*[43] in 1958, to obtain the cyclotrimerization of 1,2-propadiene under nickel(0) catalysis. The corresponding trimethylenecyclohexanes were obtained in almost perfect statistic mixture of 1,2,4 and 1,3,5 isomers. This ratio is rationalized by examining the potential metallacyclopentane intermediates. The unsymmetrical 1,2,4 isomer can be generated through the three distinct possible metallacycles, but only one of these can give access to the 1,3,5 symmetrical product (**Scheme 1.10a**). The introduction of an alkyne in the mixture, with the nickel(II) complex [$Ni(acac)_2$] as the catalyst, resulted in the formation of dimethylenecyclohexenes in good chemoselectivity (**Scheme 1.10b**).[44] Given the large number of products that could be obtained, this study provided promising results for further [2+2+2] cycloaddition reactions involving allenes, although they were not reported until three decades later.

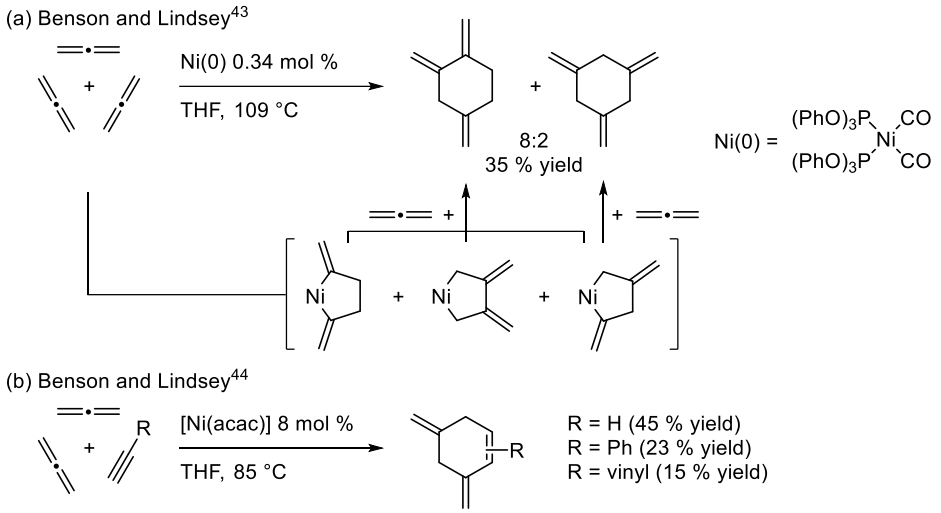

Scheme 1.10. First transition metal-catalyzed [2+2+2] cycloaddition reactions involving allenes.

In the early 90's, Diek *et al.*[45] reported a [2+2+2] cycloaddition of phenoxyallene with two molecules of dimethyl acetylenedicarboxylate using a palladacyclopentadiene complex as a catalyst. The process was found to be chemoselective towards the non-substituted double bond of the allene. Additionally, when increasing the catalyst load and the temperature to 60 ºC, an isomerization of the external double bond took place to produce a benzene derivative (**Scheme 1.11**).

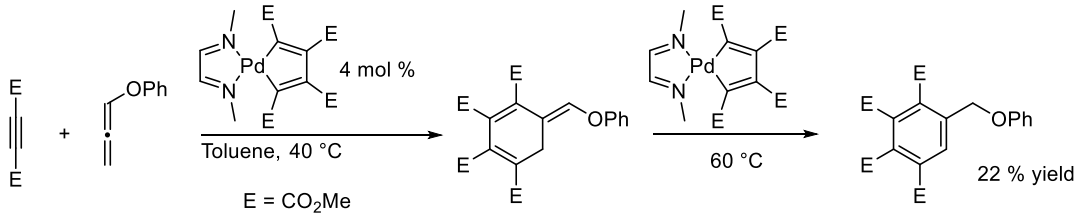

Scheme 1.11. Palladium-catalyzed [2+2+2] cycloaddition of phenoxyallene and dimethyl acetylenedicarboxylate.

Other metallacycles were used as substrates for the [2+2+2] cycloaddition with allenes, for instance a zirconacyclopentadiene as demonstrated by the group of Takahashi.[46] However, the reaction required stoichiometric amounts of nickel(II) and no chemoselectivity was obtained since both double bonds of the allene reacted.

Cheng *et al.*[47] developed a nickel(II)-catalyzed [2+2+2] cycloaddition of alkyl-monosubstituted allenes with two *in-situ*-generated arynes. Whereas arynes had already been reacted with a variety of alkynes in [2+2+2] cycloadditions, this was the first example in which they were combined with allenes, providing 10-methylene-9,10-dihydrophenantrene derivatives in good yields (**Scheme 1.12a**). The monosubstituted allene reacted chemoselectively in the internal double bond, although mixtures of the two isomers were obtained with 1,1-disubstituted allenes. Following these studies, Liang and Li *et al.*[48] obtained the same [2+2+2] cycloisomerization pattern but under palladium catalysis with di- and trisubstituted allenes. In contrast, the isomerization of the cycloadduct leading to aromatic phenantrene derivatives took place when 1,2-

disubstituted allenes bearing an electron-withdrawing group were used. In all cases, the reaction was found to be highly chemoselective as only one of the double bonds of the allene reacted in the [2+2+2] cycloaddition (**Scheme 1.12b**).

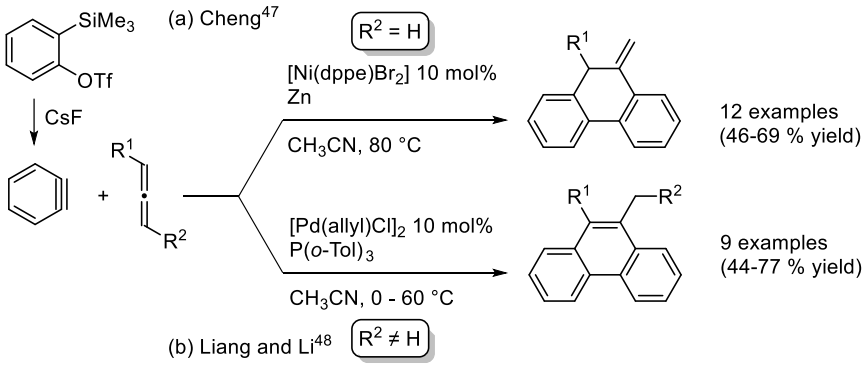

Scheme 1.12. Examples of [2+2+2] cycloaddition reactions involving arynes and allenes.

Substantial contribution to the intermolecular [2+2+2] cycloaddition was made also by Cheng *et al.*[49], who reported a highly regio- and chemoelective process combining two molecules of substituted propiolates and alkyl-monosubstituted allenes employing [Ni(acac)Br_2]/Zn as a catalytic mixture. In contrast to the [2+2+2] cycloaddition with arynes, the terminal double bond of the allene was involved in the cycloaddition. Although the reaction was limited to electron-deficient alkynes, different regioselectivities were obtained by changing the substituents in the propiolates. Esters located in *ortho* in the final product were obtained with alkylpropiolates, whereas the *meta* relative disposition was preferred for phenylpropiolate. The authors explained this regioselectivity divergence in terms of the regioselective formation of the metallacyclopentadiene (**Scheme 1.13**). The formation of the 1,4-dialkylmetallacycle would be more favorable than the 1,3-intermediate because of electronic effects. On the other hand, for phenylpropiolates the 1,3-diphenylmetallacycle was favored instead of the 1,4-substituted one due to steric congestion with the nickel moiety. Here again, the final product underwent aromatization to afford the corresponding benzene derivatives.

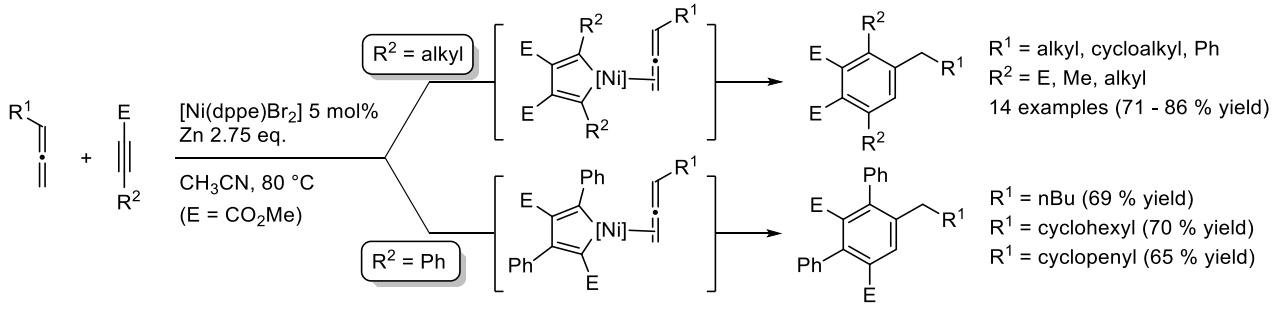

Scheme 1.13. Highly regio- and chemoselective [2+2+2] cycloaddition of propiolates and allenes.

In the reactions in which the final product aromatizes, the allene is synthetically equivalent to the corresponding alkyne, albeit in this last work the authors demonstrated the advantages on the use of allenes since performing the reaction with 1-heptyne resulted in the formation of a mixture of products with lower yields. This result suggests that allenes are much more selective than alkynes in the cocyclotrimerization. On

the other hand, the aromatization step seems to be rather difficult to predict as well as the chemoselectivity in the allene, and probably electronic and steric factors in both, the substrates and catalyst, play an important role in the whole process.

In 2016, Tanaka *et al.*[50] disclosed the first intermolecular [2+2+2] cycloaddition of two molecules of monosubstituted allenes with functionalized alkynes under rhodium(I) catalysis. The reaction tolerated both electron-deficient and electron-rich symmetrical alkynes, as well as the unsymmetrical ethyl 3-methylpropiolate, but terminal alkynes did not get the desired product since they rapidly underwent cyclotrimerization. Regarding the allene, either aliphatic, aromatic or ether-bearing ones participated in the reaction. Furthermore, the process regioselectively gave conjugated trienes, although the chemoselectivity was not complete since both double bonds of the allene reacted affording two different isomers, one of them formed in substantially major proportion (**Scheme 1.14**). It must be noted that when the reaction was performed with phenylallene (R^1 = Ph) or the ((buta-2,3-dien-1-yloxy)methyl)benzene (R^1 = CH_2OBn), the reaction was fully chemo- and regioselective, affording only one of the isomers.

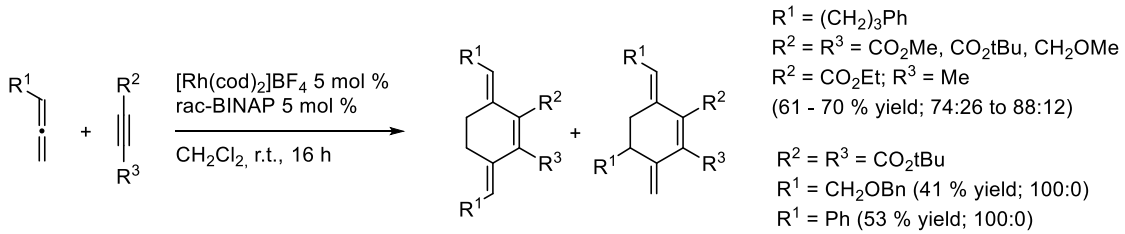

Scheme 1.14. First rhodium catalyzed [2+2+2] cycloaddition between two molecules of functionalized allenes and alkynes.

Chemoselectivity and regioselectivity are often more easily controlled in the partially intermolecular [2+2+2] cycloaddition, further extending the use of unsymmetrical substrates while maintaining good levels of selectivity. Cheng *et al.*[51] reported in 2002 a reliable procedure using unsymmetrical tethered diynes and monosubstituted allenes, in which their previously used [Ni(acac)Br_2]/Zn catalytic mixture performed well in a partially intramolecular [2+2+2] cycloaddition with high levels of chemo- and regioselectivity (**Scheme 1.15a**). A related work was reported more recently by Mukai *et al.*,[52] who described a chemo- and regioselective partially intramolecular rhodium(I)-catalyzed [2+2+2] cycloaddition of tethered allenynes with unsymmetrical alkynes (**Scheme 1.15b**). For this transformation, the use of an electron-withdrawing group in the internal carbon atom of the allene was essential.

In both cases, the allene moieties served as synthetic equivalents of alkynes as the adducts obtained aromatized to get polysubstituted benzenes. However, the use of allenes presented an important advantage since the equivalent cycloaddition with three alkynes generally suffers from poor regioselectivity.

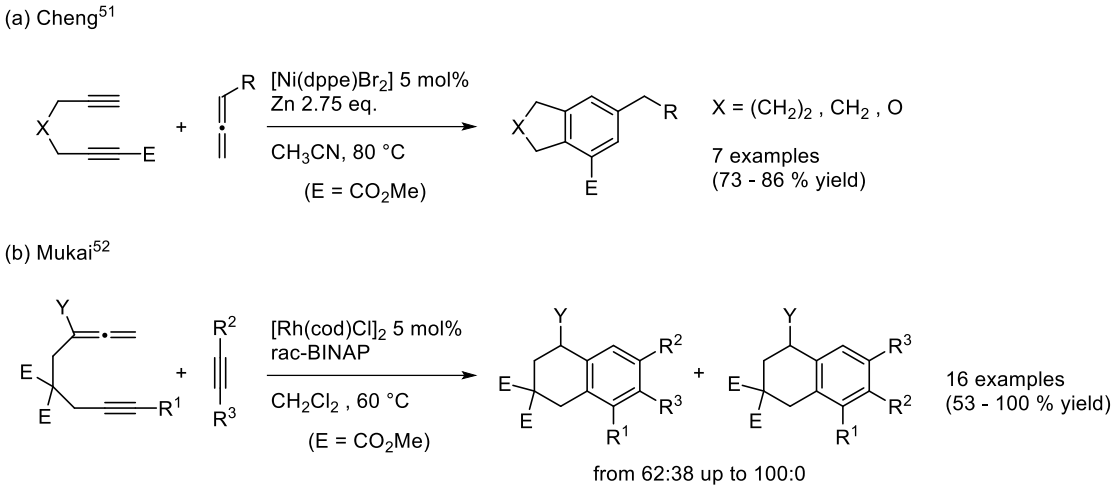

Scheme 1.15. Partially intramolecular [2+2+2] cycloadditions of two alkynes and one allene: (a) combination of a diyne and an allene; (b) combination of an allenyne and an alkyne.

The partially intramolecular [2+2+2] cycloaddition also performed well with allenynes when an allene is used as external unsaturation as shown by Arai *et al.*[53] under nickel(0) catalysis. The reaction was found to tolerate carbon-, nitrogen- and oxygen-tethered allenynes, as well as a wide variety of functionalities in the external allene. Additionally, a computational DFT study revealed that selectivity of the process is originated in the intermolecular insertion of the allene, which is strongly affected by the steric environment around the π-bonds. This observation allowed the rational design of substrates to control the regioselectivity of the reaction. As depicted in **Scheme 1.16**, alternative regioisomers were obtained by changing the substitution pattern of the participating unsaturations. As an inconvenience, the process was not completely chemoselective as low amounts of the allenyne homodimerization product were obtained.

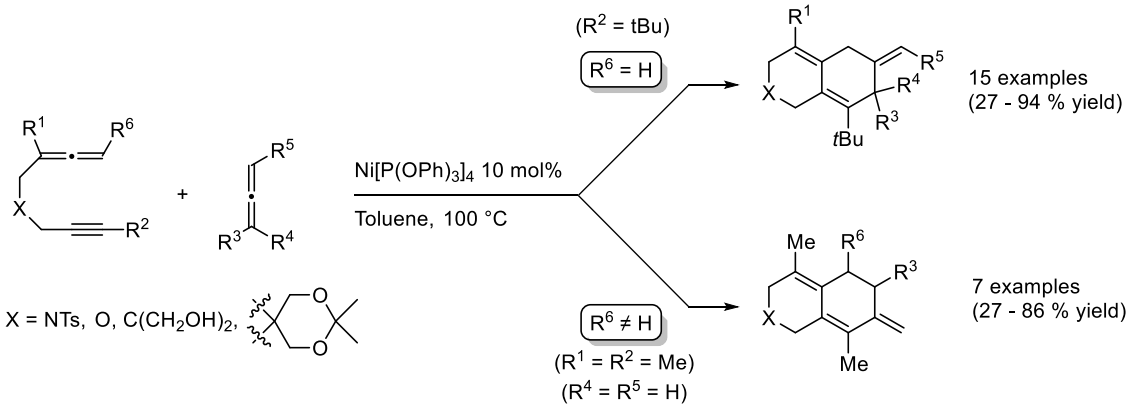

Scheme 1.16. Regioselectivity tuning in [2+2+2] cycloaddition of allenynes with allenes.

The homodimerization of propargylic allenoates was described by Ma *et al.*[54] in a process catalyzed by a modified Wilkinson's complex. A [2+2+2] cycloaddition took place between the propargylic triple bond, the allene moiety and the triple bond of a second molecule of propargylic allenoate affording 1,3-cyclohexadienes. A subsequent intramolecular Diels-Alder reaction, under the reaction conditions, efficiently afforded tricyclic scaffolds (**Scheme 1.17**). Surprisingly, only two diastereoisomers out of six possible were formed. It is to be

noted that substrates featuring H in α-position to the allene, underwent β-elimination after the initial oxidative cyclometalation affording monocyclic dihydropyranone derivatives. A previously developed dimeric [2+2+2] cycloaddition followed by a Diels–Alder process developed by the same group, but involving 1,5-bisallenes, will be overviewed in the next section dedicated exclusively to 1,5-bisallenes.

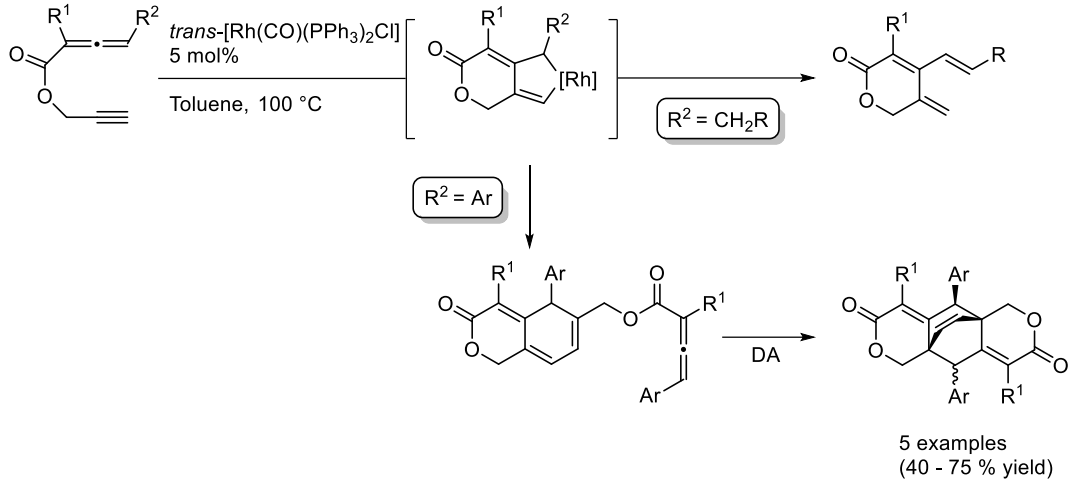

Scheme 1.17. [2+2+2] cycloaddition of propargylic allenoates.

Allenes can also react with double bonds in partially intermolecular [2+2+2] cycloadditions, affording cyclic scaffolds with up to five contiguous stereogenic centers with high levels of chemo-, regio- and stereoselectivity. In this regard, the group of Alexanian studied the [2+2+2] cycloadditon of allenenes with monosubstituted allenes under rhodium(I) catalysis, affording in a diastereoselective[55] and enantioselective,[56] manner *trans*-fused bicyclic carbocycles (**Scheme 1.18a**). Typically, the intramolecular oxidative cyclometalation of two 1,5-tethered double bonds produce the *cis*-fused metallacycles,[57] probably because their strain energy is lower than their *trans*-fused counterparts.[58] Therefore, the authors concluded that the initial oxidative cyclometalation took place in an intermolecular manner with the two internal double bonds of the allene moieties (**Scheme 1.18a**). In contrast, *cis*-fused carbocycles were obtained in a regio- and diastereoselective manner by the same group[25] under nickel catalysis when they further studied the [2+2+2] cycloaddition of allenenes with alkenes. This time, the stereoselectivity of the fused system comes from the initial intramolecular oxidative cyclometalation of the internal double bond of the allene with the linked alkene, leading to the *cis*-fused metallacycle intermediate (**Scheme 1.18b**).

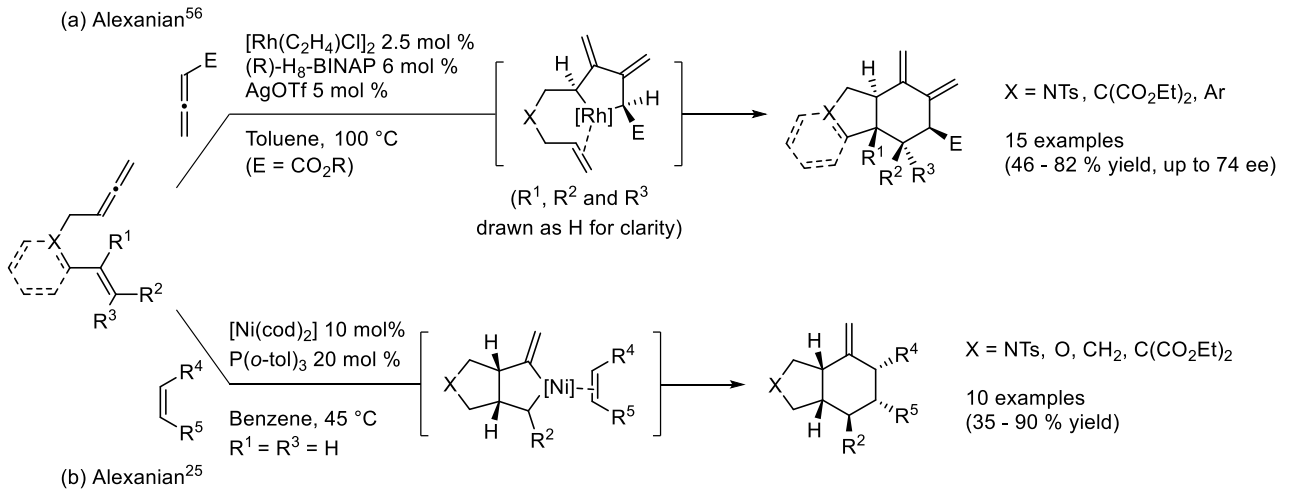

Scheme 1.18. [2+2+2] cycloaddition of allenenes with allenes and alkenes, leading to *trans*- and *cis*-fused ring systems.

The use of linear substrates containing three unsaturated carbon – carbon bonds for the totally intramolecular [2+2+2] cycloaddition allows even an easier access to complete regio-, chemo- and stereoselective methodologies given the structure constrictions generated during the process. Malacria *et al.*[59] were the first to set diverse studies employing linear allene–diynes in cobalt-mediated [2+2+2] cycloaddition reactions. Although these early examples required stoichiometric amounts of cobalt, they sparked interest in the utility of allene-containing linear triunsaturated substrates for the [2+2+2] cycloaddition. They illustrated the strong effects of the allene substitution pattern, which greatly affect the outcome of the cycloaddition, as well as the ability for these reactions to occur with effective axial to central chirality transfer.[60] However, the use of allene–diynes stands of lesser synthetic interest in their catalytic versions as the tricyclic [2+2+2] adducts undergo aromatization to yield the corresponding benzo-fused scaffolds,[61] consequently, the same structures can be easily accessed employing the analogous linear triyne precursors without chemo- or regioselectivity issues.

The combination of three different carbon – carbon unsaturated bonds (allene–ene–yne) seems to be more robust for intramolecular [2+2+2] cycloaddition. Mukai *et al.*[62] synthesized triunsaturated substrates in which the allene was placed between the alkene and the alkyne with different tether lengths and tested them in [2+2+2] cycloaddition reactions. This arrangement demonstrated to be exceptionally functional in terms of structural variability. The use of the neutral rhodium(I) catalyst $[Rh(CO)_2Cl]_2$ allowed the formation of complex tri- and tetracyclic scaffolds of different ring sizes in a completely diastereoselective manner (**Scheme 1.19**). An additional interesting feature of this approach is the possibility to form cyclopropane-fused polycyclic structures. As a drawback, the use of geminal disubstituted tether was necessary to avoid undesired side products occurring via *β*-hydride elimination.

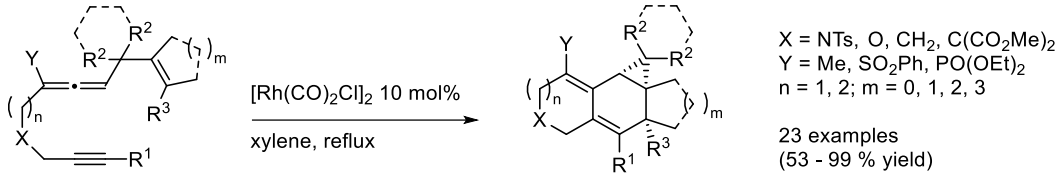

Scheme 1.19. Rhodium(I)-catalyzed intramolecular [2+2+2] cycloaddition of ene – allene – ynes.

Saito, Sato *et al.*[63] developed a ruthenium(II)-catalyzed intramolecular [2+2+2] cycloaddition of allene–yne–enes placing the allene in a terminal position. The cyclization afforded fused 5/6/5 ring systems upon cycloaddition with complete diastereoselectivity (**Scheme 1.20**). Additionally, the cycloaddition was chemoselective in the internal double bond of the allene, giving rise to an exocyclic double bond. Notably, the *β*-elimination of the ruthenacycloheptene was observed in only one example albeit most of the ruthenacycloheptene intermediates had hydrogen atoms in *β*-position amenable to *β*-elimination during the catalytic cycle.

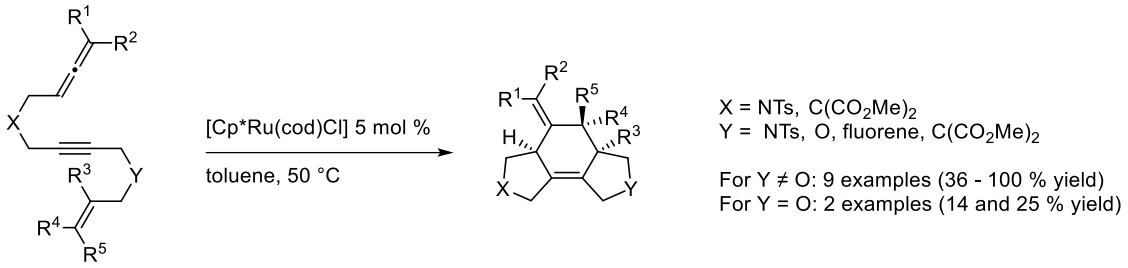

Scheme 1.20. Ruthenium(II)-catalyzed intramolecular [2+2+2] cycloaddition of allene – yne – enes.

Our research group has made great contributions in the rhodium(I)-catalyzed intramolecular [2+2+2] cycloaddition of linear substrates accommodating allenes and alkynes and/or alkenes, covering the use of allene–ene–ynes[64] and allene–yne/ene–allenes.[65] These works have been backed by means of DFT calculations and exhaustive experimental studies, letting complete understanding of the processes and rationalization of the selectivities. After demonstrating high levels of activity of the Wilkinson's complex in [2+2+2] cycloadditions in different combinations of alkynes with alkenes and nitriles,[36] the group decided to further extend this chemistry in the use of substrates containing three different carbon – carbon unsaturations.[64] In this regard, allene–ene–yne substrates were prepared, setting the allene and the alkyne moieties in the terminal positions, making the oxidative cyclometalation between them geometrically disfavored. The tricyclic derivatives were formed chemoselectively, involving the internal double of the allene. However, two diastereoisomers were obtained differing in the 6:5 ring fusion, which was either *cis*-fused (major) or *trans*-fused (**Scheme 1.21**). Then, alternative rhodium-based catalytic systems were tested to improve or switch the diastereoselectivity of the reaction, and found that the dimeric rhodium complex $[Rh(CO)_2Cl]_2$ had a preference for the formation of the *trans*-fused tricyclic derivative, while the cationic $[Rh(cod)_2]BF_4$ in combination with the bulky biphosphine (R)-DTBM-Segphos resulted in a less efficient catalytic system, probably due to steric hindrance. With this results in hand, DFT calculations were performed to understand the differences between the two neutral rhodium complexes $[Rh(PPh_3)_3Cl]$ and $[Rh(CO)_2Cl]_2$. Comparison of the two Gibbs energy profiles

allowed to computationally explain the experimental detection of two diastereoisomers since very low energetic differences were found between the intermediates leading to the *cis*- and *trans*-fused products. The difference in the selectivity can be associated to the coordination sphere of the catalytically active species. Whereas the Wilkinson complex loses all the phosphines during the catalytic cycle, the intermediates in the $[Rh(CO)_2Cl]_2$ catalytic cycle have a variable number of carbonyl units coordinated to the rhodium. This study provided evidence on the influence of fine-tuning the rhodium/ligand to provide different stereoselectivities.

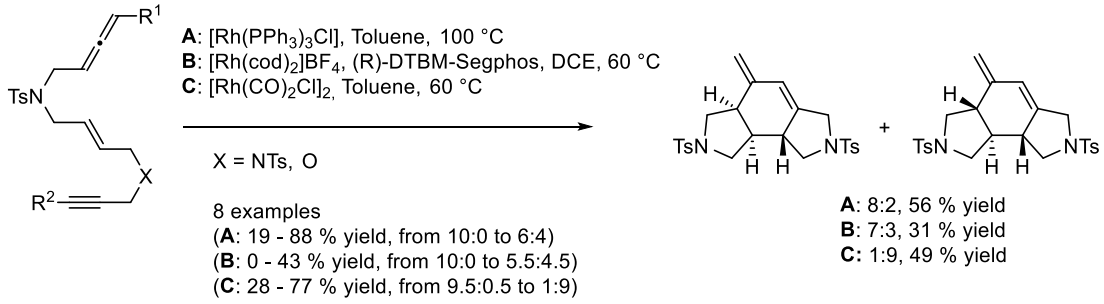

Scheme 1.21. Intramolecular rhodium-catalyzed [2+2+2] cycloaddition of allene – ene – ynes using different rhodium sources.

As part of the continued interest in the use of allenes as unsaturated motifs in the intramolecular [2+2+2] cycloaddition, our research group examined the cycloaddition of bisallenes incorporating either an alkyne or an alkene between the two allene moieties (allene–yne–allene and allene–ene–allene), first in a racemic version,[65a] and then in an enantiospecific version of the reaction.[65b] In the first study, the cycloaddition of allene–yne/ene–allenes, with *N*-tosyl- and *O*-linked tethers, took place in a fully chemo-, regio- and stereoselective manner using the Wilkinson's complex as catalyst (**Scheme 1.22**). Substrates bearing either a triple bond or a *trans* double bond in the central position, led to tricyclic structures as single diastereoisomers containing two or four stereogenic centers respectively. Additionally, all cycloadducts were formed exclusively engaging the internal double bond of both allene moieties, resulting in exocyclic dienes.

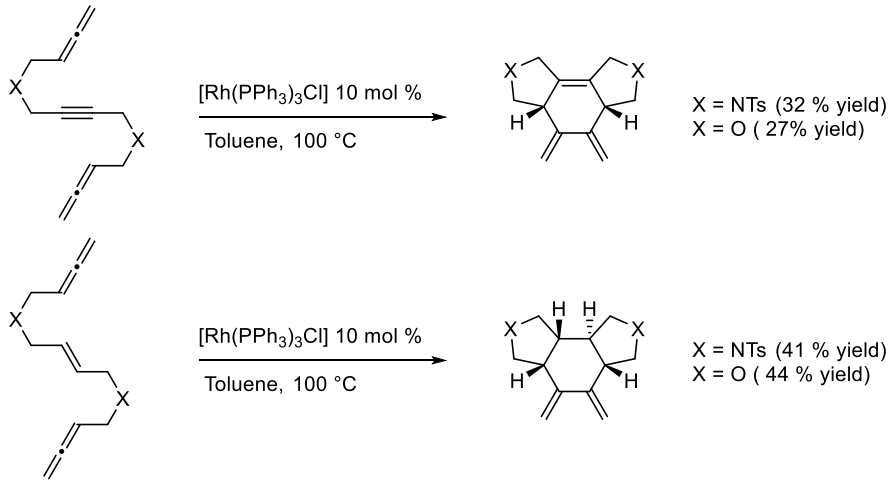

Scheme 1.22. Rhodium-catalyzed intramolecular [2+2+2] cycloaddition of linear allene – yne – enes and allene – ene – yne derivatives.

For allene–ene–allenes, exhaustive DFT calculations were performed to evaluate the chemoselectivity, along with the stereoselectivity of the process and the participation order of the different unsaturations. The initial oxidative cyclometalation was postulated to take place between the internal double bond of one of the allenes and the central alkene, generating the *cis*-fused rhodacyclopentane, then the insertion of the second allene — furnishing a *trans* ring fusion — and subsequent reductive elimination gives the tricyclic product (**Scheme 1.23**).

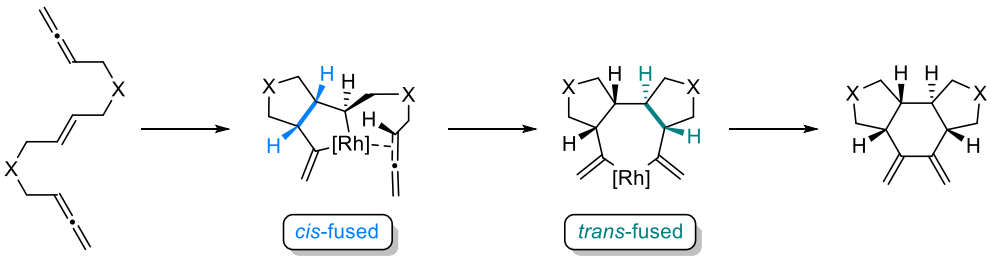

Scheme 1.23. Origin of ring-fusion stereoselectivity observed in [2+2+2] cycloaddition reactions.

This agrees to what Alexanian *et al.*[25,55,56] observed in their previous studies: intramolecular oxidative cyclometalation typically produces *cis*-fused rings, whereas *trans*-fused rings come from intramolecular insertion. In the context of this thesis, DFT computational studies are performed evaluating the stereochemistry generated in both processes, the oxidative cyclometalation and the allene insertion via Schore's mechanism. The results of these studies are discussed in chapters 5 and 6 of this manuscript.

In the second study of our group[65b] involving allene–yne/ene–enes, an enantiospecific intramolecular [2+2+2] cycloaddition was achieved by incorporating enantiomerically pure stereogenic centers in the α-position of the allene moieties. Using the non-chiral rhodium complex [$Rh(PPh_3)_3Cl$], the desired cycloadducts were obtained as single enantiomers with the *N*-tosyl tethered allene–yne/ene–allene derivatives. In contrast, two of the six possible stereoisomers were generated with the *O*-linked substrates, demonstrating an important influence of the linker in the outcome of the reaction. Based on the previous DFT calculations, the diastereoselectivity of the process can be associated to steric effects in both, the oxidative cyclometalation and the second allene insertion as shown in **Scheme 1.25**.

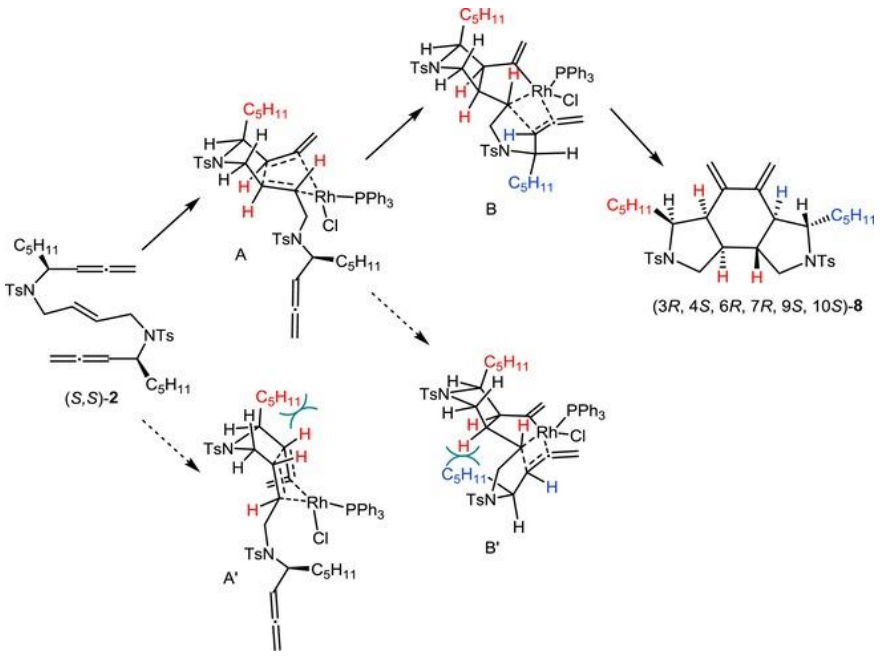

Scheme 1.24. Postulated mechanism for the selective formation of enantiomerically pure tricyclic scaffolds from *N*-tethered allene – ene – allenes. Reprinted with permission from Haraburda, E.; Fernández, M.; Gifreu, A.; Garcia, J.; Parella, T.; Pla-Quintana, A.; Roglans, A. *Adv. Synth. Catal.* **2017**, *359*, 506. Copyright 2017 2017 Wiley-VCH Verlag GmbH & Co. KGaA, Weinheim.

The different behavior of the *O*-tethered allene–ene–allene may come from the reduced steric hindrance when compared to *N*-tosyl, conferring higher flexibility to the whole system, thus, reducing the difference in energy barriers in either the oxidative cyclometalation or the insertion of the second allene moiety.

Among all the transition metal-catalyzed [2+2+2] cycloaddition reactions with allenes, reactions involving two allenes with another unsaturated carbon – carbon bond remain scarce. Therefore, as part of the continuous interest of our research group in the use of allenes as unsaturated motifs for the construction of polycyclic derivatives by rhodium-catalyzed [2+2+2] cycloadditions, we envisaged the development of partially intramolecular cycloaddition reactions of 1,5-bisallenes. Albeit 1,5-bisallenes have shown rich chemistry with transition metals, most studies consist in cyclizations and cycloisomerization reactions to furnish diversified products with 5-, 6- or 7-membered rings. Apart from the methodologies developed in this thesis, very few examples were reported involving the incorporation of a third unsaturated partner in a cycloaddition reaction.

1.3. Overview on transition metal-catalyzed cyclization reactions involving 1,5-bisallenes

Drawing inspiration from the chemistry developed on simple allenes, there has been a growing interest in studying the reactivity of bisallenes,[66] which have proven to be useful substrates in cyclization reactions to create a great variety of cyclic structures.[67] A special class of bisallenes are the 1,5-bisallenes which, when reacted in the presence of transition metals, show an intriguing and diversified reactivity to produce cyclic scaffolds.[68] The most relevant examples in the reactivity of 1,5-bisallenes are covered in this section, organized according to the nature of the process.

1.3.1. Cyclizations involving allene metalation

The metalation of an allene is a reaction in which a new bond is formed between one of the carbon atoms of the allene and a metal center, such as in insertion reactions into M–X bonds[69] (where X is a main group element) or nucleophilic additions via electrophilic π-activation[70] (**Scheme 1.25a**). More interestingly, if two linked allenes are used, the resulting complex from the metalation of one of the allenes can promote a further carbometalation into the neighboring allene to forge a cyclic scaffold (**Scheme 1.25b**).

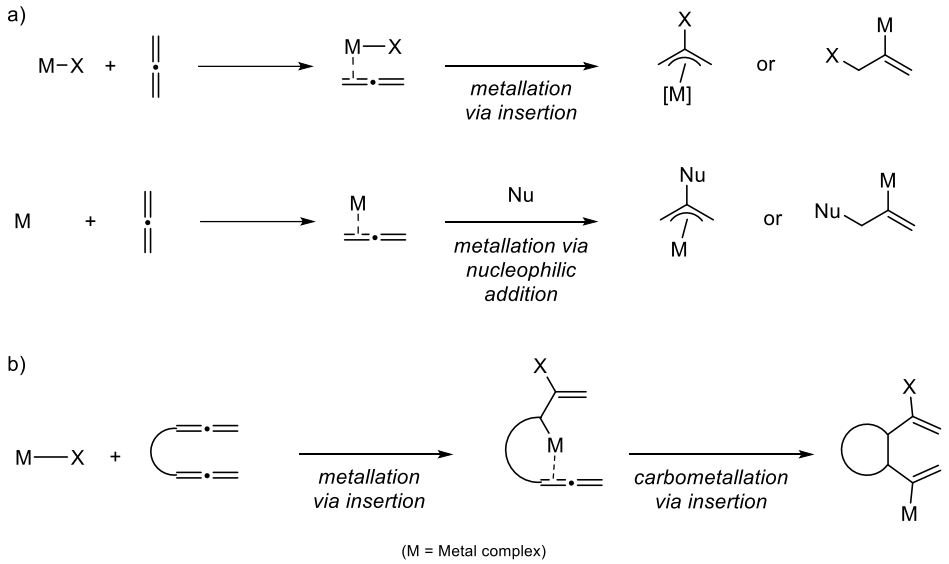

Scheme 1.25. a) Examples of allene metalation. b) Example of an allene metalation followed by an insertion to produce cyclic scaffolds.

The use of 1,5-bisallenes in cyclization reactions involving an allene metalation has proven to be effective for the formation of five and seven membered rings. The different selectivities observed in these cyclizations mainly reside in the metalation mechanism of the first allene, which is key in determining the position at which the following carbometalation into the remaining allene will take place, and thus, the ring size of the final product.

For the formation of 5-membered rings, the metalation of the first allene takes place through the insertion of one of the double bonds into an organometallic M–X bond to generate a π-allyl complex. Then, a carbometalation of the internal double bond of the remaining allene takes place to produce the 5-membered ring. This pathway to generate 5-membered rings has been observed with palladium,[71] platinum,[72] and nickel.[73] Kang and *et al.*[71a] were the first to develop this chemistry of 1,5-bisallenes with silylstannanes and distannanes (**Scheme 1.26a**), and later, the group of Yu[71b] established the equivalent addition of germylstannanes (**Scheme 1.26b**). In all of these examples[71–73], an oxidative addition of the reacting substrates into the metal center generates the organometallic complex into which the allene is inserted. Then, the carbometalation of the internal double bond of the remaining allene followed by a reductive elimination gives the final products (**Scheme 1.26c**).

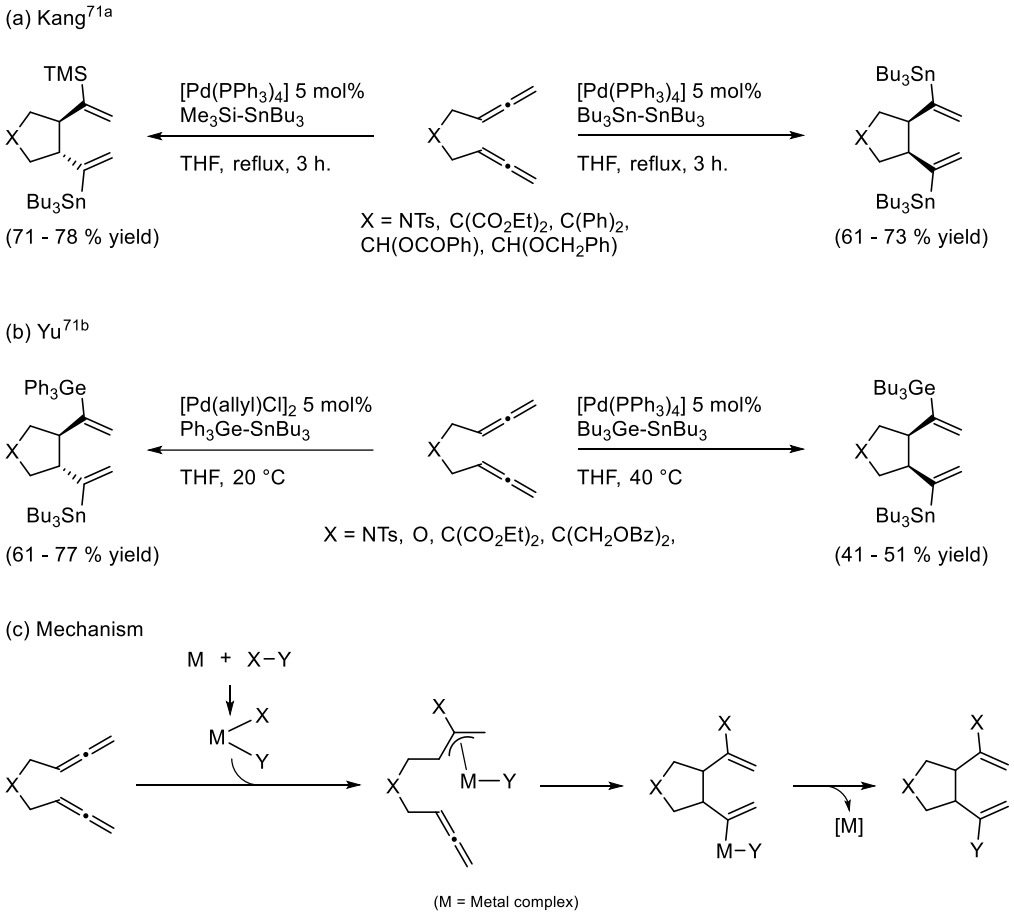

Scheme 1.26. Palladium-catalyzed carbocyclizations of 1,5-bisallenes with silylstannanes, distannanes and germylstannanes.

The *cis*-ring junction is preferred for most of these cyclizations, although the *trans*-ring junction is favored in the silylstannylation due to the steric hindrance of the bulky TMS. The *trans* stereochemistry is also adopted for the germylstannylation process with the Ph_3Ge-$SnBu_3$, presumably due to the steric hindrance of the phenyl substituents. In addition, the nature of the catalyst in the germylstannylation was found to play an important role. The palladium complex $[Pd(allyl)Cl]_2$ was effective for the reaction of 1,5-bisallenes with Ph_3Ge-$SnBu_3$ but not for the incorporation of Bu_3Sn-$SnBu_3$, whereas the opposite trend was found for $[Pd(PPh_3)_4]$.

Hydrogenative and hydrocyanative carbocyclizations have also been accomplished by Jang *et al.*[72] and Nishida *et al.*[73] respectively, affording the corresponding *cis*-5-membered rings.

More interestingly, the group of Ma described a palladium(II)-catalyzed cascade cyclization of chiral 2,3-allenoic acids with 1,5-bisallenes with excellent stereoselectivity.[71c] As opposite to the previous examples, the organometallic M–X complex is generated through a palladium(II)-catalyzed intramolecular nucleophilic cyclization of the 2,3-allenoic acid. After the following insertion of one of the allenes and the subsequent carbopalladation, a second molecule of 2,3-allenoic acid undergo a sequential coordination and cycloisomerization with the vinylpalladium complex. Then, reductive elimination releases the palladium catalyst and gives the final product (**Scheme 1.27**).

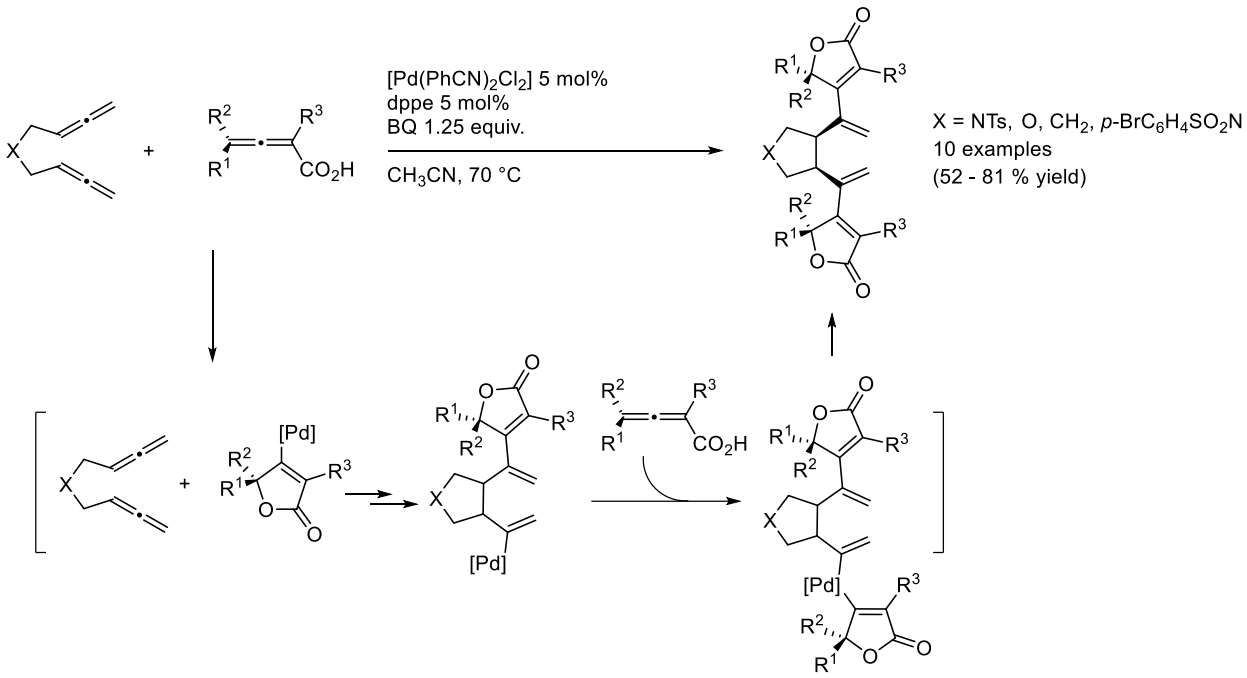

Scheme 1.27. Palladium-catalyzed sandwich type carbocyclization of 1,5-bisallenes in the presence of 2,3-allenoic acids.

Different cyclization products can be obtained when a nucleophilic addition is involved in the allene metalation of the 1,5-bisallene. The group of Ma described a tandem double cyclization of bisallenols[74] and bisallenones[75] to produce fused 5/7 membered rings, catalyzed by palladium and rhodium complexes respectively. These reactions proceed through intramolecular oxymetalation and subsequent carbometalation into the central carbon atom of the remaining allene, furnishing the final product after H_2O elimination (**Scheme 1.28a**) or protonolysis of the oxygen-bound rhodium dienolate (**Scheme 1.28b**).

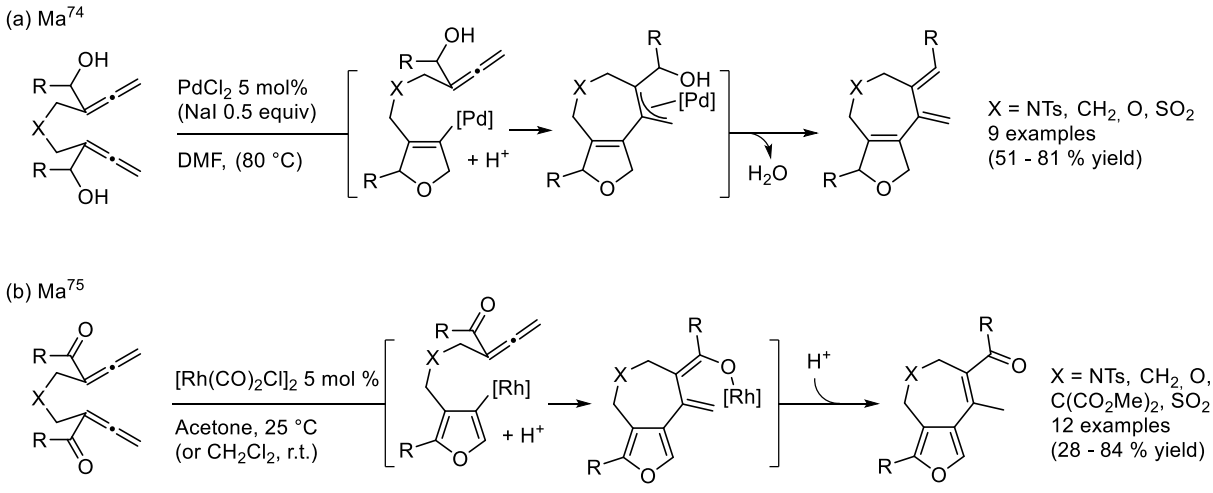

Scheme 1.28. Tandem double cyclizations of bisallenols and bisallenones.

Similar cyclization from 1,5-bisallenes is also possible with external oxygen-based nucleophiles. Muñoz *et al.*[76] reported a platinum-catalyzed cyclization of *N*-tethered 1,5-bisallenes in the presence of water to furnish tetrahydro-*1H*-azepine derivatives. Mechanistic deuterium labelling and Hammet plot studies allowed the

authors to postulate that the reaction proceeds via different mechanisms for electron-withdrawing (EW) and electron-donating (ED) groups in the sulfonamide. For EW groups the reaction proceeds through hydroxymetalation. The nucleophilic addition of the hydroxyl group takes place in the terminal allenic position, placing the organometallic bond to the platinum in the central carbon atom. Further carboplatination and subsequent protodeplatination furnishes the tetrahydro-*1H*-azepine derivatives. In contrast, for ED groups an oxidative cyclometalation is favoured to generate a platinacyclopentane intermediate. For this latter case, the final products are produced after subsequent nucleophilic substitution and protodeplatination (**Scheme 1.29**).

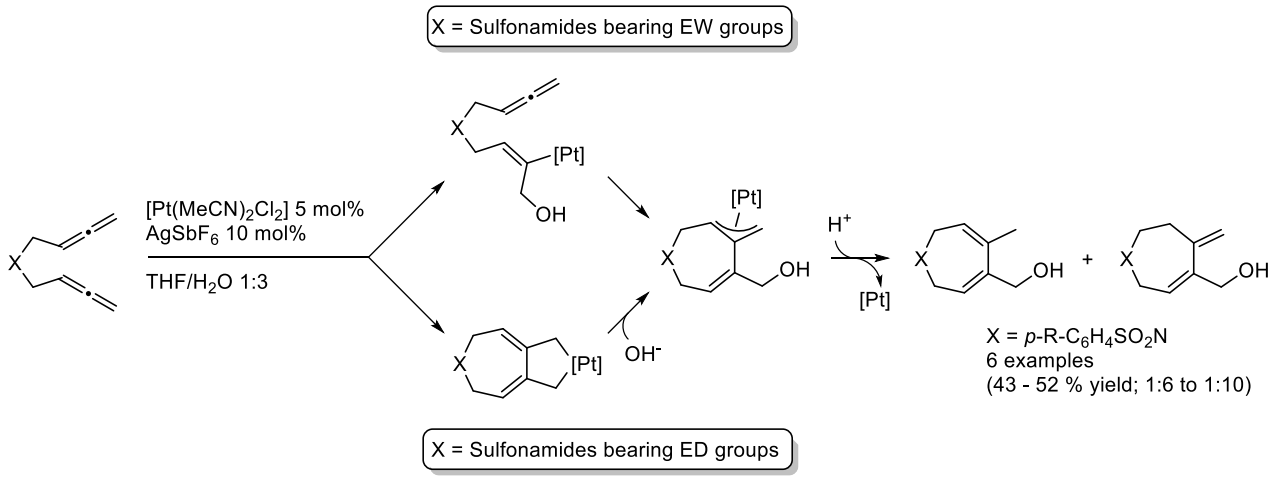

Scheme 1.29. Platinum catalyzed cyclization of 1,5-bisallenes in the presence of water.

The group of Bäckvall afforded related 7-membered rings selectively in two different studies, albeit the first metalation of the allene proceed through slightly different mechanisms. In their first study,[77] the construction of the 7-membered ring involves a palladium-catalyzed oxidative carbocyclization, followed by an alkoxycarbonylation from terminal disubstituted 1,5-bisallenes. The process is initiated by the generation of a vinylpalladium in the central allenic carbon atom via C-H bond activation, the presence of Csp^3-H bonds in the terminal allenic position is required for this step. From that point, carbometalation in the central carbon atom of the neighboring allene furnishes the 7-membered scaffold, which in the presence of CO and an alcohol evolves to the final product (**Scheme 1.30a**). Additionally, in the absence of CO and the alcohol, a *β*-hydride elimination after the carbocyclization furnishes a 7-membered cycloisomerization product of the 1,5-bisallene. In their second study,[78] a palladium-catalyzed hydroborylative carbocyclization of 1,5-bisallenes in the presence of acetic acid and bis(pinacolato)diboron, followed by a tandem cascade reaction with aldehydes, afforded diastereomerically pure alcohols featuring a quaternary carbon center. DFT calculations of the carbocyclization/borylation reaction suggest that the reaction proceeds via a concerted hydropalladation pathway from a Pd(0)-complex rather than the well-defined palladium-hydride species. This has an important impact in the outcome as the hydrogen atom is incorporated in the terminal position (and not in the central carbon atom) generating the vinylpalladium intermediate. Further carbopalladation in the central carbon atom of the remaining allene produces the π-allyl palladium cyclic intermediate. From that point, the allylboron

product is obtained after transmetalation with bis(pinacolato)diboron (**Scheme 1.30b**). Additionally, a one-pot cascade process can be triggered by the addition of the allylboron product into diverse aldehydes, in a process in which a new C-C bond is formed with concomitant formation of a secondary alcohol and a quaternary carbon center.

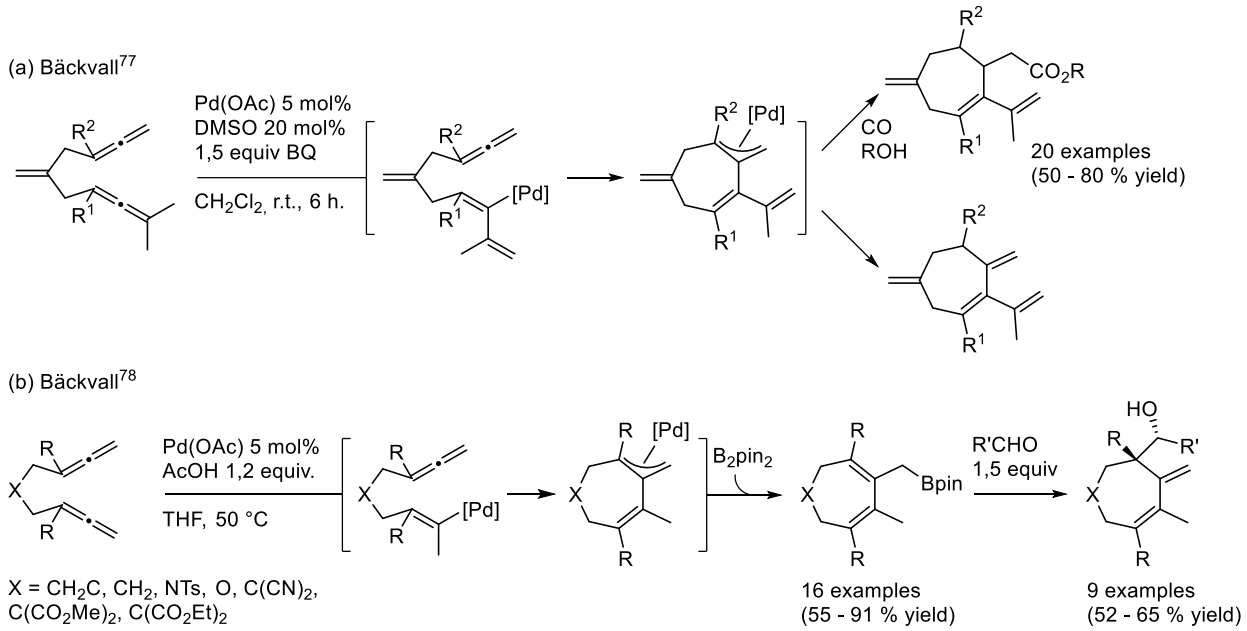

Scheme 1.30. Palladium-catalyzed carbocyclizations of 1,5-bisallenes leading to 7-membered rings.

Ma *et al.*[79] established a palladium-catalyzed three component coupling reaction of 1,5-bisallenes, propargylic carbonates and organoboronic acids affording bicyclic products as single *cis*-diastereoisomers. In the process, propargylic carbonates act as 1,2-allenyl intermediates, which are generated *in situ*, involving three allene functionalities in the reaction. According to the authors, the *in situ* generated 1,2-allenyl palladium promotes the carbopalladation in the central carbon atom of one of the allene moieties of the 1,5-bisallene. Then, two consecutive carbopalladations produce the *cis*-fused bicyclic scaffolds. The first one produces the 5-membered ring with a *cis* diastereoselectivity, as seen in previous examples. The second carbopalladation generates the fused 5/6 scaffold. Further isomerization of the π-allyl intermediate to reduce steric hindrance, subsequent double bond isomerization and Suzuki-type coupling with the organoboronic acid furnishes the final product (**Scheme 1.31**).

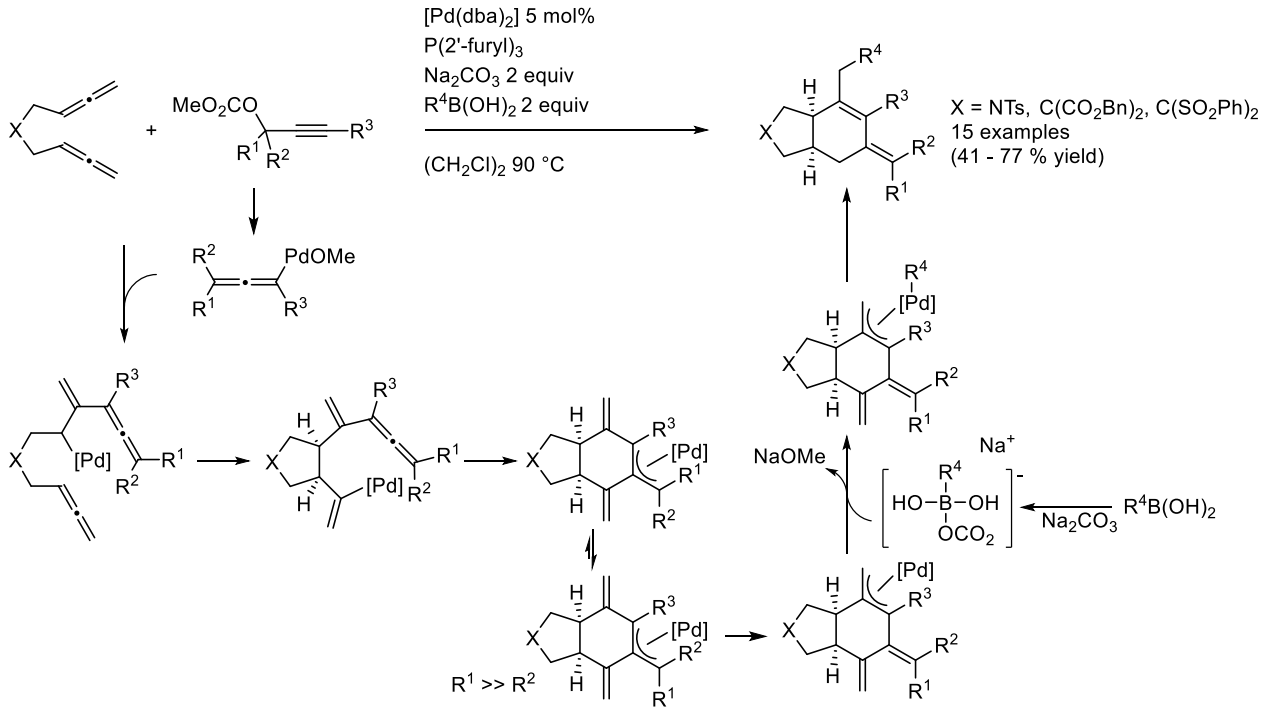

Scheme 1.31. Palladium-catalyzed three-component tandem carbocyclization of 1,5-bisallenes with propargylic carbonates and organoboronic acids.

Distinctive trends can be extracted by briefly looking at the presented cyclization examples of 1,5-bisallenes. Firstly, when a M–X (where X is a main group element) complex is formed, the metalation of the allene takes place in the internal carbon atom, and the X group ends up in the central carbon atom of the ancient allene. The subsequent carbometalation into the remaining allene occurs in the internal carbon atom of the allene to give five membered rings. Secondly, when the metal ends up directly bonded to the central carbon atom of the allene in the metalation step, the carbometalation into the second allene occurs in the central allenic carbon atom, furnishing 7-membered rings. Therefore, it can be generalized that the ring size is determined by the position at which the metal ends up in the first allene metalation: 5-membered rings will be formed when the metal is bonded into the internal carbon atom of the allene, while 7-membered rings will be the preferred choice after metalation in the central carbon atom.

1.3.2. Cycloisomerization reactions

1,5-Bisallenes have emerged as an interesting platform to develop cycloisomerization reactions, as the unsaturation spread over three contiguous carbon atoms makes the construction of various skeletons possible from one single substrate by finely controlling the selectivity of the process. Commonly, these cycloisomerizations proceed through the typical metallacyclic pathway, thus, four types of metallacycle intermediates are postulated to be possible depending on the double bonds that participate in the cyclometalation (**Scheme 1.32**): (a) the two internal double bonds (head-to-head); (b) the internal and the external double bonds (head-to-tail) or vice versa (tail-to-head); (c) the two external double bonds (tail-to-tail).

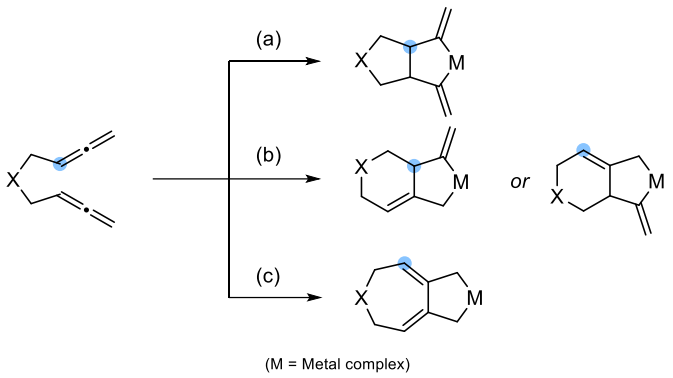

Scheme 1.32. Postulated metallacyclic intermediates of the oxidative cyclometalation of 1,5-bisallenes: (a) head-to-head; (b) head-to-tail or tail-to-head; and (c) tail-to-tail.

The direct reductive elimination of these metallacycle intermediates provides bicyclic cyclobutanes. However, it is worth mentioning that cyclobutanes coming from head-to-tail cyclometalation have not yet been reported. Head-to-head [2+2] cycloadducts[80] have been obtained by Ma *et al.*[81] under palladium catalysis, and by Nishida *et al.*[82] under nickel catalysis (**Scheme 1.33**). The *cis*-diastereoselectivity is obtained in these head-to-head cycloaddition reactions as the ring junction is constructed upon oxidative cyclometalation. The effect of the substitution pattern of the 1,5-bisallenes on the cycloaddition reaction was investigated by Nishida *et al.*[82]. Various tethers are tolerated, as well as substituents at the α position of the *N*-tosyl tether and terminal substituents in one of the allenes. However, the efficiency of the reaction is dramatically reduced when substituents are incorporated in the internal double bond of the allene. Furthermore, a Diels–Alder [4+2] cycloaddition with the resulting exocyclic diene can be performed to furnish tri- or tetracyclic scaffolds.

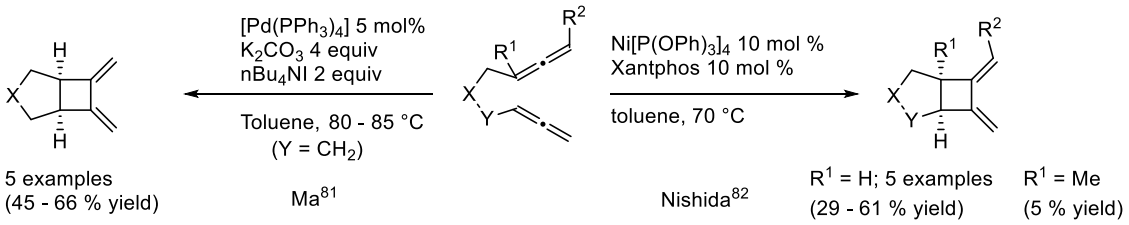

Scheme 1.33. Head-to-head [2+2] cycloaddition of 1,5-bisallenes leading to fused 5/4 scaffolds.

Upon reaction of 1,5-bisallenes under gold catalysis, Kang, Chung *et al.*[83] unexpectedly obtained a 6-membered flipped cycloisomer. DFT calculations suggested that rather than the metallacyclic pathway, the reaction proceeds through nucleophilic attack of the internal double bond of one of the allenes after electrophilic activation of the other allene. The carbocationic intermediate formed is stabilized by a bridged gold complex and concomitant C–C bond formation gives the final product (**Scheme 1.34**).

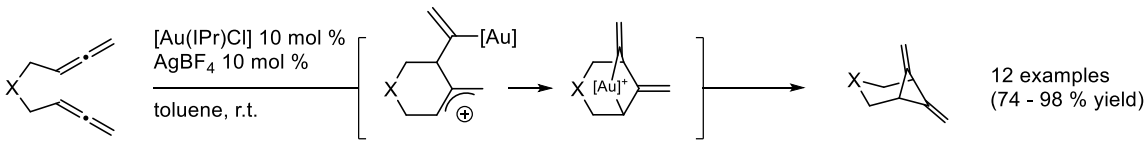

Scheme 1.34. Gold-catalyzed flipped head-to-head cycloisomerization of 1,5-bisallenes furnishing 6-membered rings.

In contrast to palladium and nickel, tail-to-tail metallacyclic intermediates are postulated when rhodium or copper are the metal of choice. Additionally, when rhodium is used, two different pathways are possible to give cycloisomerization products: (a) 1,5-hydride shift followed by reductive elimination giving 7-membered trienes; or (b) direct reductive elimination to get the [2+2] cycloadducts.

Ma *et al.*[84] described the formation of the 7-membered trienes via rhodium(I)-catalyzed cycloisomerization of 1,5-bisallenes bearing substituents at the terminal positions, which were required to avoid a dimerization via [2+2+2] cycloaddition (*vide infra*). The reaction is postulated to proceed via oxidative cyclometalation of the two external double bonds of the 1,5-bisallene, subsequent 1,5-hydride shift via *β*-hydride elimination and a final reductive elimination (**Scheme 1.35a**).

Mukai *et al.*[85] observed analogous cycloisomerization products along with the tail-to-tail cycloadducts during their studies in rhodium(I)-catalyzed carbonylative [2+2+1] cycloaddition of 1,5-bisallenes (**Scheme 1.35b**). According to the authors, the selective reaction of the terminal double bonds was facilitated on 1,5-bisallenes bearing a phenylsulfonyl substituent in the internal double bond. More recently, Peng *et al.*[86] described a tandem copper-catalyzed cross-coupling/[2+2] cycloaddition of 1,6-allenynes with diazo compounds. In this process, 1,5-bisallenes were generated *in situ*. Then, a chemoselective tail-to-tail [2+2] cycloaddition takes place to furnish the fused 7/4 scaffolds (**Scheme 1.35c**). The reaction has a broad substrate scope, providing efficient access to fused 7/4 frameworks with various functionalities under mild reaction conditions.

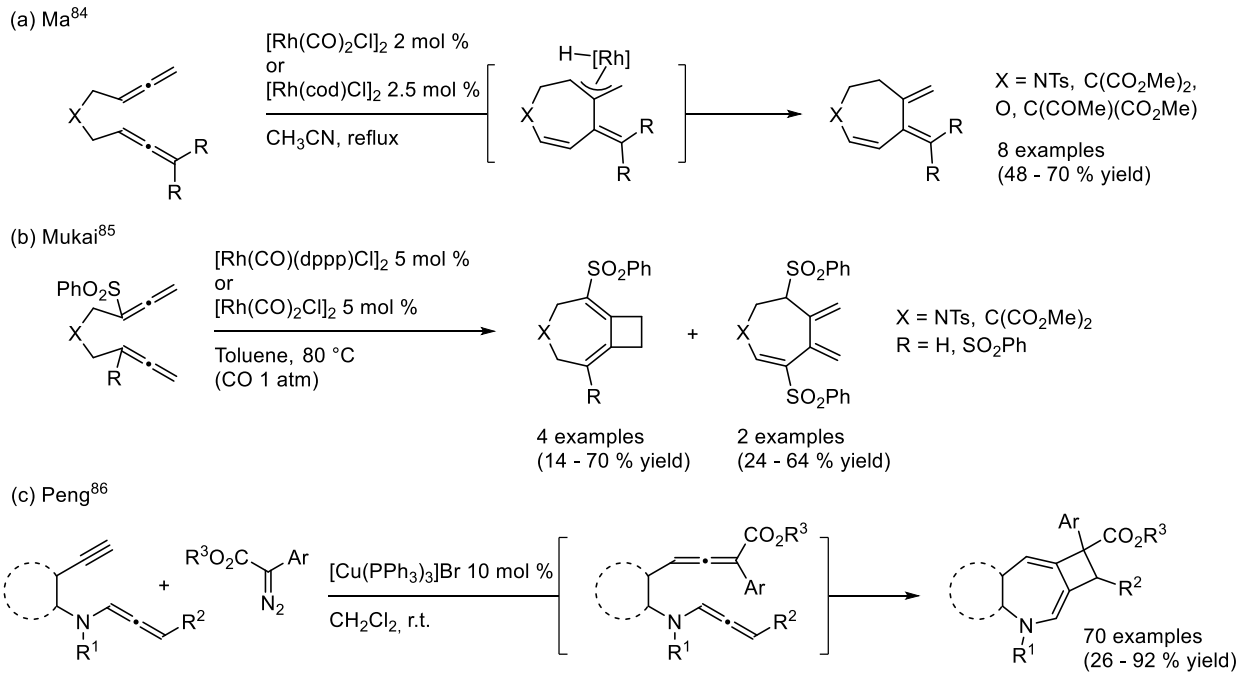

Scheme 1.35. Cycloisomerization reactions of 1,5-bisallenes involving a tail-to-tail metallacyclic intermediate using (a), (b) rhodium or (c) copper as a catalyst.

We can conclude that cycloisomerization products featuring 5-, 6- or 7-membered rings can be obtained when 1,5-bisallenes are treated under transition metals as palladium, nickel, gold, copper, or rhodium. Moreover, the choice of the metal is of vital importance, defining both, the mechanism and the chemoselectivity of the

transformation. Finally, the substitution pattern of the 1,5-bisallene is also crucial, as the presence or absence of substituents can inhibit a process or trigger alternative reaction pathways.

1.3.3. Cycloaddition reactions involving a third unsaturated motif

The examples in the literature of cycloaddition reactions of 1,5-bisallenes with a third unsaturated carbon – carbon/heteroatom bond are scarce and limited to the use of rhodium as catalyst. Most of the cycloisomerization reactions proceed through oxidative cyclometalation of the 1,5-bisallene generating a metallacycle intermediate. Under the appropriate conditions, the evolution towards the cycloisomerization can be avoided in favor of the insertion of the third unsaturated motif.

Ma *et al.*[87] were the first to show the great potential of 1,5-bisallenes in cycloaddition reactions. They found that 1,5-bisallenes without terminal substituents could undergo a dimerization process via rhodium-catalyzed partially intermolecular [2+2+2] cycloaddition to afford cross-conjugated dienes, which spontaneously undergo a Diels–Alder [4+2] cycloaddition with the remaining allene affording steroidal structures with complete chemo-, regio- and diastereoselectivity. The intramolecular oxidative cyclometalation of 1,5-bisallenes was postulated to involve either head-to-head or head-to-tail metallacyclic intermediate, in both ways the [2+2+2] cycloaddition furnishes a cross-conjugated exocyclic diene capable to undergo Diels-Alder [4+2] cycloaddition producing the steroid-like compounds (**Scheme 1.36**).

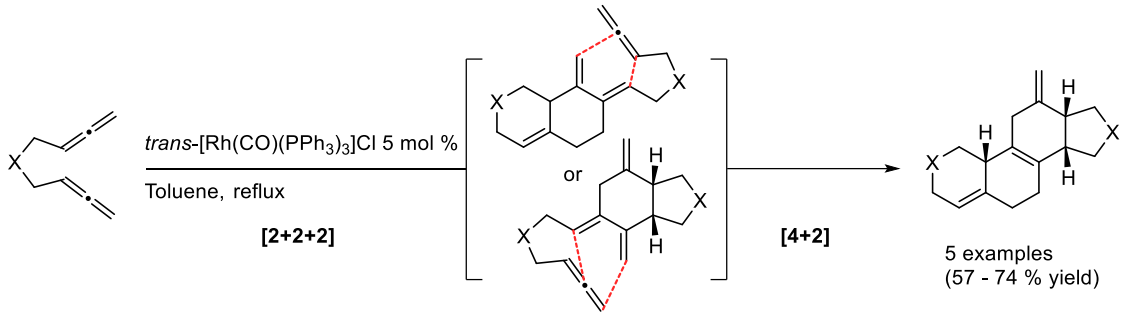

Scheme 1.36. Rhodium-catalyzed partially intermolecular [2+2+2] cycloaddition of 1,5-bisallenes to produce steroidal scaffolds in a complete chemo-, regio- and diastereoselectivity.

The same group[88] further studied this reactivity employing mixtures of two 1,5-bisallenes containing different tethers. Four possible products are possible: two homodimerization and two cross-cyclization products. Not surprisingly, this strategy furnished mixtures of the four possible products with slight preference for homocoupling products. Notably, only two products were obtained when the *O*-tethered 1,5-bisallene was used, which were the homocoupling of its partner and one of the cross-cyclization products. Probably, the large angle of the ether bond makes the oxidative cyclometalation between the two allene moieties more difficult. Interestingly, a tricyclic product was formed, along with the steroid derivative, when the *S*-tethered and the dimethyl malonate tethered 1,5-bisallenes were mixed. The process was postulated to occur via rhodium-catalyzed [2+2+2+2] cycloaddition, in which, instead of a reductive elimination after the so-called Schore

insertion, a second insertion of the remaining allene takes place, evolving then to the fused 6/8/7 tricyclic scaffold after reductive elimination.

Later on, as a follow-up approach to this rhodium-catalyzed [2+2+2] cycloaddition, Ma *et al.*[89] achieved the selective cyclization between 1,5-bisallenes and monoallenes using the same rhodium complex *trans*-$[Rh(CO)(PPh_3)_2]Cl$. The formation of the dimerization product could be avoided by slow addition of the 1,5-bisallene, achieving the [2+2+2] cycloadducts selectively (**Scheme 1.37**). Subsequent Diels–Alder reaction of the two exocyclic cross-conjugated dienes with diverse dienophiles allowed the construction of tri- or tetracyclic scaffolds. However, the yields of the whole process were moderate and only one tether was reported, often a critical point in these transformations. Overall, these tandem [2+2+2] cycloaddition/Diels–Alder reactions developed by Ma *et al.* provide an efficient and straightforward route to molecules having the tetracyclic ring systems of steroids from readily available materials.

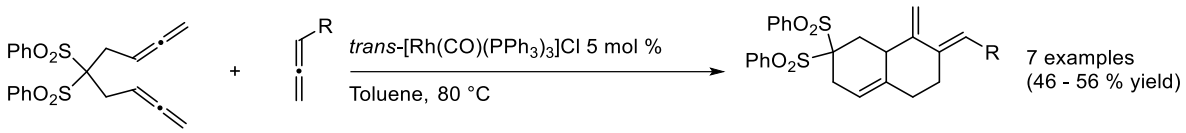

Scheme 1.37. Rhodium-catalyzed partially intermolecular [2+2+2] cycloaddition of 1,5-bisallenes and monoallenes.

Soon after, Chung *et al.*[90] established the first Pauson–Khand-type carbonylative [2+2+1] cycloaddition of 1,5-bisallenes using bimetallic Co_2Rh_2 nanoparticles as a catalyst. The process was found to be highly chemo- and regioselective, as only the distal double bonds of the bisallenes participate in the carbonylative cycloaddition. The postulated mechanism consists in a tail-to-tail oxidative cyclometalation, followed by the insertion of carbon monoxide. Subsequent reductive elimination and double bond isomerization furnishes cyclopentenones fused to 7-membered heterocycles (**Scheme 1.38a**). Similar products were obtained by Mukai *et al.*[85] in further investigations of the carbonylative [2+2+1] cycloaddition, which allowed the use of carbon-tethered 1,5-bisallenes (**Scheme 1.38b**). Treatment of 1,5-bisallenes with $[Rh(CO)(dppp)Cl]_2$ under CO atmosphere afforded the expected Pauson–Khand products, although the dimethyl malonate tethered 1,5-bisallene performed better using the rhodium complex $[Rh(CO)_2Cl]_2$. As an inconvenient, the tail-to-tail [2+2] cycloadduct (*vide supra*) was also produced along with the Pauson–Khand adducts.

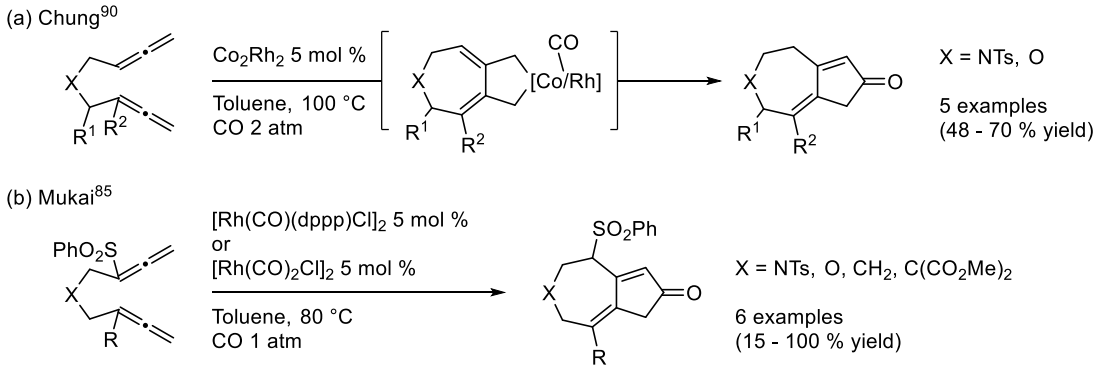

Scheme 1.38. Carbonylative [2+2+1] cycloaddition reactions of 1,5-bisallenes.

Chapter 2. General objectives

Earlier in this manuscript we have covered some aspects of the chemistry of allenes, from their structure and bond properties to their capacity to produce diversified products by finely tuning the whole system, as well as their inherent ability to behave as one, two or three carbon atoms in cyclization reactions. We have also revised in detail the versatility of allenes in the transition metal-catalyzed [2+2+2] cycloaddition reactions in their intermolecular, partially intermolecular, and intramolecular versions.

The chemistry of 1,5-bisallenes has also been examined, which present rich reactivity with transition metals affording 5-, 6- or 7-membered rings. In addition, the presence of double bonds in the cyclization products has shown the capacity to trigger cascade processes. However, cases reporting the involvement of a third unsaturation partner in a cycloaddition reaction are limited to those described by Ma,[87-89] Chung,[90] and Mukai.[85] Therefore, developing new methodologies involving 1,5-bisallenes and an unsaturated external partner in a cycloaddition reaction to efficiently prepare compounds of increased complexity, which are difficult to obtain by other means, is desirable. Besides this, further understand the electronic and steric factors that govern these processes, by computational studies for instance, may allow to increase the tools that we have to control them.

The objectives of the present thesis have been set taking into consideration the precedents that we have outlined above and the experience of our group in the field of the rhodium-catalyzed [2+2+2] cycloaddition reactions.

From a general perspective, we have envisaged developing novel cycloaddition reactions of 1,5-bisallenes involving external unsaturated partners other than allenes and carbon monoxide. Specifically, we have attempted to obtain unprecedented rhodium-catalyzed [2+2+2] cycloaddition reactions between 1,5-bisallenes and alkenes or alkynes with the aim of controlling the reaction outcome by carefully adapting the ligand for rhodium and the reaction conditions. Additionally, we have focused on rationalizing the mechanism of these transformations by performing further computational and experimental studies.

For greater clarity, the methodologies developed are divided into two main objectives. The first objective of this thesis consists in developing a partially intermolecular rhodium(I)-catalyzed [2+2+2] cycloaddition reaction of 1,5-bisallenes involving alkenes as the unsaturated partners.

Given that allenes are more reactive than alkenes in [2+2+2] cycloaddition reactions, we hypothesized that the oxidative cyclometalation may occur preferentially between two double bonds of the 1,5-bisallene, giving rise to one, two or three of the possible rhodacyclopentane intermediates. Subsequent insertion of the alkene and reductive elimination would afford the corresponding [2+2+2] cycloadduct (**Scheme 2.1**). Given the precedents, we aimed for the formation of fused 7-membered scaffolds, whose synthesis is not straightforward by other means. Chapters 3 and 4 deal with the experimental and theoretical study of these processes.

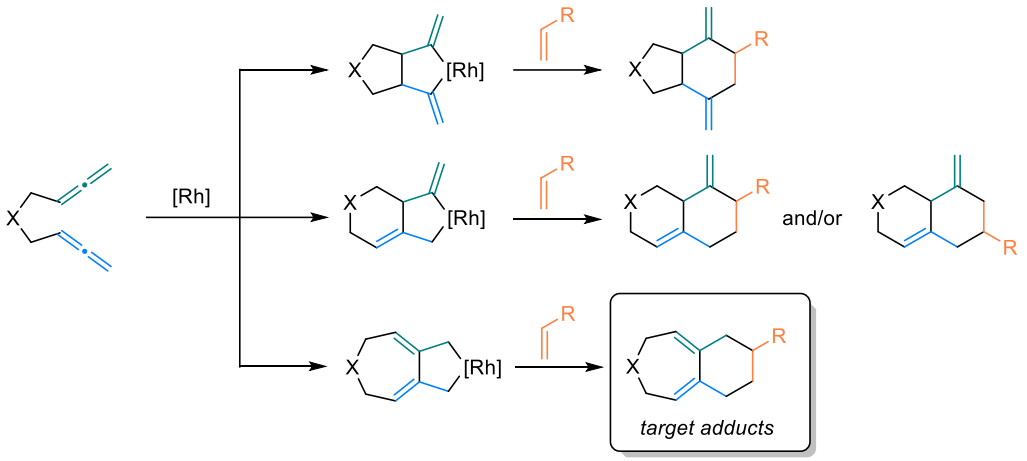

Scheme 2.1. Plausible adducts for the rhodium-catalyzed [2+2+2] cycloaddition of 1,5-bisallenes with alkenes.

Moving forward to the second objective, we aimed to develop a novel rhodium-catalyzed [2+2+2] cycloaddition reaction between 1,5-bisallenes with alkynes.

In contrast to alkenes, alkynes are more reactive than allenes in transition metal-catalyzed [2+2+2] cycloadditions. Therefore, we hypothesized that under the right conditions, the initial oxidative cyclometalation would involve one alkyne molecule and one double bond of the 1,5-bisallene. Two pathways are then possible (Scheme **2.2**): (a) the insertion of a second alkyne molecule, resulting in the formation of a [2+2+2] cycloadduct linked to an allene, which may be able to undergo a cascade process given that allenenes have shown reactivity in cyclization reactions under transition metal-catalysis (Chapter 5); or (b) the insertion of the second allene moiety and reductive elimination to generate the corresponding [2+2+2] cycloadduct (Chapter 6). Experimental and theoretical studies on these processes are outlined in Chapters 5 and 6.

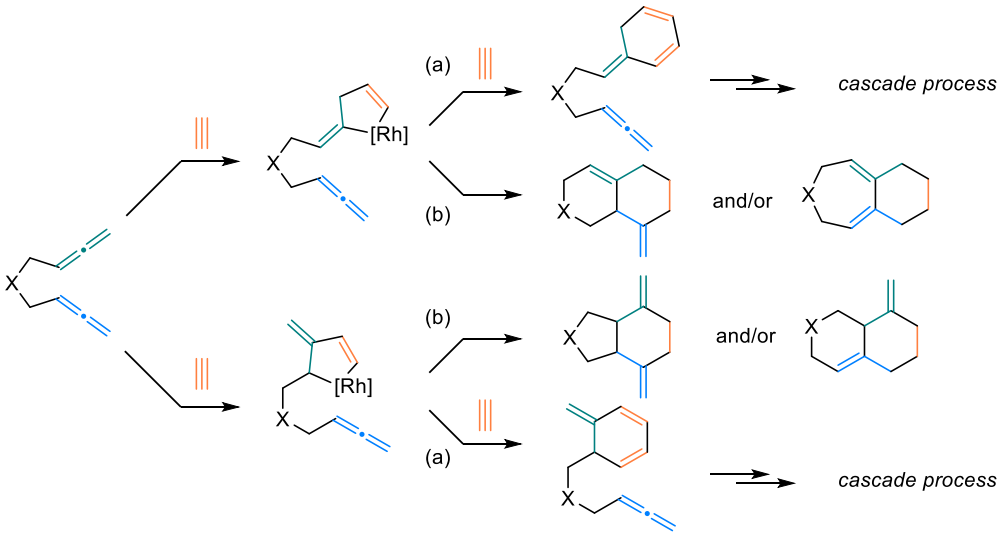

Scheme 2.2. Plausible reaction pathways for the rhodium-catalyzed [2+2+2] cycloaddition of 1,5-bisallenes with alkynes.

Chapter 3. A Rh-Catalyzed Cycloisomerization/Diels–Alder Cascade Reaction of 1,5-Bisallenes for the Synthesis of Polycyclic Heterocycles

---

Published in: *Org. Lett.* **2019**, *21*, 6608.

Authors: Artigas, A.; Vila, J.; Lledó, A.; Solà, M.; Pla-Quintana, A.; Roglans, A.

A novel methodology to transform bisallenes into a variety of polycyclic derivatives employing rhodium(I) catalysis has been developed. This transformation encompasses an intramolecular Rh-catalyzed cycloisomerization of bisallenes 1 to deliver a reactive cycloheptadiene, which concomitantly undergoes a regioselective [4 + 2] cycloaddition with alkenes. A complete mechanistic study of this transformation has been undertaken including DFT calculations. Overall, the methodology presented here constitutes a new and straightforward entry to polycyclic dihydroazepine and dihydrooxepine derivatives employing catalytic methods.

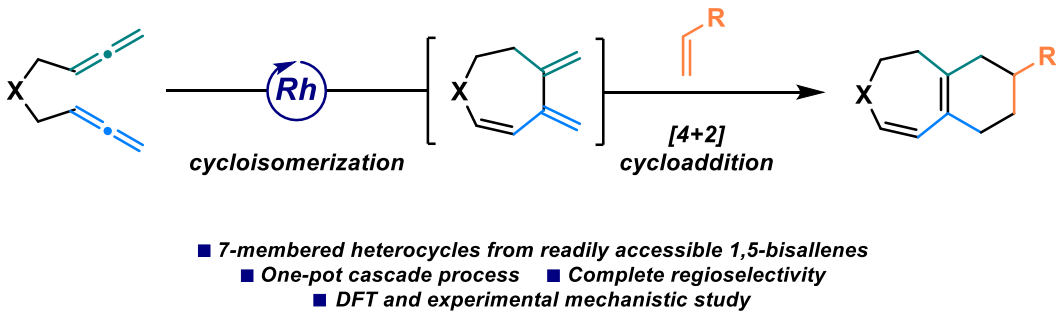

.

During the last years, our research group has focused on the use of allenes in the intramolecular rhodium-catalyzed [2+2+2] cycloaddition reactions (see chapter 1, section 2 and references cited therein). However, more recently we have been more interested in developing a partially intermolecular version of the reaction. We anticipated that 1,5-bisallenes may be good candidates for two main reasons. Firstly, they have shown great versatility with transition metals leading to 5-, 6- or 7-membered rings. Secondly, examples of cycloaddition reactions of 1,5-bisallenes with an external unsaturated partner are scarce. Given these precedents, we envisaged developing a [2+2+2] cycloaddition reaction of 1,5-bisallenes and alkenes, aiming for the control of the reaction towards the synthesis of fused 7/6-membered bicyclic systems. Azepine- and oxepine-containing scaffolds are found in some pharmacologically active and natural products,[91] and their synthesis remains highly challenging.[92]

Our initial hypothesis was that the rhodium would promote an oxidative coupling of the 1,5-bisallene to produce one, two or three of the rhodacyclopentane intermediates represented in **Scheme 3.1**. Subsequent coordination and insertion of the alkene and reductive elimination would produce one, or more, of the possible products.

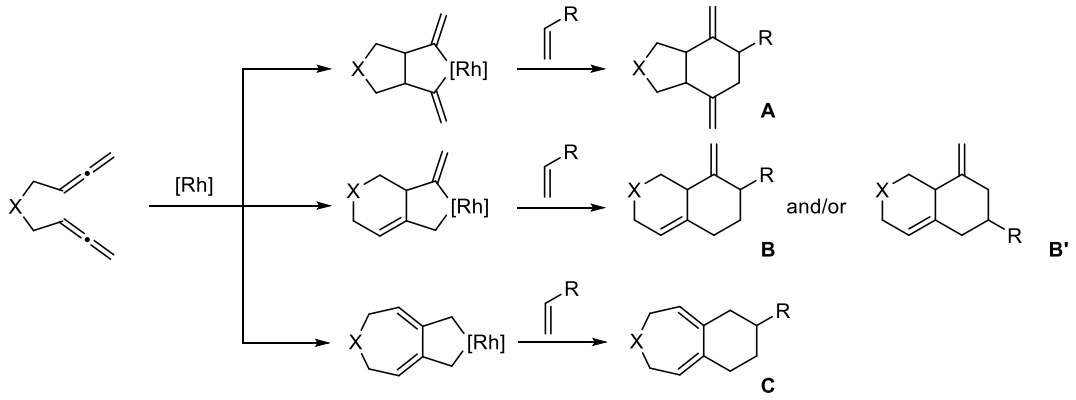

Scheme 3.1. Possible pathways for the [2+2+2] cycloaddition reaction of 1,5-bisallenes with an alkene.

Results and discussion

As the use of chiral bisphosphine ligands in conjunction with rhodium complexes is of common use for [2+2+2] cycloaddition reactions involving allenes,[50,52,56,64] we started studying the cycloaddition of the *N*-tosyl-tethered 1,5-bisallene **1a** and ethyl acrylate **2a** in the presence of a 10 mol % 1:1 mixture of the cationic rhodium(I) complex $[Rh(cod)_2]BF_4$ and (*R*)-BINAP in toluene/CH_2Cl_2 (4:1) at 65 °C. The 4:1 ratio resulted from the catalyst transfer with CH_2Cl_2 into the solution of **1a** and **2a** in toluene.

Remarkably, we found that under these conditions two different compounds were obtained, compound **3aa** in 29 % yield, and compound **4a** in 30 % yield (**Scheme 3.2**).

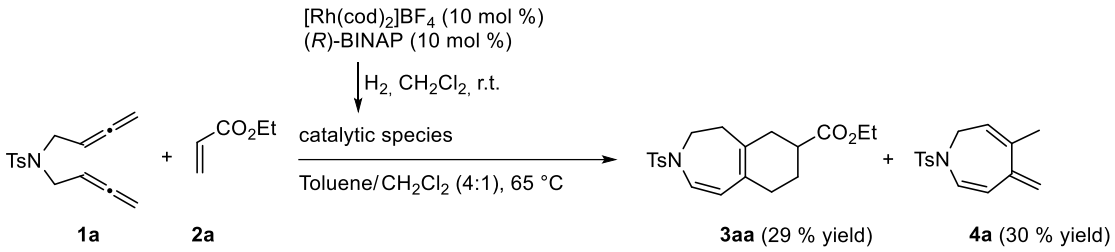

Scheme 3.2. Preliminary results of the rhodium-catalyzed cycloaddition reaction of 1,5-bisallene **1a** with ethyl acrylate **2a**.

Molecular formula of **3aa** was determined by HRMS, confirming an adduct that incorporates the 1,5-bisallene **1a** and the ethyl acrylate **2a**. Complete NMR analysis allowed us to determine the structure of the product, confirming that a single fused 7/6-membered scaffold had been forged. First, the edited HSQC was analyzed to determine the number of primary, secondary, tertiary, and quaternary carbon atoms and their hybridization. Among the possible cycloadducts represented in **Scheme 3.1**, the presence of five secondary Csp^3 (excluding the signals from the ethyl ester moiety coming from **2a** and the tosyl group) and two Csp^2–H is only compatible with the fused 7/6-membered ring system **C**. However, the exhaustive analysis of the ^{1}H-NMR chemical shifts and multiplicities, along with the COSY experiment, allowed for the determination of a slightly different product. The presence of two coupled doublets at δ = 4.86 and 6.66 ppm (**H8** and **H9**, $^3J_{cis}$ = 10.3 Hz), characteristic of a *cis*-endocyclic double bond, did not match with compound **C (Scheme 3.1**) but with an isomerized structure. The chemical shift of **H9** (δ = 6.66 ppm) indicates that the double bond is in the α-position of the nitrogen atom. Additionally, the absence of more signals in the vinylic zone, along with the presence of two Csp^2 atoms that have no hydrogen atoms attached, indicates that the second double bond is located in the fused ring junction (**C7** and **C12**), thus supporting that **3aa** is not exactly the hypothesized [2+2+2] cycloadduct (structure **C** in **Scheme 3.1**), but a closely related isomer. With this double bond distribution, two regioisomers are possible although only one is generated in the process, which means that the reaction is completely regioselective.

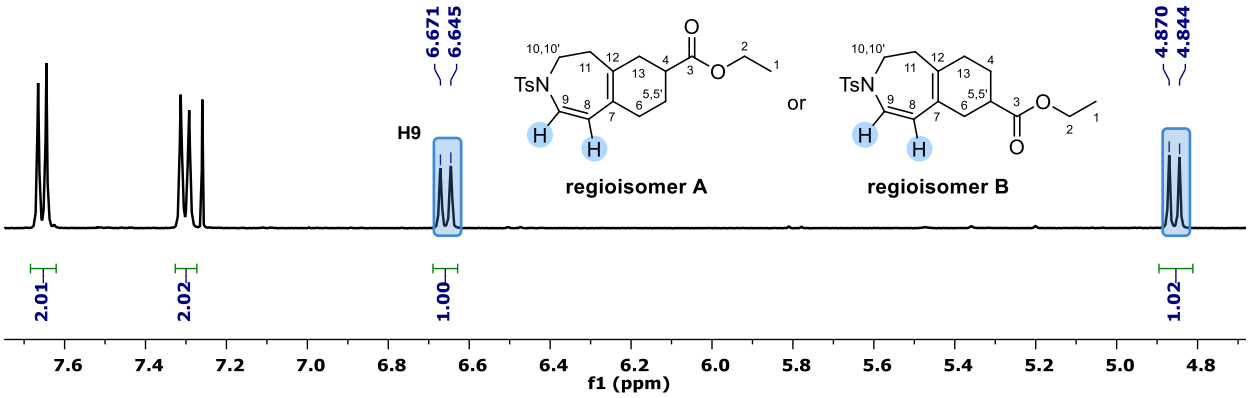

Figure 3.1. ^{1}H-NMR chemical shifts of the *cis*-endocyclic double bond.

To differentiate between the regioisomers **A** and **B**, a selective NOESY experiment was performed. NOE contacts **H6** ↔ **H8** (**H6** and **H5/5'** identified as the two contiguous methylenic groups by COSY), led us to assign regioisomer **A** as the single cycloadduct formed (**Figure 3.2**).

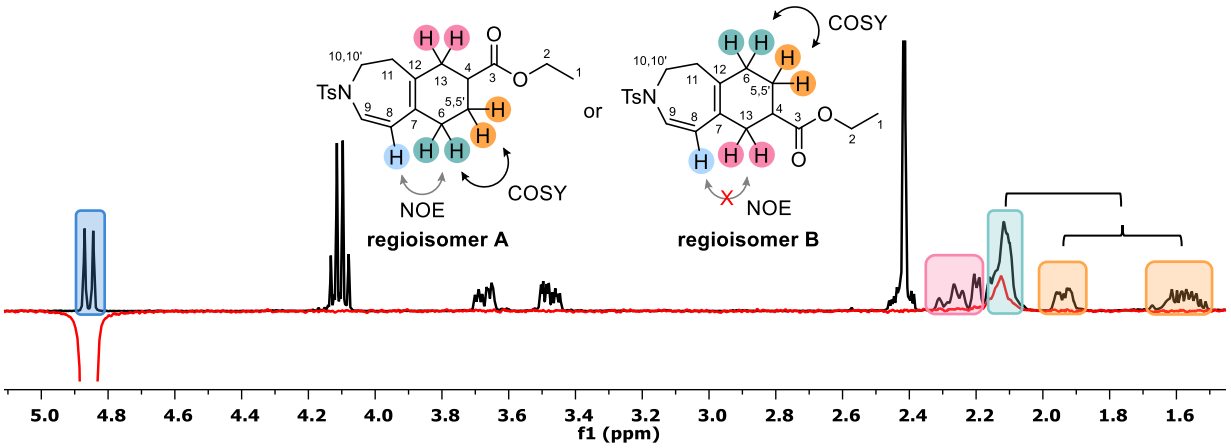

Figure 3.2. Selective NOESY experiment revealing the single regioisomer A of **3aa**.

Additionally, the HMBC three-bond correlation between **C6** and **H8** also supports the formation of the regioisomer **A** (**Figure 3.3**).

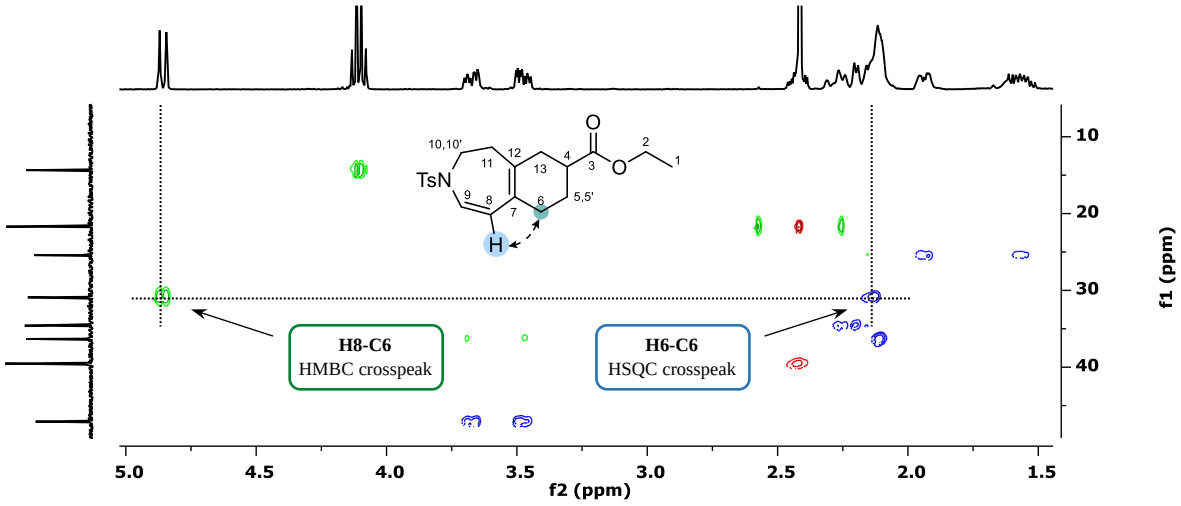

Figure 3.3. HSQC (blue for CH_2, and red for CH and CH_3) and HMBC (green) overlapped spectra showing the correlation between H8 and C6

All the key signals, COSY and HMBC crosspeaks, and NOE contacts are summarized in **Figure 3.4**.

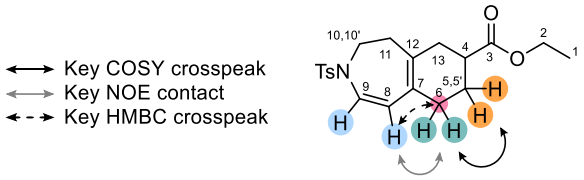

Figure 3.4. Selected signals, COSY and HMBC crosspeak, and NOE contacts confirming the structure of **3aa**.

Compound **3aa** is an isomer of one of the postulated [2+2+2] cycloadducts (structure **C** in **Scheme 3.1**), that might be formed through a latter isomerization of **C** to give **3aa**, or the reaction may proceed through a pathway other than the [2+2+2] cycloaddition.

Taking into account that **3aa** was generated alongside a novel 7-membered cross-conjugated triene **4a** presumably formed by cycloisomerization of the starting 1,5-bisallene **1a** without participation of the alkene,

and that the double bond in the *α*-position to the nitrogen atom is equivalent to the 7-membered cycloisomerization products already reported by the groups of Ma[84] and Mukai,[85] an additional pathway for the reaction was postulated, consisting in a rhodium-catalyzed cycloisomerization of the 1,5-bisallenes **1** to produce 7-membered trienes with two exocyclic double bonds. Then, in the presence of a dienophile, a tandem regioselective [4+2] cycloaddition would generate the experimentally observed product **3** (**Scheme 3.3**).

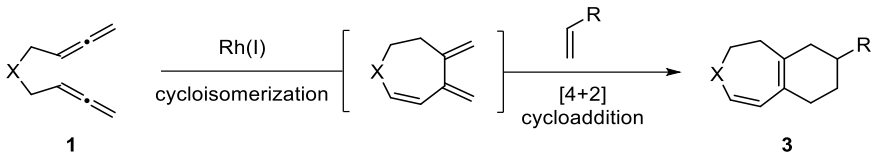

Scheme 3.3. Additional hypothesized pathway for the transformation of 1,5-bisallenes **1** into derivatives **3**.

With these promising results in hand, we proceeded to optimize the reaction conditions. Different solvent mixtures (*Solvent* / CH_2Cl_2 in 4:1 ratio) were initially tested with a 1:10 ratio of **1a**:**2a** (entries **1**-**6** in **Table 3.1**). In all the cases except when 1,2-dicloroethane (DCE) was used (entry **2**), the formation of **3aa** and **4a** in varying quantities was observed. The best result was obtained with THF/CH_2Cl_2 4:1, which improved the selectivity of **3aa** and its yield to 46 % (entry **6**). We next examined the effect of two parameters: the excess of ethyl acrylate, rising it to 50 equivalents (entry **7**), and the concentration of **1a**, reducing it to 9 mM (entry **8**). Not much of an improvement was detected in either case, albeit slightly better yield of **3aa** was obtained when both parameters were combined (entry **9**). We then assessed the use of different bisphosphine ligands (shown in **Figure 3.5**) as ligands for the cationic rhodium complex $[Rh(cod)_2]BF_4$: (*R*)-Tol-BINAP (entry **10**), (*R*)-H_8-BINAP (entry **11**), (*R*)-Monophos (entry **12**), BIPHEP (entry **13**) and (*R*)-DTBM-Segphos (entry **14**).

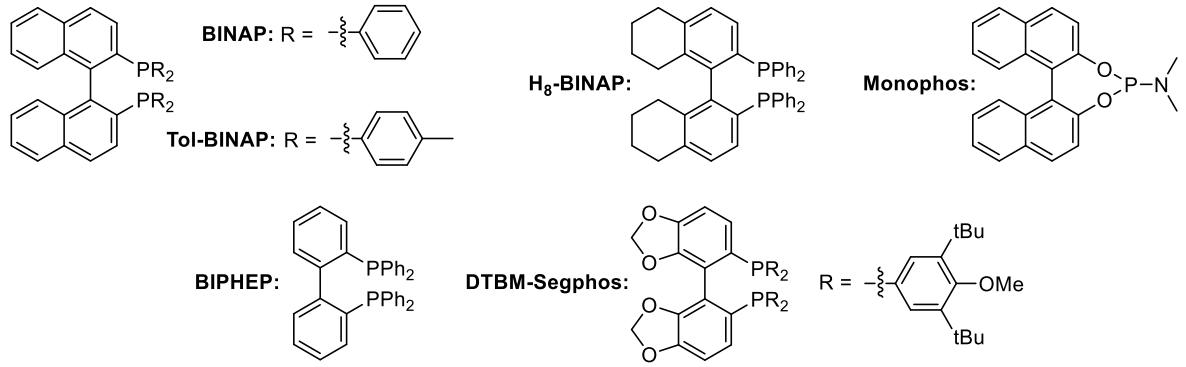

Figure 3.5. Phosphine ligands used for the optimization of the rhodiun(I)-catalyzed cycloaddition of 1,5-bisallene **1a** with alkene **2a.**

When BIPHEP was used as a ligand only cycloisomerization product **4a** was formed in a 37 % yield. Using the other ligands both **3aa** and **4a** were formed in variable ratios. Best results were obtained with the bulky electron-enriched phosphine (*R*)-DTBM-Segphos, which increased the yield of **3aa** to 65 % and reduced the yield of **4a** to 5 %. However, the [2+2] cycloisomerization byproduct **5a** was generated in 15 % yield. Fortunately, lowering the temperature to 40 °C avoided the formation of **4a**, resulting in our set of optimized conditions (entry **15**). An attempt to reduce the catalyst loading to 5 % resulted in lower yield of **3aa** (entry **16**). Furthermore, two control experiments were performed: one in the absence of the phosphine (*R*)-DTBM-

Segphos (entry **17**), and the other one without the catalytic mixture. Starting 1,5-bisallene **1a** was recovered in both cases, unveiling the essential role of the rhodium complex $[Rh(cod)_2]BF_4$ and the phosphine (*R*)-DTBM-Segphos.

Table 3.1. Optimization of the rhodiun(I)-catalyzed cycloaddition of 1,5-bisallene **1a** with alkene **2a**[a]

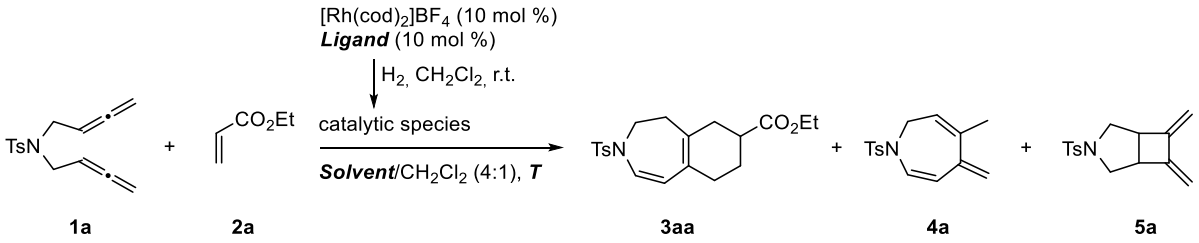

Entry	Ligand	Solvent	[**1a**] (mM)	T (ºC)	Ratio **1a**:**2a**	Yield of **3aa** / **4a** / **5a** (%)
1	(*R*)-BINAP	Toluene	18	65	1:10	30 / 29 / -
2	(*R*)-BINAP	DCE	18	65	1:10	- / - / -
3	(*R*)-BINAP	Acetonitrile	18	65	1:10	29 / 18 / -
4	(*R*)-BINAP	1,4-Dioxane	18	65	1:10	42 / 53 / -
5	(*R*)-BINAP	EtOH	18	65	1:10	18 / 24 / -
6	(*R*)-BINAP	THF	18	65	1:10	46 / 39 / -
7	(*R*)-BINAP	THF	18	65	1:50	45 / 45 / -
8	(*R*)-BINAP	THF	9	65	1:10	46 / 52 / -
9	(*R*)-BINAP	THF	9	65	1:50	49 / 45 / -
10	(*R*)-Tol-BINAP	THF	9	65	1:50	54 / 44 / -
11	(*R*)-H_8-BINAP	THF	9	65	1:50	54 / 38 / -
12	(*R*)-Monophos	THF	9	65	1:50	26 / 18 / -
13	BIPHEP	THF	9	65	1:50	- / 37 / -
14	(*R*)-DTBM-Segphos	THF	9	65	1:50	65 / 5 / 15
15	**(*R*)-DTBM-Segphos**	**THF**	**9**	**40**	**1:50**	**60 / - / 15**
16[b]	(*R*)-DTBM-Segphos	THF	9	40	1:50	44 / - / 15
17	-	THF	9	40	1:50	- / - / -
18[c]	-	THF	9	40	1:50	- / - / -

[a] Reaction conditions: 0.09 mmol of **1a,** 10-50 equivalents of **2a**, 10 mol % of Rh catalyst in 10-20 mL of *Solvent*/CH_2Cl_2 (4:1) at 65 °C for 4 h or 40 °C for 16 h. The 10% mol mixture of $[Rh(cod)_2]BF_4$ and phosphine was treated with hydrogen in dichloromethane (CH_2Cl_2) solution for catalyst activation prior to substrate addition. [b] The reaction was performed with 5% mol of $[Rh(cod)_2]BF_4$ and 5% mol of ligand. [c] The reaction was performed without $[Rh(cod)_2]BF_4$.

With the optimized reaction conditions in hand, we then evaluated the scope of the reaction (**Figure 3.6**).

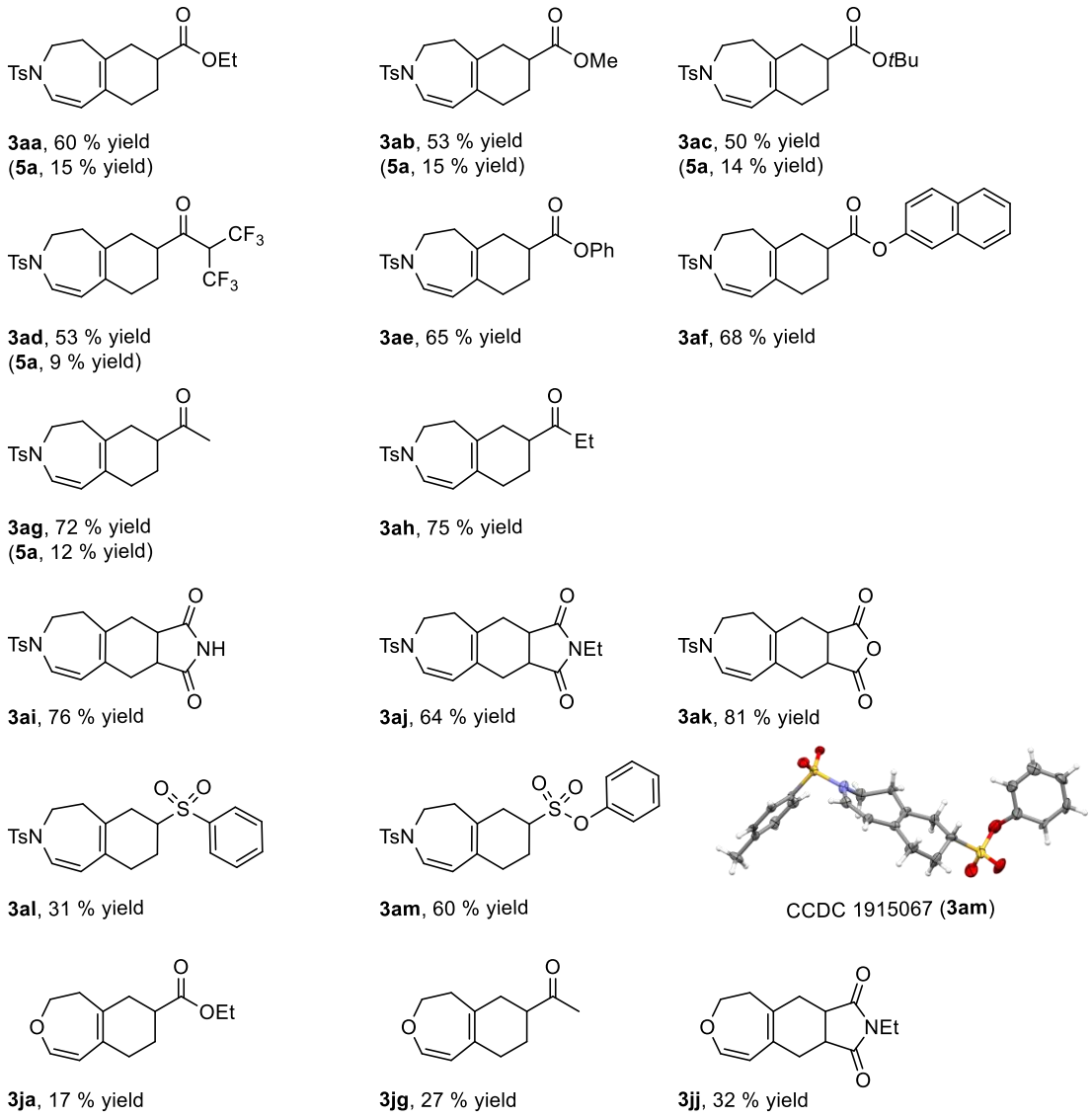

Figure 3.6. Scope of the cycloaddition of 1,5-bisallenes **1** and alkenes **2**.

Overall, the reaction performed in good to moderate yields with a wide range of alkenes. The use of alkyl and aryl acrylates delivered the desired products (**3aa** – **3af**) in yields ranging from 50 % to 68 %. Vinyl alkyl ketones also afforded the cycloadducts **3ag** and **3ah** in 72 % and 75 % yields, respectively. In some cases, the byproduct **5a** was also isolated, its formation or absence is unpredictable (especially when comparing **3ag** and **3ah**) and may account to a delicate balance of reaction rates during the multistep processes leading to products **3** and **5**. Disubstituted cyclic alkenes performed well to give the corresponding cycloadducts **3ai**, **3aj** and **3ak** in good to excellent yields, avoiding the formation of **5a**. The use of the phenyl vinyl sulfone and phenyl vinyl sulfonate produced derivatives **3al** and **3am** in 31 % and 60 % yields respectively, again, without the formation of **5a**. Single crystal diffraction of cycloadduct **3am** (CCDC 1915067) allowed us to unambiguously confirm the structure of the cycloadducts **3**.

To expand the methodology to other 1,5-bisallenes, the *O*-tethered 1,5-bisallene **1j** was prepared and the reaction with ethyl acrylate **2a**, methyl vinyl ketone **2g**, and *N*-ethylmaleimide **2j** afforded the corresponding **3ja**, **3jg** and **3jj** in low to moderate yields.

Since a stereogenic center was generated in derivatives **3**, the enantiomeric excess was measured in all cases, but no enantioinduction was observed regardless of the substrate or the ligand used. This result, along with the fact that the reaction performed better with good dienophiles, is consistent with the mechanism proposed for this transformation (*vide infra*).

To gain further understanding of the reaction mechanism, Dr. Albert Artigas (supervised by Prof. Miquel Solà) completed our study by evaluating computationally the process that transforms the 1,5-bisallene **1a** into cycloadduct **3aa**. The Gibbs energy profile computed at 313.15 K and 1 atm in a 76:24 molar mixture of THF/CH_2Cl_2 (equivalent to 4:1 v/v) at the M06L-D3/cc-pVTZ-PP // B3LYP-D3/cc-pVDZ-PP level of theory, is depicted in **Figure 3.7**. To reduce the computational costs, BINAP was chosen as the model ligand instead of the optimal phosphine (*R*)-DTBM-Segphos (see Chapter 8, section **8.1.3** for a complete description of the computational methods).

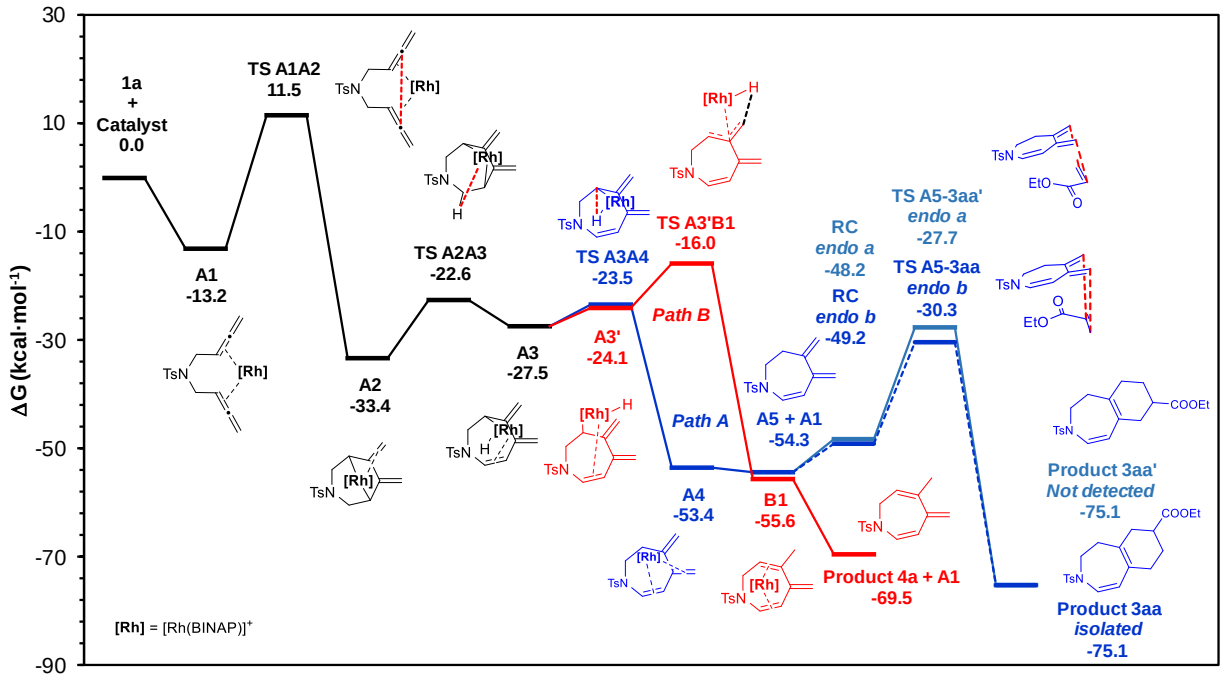

Figure 3.7. Gibbs energy profile for the tandem cycloisomerization/Diels–Alder cycloaddition leading to product **3aa**, computed at the M06L-D3/cc-pVTZ-PP/SMD(76 % THF, 24 % CH_2Cl_2) // B3LYP-D3/cc-pVDZ-PP level of theory. Reprinted with permission from Artigas, A.; Vila, J; Lledó, A.; Solà, M.; Pla-Quintana, A.; Roglans, A. *Org. Lett.* **2019**, *21*, 6608. Copyright © 2019, American Chemical Society.

The process starts with the coordination of the two internal double bonds of the 1,5-bisallene **1a** to the $[Rh(BINAP)]^+$ complex generating **A1**, a square-planar 16 e^- intermediate. This coordination is exergonic by 13.2 kcal/mol. Oxidative cyclometalation then takes place generating the C–C bond in the central allenic positions to deliver intermediate **A2**. This first step has a Gibbs energy barrier of 24,7 kcal/mol surpassing **TS**

A1A2 and is exergonic by 20.2 kcal/mol. Intermediate **A2** is a π-allyl 18 e$^-$ complex (d_{Rh-C} = 2.274, 2.196, 2.132 Å) and displays a distorted octahedral geometry in which one of the oxygen atoms of the tosyl group coordinates the rhodium atom (d_{Rh-O} = 2.231 Å). From this point, a β-hydride elimination transforms **A2** into intermediate **A3**. This process has a Gibbs energy barrier of 10.8 kcal/mol (**TS A2A3**) and is endergonic by 5.9 kcal/mol. **A4** is formed after reductive elimination, surpassing a low energy barrier of 4.0 kcal/mol (**TS A3A4**) and releasing 25.9 kcal/mol. Subsequent release of the rhodium complex leads to triene **A5**, completing the catalytic cycle (Path A in **Figures 3.7** and **3.8**). Our initial proposal for the formation of **A5** was based in a tail-to-tail oxidative cyclometalation of the 1,5-bisallene, as postulated by Ma[84] and Mukai.[85] However, this computational study revealed an unprecedented mechanism for this transformation. Alternatively, intermediate **A3** can experience a rearrangement to give **A3'**, in which the hydride is approached to one of the exocyclic double bonds at cost of 3.4 kcal/mol (Path B in **Figures 3.6** and **3.7**). Reductive elimination through **TS A3'B1** ($\Delta G^{\ddagger}$ = 8.1 kcal/mol) generates intermediate **B1** in a process that is exergonic by 31.5 kcal/mol. This alternative pathway provides rational explanation for the formation of **4a**.

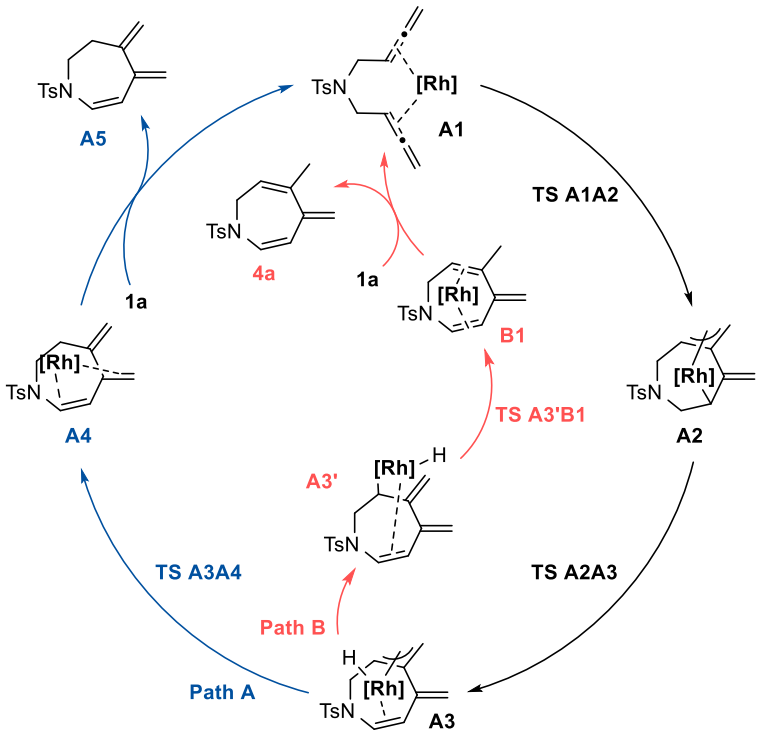

Figure 3.8. Catalytic cycle for the rhodium-catalyzed cycloisomerization of 1,5-bisallene **1a** leading to intermediate **A5**. Edited with permission from Artigas, A.; Vila, J; Lledó, A.; Solà, M.; Pla-Quintana, A.; Roglans, A. *Org. Lett.* **2019**, *21*, 6608. Copyright © 2019, American Chemical Society.

The formation of intermediate **A5** is followed by a [4+2] cycloaddition with ethyl acrylate **2a** to produce the cycloadduct **3aa** (Path A in **Figure 3.7**). The regioselectivity of this step can be also rationalized by our computed reaction mechanism. Whereas the "*endo a*" approximation of the dienophile (**TS A5–3aa'**) has a Gibbs energy barrier of 26.6 kcal/mol, the "*endo b*" approximation (**TS A5–3aa**) has a lower cost of 24.0 kcal/mol. Such difference in energy of -2.6 kcal/mol accounts for the selective formation of the product **3aa**.

As intermediates **A2**, **A3**, and **A4** are also susceptible to undergo a [4+2] cycloaddition with ethyl acrylate **2a**, all the potential reaction pathways leading to **3aa** were also computed (**Figure 3.9**). However, all the alternative paths were found to have higher energy barriers.

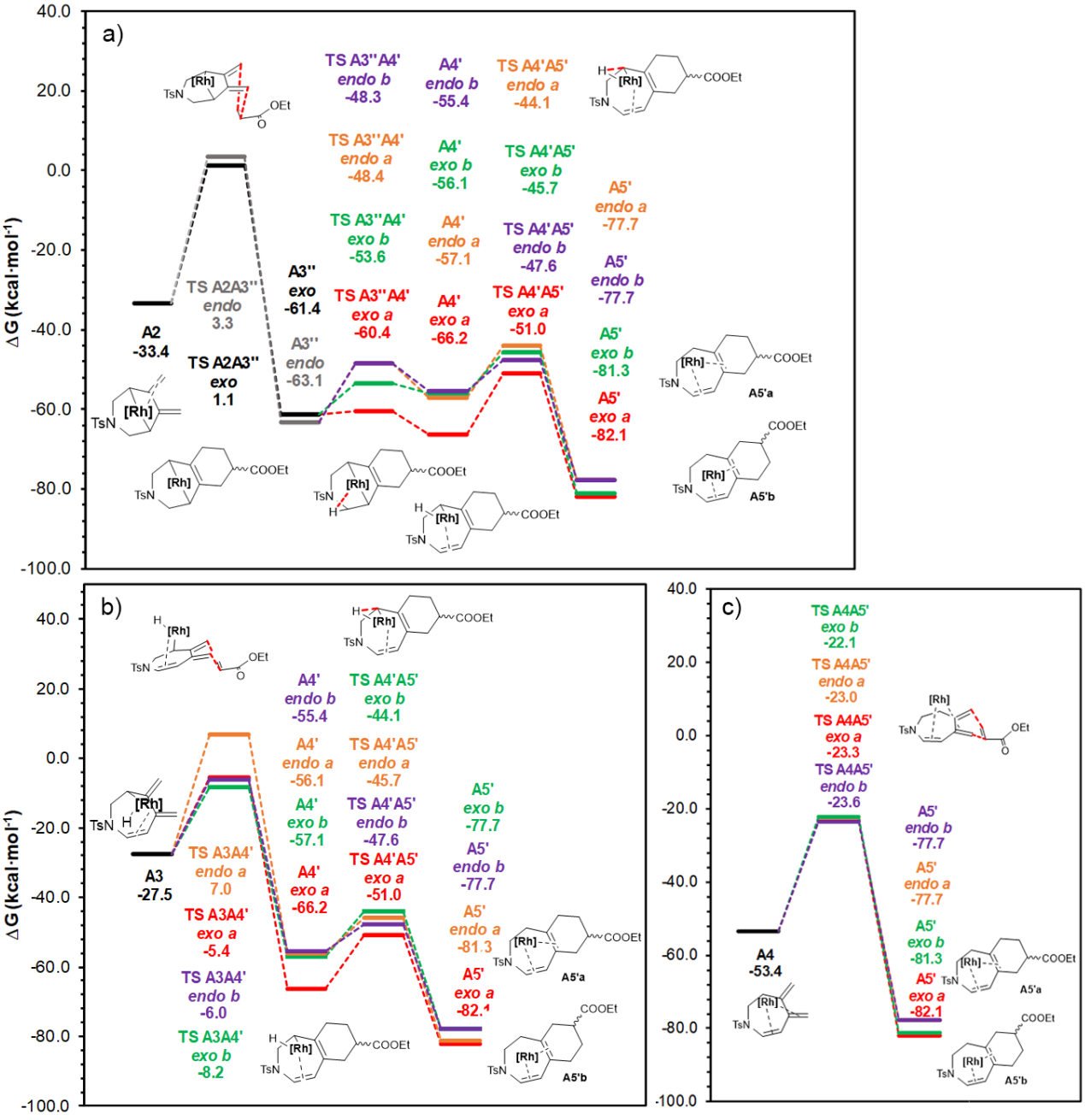

Figure 3.9. Alternative reaction paths involving a [4+2] cycloaddition from intermediates a) **A2**, b) **A3**, and c) **A4**. Gibbs energy profiles computed at the M06L-D3/cc-pVTZ-PP/SMD(76 % THF, 24 % CH_2Cl_2) // B3LYP-D3/cc-pVDZ-PP level of theory. [Rh] = $[Rh(BINAP)]^+$. Modified with permission from Artigas, A.; Vila, J; Lledó, A.; Solà, M.; Pla-Quintana, A.; Roglans, A. *Org. Lett.* **2019**, *21*, 6608. Copyright © 2019, American Chemical Society.

In summary, the reaction mechanisms leading to **A5** and **4a** have an energetic gap between the turnover frequency (TOF) determining intermediate (TDI, **A1**), and TOF determining transition state (TDTS, **TS A1A2**) of 24.7 kcal/mol.[93] Once formed, intermediate **A5** reacts with ethyl acrylate **2a** in a regioselective catalyst-free

Diels–Alder cycloaddition to provide **3aa**. Overall, the transformation of 1,5-bisallene **1a** and ethyl acrylate **2a** into the reaction product **3aa** has a total reaction energy (ΔG_r) of -71.1 kcal/mol.

To fully validate the proposed mechanism, additional experiments were performed. Firstly, we evaluated the role of the byproduct **5a** as a possible reaction intermediate by submitting it under the reaction conditions, in the presence and the absence of the catalytic mixture. In both cases, only starting materials were recovered (**Scheme 3.4**).

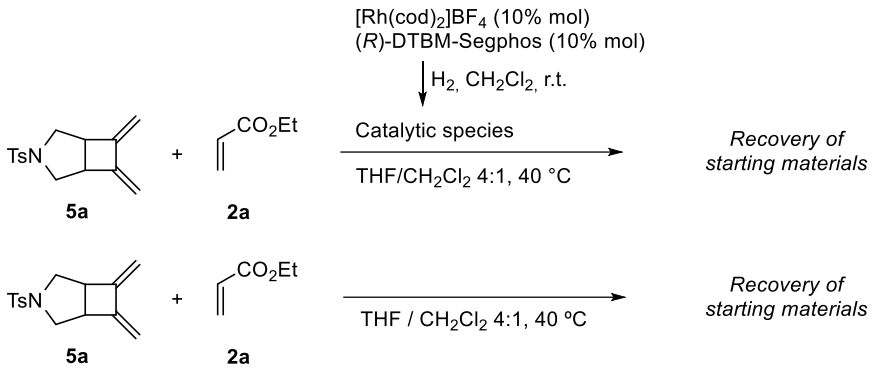

Scheme 3.4. Evaluation of the role of byproduct **5a** as a possible reaction intermediate.

Computational calculations also ruled out the involvement of byproduct **5a** as a reaction intermediate (**Figure 3.10**). The computed rhodium-catalyzed isomerization of **C1** into **A2** has a Gibbs energy barrier of 52.1 kcal/mol (**TS C1A2**), which is not experimentally feasible under the reaction conditions. Additionally, the reverse process (reductive elimination of **A2** to give **C1**) is not energetically possible either (**TS A2C1**, $\Delta G^{\ddagger}$ = 45.3 kcal/mol). This result suggests that the byproduct **5a** must be formed by an alternative pathway, probably involving a head-to-head oxidative cyclometalation of the 1,5-bisallene **1a**.[81,82]

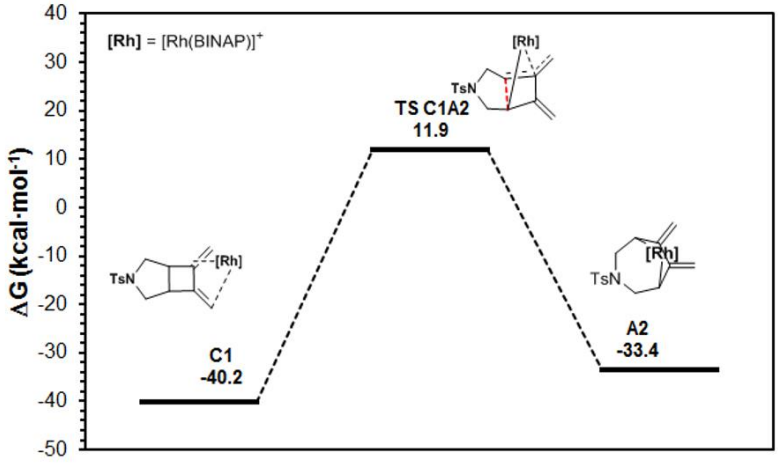

Figure 3.10. Computational evaluation of **5a** as a possible reaction intermediate. Gibbs energy profile for the transformation of **C1** into **A2**, computed at the M06L-D3/cc-pVTZ-PP/SMD(76 % THF, 24 % CH2Cl2) // B3LYP-D3/cc-pVDZ-PP level of theory. Modified with permission from Artigas, A.; Vila, J; Lledó, A.; Solà, M.; Pla-Quintana, A.; Roglans, A. *Org. Lett.* **2019**, *21*, 6608. Copyright © 2019, American Chemical Society.

Finally, as an attempt to isolate the intermediate **A5**, we performed the reaction in the absence of a dienophile (**Scheme 3.5**). Despite we could not isolate **A5** as a reaction product, we found evidence of its formation since the Diels–Alder homodimerization adduct **6a** was isolated in 58 % yield, implying that **A5** acted as the diene and the dienophile. Remarkably, only one dimer was obtained out of the six possible isomers.

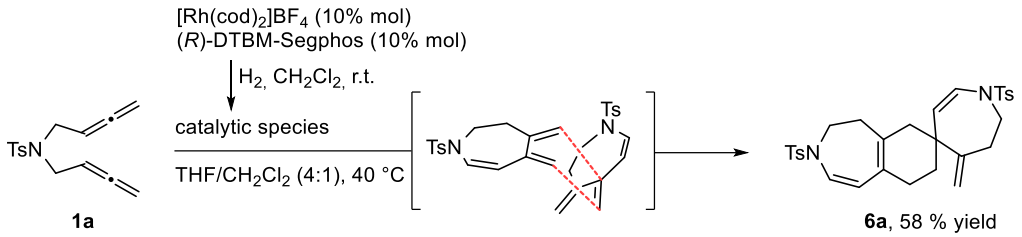

Scheme 3.5. Experimental evidence of the formation of intermediate **A5**, leading to the selective production of homodimerization spirocyclic compounds.

This result not only confirms the formation of **A5** during the reaction, but also provides a straightforward approach to generate spirocyclic compounds in a complete regioselective manner from 1,5-bisallenes. Such process has been investigated and is presented in the upcoming chapter of this manuscript.

The methodology developed in this chapter, has been further applied to the functionalization of C_{60} and C_{70} fullerenes by our group[94] to provide versatile and step-economical approach to the synthesis of fused 6/7-membered polyheterocyclic fullerene adducts (**Scheme 3.6**).

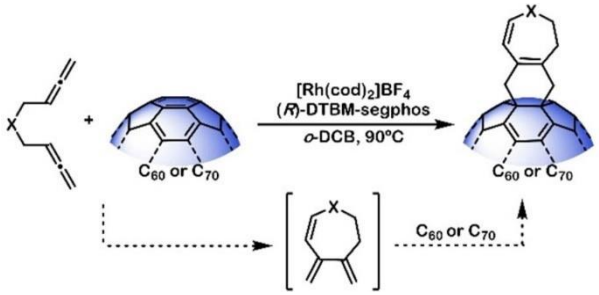

Scheme 3.6. Graphical abstract of developed methodology applied to the functionalization of fullerenes. Reprinted with permission from Artigas, A.; Castanyer, C.; Roig, N.; Lledó, A.; Solà, M.; Pla-Quintana, A.; Roglans, A. Synthesis of Fused Dihydroazepine Derivatives of Fullerenes by a Rh-Catalyzed Cascade Process. *Adv. Synth. Catal.* **2021**, *363*, 383. Copyright 2017 2017 Wiley-VCH Verlag GmbH & Co. KGaA, Weinheim.

Developing an enantioselective version

As mentioned before, a stereogenic center is generated during this cascade rhodium(I)-catalyzed cycloisomerization/Diels–Alder reaction of 1,5-bisallenes and alkenes. However, the use of chiral bisphosphine ligands does not generate enantioinduction in the product since the stereogenic carbon atom is formed in the Diels–Alder reaction. With the aim to develop a stereoselective version of this methodology and given that the chiral rhodium(I) complex participates in the cycloisomerization and not in the Diels–Alder reaction, it is straightforward to consider that the 1,5-bisallene may be modified to achieve enantioselectivity.

Our strategy was to induce enantioselectivity through a desymmetrization of the 1,5-bisallene. To produce a pro-chiral 1,5-bisallene, the nitrogen- or the oxygen-tether needs to be replaced for a carbon atom with two different substituents. In that way, the loss of symmetry during the rhodium-catalyzed cycloisomerization of the 1,5-bisallene will generate a stereogenic center (**Scheme 3.7**).

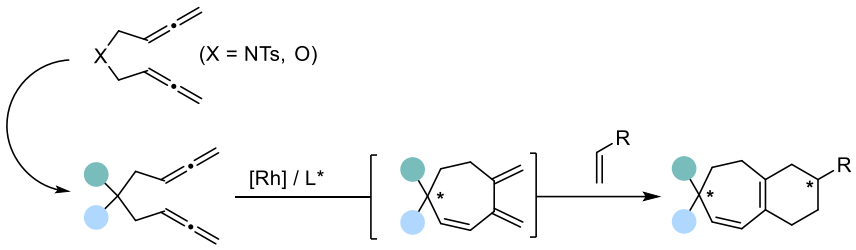

Scheme 3.7. Illustrative desymmetrization of the 1,5-bisallene to induce enantioselectivity in the tandem rhodium-catalyzed cycloisomerization/Diels–Alder cycloaddition reaction of 1,5-bisallenes.

In addition, as we know from the DFT studies, one oxygen atom of the tosyl group coordinates to the rhodium during the oxidative cyclometalation (**TS A1A2** in **Figures 3.7** and **3.8**). Accordingly, two 1,5-bisallenes were proposed to mimic this feature and favor the selective cycloisomerization: a methyl phenylacetate-tethered 1,5-bisallene, and a phenyl methylsulfone-tethered 1,5-bisallene, **1n** and **1o** respectively in **Figure 3.11**.

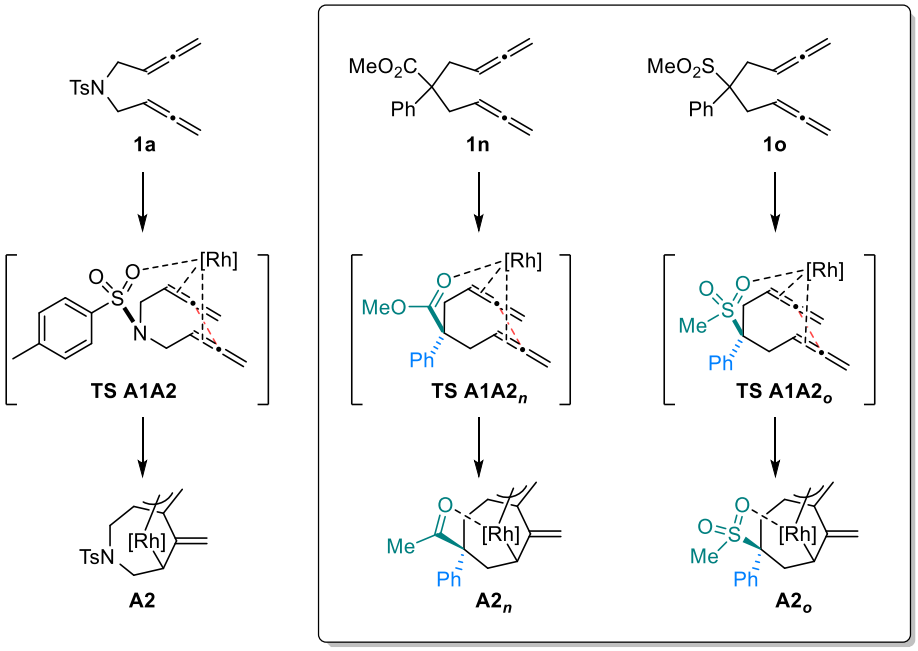

Figure 3.11. Proposed 1,5-bisallenes **1n** and **1o**, featuring oxygen atoms to coordinate the rhodium-complex during the oxidative cyclometalation.

Before proceeding with the preparation of these 1,5-bisallenes, a computational study of the oxidative cyclometalation for both 1,5-bisallenes (**1n** and **1o**) was performed to determine their capacity to give an enantioselective process. The energy barriers computed at 298K at the M06L-D3/cc-pVTZ-PP/SMD(76 % THF, 24 % CH_2Cl_2) // B3LYP-D3/cc-pVDZ-PP level of theory are depicted in **Figure 3.12**.

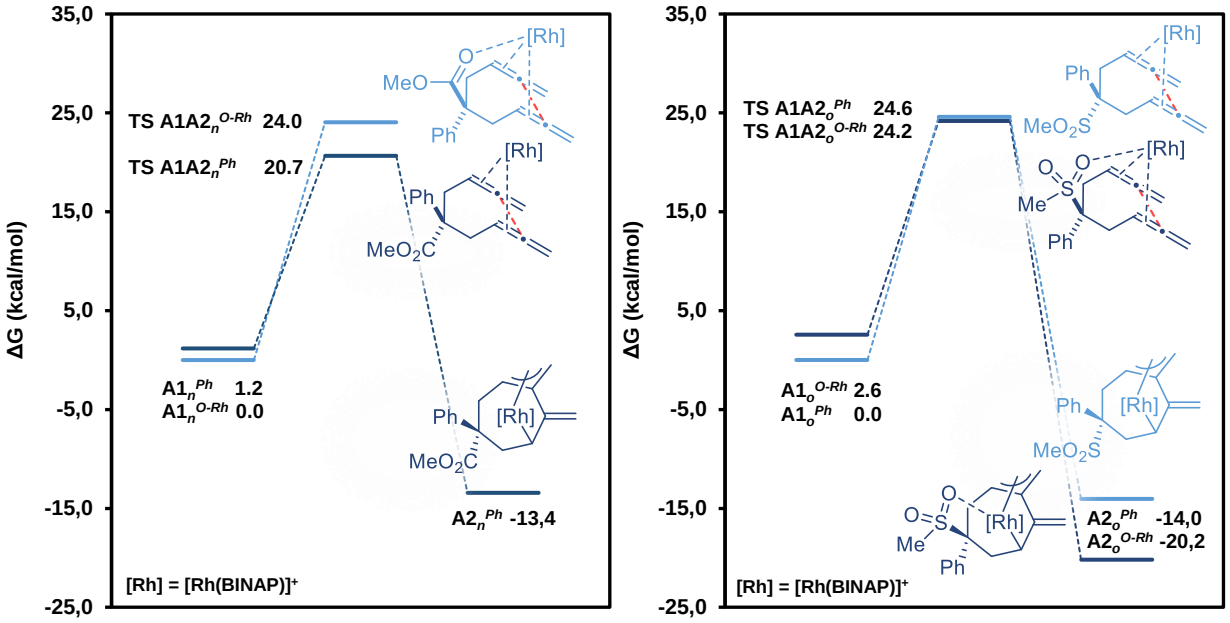

Two orientations are possible for the oxidative cyclometalation transition states: the one with the oxygen atom coordinated to the rhodium complex (superindexed as *O-Rh* in **Figure 3.12**), and the opposite, in which the phenyl points towards the rhodium complex (superindexed as *Ph* in **Figure 3.12**). Surprisingly, for the methyl phenylacetate-tethered 1,5-bisallene **1n**, the oxygen-coordinated transition-state (**TS A1A2$_n^{O\text{-}Rh}$**) was found to be energetically disfavored by 3.3 kcal/mol, thus, the orientation in which the phenyl points towards the rhodium is the preferred. In contrast, for the phenyl methylsulfone-tethered 1,5-bisallene **1o**, both transition states are almost identical in energy ($\Delta\Delta G^{\ddagger}$ = 0.4 kcal/mol), and therefore, the cycloisomerization process is expected to produce both enantiomers. According to these computational results, the methyl phenylacetate 1,5-bisallene **1n** is more likely to produce an enantioselective process as the oxidative cyclometalation is preferred to occur with the phenyl pointing towards the rhodium complex, instead of the anticipated oxygen-coordinated orientation.

Having established the 1,5-bisallene **1n** as the candidate to get an enantioselective process, we then tested its efficiency. The 1,5-bisallene **1n** was submitted under the optimized reaction conditions, but with the methyl vinyl ketone **2g** as a dienophile and employing the chiral bisphosphines (*R*)-BINAP and (*R*)-DTBM-Segphos (**Scheme 3.8**).

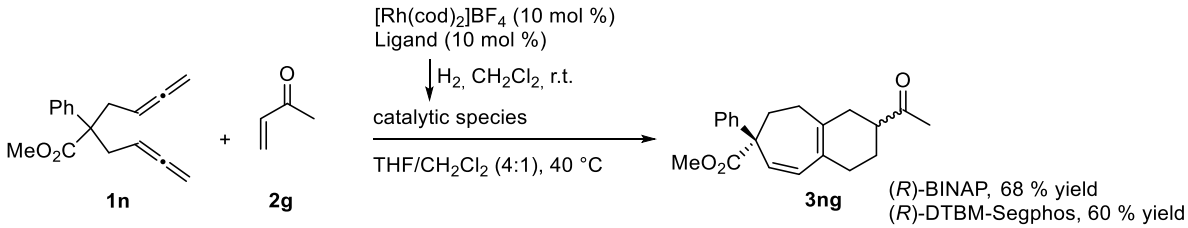

Scheme 3.8. Rhodium-catalyzed cascade cycloisomerization/Diels – Alder reaction of pro-chiral 1,5-bisallene **1n** and methyl vinyl ketone **2g**.

The reaction performed well, obtaining the cycloadduct **3ng** in good yields with both chiral bisphosphine ligands, but more importantly, we were delighted to observe that enantioinduction in the 7-membered ring was achieved as well. Although the enantiomeric excess (*ee*) could not be calculated accurately as the peaks in the HPLC were not fully resolved (see **Figures S2 – S4** in the supplementary material for Chapter 3), compound **3ng** was obtained in a 1:1 diastereomeric ratio (*d.r.*), with a promising 50 – 60 (*ee*) for both diastereoisomers. The absolute configuration of **3ng** could not be confirmed experimentally. However, according to the computational data, the *R* configuration may be adopted in the 7-membered ring.

The 1:1 diastereomeric ratio was indicative that the Diels–Alder reaction was not diastereoselective, and further experiments were directed to induce stereoselectivity in the Diels–Alder reaction by employing bulkier dienophiles (**Figure 3.13**).

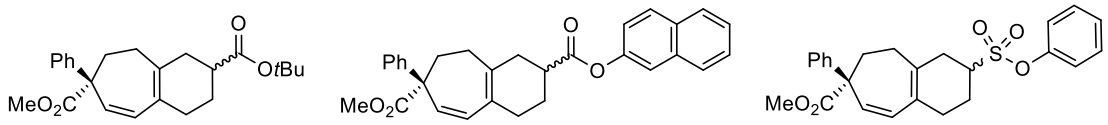

3nc, 40 % yield **3nf**, 33 % yield **3nm**, 42 % yield

Figure 3.12. Bulky dienophiles tested in the enantioselective cascade rhodium-catalyzed cycloisomerization/Diels – Alder reaction of 1,5-bisallenes and alkenes.

All the dienophiles tested, *tert*-butyl acrylate **2c**, naphtyl acrylate **2f**, and phenyl vinylsulfonate **2m**, afforded their corresponding cycloadducts in an overall yield of 40 %, 33 %, and 42 % respectively. Unfortunately, the regioselectivity of the Diels–Alder reaction decreased, resulting in unresolved mixtures in the HPLC (see **Figures S5** and **S6** in the supplementary material for Chapter 3). Therefore, the enantiomeric excess could not be calculated properly, although the diastereomeric ratio seemed to remain 1:1.

In summary, we have developed an efficient cascade process involving an intramolecular Rh-catalyzed cycloisomerization of 1,5-bisallenes **1** to deliver non-isolable cycloheptatrienes, which concomitantly undergo a regioselective [4+2] cycloaddition with alkenes **2**. The new process affords a variety of polycyclic heterocycles **3** containing dihydroazepine- and dihydrooxepine-fused ring systems. A complete mechanistic study of this transformation has been undertaken including DFT calculations. Additionally, the use of the 1,5-bisallene **1n** set a promising precedent to develop an enantioselective version of the process. Although different pro-chiral 1,5-bisallenes have not been tested, further efforts may be directed in this direction to reach higher enantiomeric excess.

Chapter 4. Highly Selective Synthesis of Seven-Membered Azaspiro Compounds by a Rh(I)-Catalyzed Cycloisomerization/Diels–Alder Cascade of 1,5-Bisallenes

---

Published in: *J. Org. Chem.* **2022**, *87*, 5279.

Authors: Vila, J.; Solà, M.; Pla-Quintana, A.; Roglans, A.

The synthesis of spiro compounds featuring seven- and six-membered rings in the spirobicyclic motif is successfully achieved through a cascade process encompassing a rhodium(I)-catalyzed cycloisomerization followed by a highly selective Diels–Alder homodimerization. The scope of the reaction is analyzed based on a series of synthetic substrates, and control experiments and DFT calculations led us to justify the exquisite degree of selectivity observed.

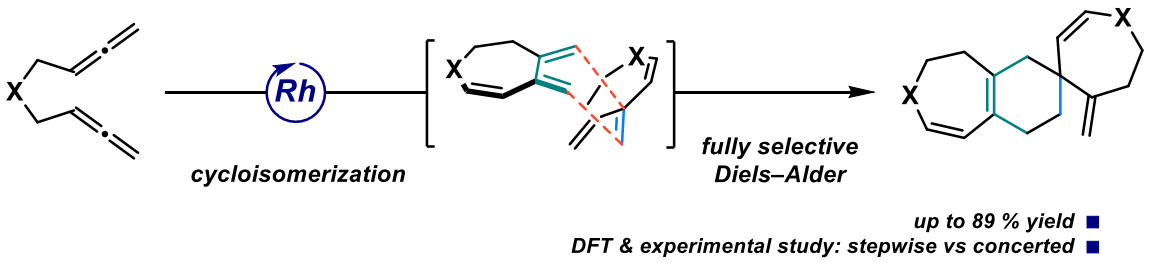

Structures containing two rings connected through a single carbon atom are referred to as spiro compounds. The synthesis of such structures has received significant attention as they have shown a broad spectrum of biological and pharmaceutical activity,[95] as well as applicability in optoelectronics.[96] Furthermore, the fact that spiro atoms can exhibit central or axial chirality, together with their inherent rigidity, can be exploited for the development of chiral ligands and catalysts for asymmetric catalysis.[97] However, the enantioselective synthesis of quaternary spiro carbon atoms poses major challenges.[98]

Although plenty of natural products contain spirocyclic moieties, compounds of 7-membered rings featuring a spiro carbon atom are not particularly common. Additionally, those that contain a nitrogen atom in the 7-membered ring show very interesting pharmaceutical properties. For instance, spirooxindole derivatives **a**, **b**, and **c** in **Figure 4.1** exhibit antimicrobial and antianxiety activity,[99] antiplasmodial activity towards the most relevant malaria parasite,[100] and antiproliferative activity on human prostatic carcinoma cell lines,[101] respectively. On the other hand, looking at spiro compounds featuring 6- and 7-membered rings (**d** and **e** in **Figure 4.1**), galanthamine (**d**) is a natural product used to slow down the neurological degeneration in Alzheimer's disease.[102] Moreover, spirolide derivatives, like pinnatoxins A–D and pteriatoxins A–C (**e**), are extremely potent marine toxins,[103] and the imine in their 7-membered ring has been found to be fundamental for their toxic activity.[104]

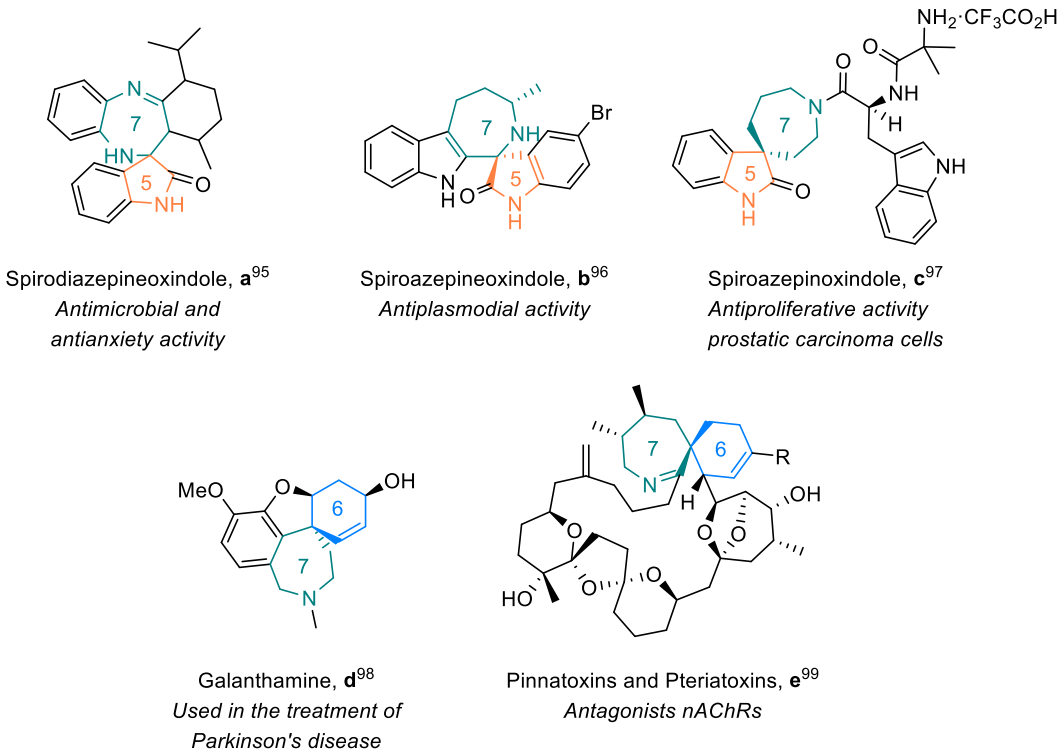

Figure 4.1. Biologically active molecules featuring 7-membered azaspiro scaffolds.

A direct method to access spirocyclic scaffolds containing 6-membered rings is based on the Diels–Alder reaction of a diene with an exocyclic dienophile. During the development of our previous project (Chapter 3 of the present manuscript), based on the rhodium-catalyzed cycloisomerization/Diels–Alder cascade reaction

of 1,5-bisallenes for the synthesis of polycyclic heterocycles,[105] we observed that a non-isolable cycloheptatriene (**cHT**) intermediate generated during the process, dimerized through Diels–Alder reaction to afford spirocyclic derivatives in a highly selective manner (**Scheme 4.1a**). This dimerization is singularly related to the postulated biosynthesis of xylopidimers **A** and **B** (**Scheme 4.1b**), in which two guaiane moieties react in a [4+2] cycloaddition. Different orientations explain the formation of the various regioisomers isolated.[106]

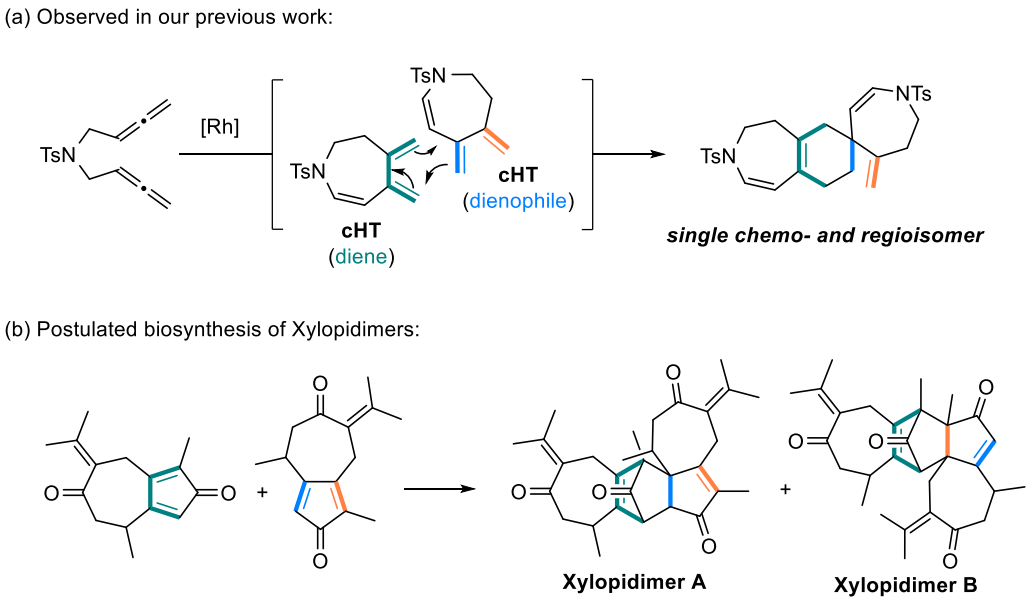

Scheme 4.1. Synthesis of spiro derivatives through Diels–Alder reaction. (a) Our previous work on rhodium-catalyzed cycloisomerization/Diels–Alder cascade reaction of 1,5-bisallenes for the synthesis of polycyclic heterocycles. (b) Postulated biosynthesis of Xylopidimer **A** and **B**.

Due to the interest in the process and the products obtained, we decided to further explore this reactivity to prepare 7-membered spiro compounds and to fully analyze the reasons behind the exquisite degree of selectivity in this transformation.

Results and discussion

Based on our earlier study,[105] submitting the 1,5-bisallene **1a** under the previously optimized reaction conditions produced two different products: compound **6a** (47 % yield) generated from the dimerization of **cHT** and isolated as a single chemo- and regioisomer, and compound **5a** (14 % yield), resulting from the [2+2] cycloaddition of the starting 1,5-bisallene **1a** (**Scheme 4.2**).

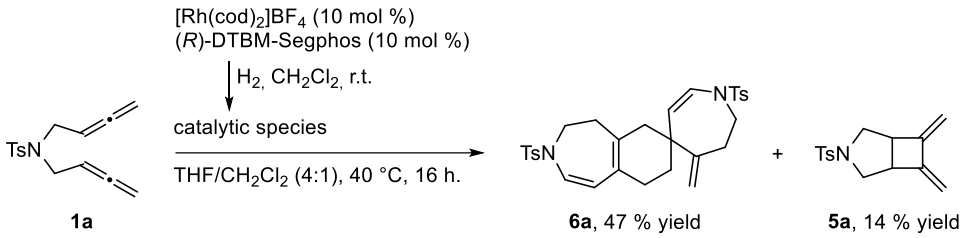

Scheme 4.2. Generation of **6a** and **5a** under the previously optimized reaction conditions.

Since the *in-situ* generated **cHT** has three double bonds susceptible to be involved in the Diels–Alder reaction as dienophiles, an exhaustive characterization of the product **6a** was mandatory. All the possible dimerization products of the **cHT** are ordered in **Figure 4.2** according to which double bond is involved as a dienophile (**dp**).

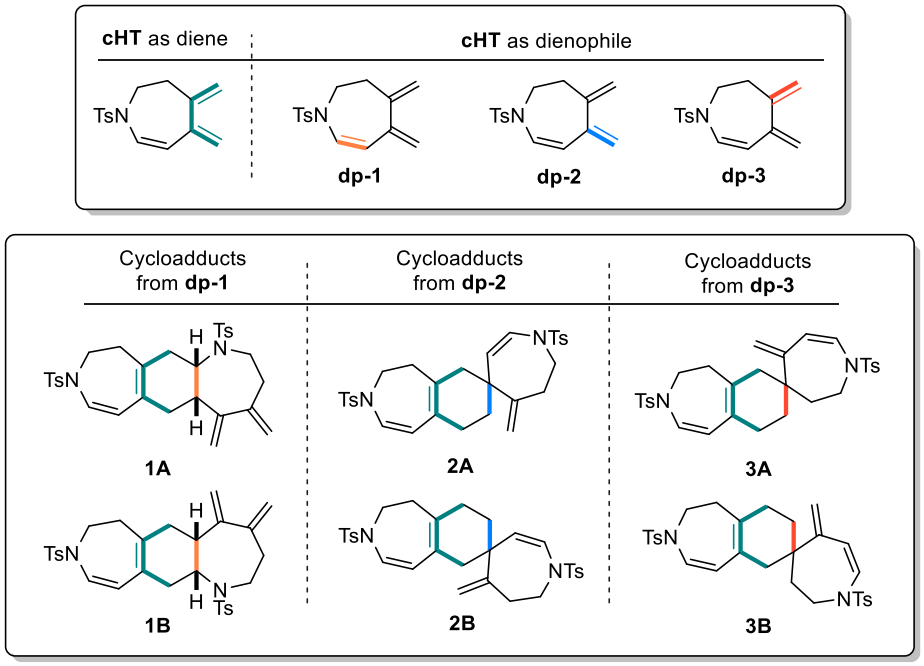

Figure 4.2. Possible dimerization products from the Diels – Alder of **cHT** according to which double bond is involved as a dienophile.

The molecular formula of the homo-dimerization product **6a** was confirmed by HRMS, showing a peak at 573.1836 corresponding to $[M+Na]^+$. Then, 1D and 2D NMR experiments allowed to confirm the formation of only one cycloadduct and its structural identification. First, the ^{1}H-NMR chemical shifts and their multiplicity were analyzed (**Figure 4.3**). The presence of two pairs of doublets at δ = 4.71 and 6.27 ppm, and δ = 4.84 and 6.64 ppm, are indicative of two *cis*-endocyclic double bonds. Furthermore, only two singlets at δ = 4.52 and 4.63 ppm are observed, from two protons attached to the same Csp^2 (confirmed at the HSQC), supporting the presence of a single exocyclic double bond. Therefore, cycloadducts **1A** and **1B** were discarded.

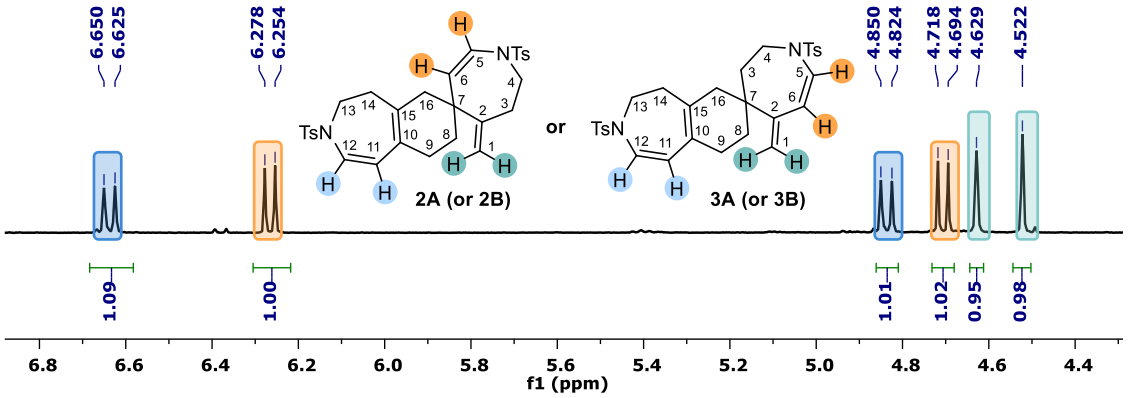

Figure 4.3. ^{1}H-NMR section of the olefinic protons showing the two pairs of doublets and the two singlets.

To distinguish between the cycloadducts formed from **dp-2** and **dp-3**, the 2D NMR HSQC and HMBC experiments were performed (**Figure 4.4**). The spiro carbon atom **C7** (Csp^3 at 42.5 ppm without any proton correlation) was identified by HSQC, as well as the carbons of the endocyclic double bonds, and the rest of the carbon atoms bonded to hydrogen atoms. The HMBC spectrum showed a three-bond correlation between the spiro carbon atom (**C7**) and the olefinic proton next to the nitrogen atom (**H5**), clearly demonstrating that the exocyclic double bond conjugated to the endocyclic double bond is involved in the Diels–Alder reaction (**dp-2**), and thus, cycloadducts **3A** and **3B** can be discarded.

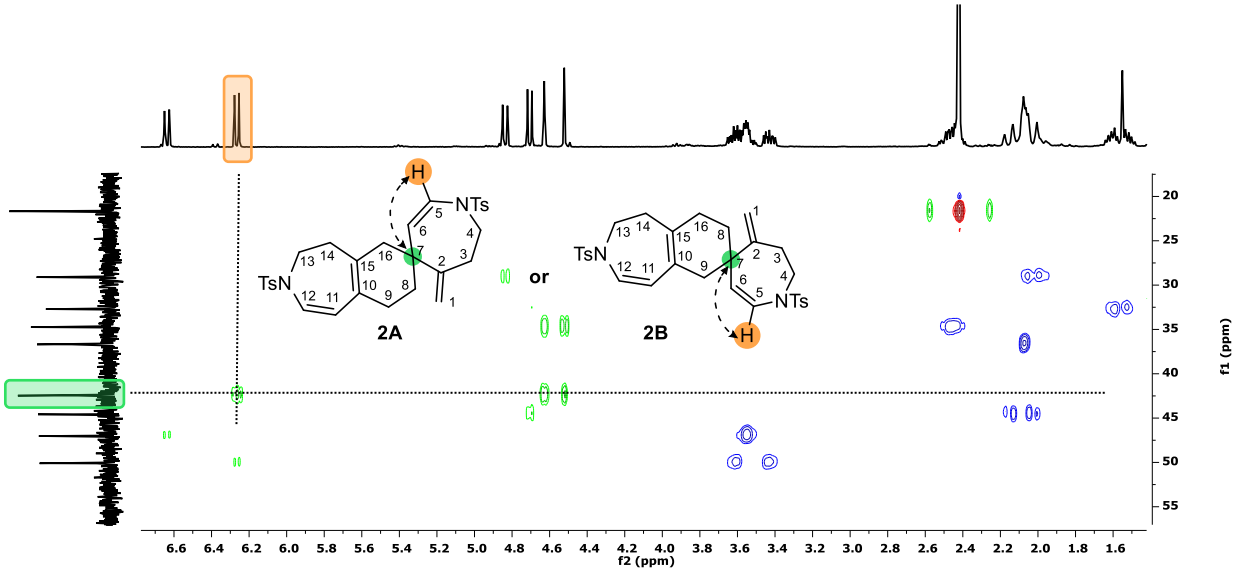

Figure 4.4. Edited HSQC (blue/red) and HMBC (green) overlapped spectra showing the correlation between spiro carbon atom **C7** and olefinic proton **H5**.

Finally, the analysis of the COSY, NOESY and HMBC experiments led us to differentiate between regioisomers **2A** and **2B**. NOE contacts **H9** ↔ **H11** (**H9** and **H8** identified as the two contiguous methylenic groups by COSY) confirmed the formation of the regioisomer **2A** as the single cycloadduct (**Figure 4.5**).

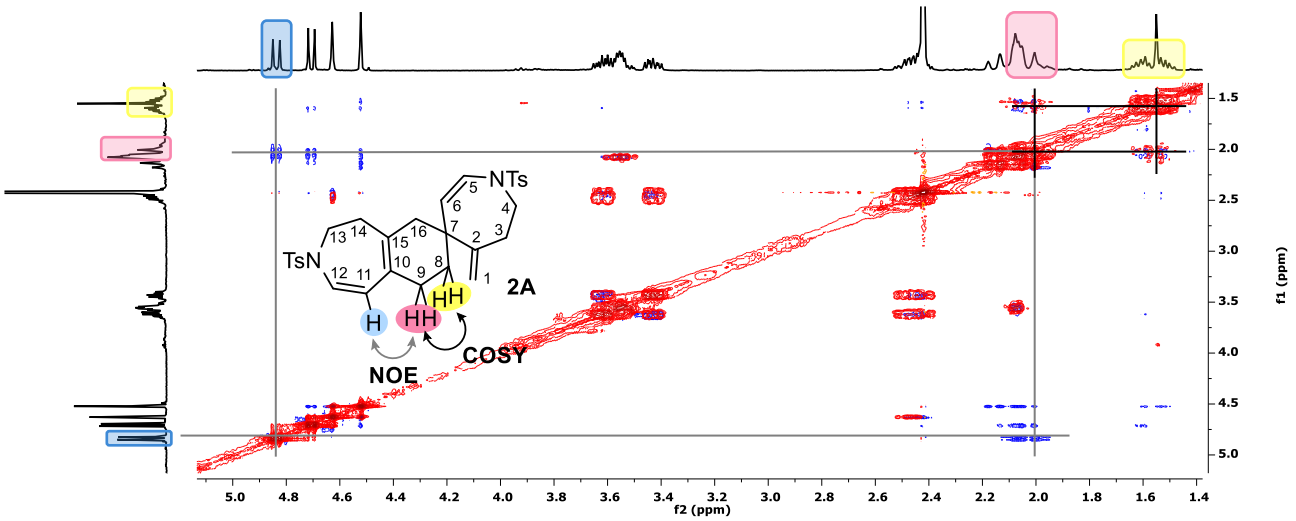

Figure 4.5. COSY (red) and NOESY (blue) overlapped spectra showing the key COSY crosspeaks (black lines) and NOE contacts (grey lines).

Additionally, the HMBC three-bond correlation between **C9** and **H11** also supports the formation of the regioisomer **2A** (**Figure 4.6**).

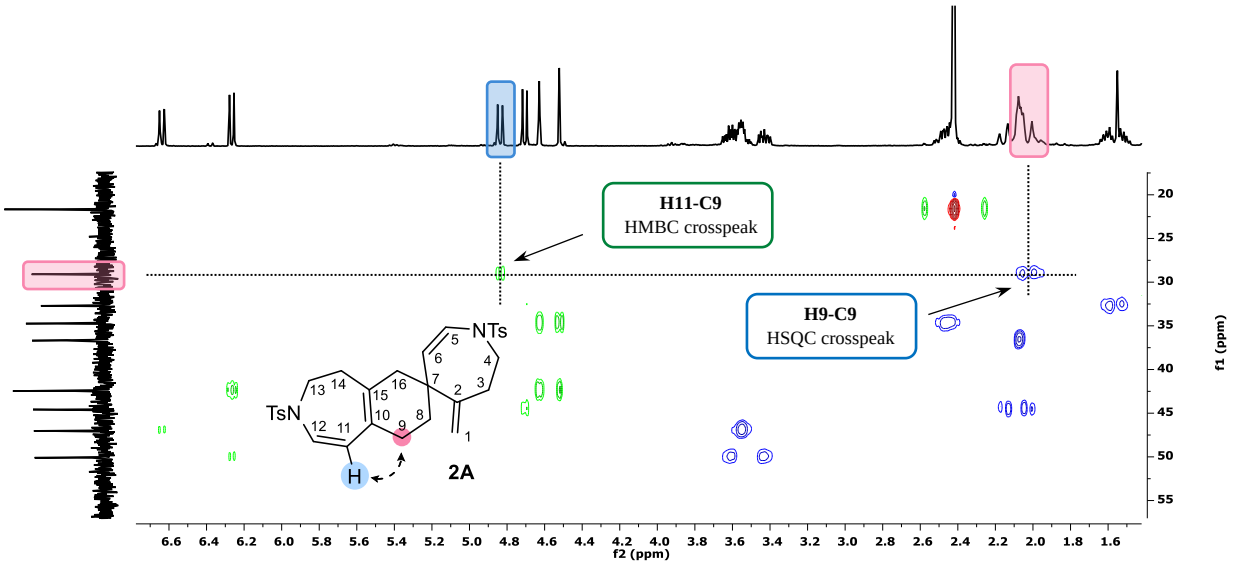

Figure 4.6. HSQC (blue for CH_2, and red for CH and CH_3) and HMBC (green) overlapped spectra showing the correlation between **C9** and **H11**.

All the key COSY and HMBC crosspeaks and NOE contacts, as well as the selected ^{1}H and ^{13}C-NMR signals are summarized in **Figure 4.7**.

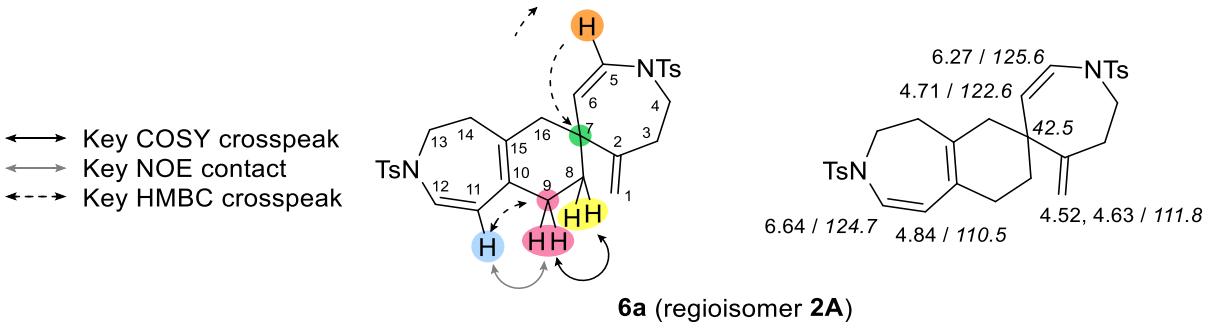

Figure 4.7. COSY and HMBC crosspeaks and NOE contact observed confirming the formation of regioisomer **2A** of **6a**, and selected ^{1}H and ^{13}C-NMR shifts (in italics). Modified with permission from Vila, J.; Solà, M.; Pla-Quintana, A.; Roglans, A. *J. Org. Chem.* **2022**, *87*, 5279. Copyright © 2022, American Chemical Society.

After the full characterization of **6a** as a single chemo- and regioisomer, we proceeded to optimize the reaction conditions to improve the production of **6a** while avoiding the formation of **5a** (**Table 4.1**). Different bisphosphine and monophosphine ligands were initially tested (shown in **Figure 4.8**). Use of BINAP, Tol-BINAP and BIPHEP afforded the spiro derivative **6a** in low yields (entries 2–4, **Table 4.1**), and Xantphos and XPhos did not promote the reaction (entries 5 and 6, **Table 4.1**). On the contrary, (*R*)-DTBM-Segphos provided **6a** in 47 % yield and was thus the ligand of choice. The effect of the concentration was then evaluated (entries 7 and 8, **Table 4.1**). Increasing the concentration to 36 mM improved the yield of **6a** to 53 %. Furthermore, the use of additives to generate different rhodium species was evaluated using the dimeric neutral rhodium complex $[Rh(cod)Cl]_2$ (entries 9 and 10, **Table 4.1**). Whereas the addition of the silver salt $AgSbF_6$ to the catalytic mixture did not improve the reaction outcome, the use of NaBArF kept the yield of **6a** while reducing the yield of the byproduct **5a** to 6 %. Finally, the effect of water in the reaction mixture was evaluated (entry 11, **Table 4.1**), the use of non-anhydrous degassed solvents, surprisingly raised the yield of **6a** to 89 %, resulting in our set of optimized reaction conditions.

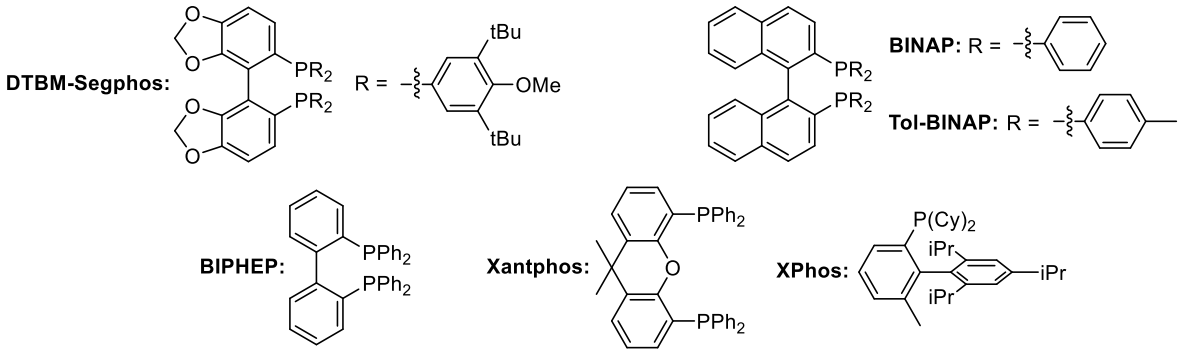

Figure 4.8. Phosphine ligands used for the optimization of the rhodium(I)-catalyzed dimerization of 1,5-bisallene **1a**.

Table 4.1. Optimization of the rhodium(I)-catalyzed dimerization of 1,5-bisallene **1a**.[a]

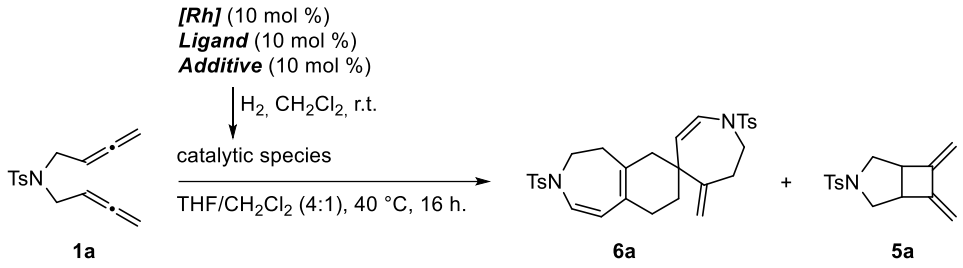

1a **6a** **5a**

Entry	[Rh] complex	Ligand	[**1a**] mM	Additive	Yield **6a**/**5a** (%)
1	$[Rh(cod)_2]BF_4$	(*R*)-DTBM-Segphos	9	-	47/14
2	$[Rh(cod)_2]BF_4$	BINAP	9	-	6/0
3	$[Rh(cod)_2]BF_4$	Tol-BINAP	9	-	10/0
4	$[Rh(cod)_2]BF_4$	BIPHEP	9	-	7/0
5	$[Rh(cod)_2]BF_4$	Xantphos	9	-	0/0
6	$[Rh(cod)_2]BF_4$	XPhos	9	-	0/0
7	$[Rh(cod)_2]BF_4$	(*R*)-DTBM-Segphos	4.5	-	44/17
8	$[Rh(cod)_2]BF_4$	(*R*)-DTBM-Segphos	36	-	53/14
9	$[Rh(cod)Cl]_2$	(*R*)-DTBM-Segphos	36	$AgSbF_6$	32/6
10	$[Rh(cod)Cl]_2$	(*R*)-DTBM-Segphos	36	$NaBArF_6$	46/6
11[b]	**$[Rh(cod)Cl]_2$**	**(*R*)-DTBM-Segphos**	**36**	**$NaBArF_6$**	**89/11**

[a] Reaction conditions: 0.09 mmol of **1a**, 10 mol % of Rh catalyst (5 % mol for $[Rh(cod)Cl]_2$) in 2.5-20 mL of THF/CH_2Cl_2 (4:1) at 40 °C for 16 h. The catalytic mixture of [Rh] complex and phosphine was treated with hydrogen in dichloromethane (CH_2Cl_2) solution for catalyst activation prior to substrate addition. [b] The solvent mixture THF/CH_2Cl_2 was non-anhydrous and degassed.

In line with our previous study,[105] the optical purity of **6a** was checked since a chiral ligand was used, but no enantioinduction was observed. This is consistent with the mechanism, which involves a rhodium-catalyzed cycloisomerization of the 1,5-bisallene followed by a catalyst-free Diels–Alder reaction.

Once the reaction conditions were optimized, diverse 1,5-bisallenes were tested to evaluate the scope of the reaction (**Scheme 4.3**). Aromatic sulfonamide-tethered 1,5-bisallenes were initially explored. The dimerization products were efficiently obtained with arylsulfonamides bearing electron-donating (**6b**, 89 % yield) and electron-withdrawing groups (**6e**, 87 % yield). Additionally, the 5-methyl-2-pyridinesulfonamide-tethered 1,5-bisallene afforded **6f** in 75% yield, showing that the potentially coordinating pyridine ring did not poison the catalyst. Aliphatic sulfonamide-tethered 1,5-bisallenes were also efficient substrates, as shown by the reactions of *tert*-butyl and trimethylsilyl sulfonamides that gave the corresponding **6g** and **6h** in 68 and 55 % yields, respectively. Furthermore, 1,5-bisallenes with tethers other than sulfonamides also gave the desired spiro derivatives. The *N*-Boc-tethered 1,5-bisallene **1i**, and the diethylmalonate carbon-tethered 1,5-bisallene **1k**, produced **6i** and **6k** in 42 and 80 % yield, respectively. It is to be noted that in all reactions, the corresponding derivatives **5** were obtained in low yields. To increase the versatility of the process, heterodimerization reaction

was attempted by mixing the 1,5-bisallenes **1e** and **1g**. Unfortunately, though not unexpectedly, the experiment resulted in a complex mixture.

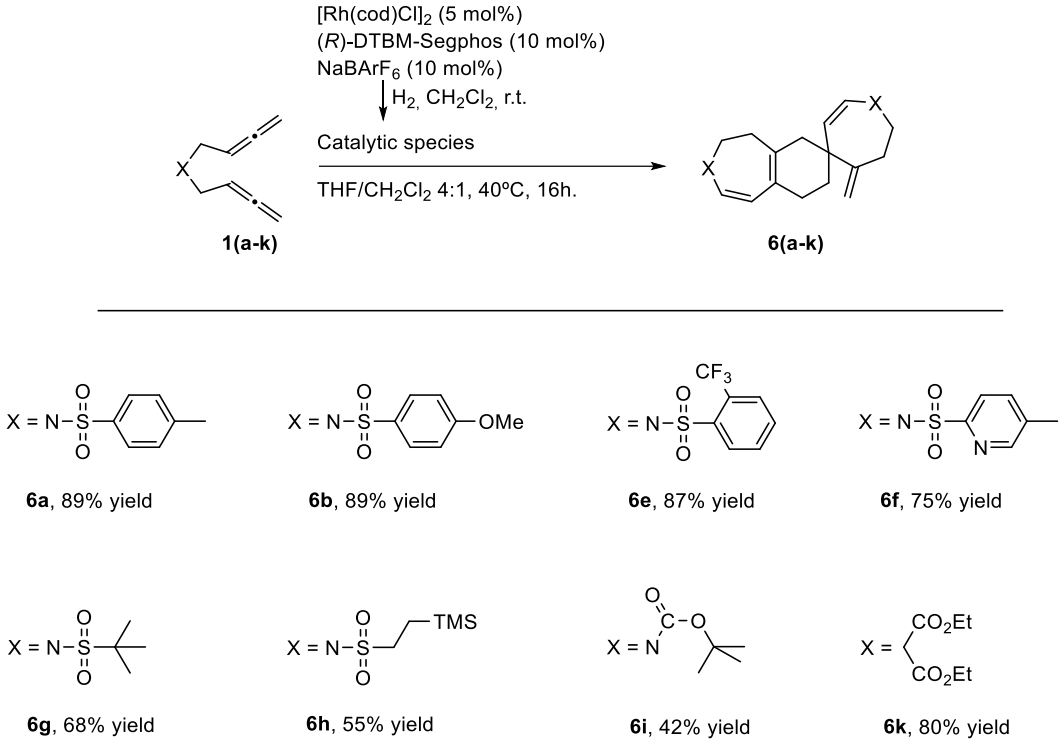

Scheme 4.3. Scope of the rhodium-catalyzed dimerization of 1,5-bisallenes **1** to produce spiro derivatives **6**.

To shed light on the reasons behind the great degree of chemo- and regioselectivity obtained in the formation of spiro derivatives **6**, a computational DFT study of the Diels–Alder reaction of **cHT-1k** was carried out. The formation of the **cHT** was omitted as it had already been studied in Chapter 3 of this manuscript. The Gibbs energy barriers were computed at 313.15K and 1 atm with the (U)B3LYP-D3/cc-pVTZ/SMD(76% THF, 24% CH_2Cl_2)//(U)B3LYP-D3/cc-pVDZ level of theory (see Chapter 8, section **8.1.3** for a complete description of the computational methods).

We first evaluated the formation of all the possible Diels–Alder cycloadducts using closed-shell (*cs*, two paired electrons for each occupied orbital) calculations, considering the *exo* and the *endo* approximations for each cycloadduct (**Figure 4.9**).

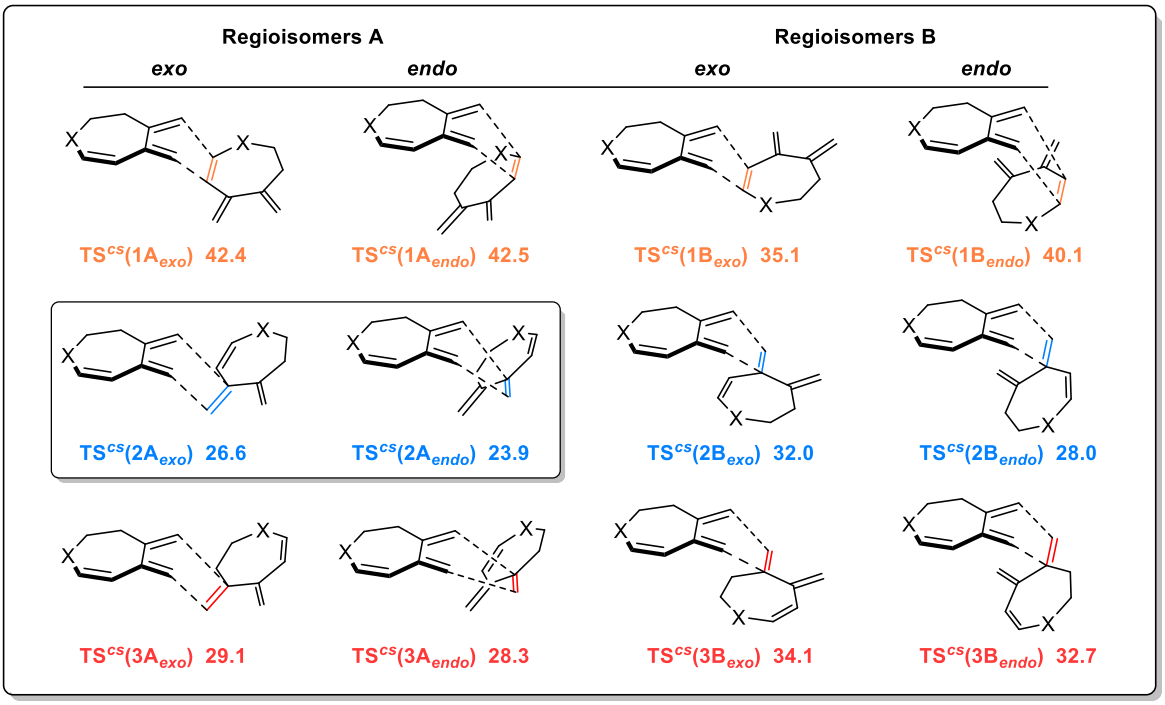

Figure 4.9. All possible orientations for the Diels–Alder cycloaddition of **cHT-1k** (X = $C(CO_2Et)_2$) and their respective Gibbs energy barriers in kcal·mol^{-1}.

We found that the most favorable approximations are those that explain the formation of our experimentally isolated product, through **TS^{cs}(2A$_{endo}$)** and **TS^{cs}(2A$_{exo}$)**, with Gibbs energy barriers of 23.9 and 26.6 kcal·mol^{-1}, respectively. It was also found that the geometries of these transition states exhibit high asynchronous character, suggesting that the reaction may occur in two steps (**Figure 4.10**). However, these transition states directly collapsed in a barrierless process to form **6k**, and an intermediate could not be found performing closed-shell calculations. Thus, the reactions can be described as concerted but highly asynchronous.

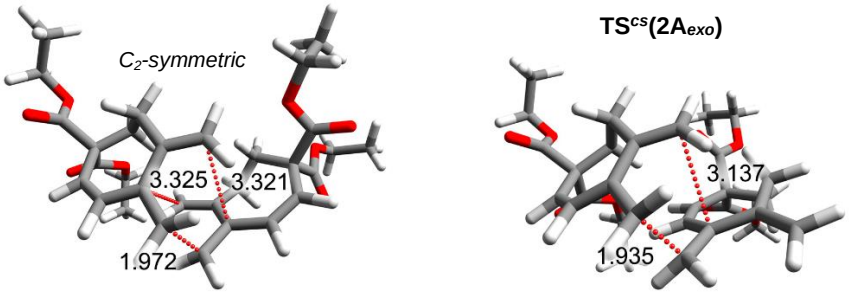

Figure 4.10. Closed-shell transition state geometries of **TS^{cs}(2A$_{endo}$)** and **TS^{cs}(2A$_{exo}$)** with an asynchronous character. Distances given in angstroms (Å).

As opposite to this, with open-shell (*os*, electrons can be unpaired) calculations the reaction was found to proceed in a two-step process involving a biradical intermediate (**Figure 4.11**). The transition states for the **2A$_{endo}$** and **2A$_{exo}$** approximations are slightly lower in energy than their closed-shell counterparts, and **TS^{os}(2A$_{endo}$)** ($\langle S \rangle^2 = 0.05$) is found to have the lowest energy barrier by 0.4 kcal·mol^{-1} and preferred over **TS^{os}(2A$_{exo}$)** ($\langle S \rangle^2 = 0.19$) by 2.1 kcal·mol^{-1}. This time, the birradical intermediate **int(2A$_{endo}$)** was localized,

which is generated at a cost of 13.1 kcal·mol^{-1}. From this point, the collapse of the biradical intermediate **int(2A$_{endo}$)** led to **6k**, surpassing a Gibbs energy barrier of 7.3 kcal·mol^{-1} through **TS^{os}(int(2A$_{endo}$))** and releasing 23.9 kcal·mol^{-1}.

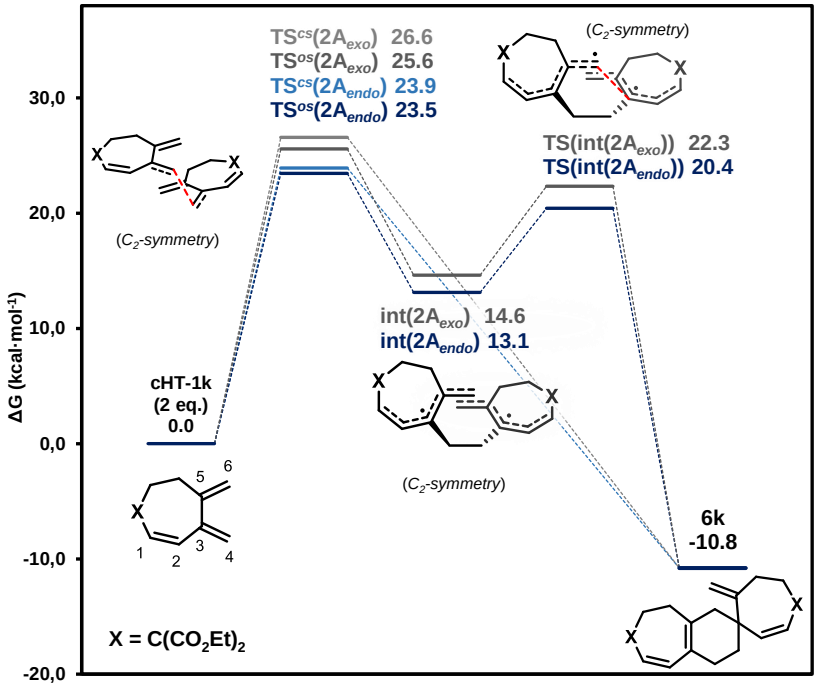

Figure 4.11. Gibbs energy profile in kcal·mol^{-1} for the transformation of **cHT** (from **1k**), into **2k**.

Overall, the two-step biradical pathway through the *endo* approximation (**TS^{os}(2A$_{endo}$)**) is the lowest in energy. However, the energetic difference of 0.4 kcal·mol^{-1} respect to its concerted asynchronous counterpart (**TS^{cs}(2A$_{endo}$)**) is not sufficient to discriminate between the two pathways and they are probably competing to generate the final product **6k**. Notwithstanding, it should be noted that the biradical pathway certainly helps to rationalize the chemo- and the regioselectivity observed, which is clearly governed by the stability of the delocalized biradical intermediate (**int(2A$_{endo}$)**) in a double allylic position. This delocalization is well depicted in the frontier orbitals HOMO of **int(2A$_{endo}$)** for both electrons α and β (**Figure 4.12**).

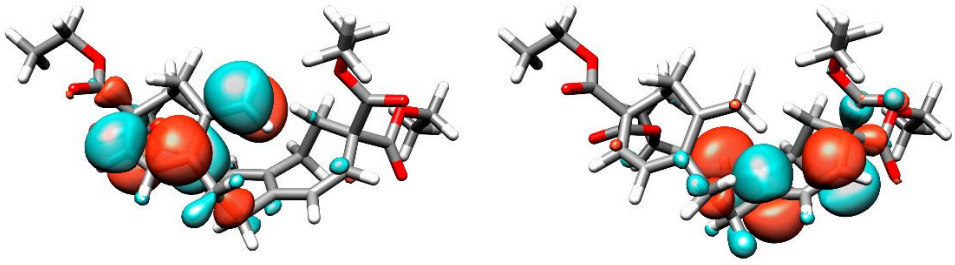

Figure 4.12. Representation of frontier orbitals HOMO of the biradical intermediate **int(2A$_{endo}$)** for electrons α and β.

Additionally, a natural population analysis (NPA) was performed of the **cHT**, the **cHT**$^{+}$ (removing 1 e^{-}) and **cHT**$^{-}$ (adding 1 e^{-}) to calculate the condensed Fukui functions (f_k^- and f_k^+),[107] which can be written as shown in eq. **4.1** and **4.2**:

$$f_k^- = q_{k(N)} - q_{k(N-1)} \quad \text{(Eq. 4.1)}$$

and

$$f_k^+ = q_{k(N+1)} - q_{k(N)} \quad \text{(Eq. 4.2)}$$

Where $q_{k(N)}$ is the natural charge on the *k*-atom of the molecule with *N* electrons, and $q_{k(N-1)}$ and $q_{k(N+1)}$ are the natural charges on the *k*-atom of the molecule with (*N-1*) and (*N+1*) electrons, respectively.

The values obtained from the condensed Fukui functions are indicative of how likely an atom is to give (f^-) or receive (f^+) an electron, in other words, which atoms are more likely to be involved in the formation of a new bond. The values of the condensed Fukui functions are shown in **Figure 4.13** on the frontier orbitals HOMO and LUMO of the **cHT**.

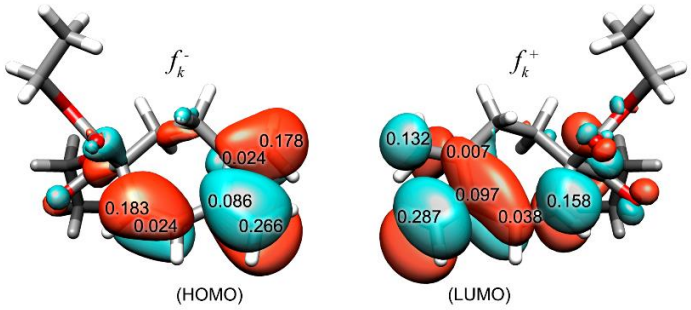

Figure 4.13. Values of the condensed Fukui functions f_k^- and f_k^+ (units are electrons) on the HOMO and LUMO orbitals.

The higher values obtained were f_4^- = 0.266 and f_4^+ = 0.287 (atom labels from **Figure 4.11**). These results support the formation of the first bond between the unsubstituted terminus of the doubly conjugated exocyclic double bond of the two **cHT** units (C_4–C_4, **Figure 4.11**), leading to the selective formation of regioisomers **2A (Figure 4.2**). The same conclusion can be extracted by looking at the frontier orbitals HOMO and LUMO, as the best molecular orbital overlap would come from the coupling of the same methylene positions.

Given these computational results, which suggest a competitive mechanism between a two-step biradical and a concerted asynchronous process in the Diels–Alder cycloaddition, we performed the reaction in the presence of 1,5 equivalents of the radical trapping agents BHT (butylhydroxytoluene) and TEMPO (2,2,6,6-tetramethylpiperidine-1-oxyl) to trap the intermediate **int(2A)** and obtain experimental evidence of its formation. The use of BHT did not alter the reaction at all, as **6a** was produced in 84 % yield. However, when the free radical TEMPO was employed, the yield towards the formation of **6a** was drastically reduced from 89 to 44 %. In addition, the yield of **5a** was not significantly reduced, indicating that the rhodium activity was not altered by the presence of TEMPO. Furthermore, an isolated fraction from the reaction crude was analyzed by ESI-MS, which showed the formation of three adducts incorporating the **int(2A)** and TEMPO moieties (**Scheme 4.4**).

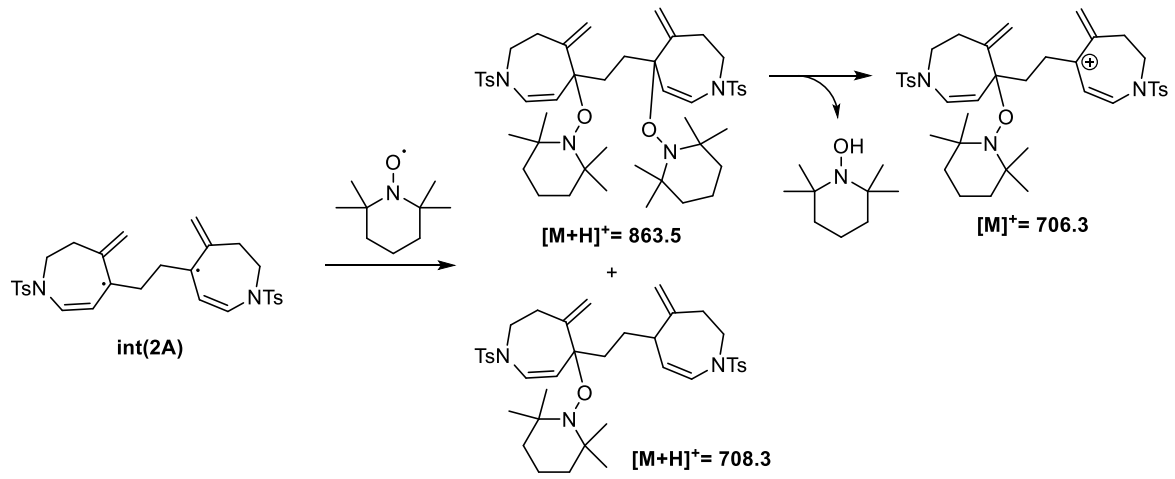

Scheme 4.4. Species detected by ESI(+)-MS when the reaction is performed in the presence of 1,5 equivalents of TEMPO.

The first adduct corresponds to the incorporation of two TEMPO units (m/z = 863.5 for [**int(2A)** + 2·TEMPO + H]$^+$) (**Figure 4.14**).

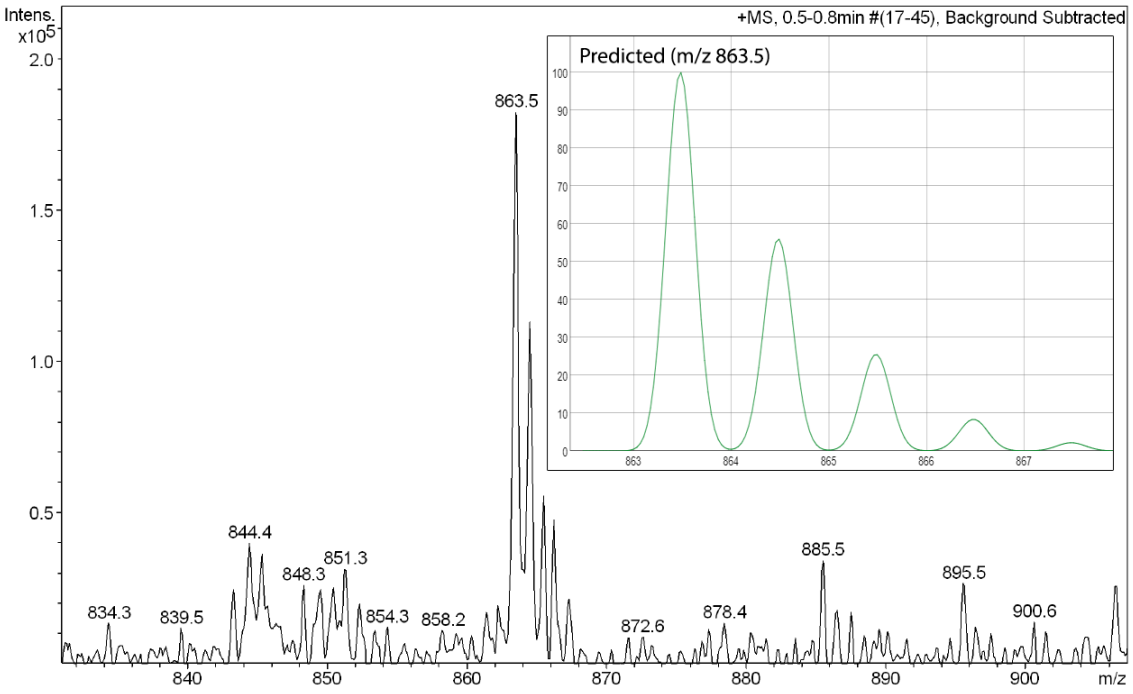

Figure 4.14. Experimental and predicted ESI(+)-MS spectra of the adduct at m/z = 863.5.

The second adduct showed the incorporation of one TEMPO unit and a hydrogen radical (m/z = 708.3 for [**int(2A)** + TEMPO + H$^{\cdot}$ + H]$^+$) (**Figure 4.15**). Finally, the third adduct resulted from the fragmentation of the adduct that incorporates two TEMPO units (m/z = 863.5) by losing a neutral TEMPO-H, giving rise to a carbocationic species (m/z = 706.3 for [**int(2A)** + TEMPO]$^+$). (**Figure 4.15**).

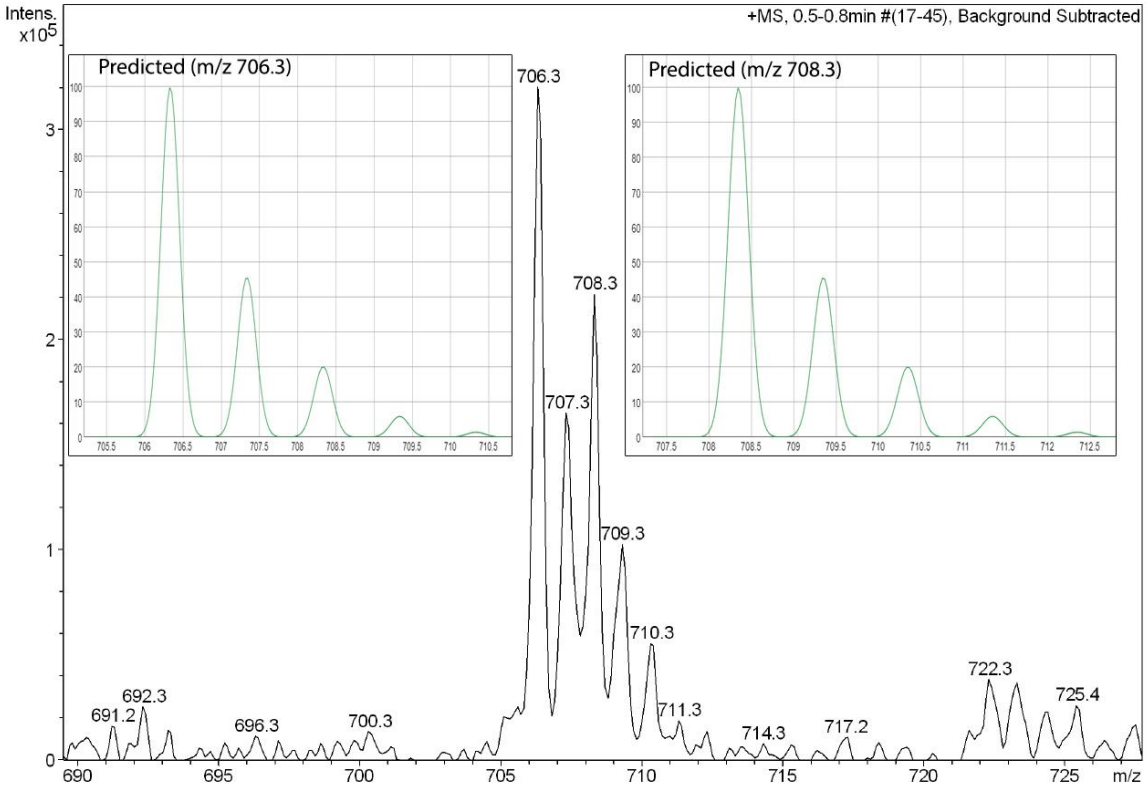

Figure 4.15. Experimental and predicted ESI(+)-MS spectras of the adducts at m/z = 706.3 and 708.3.

This fragmentation was further confirmed by an MS/MS analysis of the peak at m/z = 863.5, resulting in a peak at m/z = 706.3 (**Figure 4.16**). Therefore, we can confirm that performing the reaction in the presence of 1,5 equivalents of TEMPO clearly demonstrates the participation of the biradical intermediate **int(2A)** in the reaction that transforms 1,5-bisallenes **1** into spiro compounds **6**.

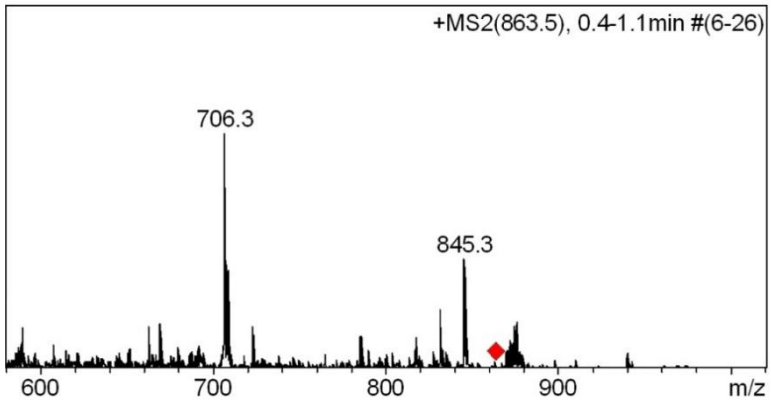

Figure 4.16. MS/MS fragmentation of m/z = 863.5 into m/z = 706.3

In summary, a method that enables rapid access to seven- and six-membered spirocyclic compounds in a complete chemo- and regioselective manner from 1,5-bisallenes has been developed. The whole process involves an initial rhodium-catalyzed cycloisomerization of 1,5-bisallenes leading to non-isolable cycloheptatrienes followed by Diels–Alder homodimerization. A set of nitrogen-tethered 1,5-bisallenes, as well as a carbon-tethered 1,5-bisallene, gave the final spirocyclic products with complete chemo- and

regioselectivity. The DFT calculations have demonstrated the selectivity observed, arising from the highly favoured homocoupling of the unsubstituted terminus of the doubly conjugated double bond. Additionally, although experimental evidence has been found for the formation of the proposed biradical intermediate, the computational study suggests that both mechanisms, the two-step biradical and the concerted asynchronous, compete to generate the spirocyclic products.

Chapter 5. A Rh(I)-Catalyzed Cascade Cyclization of 1,5-Bisallenes and Alkynes for the Formation of *cis*-3,4-Arylvinyl Pyrrolidines and Cyclopentanes

---

Published in: *Adv. Synth. Catal.* **2022**, *364*, 206.

Authors: Vila, J.; Vinardell, R.; Solà, M.; Pla-Quintana, A.; Roglans, A.

The cascade cyclization reactions of 1,5-bisallenes grant access to a great variety of products by precisely tuning the catalyst system and/or the reagents involved. Herein, we present our findings that 1,5-bisallenes react with two molecules of dimethyl acetylenedicarboxylate to afford, in a completely diastereoselective manner, *cis*-3,4-arylvinyl pyrrolidines and cyclopentanes. DFT calculations have been used to postulate a mechanism for the developed reaction, which encompasses a [2+2+2] cycloaddition reaction of the two alkynes and the external double bond of one allene, followed by a cycloisomerization involving the internal double bond of the second allene.

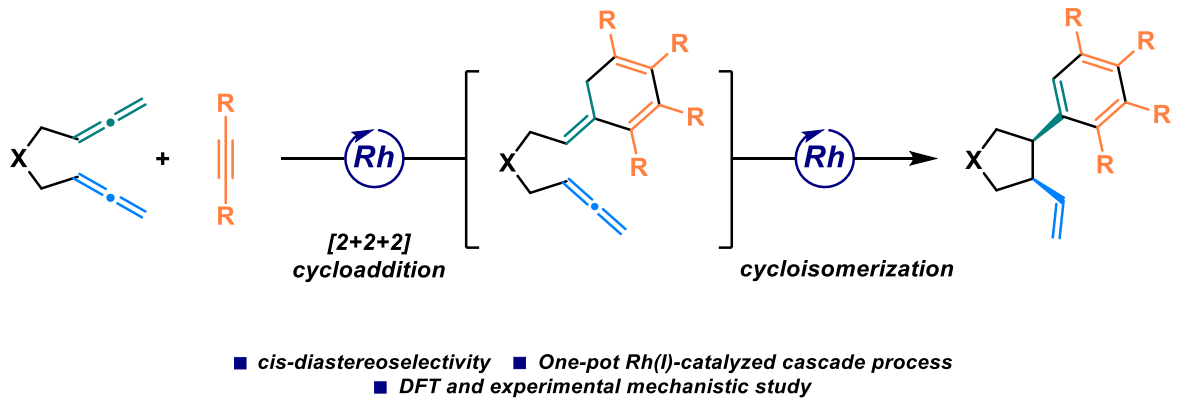

In our previous studies on the rhodium-catalyzed cycloaddition reactions of 1,5-bisallenes, the use of alkenes led to a rhodium-catalyzed cycloisomerization process of the 1,5-bisallene in which the alkene did not participate in the catalytic cycle. As a continuation of our interest in developing rhodium-catalyzed cycloaddition reactions of 1,5-bisallenes with other unsaturated C – C bonds, we asked ourselves what the favored outcome would be if instead of alkenes, alkynes were involved as external partners. Given that alkynes are much more reactive than alkenes in the rhodium-catalyzed [2+2+2] cycloaddition reaction, we anticipated that under the right conditions, either a rhodium-catalyzed [2+2+2] cyloaddition of 1,5-bisallenes with alkynes, or a fully rhodium-catalyzed cascade process might be favored.

Results and discussion

Our initial hypothesis was that, under the right conditions, the oxidative cyclometalation would involve one molecule of alkyne and one double bond of the 1,5-bisallene. From that point, two pathways should be possible (**Scheme 5.1**): (a) insertion of a second alkyne molecule, resulting in the formation of the [2+2+2] cycloadducts **A** or **E** (which may be able to undergo a rhodium-catalyzed cascade process); or (b) insertion of the second allene moiety and reductive elimination to generate the corresponding [2+2+2] cycloadducts **B**, **C** or **D**.

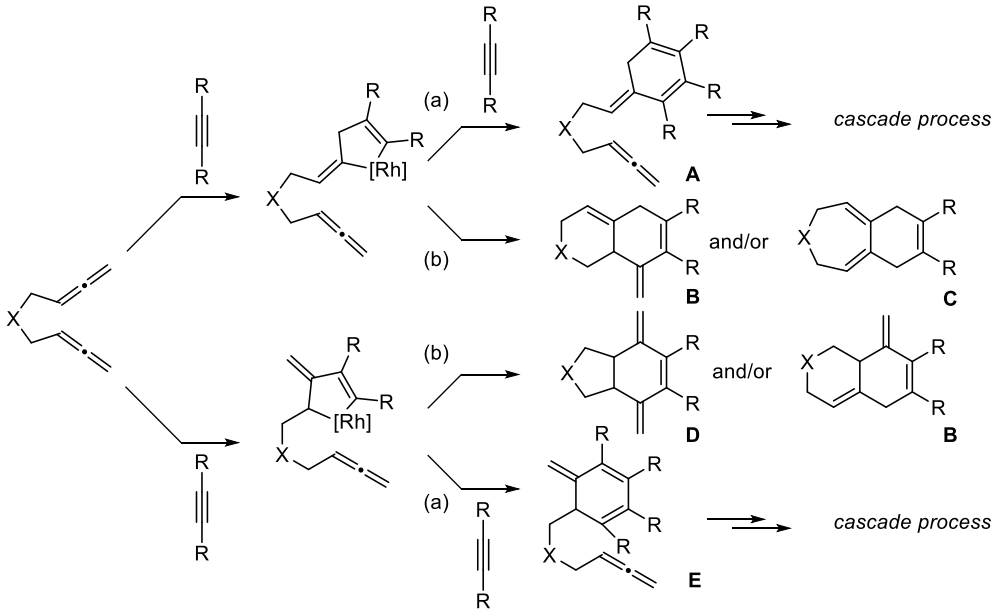

Scheme 5.1. Possible reaction outcomes from the rhodium-catalyzed [2+2+2] cycloaddition of 1,5-bisallenes and alkynes.

As starting point, we decided to study the reaction between the *N*-tosyl-tethered 1,5-bisallene **1a** and the dimethyl acetylenedicarboxylate (DMAD) **2n**. Our first attempts consisted in employing a 10 mol % mixture of the cationic rhodium complex $[Rh(cod)_2]BF_4$ with a set of different phosphine and bisphosphine-based ligands (shown in **Figure 5.1**), in THF/CH_2Cl_2 4:1 at 40 ºC (see **Table 5.1**). The use of BINAP, Tol-BINAP, BIPHEP, DPEphos, Xantphos and XPhos resulted in the production of undefined products and complex mixtures in low quantities (entries 1–6, **Table 5.1**). Nonetheless, the formation of a new product was observed when we switched to the Segphos-type family ligands, with the (*R*)-DTBM-Segphos producing the largest

amount of the new compound **7an** (entries 7–10, **Table 5.1**). Along with the new product **7an**, the cyclotrimerization adduct of DMAD, **8n**, was also observed in a significant 8 % yield at 40 °C with the (*R*)-DTBM-Segphos (entry 9, **Table 5.1**). Performing the reaction at room temperature prevented its formation without any detrimental effect on the amount of **7an**, yet to be identified.

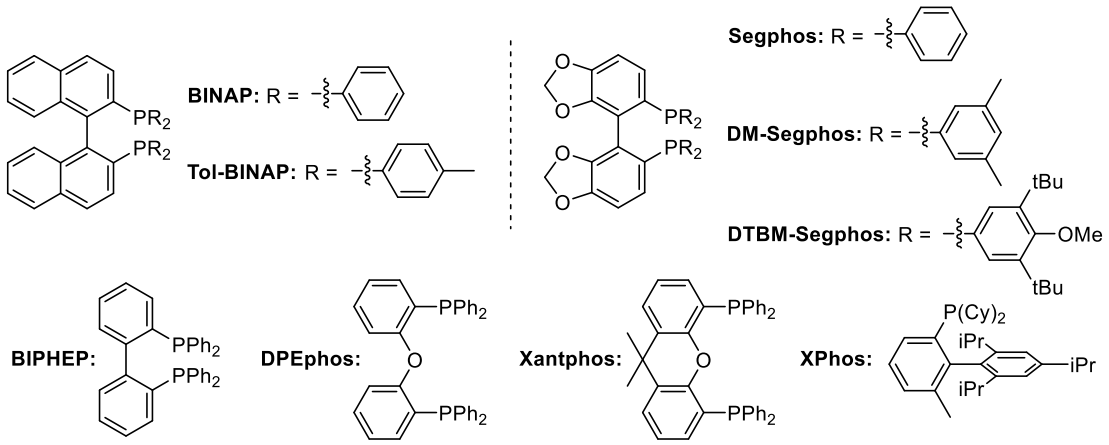

Figure 5.1. Phosphine ligands used in the ligand screening of the rhodium-catalyzed [2+2+2] cycloaddition of 1,5-bisallene **1a** and DMAD **2n**.

Table 5.1. Ligand screening for the rhodium-catalyzed [2+2+2] cycloaddition of 1,5-bisallene **1a** and DMAD **2n**.[a]

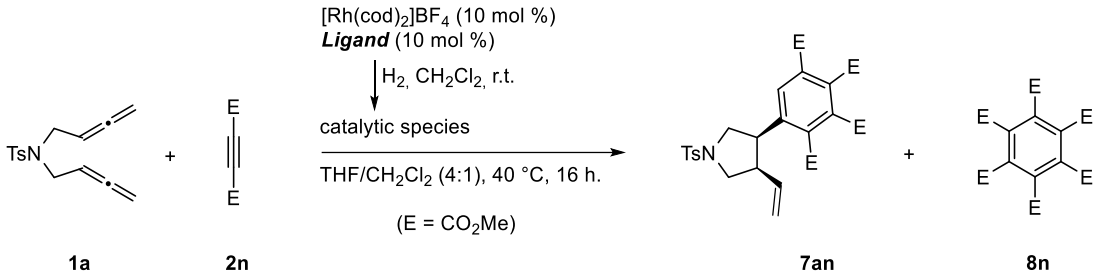

Entry	Ligand	Yield 7an / 8n (%)
1	BINAP	0 / 0
2	Tol-BINAP	0 / 0
3	BIPHEP	0 / 0
4	DPEphos	0 / 0
5	Xantphos	0 / 0
6	XPhos	0 / 0
7	Segphos	10 / 0
8	DM-Segphos	14 / 0
9	(*R*)-DTBM-Segphos	57 / 8
10[b]	(*R*)-DTBM-Segphos	56 / traces

[a] Reaction conditions: 0.09 mmol of **1a** ([**1a**] = 9 mM), 50 equiv. of **2n**, 10 mol% of $[Rh(cod)_2]BF_4$ and phosphine in 10 mL of THF/CH_2Cl_2 (4:1) at 40 ºC (unless indicated) for 16 h. The 10 mol% mixture of $[Rh(cod)_2]BF_4$ and phosphine was treated with hydrogen in dichloromethane (CH_2Cl_2) solution for catalyst activation prior to substrate addition. [b] Reaction carried out at room temperature.

The ESI-MS spectra of the new compound **7an** rapidly revealed that it was formed by reaction of one molecule of the 1,5-bisallene **1a** and two molecules of DMAD. Therefore, neither of the products **B**, **C** or **D** in **Scheme 5.1** were formed in the reaction. In addition, the ^{1}H-NMR unveiled the presence of a single aromatic proton (apart of the two doublets of the tosyl group aromatic protons), at δ = 7.94 ppm, which discards a possible cascade reaction from **E**, as an aromatic ring from a further reaction would be fully substituted. Taking this into account, exhaustive analysis of the 1D and 2D NMR data allowed us to propose a structure for **7an**. The presence in the ^{1}H-NMR of four non-equivalent signals for the methyl moieties of the DMAD (δ = 3.81, 3.84, 3.92 and 3.93), together with the aromatic proton, are consistent with the construction of an aromatic ring (**Figure 5.2**).

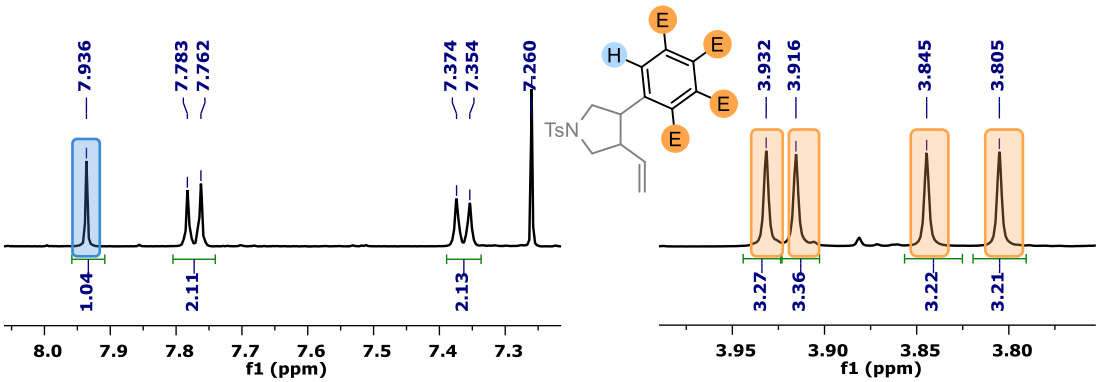

Figure 5.2. ^{1}H-NMR chemical shifts constructing the aromatic ring of **7an**.

A vinyl moiety was then elucidated by COSY and HSQC, one proton as a multiplet at δ = 5.19 – 5.30 ppm, coupled with two terminal protons, as doublets with *trans* and *cis* coupling constants (**Figure 5.3**).

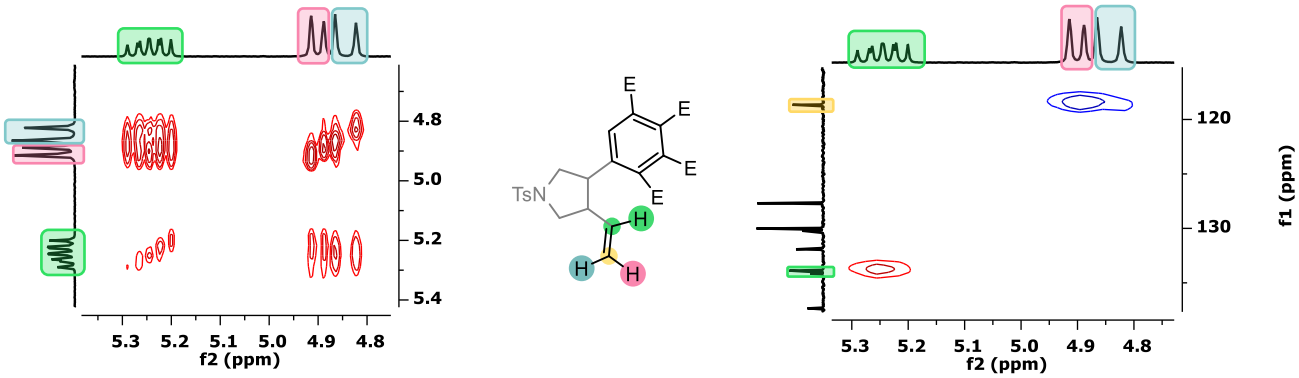

Figure 5.3. 2D COSY (left) and edited HSQC (right) of the vinyl moiety.

Following analysis of the COSY, and the chemical shifts, allowed to construct the proposed vinylpyrrolidine scaffold connected to the aromatic ring. The structure of **7an**, as well as the *cis* diastereoselectivity, was further confirmed by single crystal X-Ray crystallographic analysis (CCDC 2098127, **Figure 5.4**).

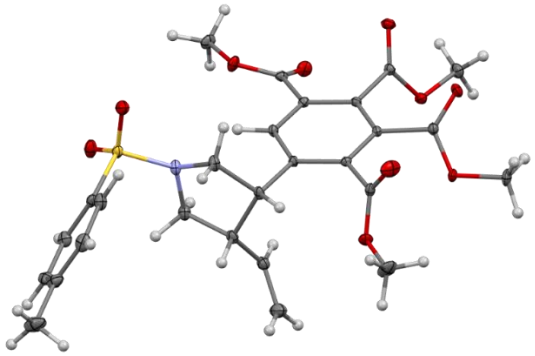

Figure 5.4. ORTEP representation of **7an** at 50% of probability level (CCDC 2098127).

The development of new methods to construct vinylpyrrolidine derivatives is of great interest in medicinal and synthetic organic chemistry, as pyrrolidine cores are widely found in drug fragments.[108] Furthermore, the vinyl substituent in the heterocyclic moiety can be further functionalized or may impart interesting physico-chemical properties. Therefore, as we were very interested in exploring this new cyclization process in depth, we proceeded to optimize the reaction conditions (**Table 5.2**).

First, different solvents were tested (entries 1–6, **Table 5.2**). Whereas the use of the initial mixture THF/CH_2Cl_2 4:1 provided the highest amount of **7an**, using CH_2Cl_2 and THF independently, resulted in either low yield or no production of the desired product **7an**. Other halogenated solvents, such 1,2-dichloroethane gave comparable results to CH_2Cl_2. The strong coordinating solvent CH_3CN or the toluene/CH_2Cl_2 mixture 4:1 were also tested, but no improvement in the production of **7an** was observed. We then evaluated the influence of the quantity of DMAD and the concentration of **1a** (entries 7–11, **Table 5.2**). Reducing the equivalents of DMAD from 50 to 40 resulted in lower yield of **7an**. In another attempt to reduce the amount of DMAD, we increased the concentration of **1a** up to 36 mM reducing the equivalents of DMAD to 25 equiv., but no improvement was observed either. The nature of the counterion was also evaluated using the neutral complex $[Rh(cod)Cl]_2$ together with silver and sodium salts (entries 12–14, **Table 5.2**). Slightly larger anions, as hexafluoroantimoniate and hexaflorophosphate resulted in slightly lower production of **7an**, whereas the yield of **7an** was significantly reduced to 27 % with the very bulky borate anion $BArF^-$. Wilkinson's catalyst was also tested but only starting materials were recovered (entry 15, **Table 5.2**). We also attempted to reduce the catalyst load to 5 %, but the yield was drastically reduced to 24 % (entry 16, **Table 5.2**). Finally, a control experiment with the absence of the catalytic mixture resulted in recovery of the starting materials, demonstrating the role of the rhodium and the (*R*)-DTBM-Segphos in the cyclization process. Therefore, the optimal reaction conditions for the upcoming studies were set as [**1a**] = 9 mM, DMAD **2n** (50 equiv.), $[Rh(cod)_2]BF_4$ (10 mol%), (*R*)-DTBM-Segphos (10 mol%) in THF/CH_2Cl_2 4:1 at room temperature for 16 hours (entry 7, **Table 5.2**).

Table 5.2. Reaction conditions optimization for the rhodium-catalyzed [2+2+2] cycloaddition of 1,5-bisallene **1a** and DMAD **2n**[a]

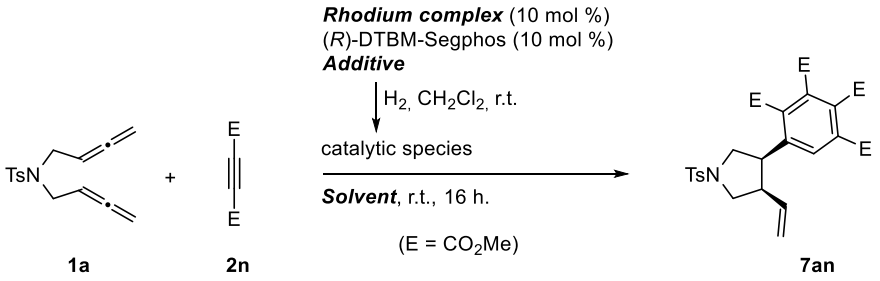

Entry	[Rh] complex	Additive	Solvent	[1a] mM	2n (equiv.)	Yield 7an (%)[b]
1	$[Rh(cod)_2]BF_4$	-	THF/CH_2Cl_2 4:1	9	10	20
2	$[Rh(cod)_2]BF_4$	-	CH_2Cl_2	9	10	7
3	$[Rh(cod)_2]BF_4$	-	THF	9	10	No rx.
4	$[Rh(cod)_2]BF_4$	-	CH_3CN	9	10	10
5	$[Rh(cod)_2]BF_4$	-	$Toluene/CH_2Cl_2$ 4:1	9	10	8
6	$[Rh(cod)_2]BF_4$	-	1,2-DCE	9	10	6
7	**$[Rh(cod)_2]BF_4$**	**-**	**THF/CH_2Cl_2 4:1**	**9**	**50**	**56[c]**
8	$[Rh(cod)_2]BF_4$	-	THF/CH_2Cl_2 4:1	9	40	41[c]
9	$[Rh(cod)_2]BF_4$	-	THF/CH_2Cl_2 4:1	18	50	50
10	$[Rh(cod)_2]BF_4$	-	THF/CH_2Cl_2 4:1	36	50	51
11	$[Rh(cod)_2]BF_4$	-	THF/CH_2Cl_2 4:1	36	25	32
12	$[Rh(cod)Cl]_2$	$AgSbF_6$	THF/CH_2Cl_2 4:1	9	50	45
13	$[Rh(cod)Cl]_2$	$AgPF_6$	THF/CH_2Cl_2 4:1	9	50	39
14	$[Rh(cod)Cl]_2$	NaBArF	THF/CH_2Cl_2 4:1	9	50	27
15[d]	$[Rh(PPh_3)_3Cl]$	-	THF/CH_2Cl_2 4:1	9	50	No rx.
16[e]	$[Rh(cod)_2]BF_4$		THF/CH_2Cl_2 4:1	9	50	24
17[d]	-	-	THF/CH_2Cl_2 4:1	9	50	No rx.

[a] Unless otherwise noted: reaction conditions: 0.09-0.018 mmol of **1a**, 50 equiv. of **2n**, 10 mol% mixture of the rhodium(I) complex and (*R*)-DTBM-Segphos in 5-20 mL of the indicated solvent at room temperature for 16 h. The 10 mol% catalytic mixture was treated with hydrogen in dichloromethane (CH_2Cl_2) solution for catalyst activation prior to substrate addition. [b] Yields calculated by ^{1}H-NMR using mesitylene as internal standard. [c] Isolated yield. [d] Reaction performed without (*R*)-DTBM-Segphos. [e] Load of the catalytic mixture reduced to 5 mol %.

The scope of the reaction was then evaluated with diverse sulfonamide-tethered 1,5-bisallenes **1b**–**1h** (**Scheme 5.2**). The desired derivatives **7** were successfully obtained with a set of aryl sulfonamides bearing substituents of different electronic demand in the *para* and *ortho* positions (**7an**, **7bn** and **7en**). Alkyl sulfonamide-tethered 1,5-bisallenes **1g** and **1h** were also active in the process, affording **7gn** and **7hn** in 51 and 23 % yield respectively. However, the pyridine sulfonamide-tethered 1,5-bisallene **1f** did not afford the desired product **7fn**, probably due to the presence of a strong coordinating nitrogen atom that might poison the rhodium catalyst.

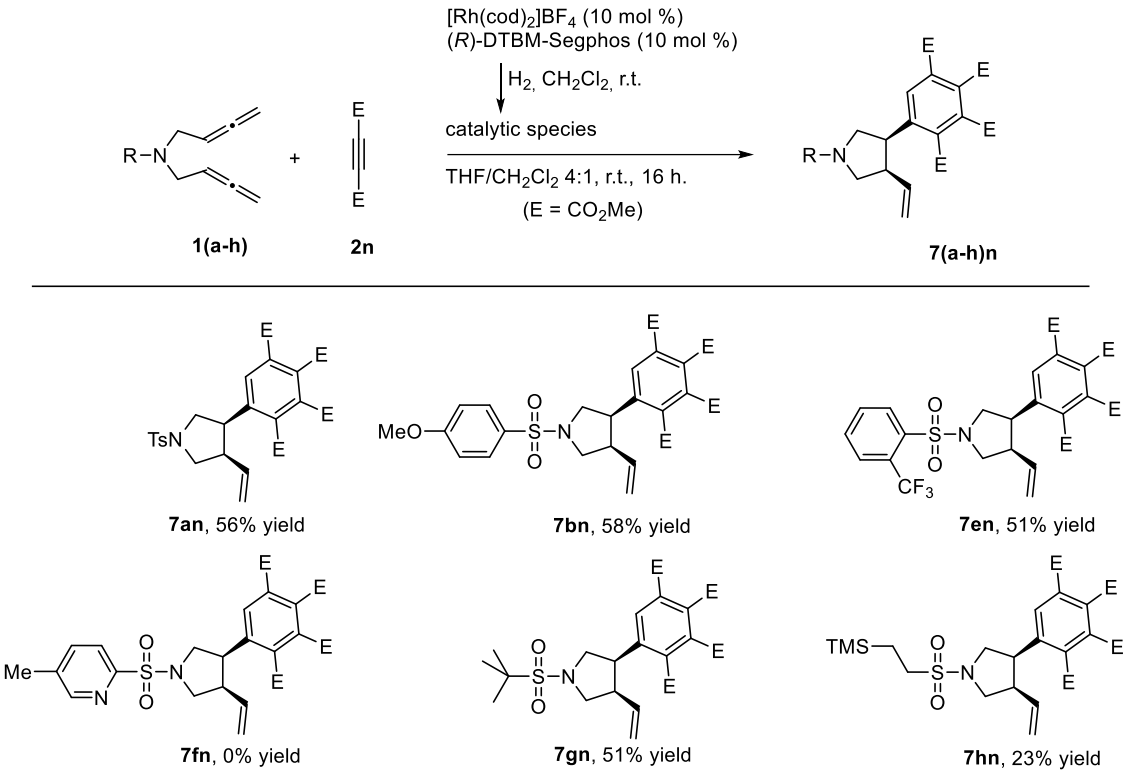

Scheme 5.2 Scope of the sulfonamide-tethered 1,5-bisallenes **1a** – **1h**.

To broaden the scope of this cyclization towards the synthesis of *cis*-3,4-arylvinylcyclopentanes, a set of carbon-tethered 1,5-bisallenes were tested (**Scheme 5.3**).

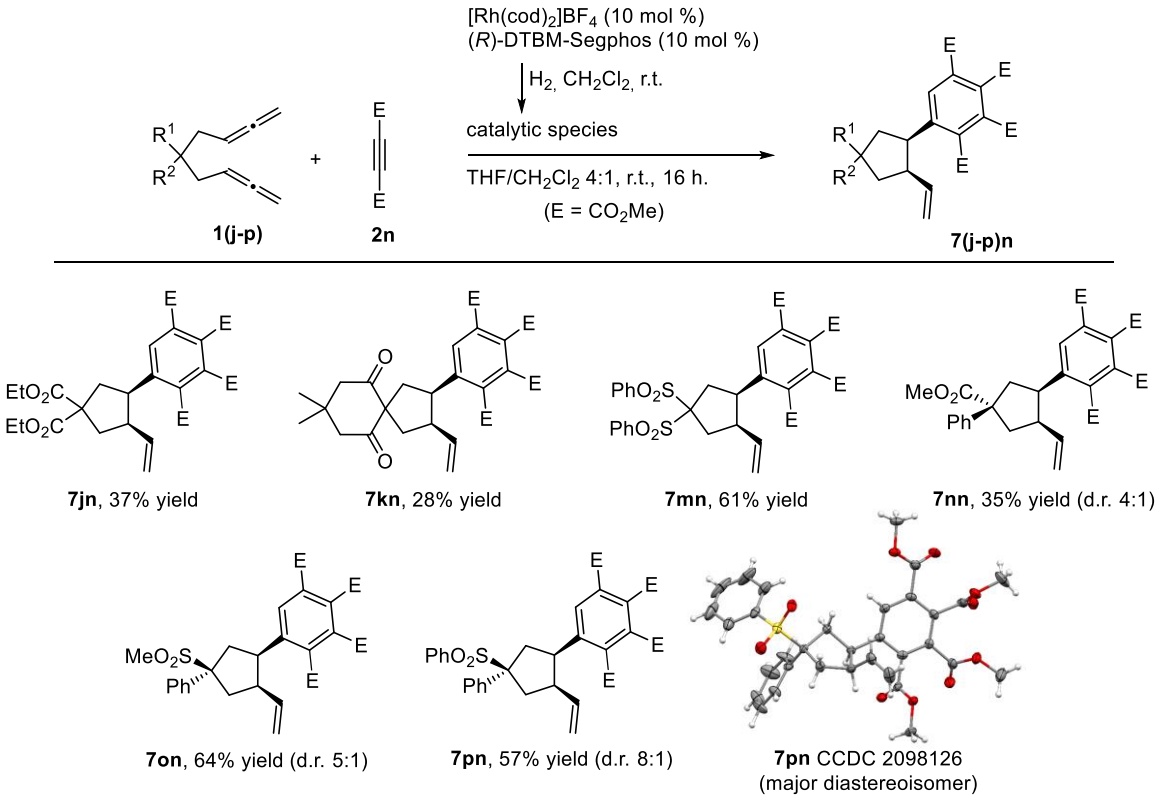

Scheme 5.3. Scope of the carbon-tethered 1,5-bisallenes **1j** – **1p**.

Substrates bearing a carbonyl moiety adjacent to the quaternary carbon atom of the tether of the 1,5-bisallenes, produced derivatives **7jn**, **7kn**, and **7nn** in moderate yields. In contrast, the substitution of the carbonyl for an alkyl- or an arylsulfonyl group, resulted in better yields, producing **7mn**, **7on** and **7pn** in 61, 64 and 57 % yields, respectively.

In addition, as **1n**, **1o** and **1p** are pro-chiral 1,5-bisallenes, derivatives **7nn**, **7on** and **7pn** were obtained as a mixture of diastereoisomers, and its diastereoisomer ratio was calculated by ^{1}H-NMR spectroscopy (**Figure 5.5**).

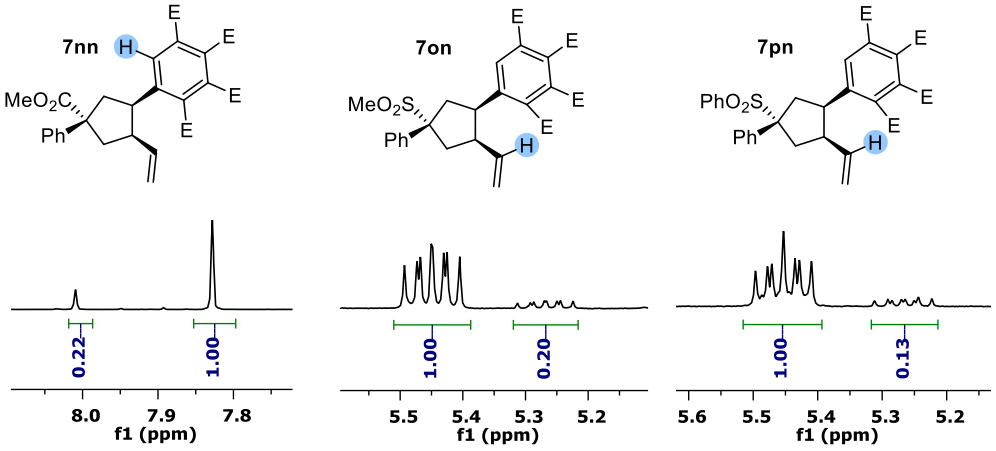

Figure 5.5. Diastereoisomer ratios of **7nn**, **7on** and **7pn** in the ^{1}H-NMR spectra. Major diastereoisomers drawn (E = CO_2Me).

The assignment of the major and minor diastereoisomers was determined by NOESY experiments. The NOE contacts between the two *cis*-protons of the cyclopentane with the aromatic protons from the tether, allowed us to identify the major and the minor diastereoisomers of **7nn** and **7on** (**Figure 5.6** and **5.7**, respectively). For **7nn**, the NOE contacts were not observed for the major diastereoisomer, but increasing the intensity of the NOESY signals revealed the expected NOE contacts in the minor diastereoisomer.

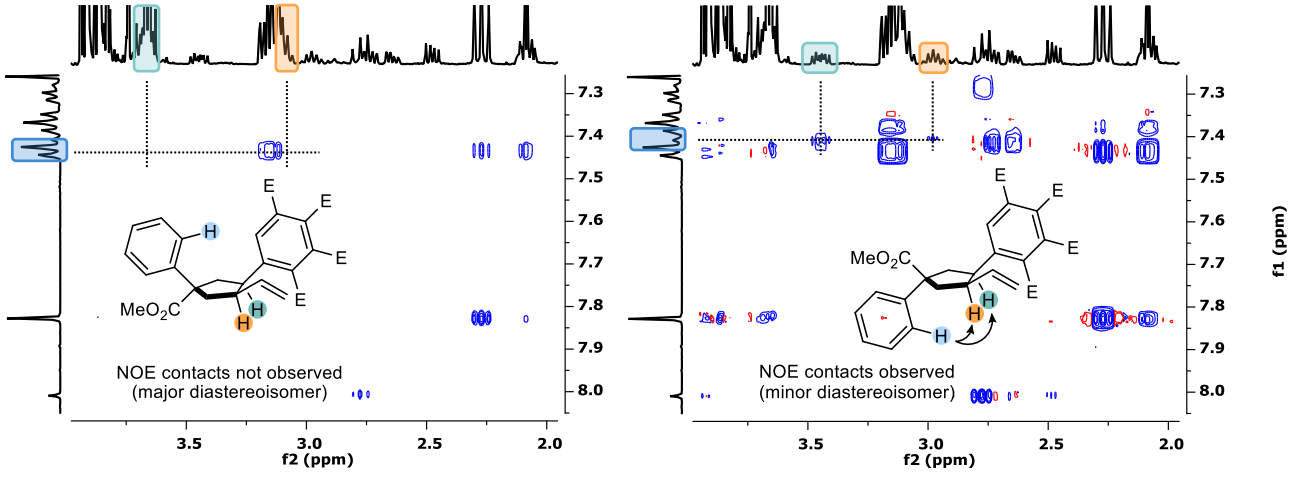

Figure 5.6. NOESY experiments of **7nn** (left and right, same spectra with different signal intensity) that allow the identification of the major and minor diastereoisomers (E = CO_2Me).

On the other hand, for **7on** the NOE contacts were observed in the signals of the major diastereoisomer.

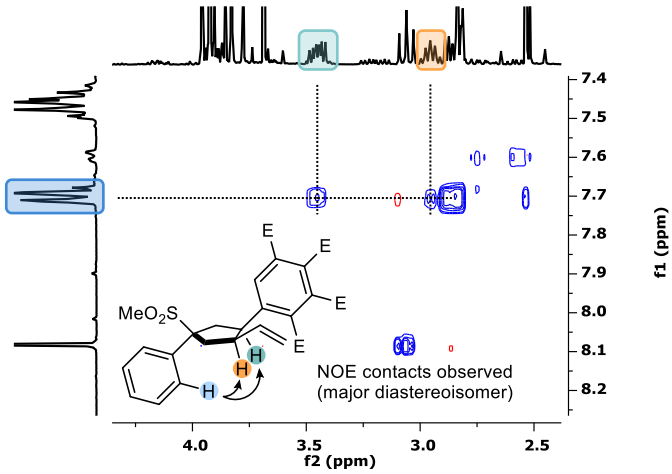

Figure 5.7. NOESY experiments of **7on** that allow the identification of the major and minor diastereoisomers (E = CO_2Me).

As opposite to this, the diastereoisomers of derivative **7pn** could not be identified using this method, as the aromatic protons in both substituents of the tether are not distinguishable by NMR, and the stereochemistry of the major diastereoisomer was confirmed by X-ray crystallographic analysis (**Scheme 5.3**, CCDC 2098126).

To further extend the scope of the reaction, diverse disubstituted alkynes were evaluated with the *N*-tosyl-tethered 1,5-bisallene **1a**. However, the reaction was found to be limited to the dimethyl acetylenedicarboxylate **2n**, as the use of other type of alkynes, such as diphenylacetylene, 2-butyne-1,4-diol, ethyl phenylpropiolate, or di-*tert*-buthyl acetylenedicarboxylate, led alkyne cyclotrimerization products or undefined complex mixtures.

Nonetheless, the desired derivatives **7** were obtained when we moved to monosubstituted alkynes (**Scheme 5.4**). Surprisingly, the reaction was completely regioselective when the propargyl alcohol **2o** was used, producing only the 2,4-regioisomer in 56 % yield. On the other hand, the use of the methyl propiolate **2p** led to a mixture of three regioisomers (**7ap**$^{2\text{-}4}$, **7ap**$^{2\text{-}5}$ and **7ap**$^{3\text{-}5}$) in 35 % overall yield.

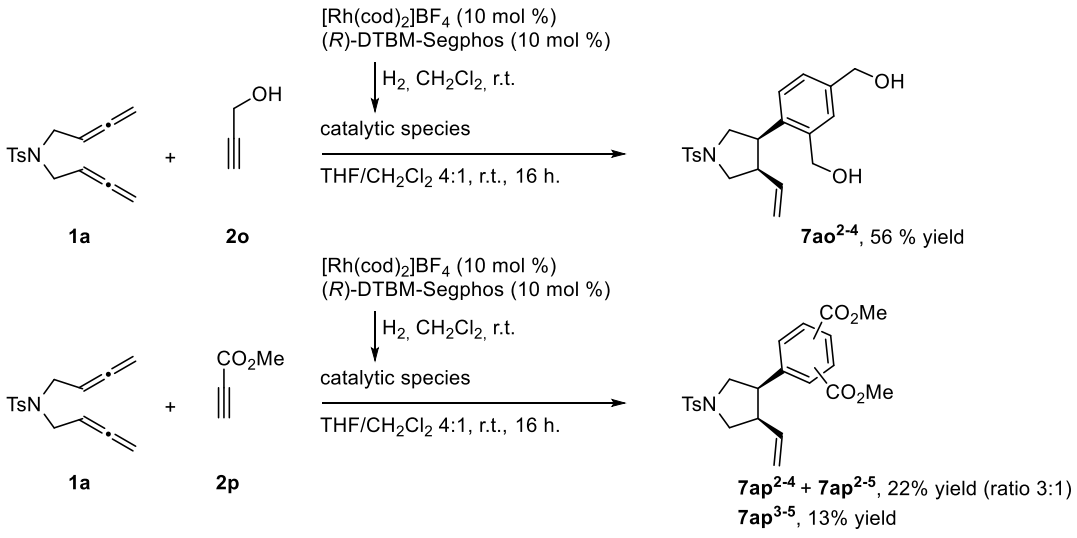

Scheme 5.4. Scope of the monosubstituted alkynes **2o** and **2p** with the 1,5-bisallene **1a**.

The ^{1}H-NMR spectroscopy confirmed the formation of only one regioisomer of **7ao**, which was identified with 2D NMR NOESY experiment (**Figure 5.8**). At first, the isomer **7ao**$^{3\text{-}5}$ was discarded due to the lack of symmetry in the signals from the aromatic ring. Then, the NOE contact between a pair of *ortho* aromatic protons with the two protons next to the nitrogen atom in the pyrrole ring (NOE_a in **Figure 5.8**), together with the NOE contact of the aromatic –C**H**$_2$OH with one of the *cis*-protons of the pyrrole (NOE_b, in **Figure 5.8**), are only compatible with regioisomer **7ao** $^{2\text{-}4}$, as **7ao** $^{2\text{-}5}$ and **7ao** $^{3\text{-}4}$ cannot present both contacts, NOE_a and NOE_b.

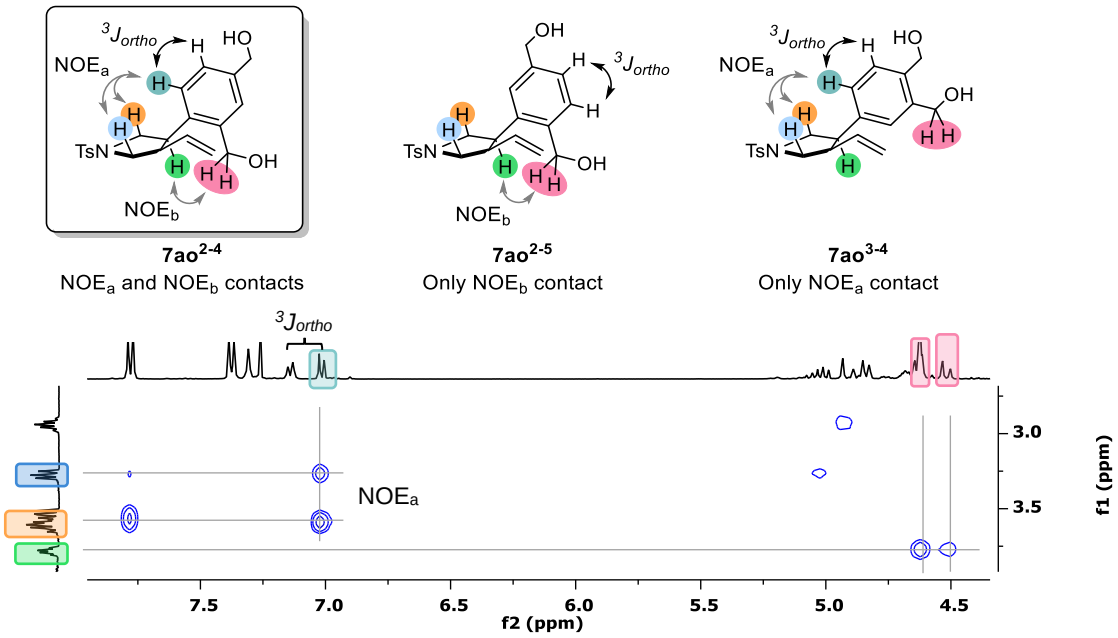

Figure 5.8. 2D NMR NOESY experiment with the key NOE contacts for the identification of the 2,4-regioisomer of **7ao**$^{2\text{-}4}$.

At this point, we proceeded to evaluate the process computationally to gain further understanding of the reaction mechanism. The Gibbs energy profiles computed at 298K and 1 atm at M06L−D3/ccpVTZ-PP/SMD (76% THF, 24% CH_2Cl_2)//B3LYP−D3/ccpVDZ-PP level of theory are shown in **Figure 5.9** and **Figure 5.10**. To reduce computational costs, the ligand (*R*)-Segphos was chosen as the model bisphosphine ligand instead of the optimal (*R*)-DTBM-Segphos (see Chapter 8, section **8.1.3** for a complete description of the computational methods).

The first part of the mechanism consists in a classical [2+2+2] cycloaddition. The reaction starts with the coordination equilibrium of one molecule of DMAD (**A1**) or 1,5-bisallene (**A1'**) with the rhodium complex, with the formation of **A1** as the most exergonic process, releasing 14.6 kcal·mol^{-1}. From **A1**, either a second molecule of DMAD or one of the distal double bonds of the allene can coordinate to the rhodium center. The incorporation of the second DMAD unit gives **A2** at cost of 3.7 kcal·mol^{-1}. On the other hand, two different orientations for the 1,5-bisallene coordination generate **A2'** or **A2''**, at cost of 4.5 and 6.4 kcal·mol^{-1}, respectively. For the following oxidative cyclometalation, the new C–C bond can be formed in either the terminal or the central carbon atom of the allene. Since **A1**, **A2**, **A2'** and **A2''** are all in equilibrium, according

to the Curtin–Hammett principle[109] the major rhodacyclopentene intermediate should come from the lowest energy transition state, which is the Csp^2–Csp^3 bond formation from the orientation **A2'** (**TS^1(A2'A3)**, $\Delta G^{\neq}$ = 11.4 kcal·mol^{-1}) giving the rhodacyclopentene intermediate **A3**. This step **A1→A3** is exergonic by 26.8 kcal·mol^{-1}.

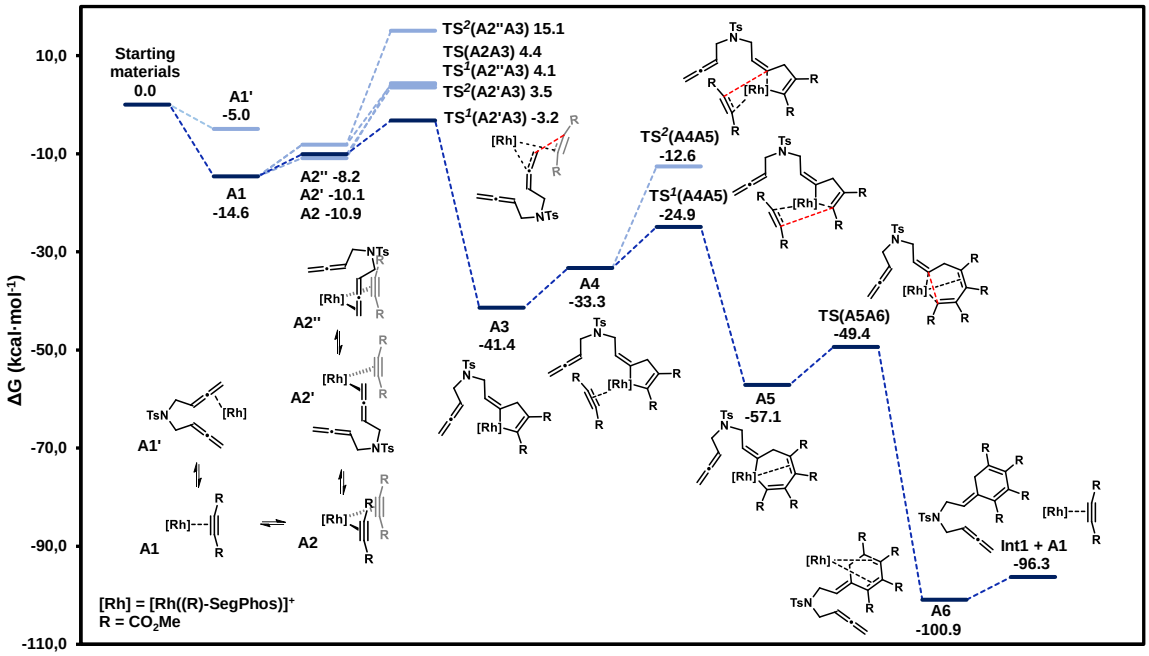

Figure 5.9. Gibbs energy profile (in kcal · mol^{-1}) for the [2+2+2] cycloaddition of 1,5-bisallene **1a** and dimethyl acetylenedicarboxylate (DMAD) **2n** leading to **Int1**. Reprinted with permission from Vila, J.; Vinardell, R.; Solà, M.; Pla-Quintana, A.; Roglans, A. *Adv. Synth. Catal.* **2022**, *364*, 206. Copyright 2021 Wiley-VCH Verlag GmbH & Co. KGaA, Weinheim.

The coordination of DMAD to **A3** gives **A4**, a 16-electron square-pyramidal complex. The upcoming alkyne insertion (Schore mechanism[40]) occurs in the equatorial Rh–C bond to produce the conjugated rhodacycloheptadiene **A5** through **TS^1(A3A4)**, overcoming a Gibbs energy barrier of 16.5 kcal·mol^{-1}. This step is exergonic by 15.7 kcal·mol^{-1}. Reductive elimination from **A5** leads to intermediate **A6** (**TS(A5A6)**, $\Delta G^{\neq}$ = 7.7 kcal·mol^{-1}), releasing 43.8 kcal·mol^{-1} in the process. **A6** has a distorted square-planar geometry in which the two endocyclic double bonds are η^4-coordinated to the rhodium center (d_{Rh-C} = 2.317, 2.136, 2.216 and 2.275 Å). Intermediate **A6** can now release the catalyst to give the [2+2+2] cycloadduct **Int1** and reinitiate the [2+2+2] catalytic cycle, or rearrange into **A6^s**, an 18-electron complex, to start a tandem reaction (**Figure 5.10**). In **A6^s**, one of the oxygen atoms of the carboxylate is coordinated to the rhodium center (d_{Rh-O} = 2.219 Å), and the exocyclic double bond and the internal double bond of the allene are both η^2-coordinated to the rhodium center. The oxidative cyclometalation of this intermediate leads to the *syn*-fused rhodacyclopentane **A7**. The combined Gibbs energy barrier for the rearrangement and the oxidative cyclometalation (**TS^{s}A6A7**) is 25.8 kcal·mol^{-1} and is slightly endergonic by 2.4 kcal·mol^{-1}. Alternatively, the transition state leading to the *anti*-fused rhodacyclopentane has a higher energy barrier of 27.2 kcal·mol^{-1} (**TS^{a}A6A7**). From that point, **A7** easily rearranges into **A7'** to create an agostic Rh – H interaction (d_{Rh-H} = 1.74Å), getting predisposed for the following β-hydride elimination to generate **A8**. This step has a low Gibbs energy barrier of 1.9 kcal·mol^{-1}

(**TS(A7'A8)**) and releases 8.4 kcal·mol^{-1}. Finally, reductive elimination of **A8** gives **A9** through **TS(A8A9)**, surpassing a Gibbs energy barrier of 7.4 kcal·mol^{-1} and releasing 19.6 kcal·mol^{-1}. Subsequent release of the catalyst leads to **7an** and completes the catalytic cycle.

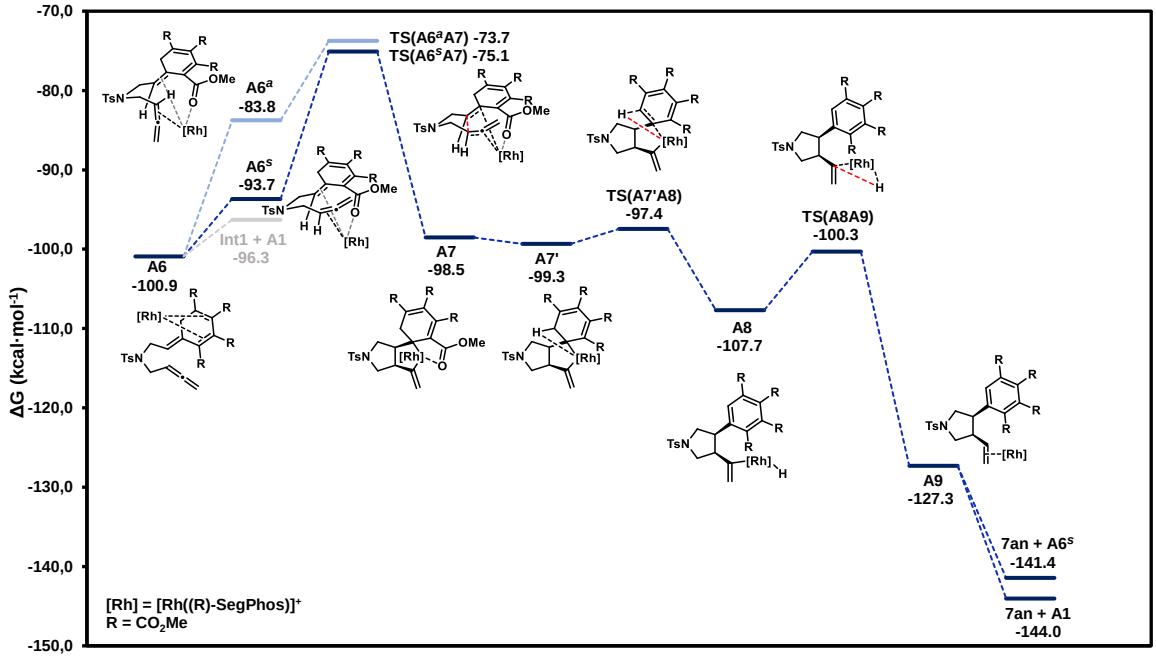

Figure 5.10. Gibbs energy profile (in kcal · mol^{-1}) for the cycloisomerization of **Int1** leading to **7an**. Reprinted with permission from Vila, J.; Vinardell, R.; Solà, M.; Pla-Quintana, A.; Roglans, A. *Adv. Synth. Catal.* **2022**, *364*, 206. Copyright 2021 Wiley-VCH Verlag GmbH & Co. KGaA, Weinheim.

Additionally, it did not escape to our attention that the exocyclic double bond in **A6** can isomerize to give an aromatic derivative (**Scheme 5.5**). However, it was found that this process has a high energy barrier of 29.5 kcal·mol^{-1}, and thus, is not likely to occur (**Figure 5.11**).

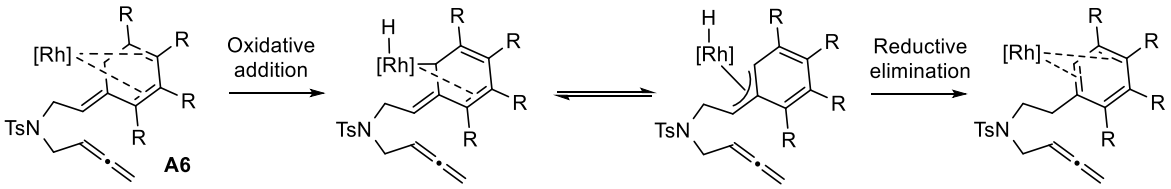

Scheme 5.5. Alternative path leading to the exocyclic double bond isomerization from **A6**.

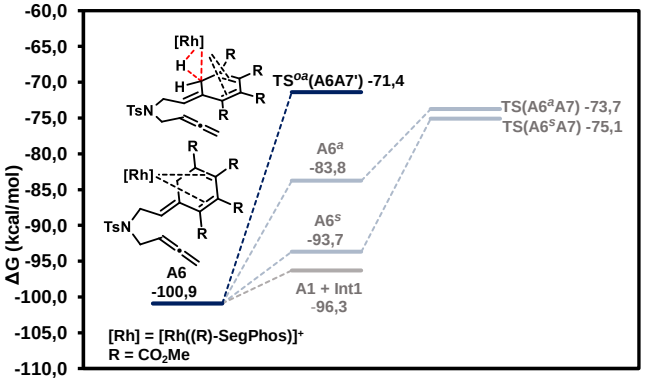

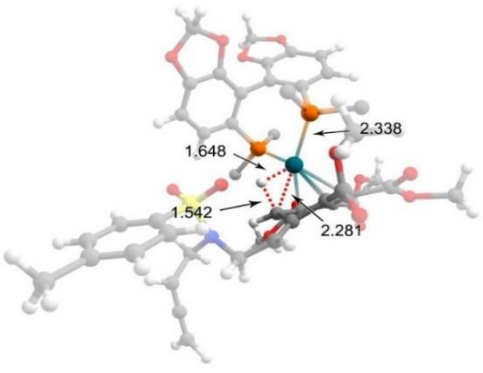

To sum up, the complete reaction mechanism that transforms the 1,5-bisallene **1a** and DMAD **2n** into **7an** (depicted in **Scheme 5.6**), has an overall reaction energy of –129.4 kcal·mol^{-1} ($\Delta G = G_{\mathbf{7an}} - [G_{\mathbf{1a}} + 2 \cdot G_{\mathbf{2n}}]$). The overall process has an energetic span between the turnover frequency (TOF) determining intermediate (TDI, **A6**) and the TOF determining transition state (TDTS, **TS^{s}(A6A7)**) of 25.8 kcal·mol^{-1}.[93]

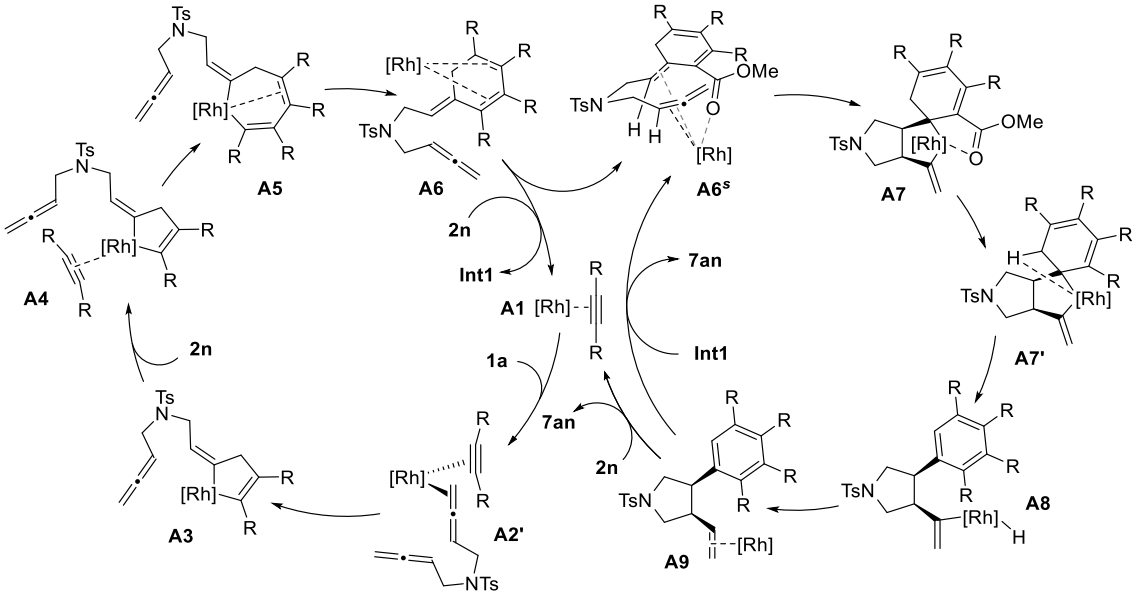

Scheme 5.6. Catalytic cycle for the cascade cyclization reaction of 1,5-bisallene **1a** and dimethyl acetylenedicarboxylate **2n** leading to **7an**. Reprinted with permission from Vila, J.; Vinardell, R.; Solà, M.; Pla-Quintana, A.; Roglans, A. *Adv. Synth. Catal.* **2022**, *364*, 206. Copyright 2021 Wiley-VCH Verlag GmbH & Co. KGaA, Weinheim.

To obtain experimental evidence of the proposed mechanism, we carried out the reaction with the 1,5-bisallene **1a-*d*$_4$**, deuterated in the terminal positions (**Scheme 5.7**). According to the proposed mechanism, a deuterium atom should get incorporated in the internal carbon atom of the vinyl moiety through a *β*-hydride elimination (**A6**, **A7'**, and **A8** are drawn in **Scheme 5.7** to better illustrate the process). Performing the reaction under the optimized conditions, the expected product **7an-*d*$_4$** was obtained in a 26 % yield.

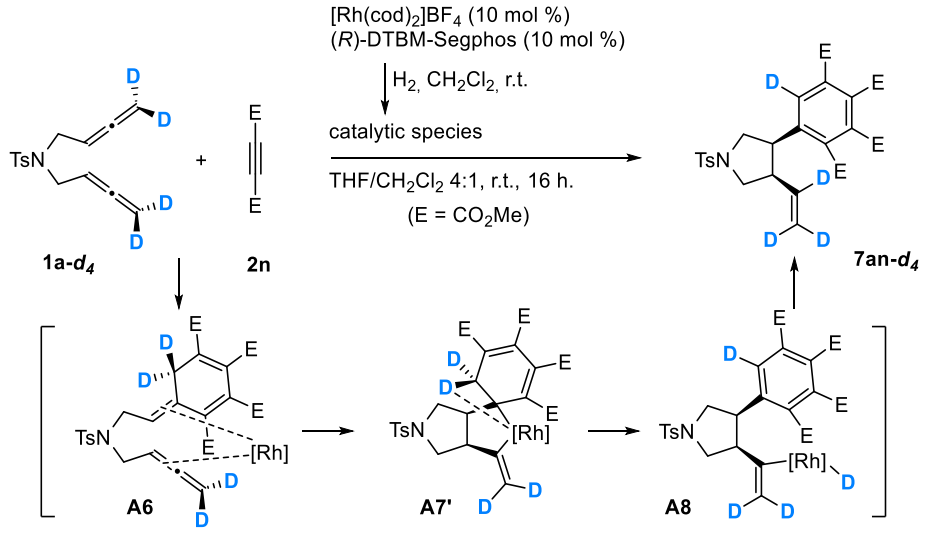

Scheme 5.7. Deuterium-labelling experiment for the cascade reaction of 1,5-bisallene **1a-*d*$_4$** and **2n** (E = CO_2Me).

The composition of the deuterated product was confirmed by ESI-HRMS (m/z = 586.1647 for $[M+H]^+$) and characterized by ^{1}H-NMR spectroscopy. As shown in **Figure 5.12**, comparing the ^{1}H-NMR of **7an** and **7an-*d*$_4$** clearly shows the absence of the vinylic and the aromatic protons signals for **7an-*d*$_4$**. In addition, the multiplicity of the allylic proton changed from an apparent quintuplet to an apparent quadruplet.

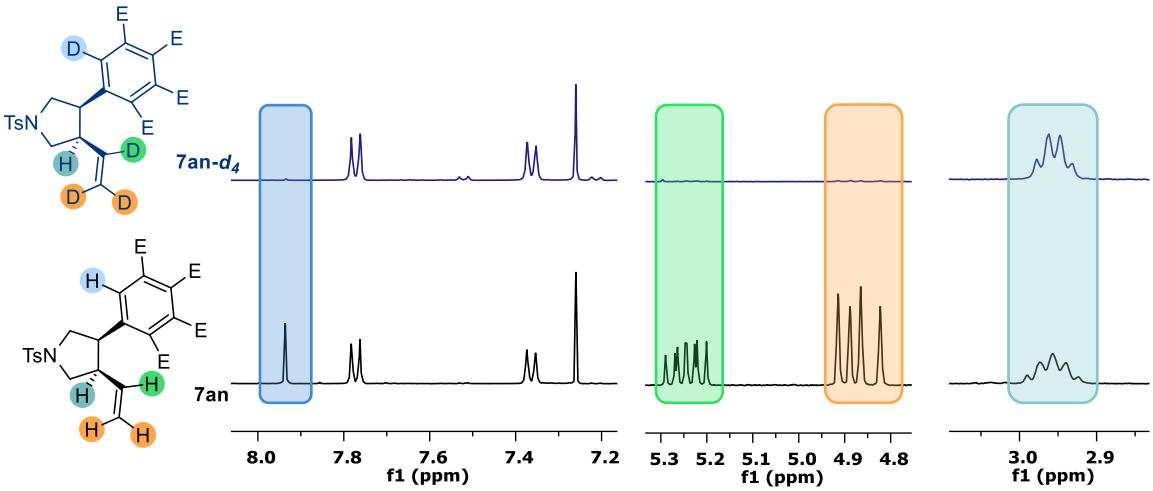

Figure 5.11. Comparison of the ^{1}H-NMR spectra of **7an-*d*$_4$** (above), and **7an** (below) (E = CO_2Me).

To prove the potential synthetic capabilities of this rhodium-catalyzed tandem process, several further transformations of **7an** were accomplished (**Scheme 5.8**). The vinyl moiety of the pyrrolidine derivative **7an** was both hydrogenated and epoxidated. For the hydrogenation, H_2 was bubbled at atmospheric pressure in the presence of Pd/C as a catalyst, affording the corresponding derivative **9** in quantitative yield. The epoxidation was carried out by adding meta-chloroperbenzoic acid at 0 ºC, after stirring for 48 h at room temperature product **11** was obtained with an excellent 75 % yield as a 3:1 diastereomeric mixture. The structure of the major isomer was identified by X-ray diffraction analysis (CCDC 2098128).

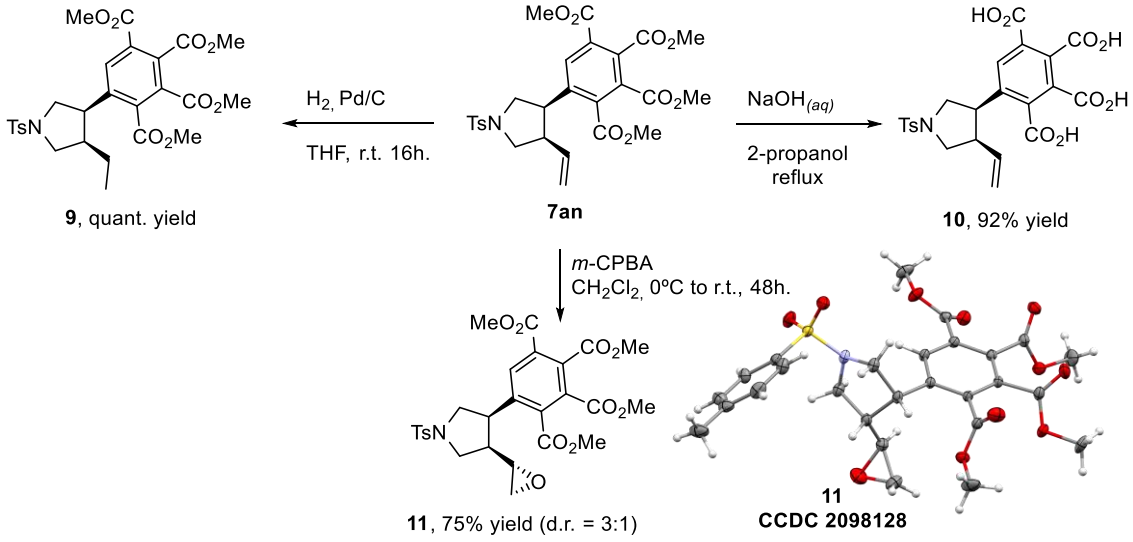

Scheme 5.8. Further transformations of **7an.**

Finally, the hydrolysis of the four ester groups was performed using an aqueous solution of sodium hydroxide in 2-propanol under reflux conditions. The tetra acid derivative **10** was obtained in an excellent 92 % yield. This process habilitates the generation of dianhydride derivatives for the preparation of polyamide polymers, which are used in membrane technology.[110] In addition, dianhydride monomers together with the vinyl motif could produce cross-linked polymers with interesting properties.

In summary, we have developed a diastereoselective method for the rapid construction of *cis*-3,4-arylvinyl pyrrolidine and cyclopentane derivatives through a new rhodium-catalyzed cascade process involving 1,5-bisallenes and alkynes. The complete mechanism of this transformation has been rationalized by DFT calculations and experimental procedures. The global process encompasses a Rh-catalyzed [2+2+2] cycloaddition between two units of alkyne and one unit of allene, followed by a Rh-catalyzed cycloisomerization reaction involving the second allene unit in the molecule affording the disubstituted arylvinylcyclic derivative.

Chapter 6. Rh(I) complexes with hemilabile thioether-functionalized NHC ligands as catalysts for [2+2+2] cycloaddition of 1,5-bisallenes and alkynes

---

Published in: *ACS Catal.* **2023**, *13*, 3201.

Authors: Vila, J.; Solà, M.; Achard, T.; Bellemin-Laponnaz, S.; Pla-Quintana, A.; Roglans, A.

The selectivity of the reactions involving 1,5-bisallenes can be controlled by fine-tuning the catalytic system. Herein, we report a completely chemo- and diastereoselective rhodium(I)-NHC catalyzed [2+2+2] cycloaddition reaction of 1,5-bisallenes with one molecule of dimethyl acetylenedicarboxylate to afford *trans*-fused 5/6-membered scaffolds with two exocyclic double bonds. DFT calculations have been used to elucidate the mechanism and to understand the role of the thioether functionality of the NHC ligand, which has been found to facilitate both the oxidative cyclometalation and the reductive elimination by a dynamic chelating effect.

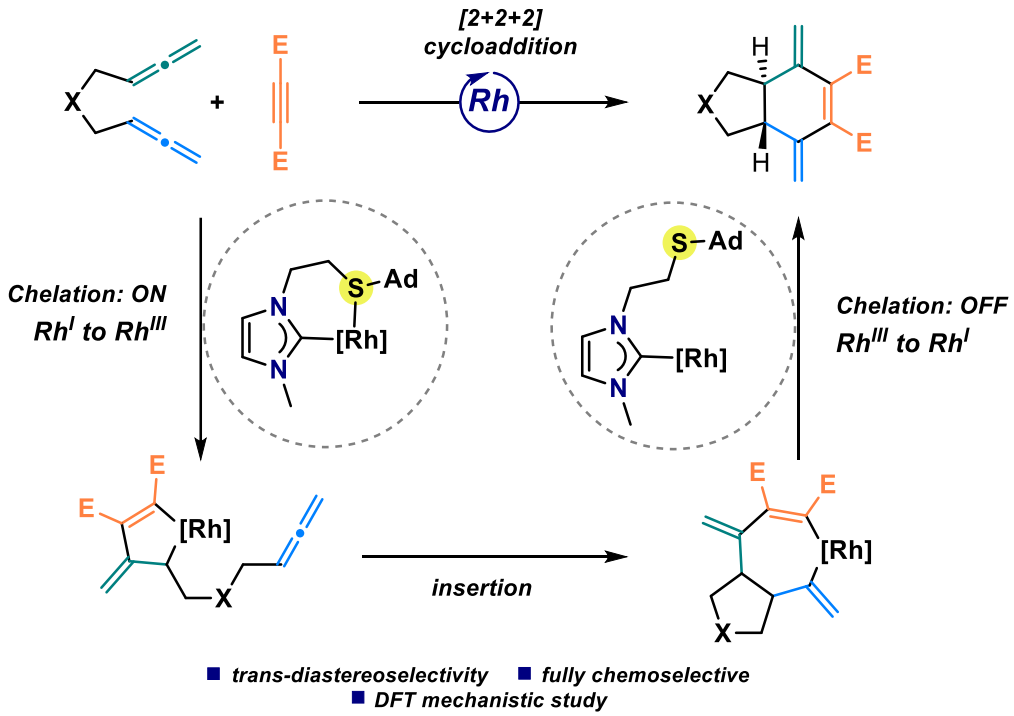

During this thesis, we have seen the importance of the coordination environment around the metal in favoring disparate reaction outcomes in cycloaddition reactions of 1,5-bisallenes. For instance, when Ma *et al.*[87] used the *trans*-[Rh(CO)(PPh_3)$_2$Cl] in the presence of 1,5-bisallenes, a dimerization process involving a rhodium-catalyzed [2+2+2] cycloaddition/DA produced steroidal scaffolds (**Scheme 6.1a**). In contrast, when we[111] used the [Rh(cod)Cl]$_2$ in combination with the bisphosphine ligand (*R*)-DTBM-Segphos and $NaBArF_6$, spirocyclic compounds were obtained through rhodium-catalyzed cycloisomerization of 1,5-bisallenes followed by a DA homodimerization (**Scheme 6.1b**). Furthermore, the addition of an alkene in the reaction mixture avoided the DA homodimerization in favor of the formation of dihydroazepine and dihydrooxepine derivatives (**Scheme 6.1c**).[105] On the other hand, the addition of an alkyne led to the diastereoselective formation of *cis*-3,4-arylvinyl pyrrolidines and cyclopentanes through a fully rhodium-catalyzed cascade process,[112] encompassing a [2+2+2] cycloaddition reaction between the external doble bond of one allene of the 1,5-bisallene and two molecules of dimethyl acetylenedicarboxylate, followed by a cycloisomerization reaction involving internal double bond of the remaining allene (**Scheme 6.1d**).

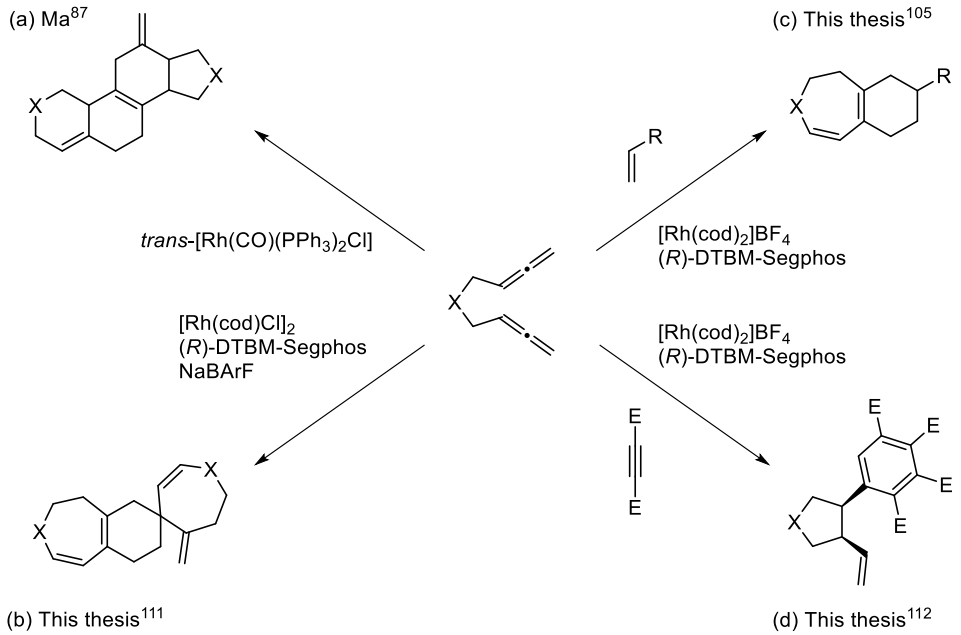

Scheme 6.1. Disparate reaction outcomes in cycloaddition reactions of 1,5-bisallenes.

Still with the idea of developing a [2+2+2] cycloaddition reaction involving the two allene moieties of 1,5-bisallenes, we thought of testing ligands other than bisphosphines to drastically change the coordination environment and electronics of the rhodium center. With this aim, we set out a collaboration project with Dr. Thierry Achard and Dr. Stéphane Bellemin-Laponnaz from the DMO (Departement du Matériaux Organiques) group at the IPCMS (Institut de Physique et de Chimie des Matériaux) in Strasbourg (France). Within the framework of this collaboration, I carried out a three-month predoctoral stay in their laboratories. The DMO group has experience in the synthesis of phosphine-based and *N*-heterocyclic carbene (NHC) ligands and the study of their applications in catalysis.

In this chapter, a variety of phosphine, SPO (secondary phosphine oxide), and mono- and bidentate NHC ligands with diversified steric and electronic properties are evaluated with the aim of triggering a selective rhodium-catalyzed [2+2+2] cycloaddition of 1,5-bisallenes involving the two allene moieties and an alkyne towards the synthesis of adducts **A**, **B** or **C** in **Scheme 6.2**.

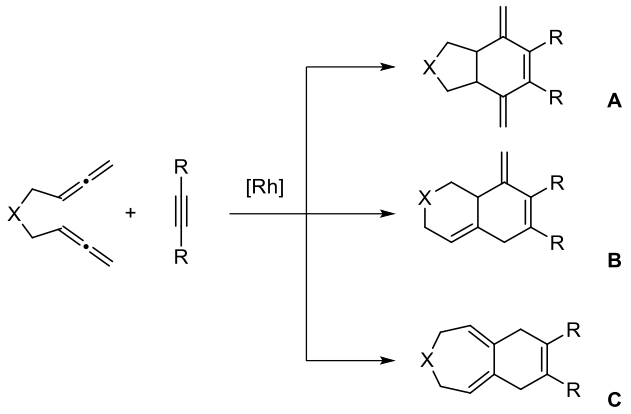

Scheme 6.2. Possible rhodium-catalyzed [2+2+2] cycloaddition products involving the two allene moieties and an alkyne.

Results and discussion

We started our study by analyzing the reaction of *N*-tosyl-tethered 1,5-bisallene **1a** and dimethyl acetylenedicarboxylate **2n** in the presence of a 10 mol % of the rhodium complex $[Rh(cod)_2]BF_4$ with a set of different monophosphines and bisphosphine ligands (**L1**-**L5**, **JohnPhos** and **CataCXium** shown in **Figure 6.1**) in THF/CH_2Cl_2 4:1, at 40 and 65 °C (**Table 6.1**).

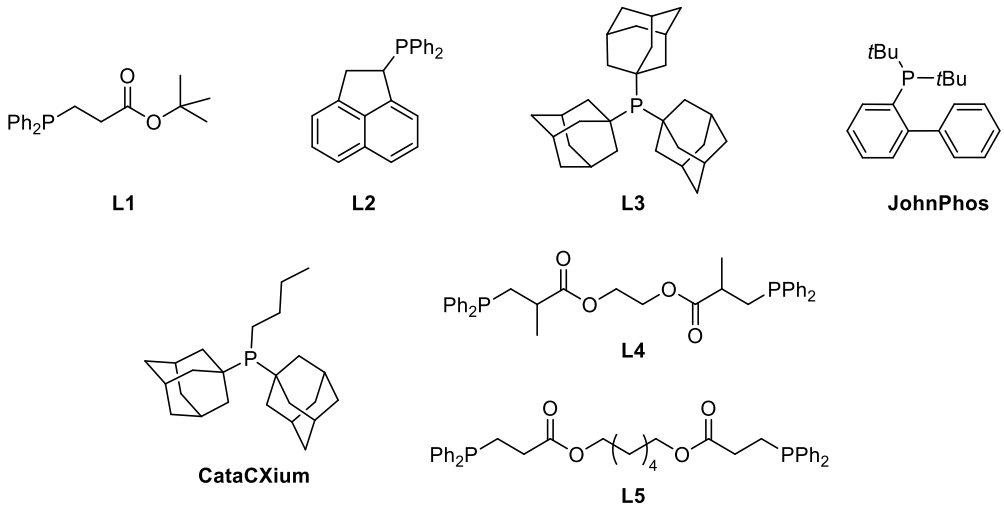

Figure 6.1. Mono- and bisphosphine ligands used in the screening.

Table 6.1. Mono- and bisphosphine ligand screening.[a]

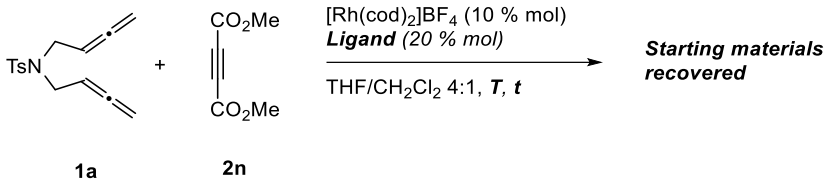

1a 2n

Entry	Ligand	T (ºC)	t (h)	Conversion (%)
1	L1	40	16	0
2	L2	40	16	0
3	L3	40	16	0
4	L3	65	4	0
5	JohnPhos	65	4	0
6	CataCXium	65	4	0
7[b]	L4	65	4	0
8[b]	L5	65	4	0

[a] Reaction conditions: 0.09 mmol of **1a** ([**1a**] = 9 mM), 5 equiv. of **2n**, 10 mol% of $[Rh(cod)_2]BF_4$ and 20 mol% of phosphine in 10 mL of THF/CH_2Cl_2 (4:1) at the indicated temperature and reaction time. [b] Reaction carried out with 10 mol % of the ligand.

Unfortunately, in all cases the starting 1,5-bisallene **1a** was recovered. The absence of catalytic activity was found to be caused by an undesired side reaction of the phosphine ligands with **2n**. Presumably, these phosphine ligands are in constant coordination equilibrium with the rhodium center as they lack chelating effect. Although **L4** and **L5** are bisphosphine ligands, their long chain between phosphines results in a low entropic contribution in favoring the chelation. The free phosphine (either unreacted or upon dissociation), nucleophilically adds into DMAD **2n** to produce diverse zwitterionic and neutral adducts (**Scheme 6.3**).[113]

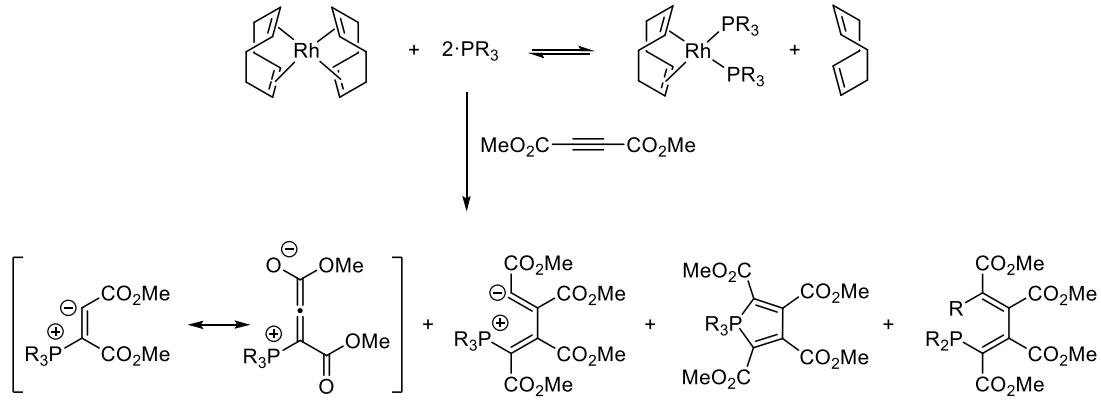

Scheme 6.3. Consumption of phosphine ligands by addition to dimethyl acetylenedicarboxylate **2n**.

To avoid the consumption of the phosphine ligand upon dissociation, we decided to switch to secondary phosphine oxides (SPOs), a lesser explored phosphorous-based ligands.[114] SPOs present a tautomeric equilibrium between their pentavalent form (SPO) and the trivalent phosphinous acid (PA). One of the characteristic advantages of SPOs compared to phosphines is their high air and moisture stability, as the

pentavalent form usually predominates. However, the PA tautomer can coordinate to metal centers, shifting the equilibrium towards the metal complex and act as an ordinary phosphine ligand. A particularity of these ligands is that they form hydrogen-bonded pseudo-chelated complexes upon coordination, which can be then transformed into completely chelated complexes, for instance by treatment with tetrafluoroboric acid (**Scheme 6.4**).[115]

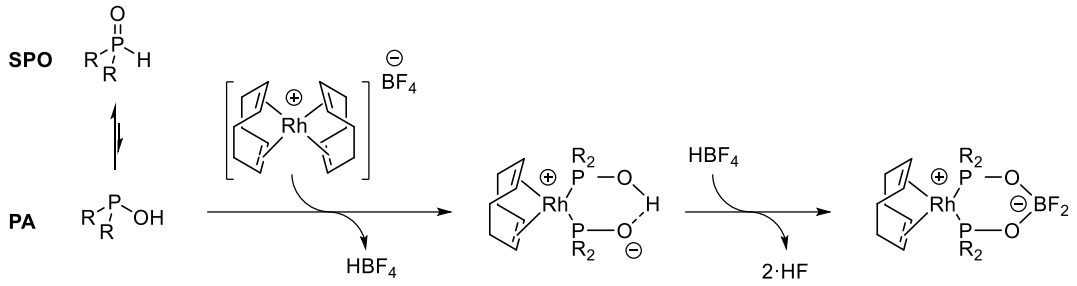

Scheme 6.4. Preparation of chelated rhodium complexes from SPOs.

Rhodium-SPO complexes have been successfully applied to the hydroformylation of linear olefins,[116] to the asymmetric hydrogenation of functionalized olefins,[117] and to the enantioselective hydroamination of allenes and alkynes.[118] For cycloaddition reactions involving SPO ligands, the examples are limited to the use of palladium and platinum, mostly in [2+1] cycloadditions.[119] Nonetheless, metal-SPO complexes have shown the ability to catalyze oxidative cyclometalations, as reported by Buono *et al.*[120] in a regio- and diastereoselective platinum-catalyzed tandem [2+1]/[3+2] cycloaddition, in which a platinacyclopentene was postulated to be formed during the process.

Considering this, we ran the reaction with 1,5-bisallene **1a** and DMAD **2n** using a 20 mol % of the SPO bis(4-methoxyphenyl)phosphine oxide (**L6**), in combination with 10 mol % of the rhodium complex $[Rh(cod)_2]BF_4$ in THF at 65 ºC for 120 minutes. The reaction resulted in low catalytic activity (observed via TLC), but rising the temperature to 100 ºC for an additional 16 hours, gave the *cis*-arylvinyl pyrrolidine derivative **7an**, already reported by us,[112] in 39 % yield along with the DMAD cyclotrimerization adduct **8n** and a new product, **12an**, in 19 % yield (**Scheme 6.5**).

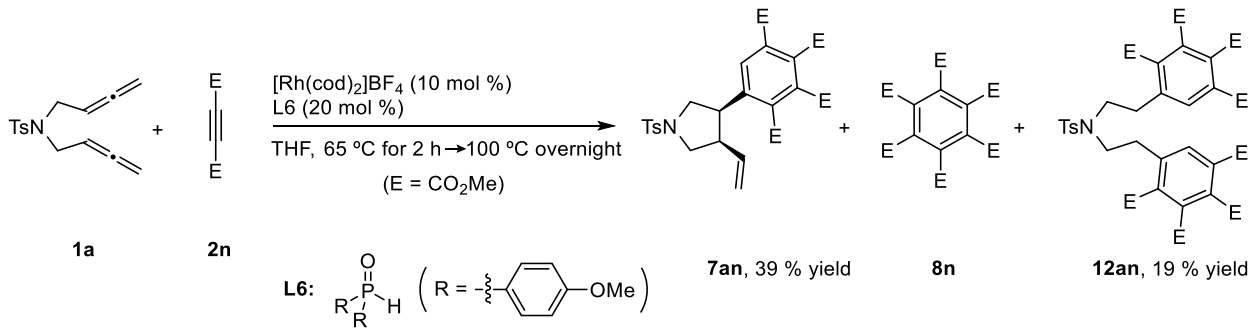

Scheme 6.5. Rhodium-SPO-catalyzed [2+2+2] cycloaddition reaction of 1,5-bisallene **1a** and DMAD **2n**.

Although this experiment proved the capacity of the Rh-SPO complex to catalyze [2+2+2] cycloaddition reactions, the selectivity observed towards the production of **7an** and **12an** was not of our interest, and thus, the use of the SPOs as ligand precursors was not further explored.

We then decided to explore *N*-heterocyclic carbenes (NHC). The use of NHC ligands have shown dramatic effects in rhodium-catalyzed transformations in terms of both reactivity and selectivity, which are often complementary to those of phosphines.[121] NHCs are strong σ-donor ligands, which can effectively stabilize electron-deficient metal species generated during a catalytic process. In addition, as NHCs form strong metal-ligand interactions, they can prevent the catalyst decomposition by the loss of the ligand under the reaction conditions. Moreover, NHCs are synthetically accessible and their steric and electronic properties are easily tuned by modifying either the nitrogen atom or the backbone substituents, making them very attractive for rapid ligand screening. Generally, NHCs are monodentate ligands although there is an increasing interest for the chemistry of functionalized NHC in which a Lewis base (often a N, P or O atom) is attached to the imidazolylidene ring.[122] Even though thioether-functionalized NHCs are less represented,[123] they are an interesting class of ligands as they can potentially provide an on-demand dynamic chelating effect for the metal complex during the catalytic cycle.[124] To the best of our knowledge, only two examples were reported for rhodium(I)-NHC-SR complexes, by Poli *et al*.[125] and Lassaletta *et al*.,[126] and none of them were applied to cycloaddition reactions.

Several examples are found in the literature of transition metal-catalyzed [2+2+2] cycloadditions with NHC ligands, mainly involving the use of nickel,[127] and in a lesser extent, the use of cobalt.[128] As regards to rhodium, there are only two previous examples in which NHC ligands were tested for the [2+2+2] cycloaddition reaction of alkynes, both reported by our group in either homogeneous[129] or heterogeneous[130] catalysis.

A couple of monodentate and a variety of bidentate NHC-imidazole precursors with different bite angles and binding modes were selected for its evaluation (shown in **Figure 6.2**). The various bidentate NHC-imidazole precursors differ in the substituent on the sulfur and the size of the thioether chain attached to the imidazolylidene ring. Both parameters influence the ability of the ligands to coordinate to the rhodium center, and thus, its hemilability. To evaluate these effects, groups with different steric hindrances and chain lengths were attached to the sulfur.

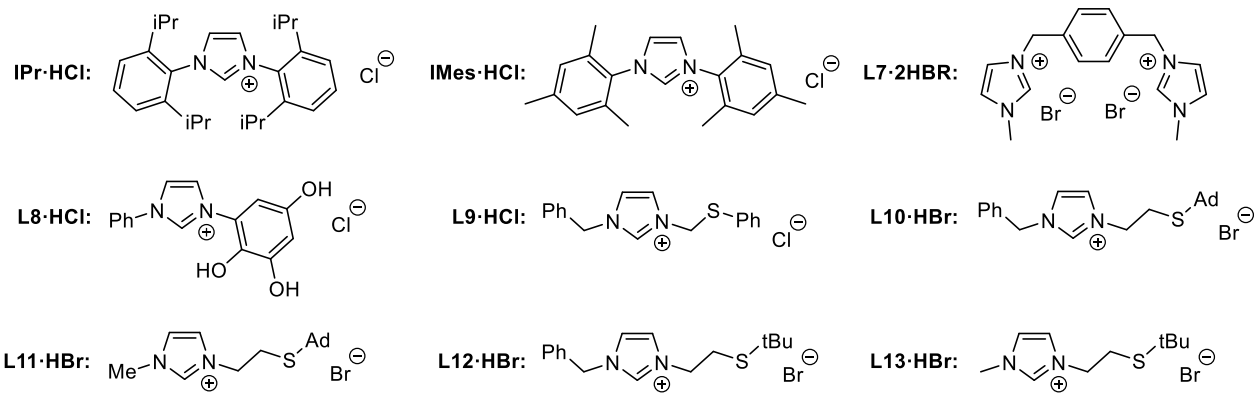

Figure 6.2. NHC precursors evaluated in the rhodium-catalyzed reaction of 1,5-bisallene **1a** and DMAD **2n**.

In the initial tests, the rhodium-NHC complexes were generated *in situ* by treatment of the corresponding imidazolium salt (NHC·HX) with *t*BuOK at -35 ºC in the presence of the rhodium complex using 1,2-dichloroethane as solvent (**Scheme 6.6**).

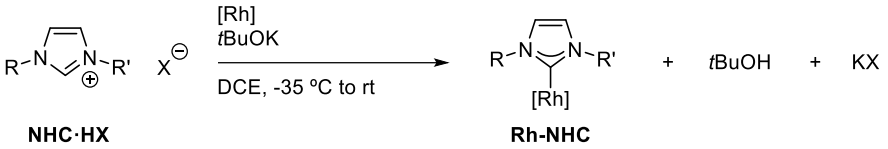

Scheme 6.6. *In situ* generation of the rhodium-NHC complexes.

First, we evaluated the use of the NHC ligand **IPr** (1,3-bis(2,6-diisopropylphenyl)imidazol-2-ylidene) with both the cationic $[Rh(cod)_2]BF_4$ and the neutral $[Rh(cod)Cl]_2$ complexes (**Scheme 6.7**). The reaction using the cationic $[Rh(cod)_2]BF_4$ gave a complex mixture of undefined products, while two products were detected with the dimeric rhodium complex $[Rh(cod)Cl]_2$ (**Scheme 6.7**). The product **13an**, was obtained as a diastereomeric mixture of *trans* and *cis* isomers, in a 23 % yield and 78:22 ratio. In addition, **3an** was obtained in a 13 % yield, which was found to come from our previously described cascade cycloisomerization/Diels–Alder process, acting the DMAD as a dienophile instead of an alkene.[105]

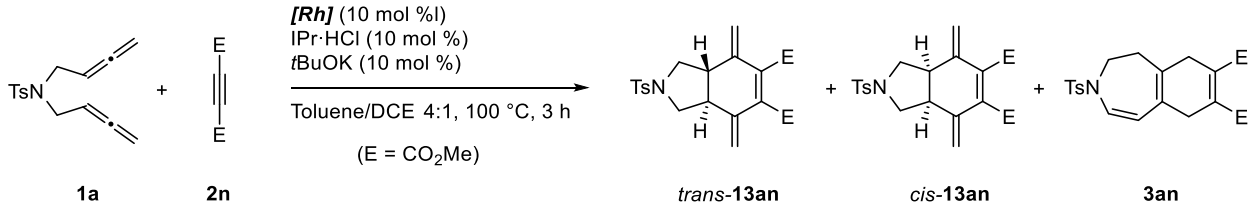

Rh complex	Yield 13an (*trans*:*cis*) / 3an (%)
$[Rh(cod)_2]BF_4$	Complex mixture
$[Rh(cod)Cl]_2$	23 (78:22) / 13

Scheme 6.7. Evaluation of the cationic and the neutral rhodium-IPr complexes for the reaction between 1,5-bisallene **1a** and DMAD **2n**.

The ESI-HRMS confirmed the formation of a 1:1 adduct of the 1,5-bisallene **1a** and the DMAD **2n**. The molecular structure of **13an** was identified by 1D and 2D NMR spectroscopy. The low number of signals in

the ^{1}H-NMR rapidly evidenced the formation of a symmetrical product. In addition, the presence of the two singlets at δ = 5.06 and 5.38 ppm and their integrations (**Figure 6.3**) are consistent with the presence of two equivalent exocyclic double bonds. Then, the information from the HSQC and the COSY gave us enough evidence to anticipate the formation of the [2+2+2] cycloadduct **A** of the **Scheme 6.2**. The molecular structure and the stereochemistry of the major diastereoisomer **13an**, which was found to be the *trans* isomer, were confirmed by X-ray crystallographic analysis (CCDC 2209948, **Figure 6.4**).

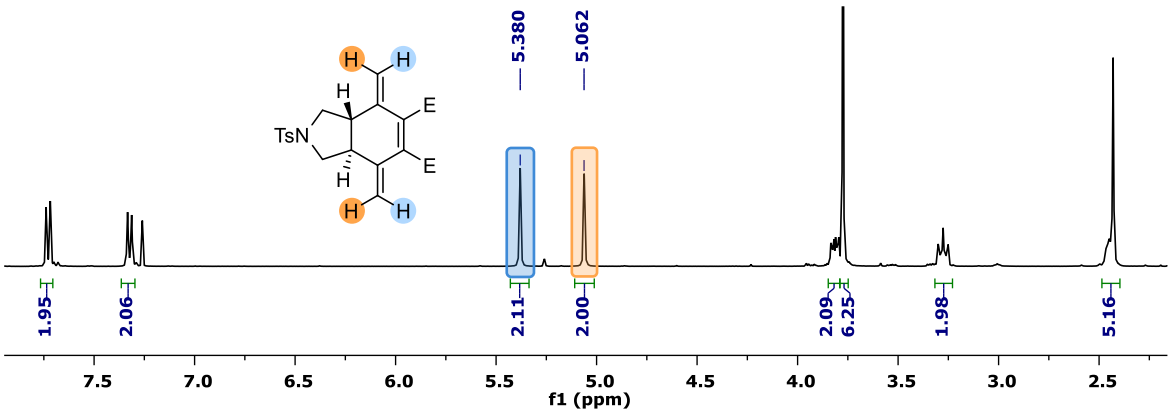

Figure 6.3. ^{1}H-NMR spectra of compound **13an**.

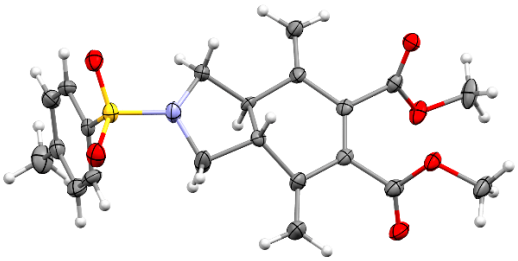

Figure 6.4. ORTEP representation of **13an** at 50% of probability level.

Encouraged by the selective formation of the [2+2+2] cycloadduct **13an** with the **Rh-IPr** complex, we decided to test other NHC ligands and optimize the reaction conditions towards the formation of *trans*-**13an** (**Table 6.2**). The monodentate NHC ligand **IMes** gave comparable results to **IPr** (entries 1 and 2, **Table 6.2**), this was not surprising as both ligands exhibit comparable electronic and steric properties.[131] We then decided to test bidentate NHCs. Neither the use of the large bite angle biscarbene **L7** nor the strong coordinating *OH*-functionalized **L8** improved the outcome (entries 3 and 4, **Table 6.2**), as slightly lower yields of **13an** and higher amounts of the *cis* isomer were obtained. However, switching to the *S*-functionalized NHCs resulted in considerable improvement on the yields (entries 5–10, **Table 6.2**). While the **L9** with the shortest chain resulted in a 35 % yield of **13an** in an 83:17 *trans:cis* ratio (entry 5, **Table 6.2**), the use of the **L10** with the flexible ethylene backbone gave **13an** in a 51% yield and better selectivity towards the *trans* isomer (entry 6, **Table 6.2**). Interestingly, performing the reaction at 80 ºC for two hours, drastically improved the yield of **13an** while maintaining the selectivity (entry 7, **Table 6.2**), suggesting that **13an** may undergo thermal decomposition at

100 ºC. Under these conditions, the steric and electronic effects of the thioether-functionalized **L11**–**13** were evaluated (entries 8–10, **Table 6.2**). Use of the ligand **L11** provided the best yield and selectivity towards the formation of **13an** (entry 8, **Table 6.2**), and was thus the ligand of choice for further optimization tests. Performing the reaction in toluene without DCE led to an improved *trans*:*cis* ratio and reduced the amount of **3an** (entry 11, **Table 6.2**). Reducing the concentration of the 1,5-bisallene **1a** from 18 mM to 9 mM resulted in similar yields and selectivities (entry 12, **Table 6.2**), whereas increasing the concentration from 18 mM to 36 mM suppressed the formation of **3an** (entry 13, **Table 6.2**) providing an excellent 76% yield of **13an** with a 93:7 *trans*:*cis* ratio. Finally, increasing or reducing the equivalents of DMAD **2n** did not improve the results (entries 14 and 15, **Table 6.2**).

Table 6.2. NHC ligand screening for the reaction of 1,5-bisallene **1a** and DMAD **2n**.[a]

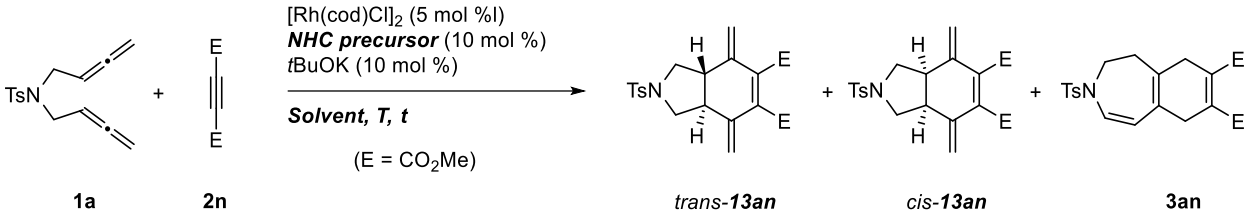

Entry	Rh complex	NHC	Solvent	T (ºC)	t (h)	[1a] (mM)	2a (equiv.)	Yield[b] (%) 13an (*trans*:*cis*) / 3an
1	$[Rh(cod)Cl]_2$	IPr	Toluene/DCE	100	3	18	5	23 (78:22) / 13
2	$[Rh(cod)Cl]_2$	IMes	Toluene/DCE	100	3	18	5	24 (75:25) / 5
3	$[Rh(cod)Cl]_2$	L7	Toluene/DCE	100	3	18	5	18 (55:45) / 9
4	$[Rh(cod)Cl]_2$	L8	Toluene/DCE	100	3	18	5	19 (47:53) / 9
5	$[Rh(cod)Cl]_2$	L9	Toluene/DCE	100	3	18	5	35 (83:17) / 4
6	$[Rh(cod)Cl]_2$	L10	Toluene/DCE	100	3	18	5	51 (86:14) / 10
7	$[Rh(cod)Cl]_2$	L10	Toluene/DCE	80	2	18	5	66 (86:14) / 13
8	$[Rh(cod)Cl]_2$	L11	Toluene/DCE	80	2	18	5	74 (89:11) / 8
9	$[Rh(cod)Cl]_2$	L12	Toluene/DCE	80	2	18	5	61 (87:13) / 8
10	$[Rh(cod)Cl]_2$	L13	Toluene/DCE	80	2	18	5	61 (90:10) / 7
11	$[Rh(cod)Cl]_2$	L11	Toluene	80	2	18	5	73 (93:7) / 4
12	$[Rh(cod)Cl]_2$	L11	Toluene	80	2	9	5	74 (92:8) / 6
13	**$[Rh(cod)Cl]_2$**	**L11**	**Toluene**	**80**	**2**	**36**	**5**	**76 (93:7) / 0**
14	$[Rh(cod)Cl]_2$	L11	Toluene	80	2	36	2	66 (91:9) / 8
15	$[Rh(cod)Cl]_2$	L11	Toluene	80	2	36	10	77 (92:8) / 0

[a] Reaction conditions (unless otherwise noted): 0.09 mmol of **1a** (at the indicated concentration), 5 equiv. of **2n**, 5 mol % of $[Rh(cod)Cl]_2$ and NHC/tBuOK (10 mol%) at the indicated solvent and temperature. [b] Yield and ratios calculated by NMR from the reaction crude using mesitylene as internal standard.

Having optimized the reaction conditions for the ligand, we then proceeded to prepare and isolate the rhodium complex with the NHC precursor **L11** to precisely tune the catalyst load. The NHC-rhodium(I) complex **Rh-L11** was prepared by the reaction of 2 equiv. of the imidazolium salt **L11** with 1 equiv. of the neutral

$[Rh(cod)Cl]_2$ in the presence of 2.2 equiv. of *t*BuOK in THF (**Scheme 6.8**) following a procedure described in the literature.[132] The **Rh-L11** complex was successfully obtained in a very satisfactory 95 % yield as a shiny yellow solid, which was fully characterized by Dr. Thierry Achard from the DMO group at the IPCMS.

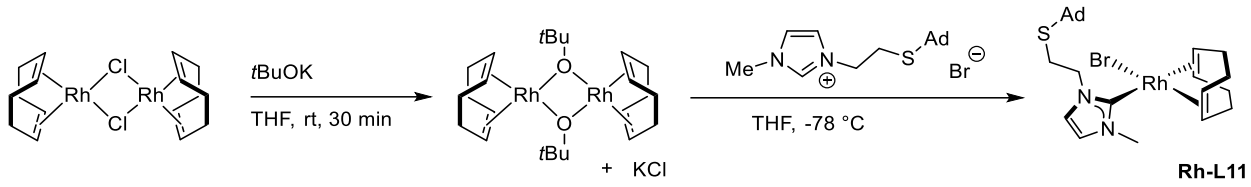

Scheme 6.8. Preparation of the NHC-rhodium(I) catalyst **Rh-L11** from the neutral rhodium complex $[Rh(cod)Cl]_2$ and the imidazolium salt **L11**.

Single crystals of the **Rh-L11** complex suitable for X-ray diffraction analysis confirmed the molecular structure of the complex (**Figure 6.5**). The rhodium-carbene distance was found to be within the range of other [Rh(cod)(imidazole-2-ylidene)Cl] complexes ($d_{Rh\text{-}C(1)}$ = 2.033 Å).[132,133] On the other hand, a strong *trans* influence of the NHC was observed in the complex, as Rh–C bond distances of the cyclooctadiene were significantly elongated in the relative *trans* position to the carbene ($d_{Rh\text{-}C(2)}$ = 2.207 Å, $d_{Rh\text{-}C(3)}$ = 2.227 Å) compared to those *trans* to the bromide ligand ($d_{Rh\text{-}C(4)}$ = 2.109 Å, $d_{Rh\text{-}C(5)}$ = 2.102 Å). The imidazol-2-ylidene ring was almost perpendicular to the coordination plane of the rhodium center (dihedral angle = 88.64 °), which was consistent with the ^{1}H NMR observation that the proton signals from the ethylene chain are not homotopic.

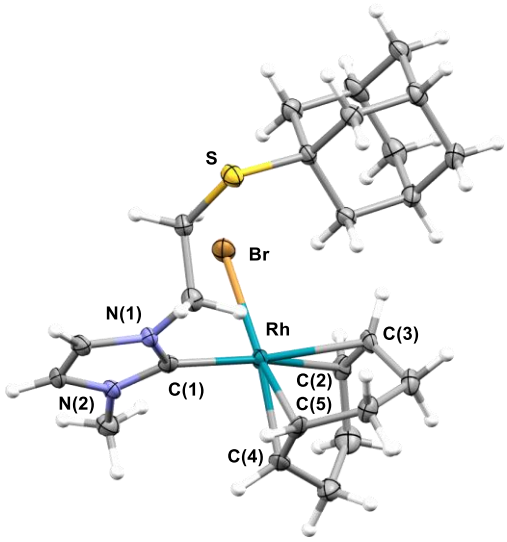

Figure 6.5. ORTEP representation of **Rh-L11** at 50% of probability level.

Once synthetized the **Rh-L11** complex, we ran different tests with catalysts loads ranging from 1 mol % to 10 mol % (**Table 6.3**). In all cases, the *trans*:*cis* ratio was maintained. Experiments with a catalyst load below 5 mol % resulted in lower yields of **13an** (entries 1–3, **Table 6.3**), while the use of 10 mol % of the **Rh-L11** complex did not improve the yield of **13an** when compared to the use of 5 mol %. Therefore, our set of optimized reaction conditions were defined as 1,5-bisallene **1a** ([**1a**] = 36 mM), **2n** (5 equiv.), **Rh-L11** (5 mol %) in toluene at 80 ºC for 2 h.

Table 6.3. Catalyst load optimization for the NHC-rhodium(I)-catalyzed [2+2+2] cycloaddition of 1,5-bisallene **1a** and DMAD **2n**.[a]

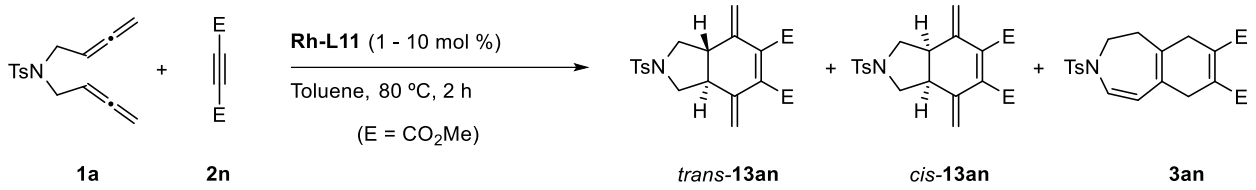

1a **2n** *trans*-**13an** *cis*-**13an** **3an**

Entry	Catalyst load	t (h)	Yield[b] (%) 13an (*trans*:*cis*) / 3an
1	1 mol %	2	31 (91:9) / 0
2	2.5 mol %	2	55 (92:8) / 0
4	2.5 mol %	6.5	68 (91:9) / 2
4	**5 mol %**	**2**	**82 (92:8) / 0**
5	10 mol %	2	81 (92:8) / 0

[a] Reaction conditions: 0.09 mmol of **1a** ([**1a**] = 36 mM), 5 equiv. of **2n**, 1–10 mol % of **Rh-L11** in 2.5 ml of toluene at 80 ºC for 2 h (unless otherwise noted). [b] Yield and ratios calculated by NMR from the reaction crude using mesitylene as internal standard.

With the set of optimized reaction conditions, the scope of the reaction was evaluated (**Scheme 6.9**). Methyl, ethyl and *tert*-butyl acetylenedicarboxylates reacted with 1,5-bisallene **1a** to afford their corresponding adducts **13an, 13aq** and **13ar** in excellent yields and *trans*:*cis* ratios. Unfortunately, the reaction was found to be limited to activated acetylenedicarboxylates, as the use of less activated alkynes such as methyl propiolate, ethyl phenylpropiolate or 4-phenyl-3-butyn-2-one, led to the recovery of 1,5-bisallene **1a** and to the formation of the spirocyclic derivative **6a** (see Chapter 4) in low quantities.

The nature of the 1,5-bisallene was then explored. First, diverse aromatic and aliphatic sulfonamide-tethered 1,5-bisallenes were examined. The reaction proceeded efficiently with phenyl sulfonamides with electrondonating (**13bn**) and electronwithdrawing groups (**13cn**) in the *para* position, as well as with *ortho*-substituted phenyl sulfonamides (**13dn** and **13en**). The 5-methyl-2-pyridinesulfonamide tethered 1,5-bisallene also produced the desired adduct **13fn** in 60 % yield, indicating that the potentially coordinating nitrogen atom did not poison the catalyst. Aliphatic sulfonamide-tethered 1,5-bisallenes were also efficient, as *tert*-butyl- and trimethylsilyl-substituted sulfonamides delivered the cycloadducts **13gn** and **13hn** in 79 and 58% yields respectively. All the sulfonamide-tethered 1,5-bisallenes gave the expected cycloadducts **13** with excellent yields and good diastereoselectivity. However, changing the substitution on the nitrogen atom for the *tert*-butyl carbamate (Boc) resulted in a 53 % yield of **13in** with complete loss of diastereoselectivity (d.r. 50:50), suggesting an important role of the sulfonamide functional group on the diastereoselectivity of the process. The *O*-tethered 1,5-bisallene **1j** produced the cycloadduct **13jn** in a good 61 % yield and an excellent *trans*:*cis* ratio. 1,5-Bisallenes containing carbonyl groups in the quaternary carbon atom of the tether also participated in the [2+2+2] cycloaddition, affording **13kn** and **13ln** in a 61 and 81 % yield with moderate and low diastereoselectivity, respectively. When the carbonyl groups were substituted by arylsulfonyl groups, **13mn**

was obtained in a 54 % yield and excellent diastereoselectivity, highlighting once more the importance of the SO_2 group. For the pro-chiral 1,5-bisallene **1p**, **13pn** was obtained in a 57 % yield as an inseparable mixture of diastereoisomers, making difficult to determine the diastereomeric ratios.

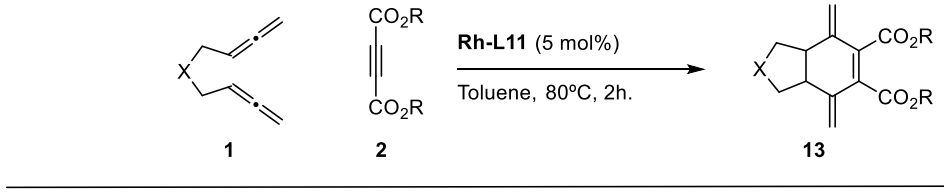

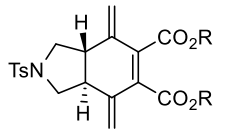

13an R = Me, 80% yield (d.r. 92:8)
13aq R = Et, 84% yield (d.r. 97:7)
13ar R = *t*Bu, 79% yied (d.r. 92:8)

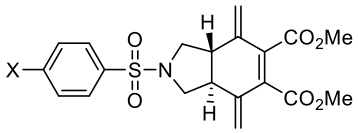

13bn X = OMe, 78% yield (d.r. 91:9)
13cn X = NO_2, 65 % yield (d.r. 100:nd)

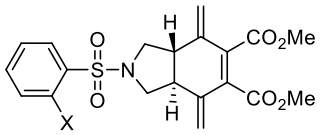

13dn X = CH_3, 79% yield (d.r. 90:10)
13en X = CF_3, 81% yield (d.r. 92:8)

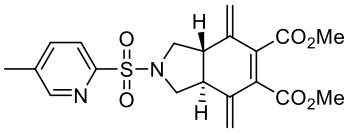

13fn, 60% yield (d.r. 87:13)

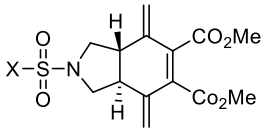

13gn X = *t*Bu, 79% yield (d.r. 83:17)
13hn X = CH_2CH_2TMS, 58% yield (d.r. 89:11)

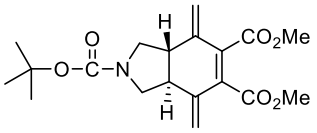

13in, 53% yield (d.r. 50:50)

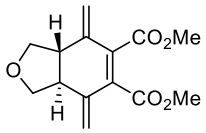

13jn, 61% yield (d.r. 96:4)

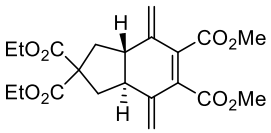

13kn, 61% yield (d.r. 80:20)

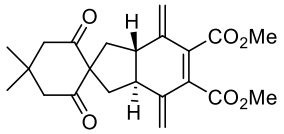

13ln, 81% yield (d.r. 61:39)

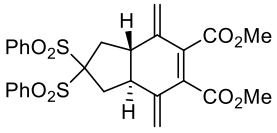

13mn, 54% yield (d.r. 91:9)

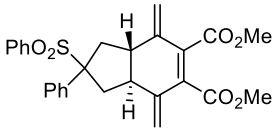

13pn, 57% yield (mix of diastereoisomers)

Scheme 6.9. Scope of the NHC-rhodium(I)-catalyzed [2+2+2] cycloaddition reaction of 1,5-bisallenes with acetylenedicarboxylates.

Interested in understanding the role of the *S*-functionalized NHC as a ligand in the [2+2+2] cycloaddition, as well as the origin of the selective formation of a *trans* ring junction, we performed DFT calculations of the whole catalytic process. The Gibbs energy profile computed at 353.15K and 1 atm with the ωB97X-D/cc-pVTZ-PP/SMD(Toluene)//B3LYP–D3/cc-pVDZ-PP method is depicted in **Figure 6.6**, (see Chapter 8, section **8.1.3** for a complete description of the computational methods).

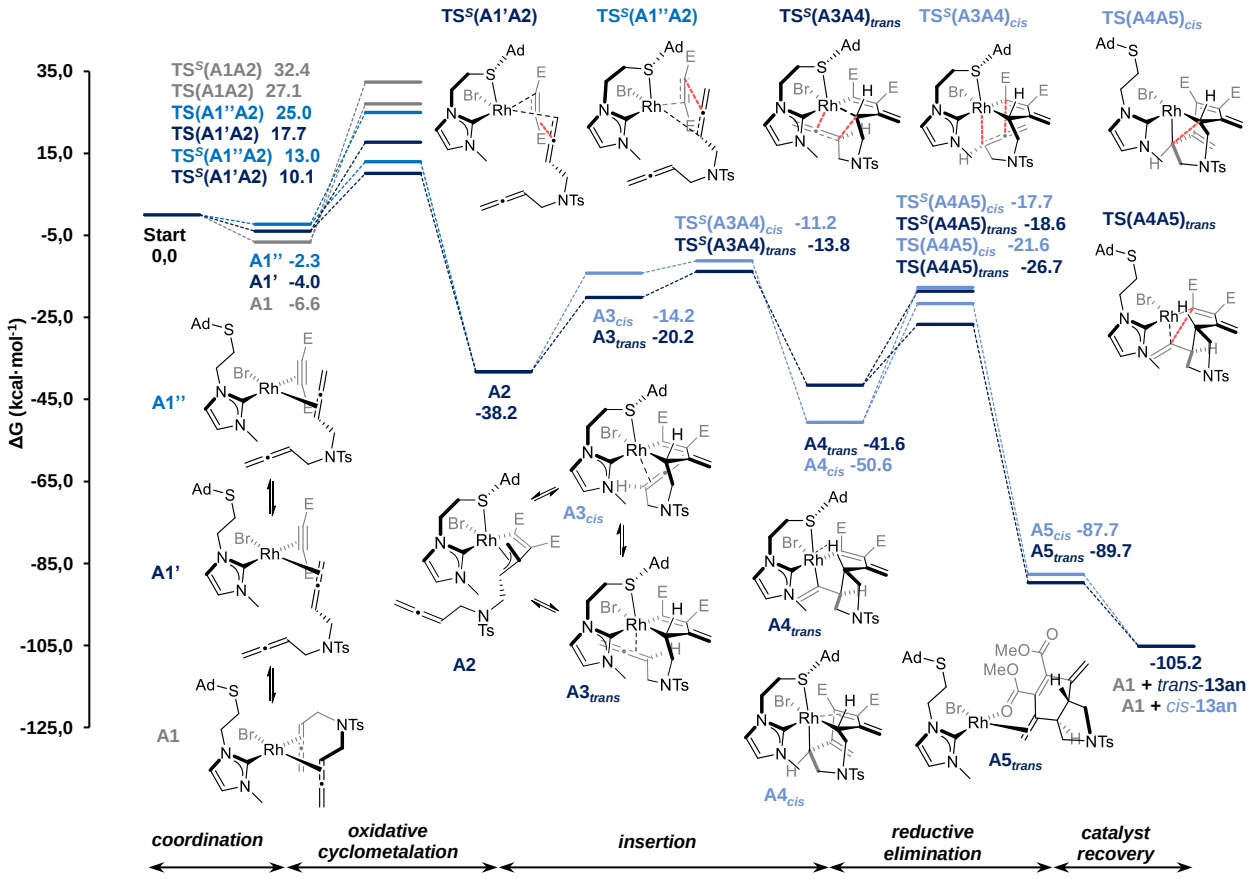

Figure 6.6. Gibbs energy profile (in kcal·mol^{-1}) computed at 353.15K and 1 atm for the cycloaddition of 1,5-bisallene **1a** and dimethylacetylenedicarboxylate **2n** leading to **13an** (E = CO_2Me). Modified from Vila, J.; Solà, M.; Achard, T.; Bellemin-Laponnaz, S.; Pla-Quintana, A.; Roglans, A. Rh(I) Complexes with Hemilabile Thioether-Functionalized NHC Ligands as Catalysts for [2 + 2 + 2] Cycloaddition of 1,5-Bisallenes and Alkynes. *ACS Catal.* **2023**, *13*, 3201. Copyright © Creative Commons 4.0 public license.

The reaction starts with the coordination equilibrium of 1,5-bisallene **1a** and DMAD **2n** with the rhodium catalyst to give the Rh(I) 16 e$^-$ square planar complexes **A1**, **A1'** and **A1''** (**Figure 6.6**) (see **Figure S7** in the Supplementary materials for the whole set of coordination complexes evaluated). The coordination of the two internal double bonds of the 1,5-bisallene (**A1**) is the most exergonic process, releasing 6.6 kcal·mol^{-1}. For the upcoming oxidative cyclometalation, all the possible orientations were evaluated along with the dynamic chelating effect of the sulfur (see **Figures S8** and **S9**), resulting in two possible transition states for each orientation: one with the sulfur chelating the rhodium center (TSs superindexed with *S* in **Figure 6.6**), and the other without such a chelation. Since **A1**, **A1'** and **A1''** (and the rest of possible coordination complexes) are in equilibrium, according to the Curtin–Hammett principle,[109] the major rhodacyclopentene or rhodacyclopentane intermediate formed is the one generated through the lowest in energy transition state (TS), in this case, **TS^S(A1'A2)**. This TS involves an oxidative cyclometalation between the central carbon atom of one of the allenes of the 1,5-bisallene **1a** and DMAD **2n** with the sulfur chelating the rhodium center. Formation of intermediate **A2** takes place with an affordable barrier of 16.7 kcal·mol^{-1} (**A1** to **TS^S(A1'A2)**, being 7.6 kcal·mol^{-1} lower than its non-chelating counterpart (**TS(A1'A2)**, $\Delta G^{\ddagger}$ = 24.3 kcal·mol^{-1}). This step **A1** ⇌ **A1'** → **A2** is exergonic by 31.6 kcal·mol^{-1}. An alternative way to generate **A2** could be through

TS^S(A1''A2), although the energy barrier for this transformation is 2.9 kcal·mol^{-1} higher than via **TS^S(A1'A2)**. For these two paths (and all the other allene–alkyne oxidative couplings evaluated), the sulfur-assisted transition states (**TS^S(A1'A2)**, **TS^S(A1''A2)**) are lower in energy than their analogues in which the sulfur is not coordinated to the rhodium center (**TS(A1'A2)**, **TS(A1''A2)**) due to the electron-donating character of the *S*-adamantyl functionality, which adds electronic density to the rhodium center through the sulfur and facilitates its oxidation [NPA charges on Rh are −0.101 e in **TS(A1′A2)** and −0.443 e in **TS^S(A1'A2)**]. However, in the oxidative cyclometalation from **A1**, the steric hindrance between the tether in the 1,5-bisallene and the *S*-adamantyl group coordinated to the rhodium center in **TS^S(A1A2)** inverts this trend. As a result, the non-chelated transition state **TS(A1A2)** is lower in energy than **TS^S(A1A2)** by 5.3 kcal·mol^{-1}. **A2** is a Rh(III) 18 e$^-$ complex and exhibits an octahedral geometry in which the three carbon atoms from the reacted allene are η^3-coordinated to the rhodium center ($d_{Rh–C}$ = 2.217, 2.129, and 2.218 Å). This type of π-allyl metallacycle intermediates have previously been postulated in cycloaddition reactions.[134] From this point, **A2** needs to rearrange to set a coordination position free for the second allene unit, giving either **A3$_{trans}$** or **A3$_{cis}$** at cost of 18.0 and 24.0 kcal·mol^{-1} respectively. For the formation of the *trans*-fused rhodabicyclo intermediate **A4$_{trans}$** through **A3$_{trans}$**, the insertion (via Schore mechanism[40]) of the internal double bond of the second allene takes place in the Rh–Csp^3 bond through **TS(A3A4)$_{trans}$**. This process **A2 → A4$_{trans}$** has a total Gibbs energy barrier of 24.4 kcal·mol^{-1} and is exergonic by 3.4 kcal·mol^{-1}. In contrast, for the formation of **A4$_{cis}$**, the insertion is found to occur in the Rh–Csp^2 bond, surpassing a Gibbs energy barrier of 27.0 kcal·mol^{-1} (**TS(A3A4)$_{cis}$**) and releasing 12.4 kcal·mol^{-1}. For the last reductive elimination step, the *S*-adamantyl functionality is dissociated from the rhodium center to remove electronic density, drastically reducing the Gibbs energy barriers by 8.1 kcal·mol^{-1} (**TS(A4A5)$_{trans}$** vs **TS^S(A4A5)$_{trans}$**) and 3.9 kcal·mol^{-1} (**TS(A4A5)$_{cis}$** vs **TS^S(A4A5)$_{cis}$**). The formation of **A5$_{trans}$** and **A5$_{cis}$** are exergonic processes by 48.1 and 37.1 kcal·mol^{-1}, respectively. Finally, ligand exchange from **A5$_{trans}$** and **A5$_{cis}$** releases *trans*-**13an** and *cis*-**13an** and gives **A1** to restart the catalytic cycle.

Overall, the reaction follows the typical [2+2+2] cycloaddition mechanism[42] and has an overall reaction energy of -98.6 kcal·mol^{-1} ($\Delta G = G_{3a} – [G_{1a} + G_{2a}]$) almost identical for both diastereoisomers. For *trans*-**13an**, the energetic span between the turnover frequency (TOF) determining intermediate (TDI, **A2**) and the TOF determining transition state (TDTS, **TS(A3A4)$_{trans}$**) is 24.4 kcal·mol^{-1}. For *cis*-**13an**, the energetic span between TDI (**A4$_{cis}$**) and the TDTS (**TS(A4A5)$_{cis}$**) is 29.0 kcal·mol^{-1}.[93]

The allene–allene oxidative cyclometalation is found to be much higher in energy than the allene–alkyne oxidative cyclometalation ($\Delta\Delta G^{‡}$ = 16.0 kcal·mol^{-1}), indicating that the ring fusion stereochemistry comes from the latter insertion of the second allene. The insertion leading to the *trans* isomer (**TS(A3A4)$_{trans}$**) is preferred over the *cis* (**TS(A3A4)$_{cis}$**) by 2.6 kcal·mol^{-1}. This difference in energy is translated into a 98:2 *trans*:*cis* ratio using the Eyring equation, in perfect agreement with the experimental data.

Alternative pathways towards the formation of by-product **3an**, as well as the formation of our previously reported *cis*-3,4-arylvinyl pyrrolidine derivative **7an**,[112] were also evaluated (**Scheme 6.10**). The Gibbs energy

profile for these transformations computed at 353.15K and 1 atm with the ωB97X-D/cc-pVTZ-PP/SMD(Toluene)//B3LYP–D3/cc-pVDZ-PP method is depicted in **Figure 6.7**.

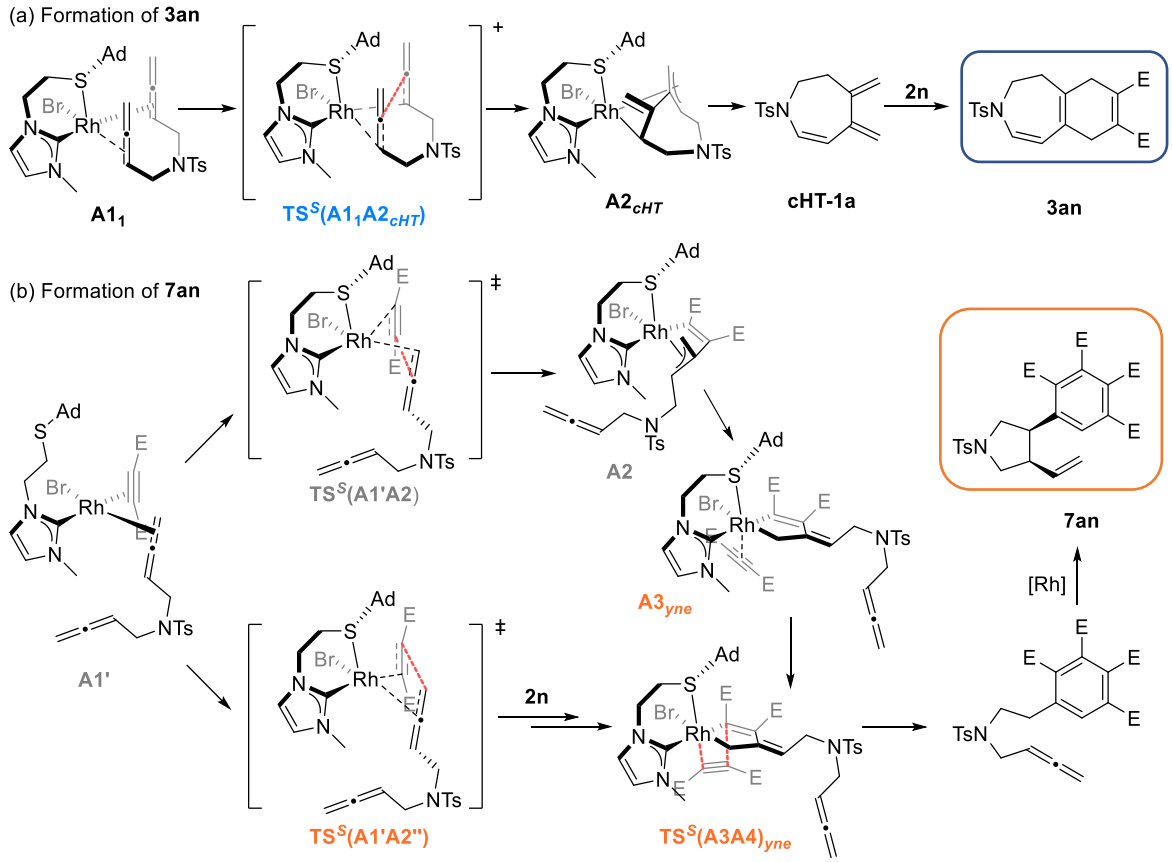

Scheme 6.10. Alternative pathways evaluated towards the formation of **3an** and **7an.** Modified from Vila, J.; Solà, M.; Achard, T.; Bellemin-Laponnaz, S.; Pla-Quintana, A.; Roglans, A. Rh(I) Complexes with Hemilabile Thioether-Functionalized NHC Ligands as Catalysts for [2 + 2 + 2] Cycloaddition of 1,5-Bisallenes and Alkynes. *ACS Catal.* **2023**, *13*, 3201. Copyright © Creative Commons 4.0 public license.

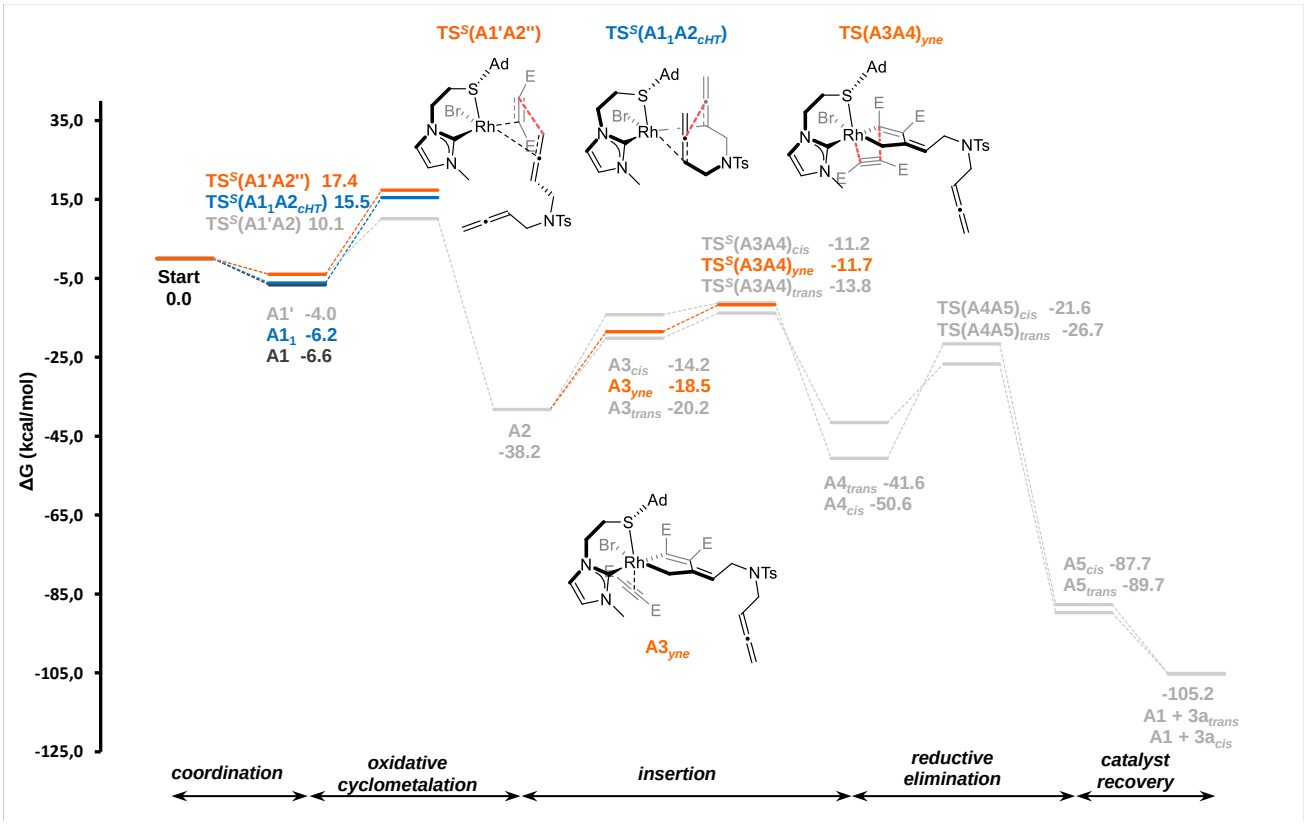

Figure 6.7. Gibbs energy profile (in kcal·mol^{-1}) computed at 353.15K and 1 atm for the cycloaddition of 1,5-bisallene **1a** and dimethylacetylenedicarboxylate **2n** leading to **13an** (E = CO_2Me). Reprinted from Vila, J.; Solà, M.; Achard, T.; Bellemin-Laponnaz, S.; Pla-Quintana, A.; Roglans, A. Rh(I) Complexes with Hemilabile Thioether-Functionalized NHC Ligands as Catalysts for [2 + 2 + 2] Cycloaddition of 1,5-Bisallenes and Alkynes. *ACS Catal.* **2023**, *13*, 3201. Copyright © Creative Commons 4.0 public license.

For the formation of **3an**, the energy barrier for the oxidative cyclometalation between the two central carbon atoms of the 1,5-bisallene, leading to $\mathbf{A2}_{cHT}$ ($\mathbf{TS^S(A1_1A2}_{cHT}\mathbf{)}$), is found to be 5.4 kcal·mol^{-1} higher than $\mathbf{TS^S(A1'A2)}$, which explains the absence of **3an** under the optimized reaction conditions. However, the production rate of **A2** depends on the concentration of DMAD, which is consumed during the reaction to produce its cyclotrimerization adduct and **13an**. Therefore, we must use the Eyring equation to compare both processes at different concentrations of **2n**. The formation rates of **A2** and $\mathbf{A2}_{cHT}$ are:

$$v_{\mathbf{A2}} = \frac{d[\mathbf{A2}]}{dt} = k_{\mathbf{A2}}[\mathbf{A1}][\mathbf{2n}] \qquad \text{(Eq. 6.1)}$$

and

$$v_{\mathbf{A2}_{cHT}} = \frac{d[\mathbf{A2}_{cHT}]}{dt} = k_{\mathbf{A2}}[\mathbf{A1}] \qquad \text{(Eq. 6.2)}$$

Then:

$$\frac{v_{\mathbf{A2}}}{v_{\mathbf{A2}_{cHT}}} = \frac{k_{\mathbf{A2}}[\mathbf{A1}][\mathbf{2n}]}{k_{\mathbf{A2}_{cHT}}[\mathbf{A1}]} = \frac{k_{\mathbf{A2}}}{k_{\mathbf{A2}_{cHT}}}[\mathbf{2n}] \qquad \text{(Eq. 6.3)}$$

Considering that the Eyring equation is :

$$k_i = \frac{k_B T}{h} e^{\frac{-\Delta G_i^{\ddagger}}{RT}} \qquad \text{(Eq. 6.4)}$$

Then:

$$\frac{v_{A2}}{v_{cHT}} = \frac{e^{\frac{-\Delta G^{\ddagger}_{A2}}{RT}}}{e^{\frac{-\Delta G^{\ddagger}_{A2_{cHT}}}{RT}}}[\mathbf{2n}] = [\mathbf{2n}]e^{\frac{\Delta G^{\ddagger}_{A2_{cHT}} - \Delta G^{\ddagger}_{A2}}{RT}} \quad \text{(Eq. 6.5)}$$

If the values obtained for Eq. 6.5 are normalized and plotted versus decreasing concentration of **2n**, **Figure 6.8** is obtained.

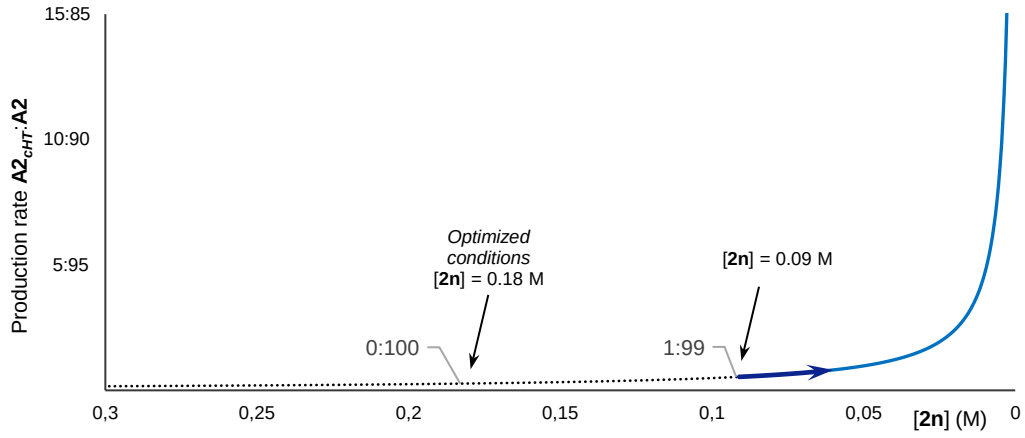

Figure 6.8. Graphical representation of the **cHT:A2** production rate as a function of the concentration of **2n**. Reprinted from Vila, J.; Solà, M.; Achard, T.; Bellemin-Laponnaz, S.; Pla-Quintana, A.; Roglans, A. Rh(I) Complexes with Hemilabile Thioether-Functionalized NHC Ligands as Catalysts for [2 + 2 + 2] Cycloaddition of 1,5-Bisallenes and Alkynes. *ACS Catal.* **2023**, *13*, 3201. Copyright © Creative Commons 4.0 public license.

At higher starting concentrations of DMAD ([**2n**] = 0.18 M, optimized conditions), the amount of DMAD is not reduced enough during the reaction to significantly reduce the production rate of **A2**. However, the amount of DMAD rapidly decreases at lower concentrations, and thus, the oxidative cyclometalation towards **A2*cHT*** is less disfavored. This explains the production of **3an** in low amounts during the optimization of the reaction conditions at lower concentrations of **2n**.

For the formation of the *cis*-3,4-arylvinyl pyrrolidine derivative **7an**, the oxidative cyclometalation between the terminal carbon atom of the allene and the DMAD through **TS^S(A1'A2'')** is 7.3 kcal·mol^{-1} higher than **TS^S(A1'A2)**, which allowed us to discard this pathway. Another possible pathway to produce **7an**, was by coordination of a second DMAD unit into **A2** to produce intermediate **A3*yne*** and subsequent insertion (via Schore mechanism[40]) of DMAD. The transition state for the insertion (**TS^S(A3A4)*yne***) was found to be slightly lower in energy than **TS^S(A3A4)*cis*** ($\Delta\Delta G^{\ddagger}$ = -0.5 kcal·mol^{-1}). However, the production rate of **A4*yne*** depends on the concentration of DMAD, therefore, we must use again the Eyring equation to compare both processes at different concentrations of **2n**. Using the same method as before, we obtain:

$$\frac{v_{A4_{cis}}}{v_{A4_{yne}}} = \frac{1}{[\mathbf{2a}]}e^{\frac{\Delta G^{\ddagger}_{yne} - \Delta G^{\ddagger}_{cis}}{RT}} \quad \text{(Eq. 6.6)}$$

If the values obtained for Eq. 6.6 are normalized and plotted versus decreasing concentration of **2n**, **Figure 6.9** is obtained.

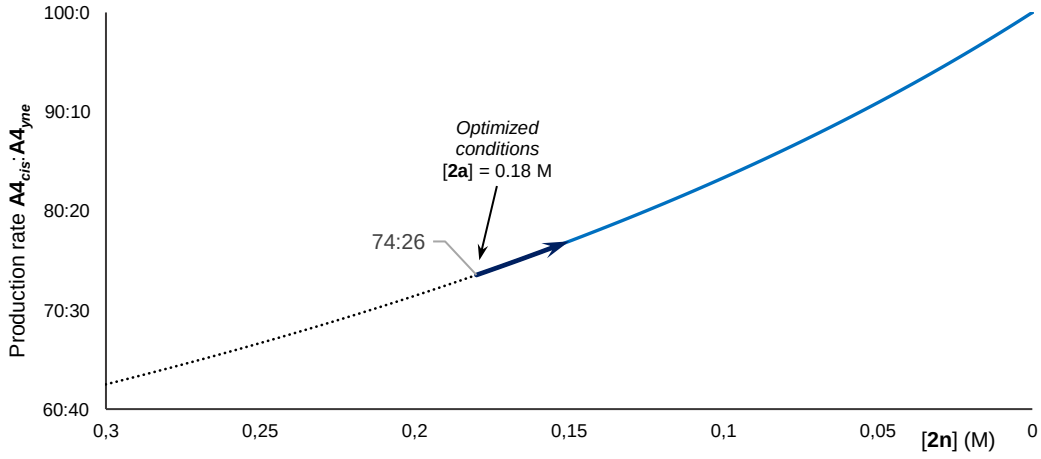

Figure 6.9. Graphical representation of the $\mathbf{A4}_{cis}$:$\mathbf{A4}_{yne}$ production rate as a function of the concentration of **2n**. Reprinted from Vila, J.; Solà, M.; Achard, T.; Bellemin-Laponnaz, S.; Pla-Quintana, A.; Roglans, A. Rh(I) Complexes with Hemilabile Thioether-Functionalized NHC Ligands as Catalysts for [2 + 2 + 2] Cycloaddition of 1,5-Bisallenes and Alkynes. *ACS Catal.* **2023**, *13*, 3201. Copyright © Creative Commons 4.0 public license.

At the starting concentration of DMAD, the production rate $\mathbf{A4}_{cis}$:$\mathbf{A4}_{yne}$ is 74:26, which is even increased during the reaction as the DMAD is consumed. Considering that this $\mathbf{A4}_{cis}$:$\mathbf{A4}_{yne}$ ratio is applied over a 98:2 $\mathbf{A4}_{trans}$:$\mathbf{A4}_{cis}$ ratio (computationally calculated), the production of $\mathbf{A4}_{yne}$ is completely disfavored, and thus, not observed experimentally.

In summary, the [2+2+2] cycloaddition of 1,5-bisallenes and alkynes under the catalysis of Rh(I) with hemilabile thioether-functionalized NHC ligands has been described. This protocol effectively provides an entry to different *trans*-5,6-fused bicyclic systems with two exocyclic double bonds in the cyclohexene ring. The process is totally chemoselective involving the two internal double bonds of the 1,5-bisallenes and one alkyne in the cycloaddition. The complete mechanism of this transformation as well as the preference for the *trans*-fusion over the *cis*-fusion has been rationalized by DFT calculations. The reaction is found to follow the typical [2+2+2] cycloaddition mechanism, in which the initial oxidative addition takes place between the alkyne and one of the allenes, coming the *trans* ring fusion from the subsequent insertion of the second allene unit. Remarkably, the hemilabile character of the sulfur atom in the NHC ligand modulates the electron density in the key intermediates, facilitating the overall transformation.

Chapter 7. General conclusions

The first objective proposed in this thesis consisted of developing a partially intermolecular rhodium(I)-catalyzed [2+2+2] cycloaddition reaction of 1,5-bisallenes involving alkenes as unsaturated partners. In the context of this project, an efficient cascade process encompassing an intramolecular Rh(I)-catalyzed cycloisomerization of 1,5-bisallenes followed by a regioselective Diels–Alder with alkenes was developed. The experimental and computational studies performed allowed us to extract the following conclusions:

- A variety of polycyclic heterocycles containing fused dihydroazepine and dihydrooxepine scaffolds were obtained with moderate to good yields.
- An unprecedented mechanism, other than a [2+2+2] cycloaddition, was revealed for this transformation. The reaction was found to involve an oxidative coupling of the two central carbon atoms of the 1,5-bisallenes with the rhodium center, followed by a β-hydride elimination and reductive elimination, to give a nonisolable cycloheptatriene intermediate, which in the presence of a dienophile underwent a regioselective Diels–Alder reaction to give the observed products.
- Experimental mechanistic studies were in complete agreement with the computational results.
- Although enantioselectivity was achieved in the formation of the cycloheptatriene using pro-chiral 1,5-bisallenes, the Diels–Alder reaction was not diastereoselective.

Derived from the results obtained in chapter 3 when the reaction was performed in the absence of an external alkene, we envisaged the synthesis of seven- and six-membered spiro compounds by a Rh(I)-catalyzed cycloisomerization/Diels–Alder cascade process (Chapter 4). An exhaustive mechanistic study of the process by means of DFT calculations and experimental work, allowed us to conclude:

- A method that enables rapid access to seven- and six- membered spirocyclic substrates in good to excellent yields was successfully achieved.
- The process was found to be completely chemo- and regioselective, obtaining a single isomer out of six different possibilities.
- A ‘two-step birradical’ and a ‘concerted asynchronous’ processes compete to generate the spirocyclic products. The formation of a biradical intermediate was confirmed by performing additional experiments.
- The selectivity observed arose from the highly favored homocoupling of the unsubstituted terminus of the doubly conjugated double bond of the cycloheptatriene in the Diels–Alder reaction.

The second goal proposed in this thesis was to develop a novel rhodium-catalyzed [2+2+2] cycloaddition reaction between 1,5-bisallenes and alkynes. In our initial approach, a Rh(I)-catalyzed cascade process involving a [2+2+2] cycloaddition between two alkyne molecules and one allene, followed by a

cycloisomerization of the remaining allene of the 1,5-bisallene was achieved (Chapter 5). Computational and experimental evaluation of the process lead to the following conclusions:

- A variety of *cis*-3,4-arylvinyl pyrrolidines and cyclopentanes were synthetized with moderate to good yields in a complete diastereoselective manner.
- The introduction of an alkyne in the reaction mixture instead of an alkene, led to the oxidative cyclometalation of one of the external double bonds of the 1,5-bisallene with an alkyne. Subsequent insertion of a second alkyne unit and reductive elimination produced the [2+2+2] cycloadduct. Then, the internal double bond of remaining allene and the exocyclic double bond of the [2+2+2] adduct participated in an oxidative cyclometalation, affording the final product after *β*-hydride elimination and following reductive elimination. The results obtained from performing the reaction with 1,5-bisallene deuterated in the terminal positions were consistent with the mechanism.
- The products obtained were further functionalized to demonstrate potential synthetic utilities of the process.

In Chapter 6, we set the goal of involucrate both allenes of the 1,5-bisallene in the [2+2+2] cycloaddition reaction. In that way, the use of different ligands for the rhodium atom and exhaustive tuning of the reaction conditions, along with a complete computational study of the process, allowed us to conclude:

- The desired selectivity was only achieved with rhodium(I)–*N*-heterocyclic carbene complexes, leading to the diastereoselective formation of bicyclic *trans*-fused 3,6-dimethylenecyclohex-1-ene derivatives in good yields.
- Several *N*-, *O*-, and *C*-tethered 1,5-bisallenes, as well as different acetylenedicarboxylates were successfully used in the reaction.
- The mechanism was found to follow a classical [2+2+2] cycloaddition pathway.
- The hemilabile character of the sulfur in the ligand was found to precisely modulate the electron density in key intermediates and facilitate both, the initial oxidative cyclometalation upon coordination, and the reductive elimination after dissociation.
- In terms of chemoselectivity, the oxidative cyclometalation between the central carbon atom of one of the allenes and an alkyne was preferred over the allene–allene oxidative cyclometalation, coming the *trans*/*cis* junction from the later insertion of the second allene unit and explaining the *trans*:*cis* ratio observed. Additionally, the insertion of a second alkyne unit instead of the second allene was found to be completely disfavored.

In all the projects developed in this thesis, the coordination environment of the rhodium center was found to be of utmost importance, as small changes in either the catalyst or the substrates employed produced disparate outcomes.

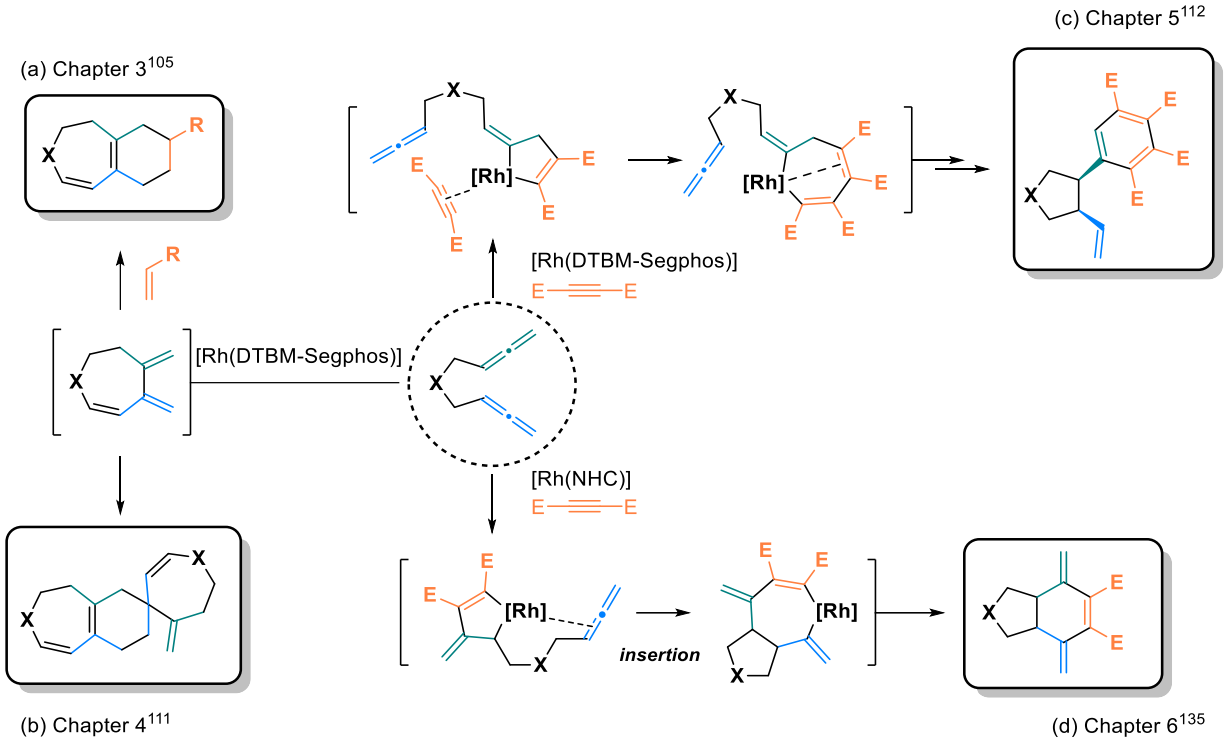

Scheme 7.1. Summary of all the reactions developed in this thesis from 1,5-bisallenes.

When the chiral (*R*)-DTBM-Segphos was used as a ligand for rhodium(I) in the absence of an alkyne, a rhodium-catalyzed cycloisomerization of the 1,5-bisallene afforded the nonisolable cycloheptatriene, followed by a Diels–Alder, with either an external alkene (**Scheme 7.1a**)[105] or another molecule of cycloheptatriene (**Scheme 7.1b**).[111] In contrast, the addition of an alkyne in the reaction mixture avoided the formation of the cycloheptatriene in favor of the oxidative cyclometalation between the external double bond of the allene and the alkyne. The insertion of a second alkyne ended up to the formation of the *cis*-3,4-arylvinyl pyrrolidine and cyclopentane derivatives **(Scheme 7.1c**).[112] On the other hand, switching to rhodium(I)–*N*-heterocyclic carbene complexes favored the oxidative cyclometalation between the central carbon atom of the allene and the alkyne, as well as the following insertion of the second allene instead of the alkyne. Finally leading to the bicyclic 3,6-dimethylenecyclohex-1-ene derivatives (**Scheme 7.1d**).[135]

Chapter 8. Methods

8.1. Computational chemistry: modeling reaction mechanisms

8.1.1. Examination of the PES

Given a molecular system, the potential-energy surface (PES) is a mathematical representation in which the potential energy is plotted as a function of the coordinates that represent the molecular geometries of the system. A molecular geometry can be described with three parameters: bond distances, bond angles, and dihedral angles; and every point of the PES corresponds to a unique combination of those parameters. Consequently, for a non-linear system with more than two atoms (N > 2) the PES has 3N – 6 dimensions. However, the potential energy can be graphically represented as a function of two geometric parameters to define the potential-energy contour map (**Figure 8.1a**), or as a function of a single geometric parameter to define a potential-energy profile (**Figure 8.1b**).

Extrapolating this to a given chemical reaction, the molecular structures of the reactants and products are in the deepest points of the valleys (points A and C in **Figure 8.1**) in the potential-energy contour map, whereas the saddle point connecting two valleys correspond to the transition-state (point B in **Figure 8.1**). Mathematically, a saddle point is a local maximum in one direction and a minimum in all other directions. The energetically easiest route from reactants to products defines the potential-energy profile of the reaction (blue line in **Figure 8.1**). For an elementary reaction, the geometric parameter represented in the potential-energy profile is the reaction coordinate; for a stepwise reaction it is a succession of reaction coordinates for each individual reaction step.

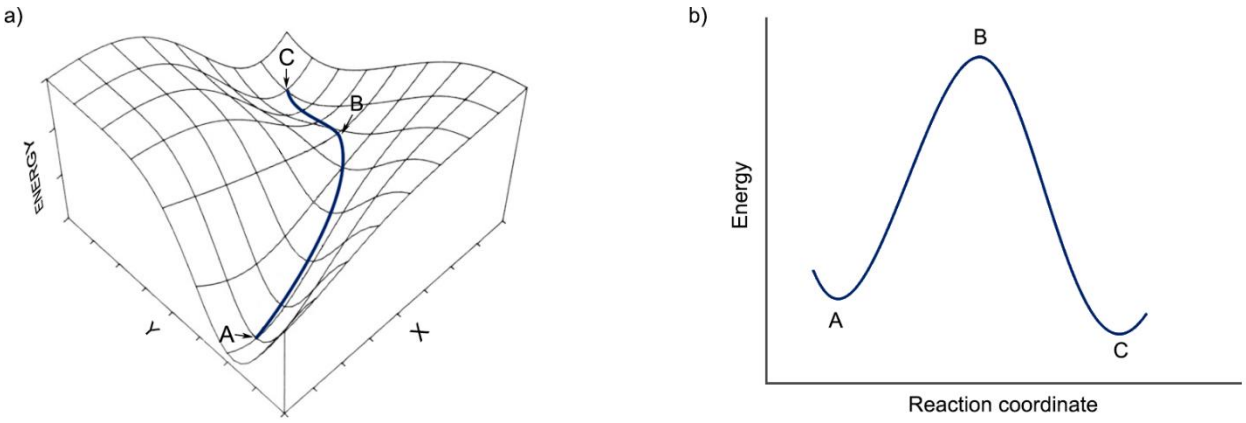

Figure 8.1. Representation of the PES as a function of a) two geometric parameters or b) one geometric parameter. a) Modified with permission from Schlegel, H. B. *Adv. Chem. Phys.* **1987**, *67*, 249. Copyright 2007 Wiley-VCH Verlag GmbH & Co. KGaA, Weinheim.

These minimum and saddle points are stationary points, and have the shared property that their gradient, which is the first derivative of the potential-energy (E) with respect to their cartesian coordinates ($\vec{R}$), is equal to zero.

$$\frac{\partial E}{\partial \vec{R}} = 0 \qquad \text{(Eq. 8.1)}$$

Stationary points can be found by running geometry optimizations.[136] To do so, the Gaussian uses numerical methods and algorithms that help to predict increasingly more stable structures. After applying a series of

iterations in which the geometry is modified in each step, the gradient is reduced until the energy of the system cannot become lower, leading to the converged (or optimized) geometry (**Figure 8.2**).

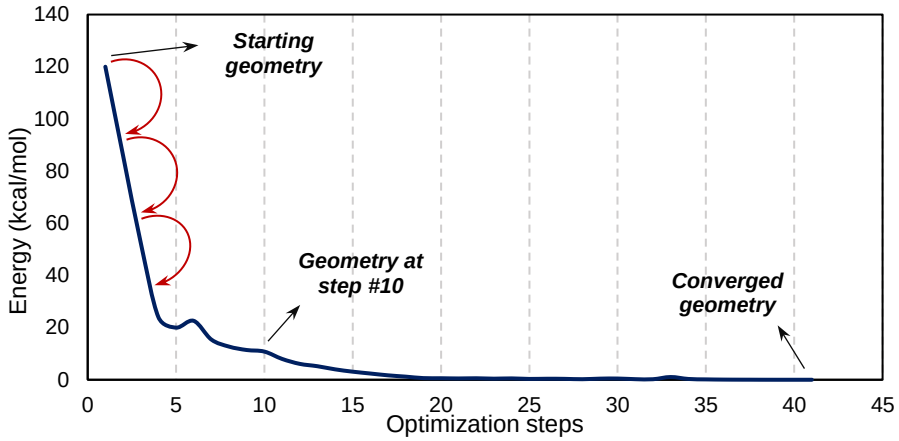

Figure 8.2. Evolution of the energy through the iterative steps during a geometry optimization. Curly arrows represent three consecutive optimization steps.

Optimization of equilibrium species (minimum points in the PES) are often performed from an estimated geometry since the optimization algorithm will reduce the gradient in a "downhill" direction along the PES. In contrast, locating the structure of a TS results in a more laborious task as it requires a starting guess much closer to the converged geometry to avoid missing the saddle point, this is because the algorithm will perform "uphill" steps to find a TS. To get an accurate starting guess, a scan of one reaction coordinate can be done. This consists in perform sequential geometry optimizations while freezing the reaction coordinate at increasing or decreasing values, usually the distance between two atoms that are forming or breaking a bond (**Figure 8.3a**). The energy maximum of the profile obtained from the scan has a TS-like geometry that can be picked for further TS optimization (**Figure 8.3b**).

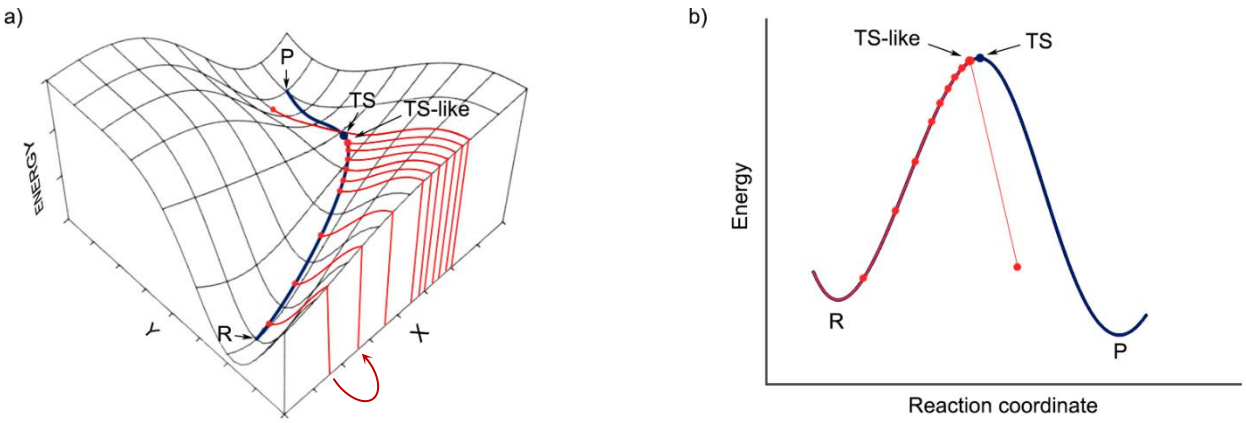

Figure 8.3. Representation of a reaction coordinate scan on the a) potential-energy contour map and the b) energy profile. In blue, the reaction path, in red the scanned reaction coordinate. Red dots are the converged energies along the reaction coordinate **X**.

To characterize the stationary points obtained from geometry optimizations (minimum and saddle points), the vibrational frequencies must be computed. As each eigenvector obtained corresponds to a normal vibrational

mode, a minimum on the PES will provide only positive eigenvalues (real frequencies). On the other hand, given that a saddle point is a maximum along the reaction path and a minimum in all other directions, a TS will provide a single negative eigenvalue (imaginary frequency). Nonetheless, the presence of an imaginary frequency is not necessary indicative that we have located the desired TS. The vibrational mode associated to the imaginary frequency needs to be checked to confirm that it matches the desired reaction path.

Finally, to unquestionably verify that our optimized TS structure is connected to the desired minimum points (reactants and products), an intrinsic reaction coordinate (IRC) calculation[137] is carried out. The IRC calculation follows the reaction path downhill from our optimized TS structure to reactants and products, whose must match our expected species (**Figure 8.4**).

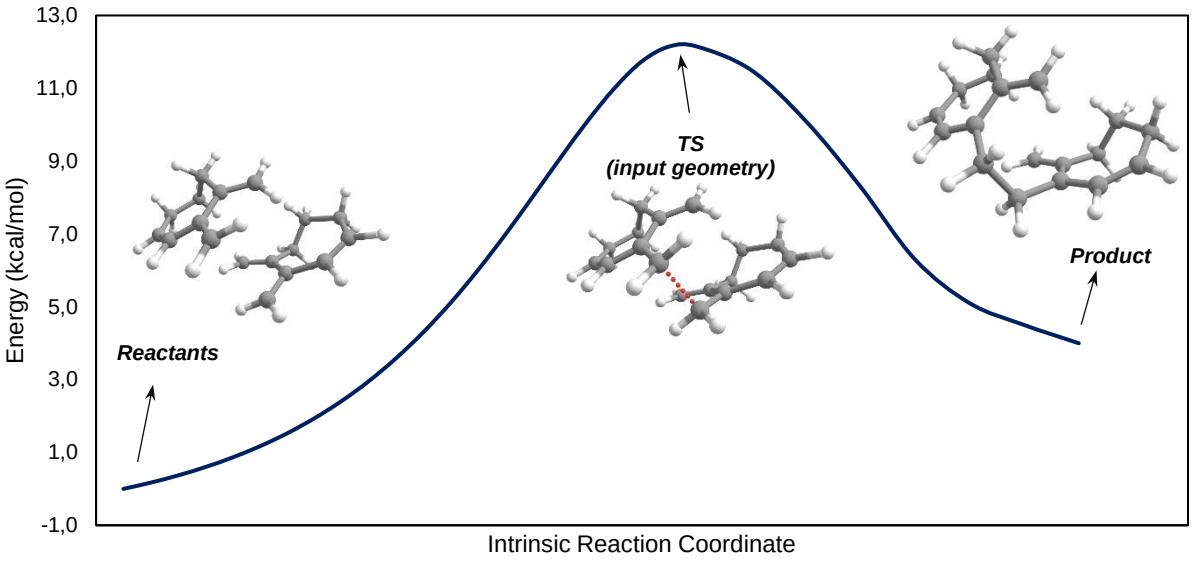

Figure 8.4. Representation of the IRC for the formation of the first C – C bond in a stepwise DA reaction.

8.1.2. Gaussian thermochemistry output

The computed energy obtained from an optimization calculation is the *electronic energy* (*E*) of a given molecule at the stationary point. However, for the study of chemical reactions it is usually more convenient to use the Gibbs free energy or the enthalpy rather than potential electronic energy. These thermochemical properties are automatically calculated by Gaussian after applying approximated corrections to the *electronic energy* (*E*) based on standard statistical-mechanics and thermodynamic equations.[138] A frequency calculation is needed to extract the values of these corrections as some of their components depend on the normal vibrational modes of the molecule, but this calculation does not involve extra computational work since the frequency calculation is always performed to characterize stationary points.

The Gaussian's output file contains the following thermochemistry results computed at the given temperature and pressure (298,15 K and 1 atm by default).

1. The *zero-point correction* (E_{ZPE}) results from the vibrational motion of the molecule at 0 K and is calculated using the harmonic oscillator model as a sum of contributions from all *i* vibrational modes of the system.

   - *Zero-point correction* $= E_{ZPE} = \sum_{i}^{3N-6} \frac{1}{2} h\omega_i$ (Eq. 8.2)

2. The correction to the *internal energy* (*U*) at a given temperature is defined as the sum of electronic, vibrational, rotational, and translational internal energies of the molecule. This correction already includes the *zero-point correction* (E_{ZPE}).

   - *Thermal correction to Energy* $= U_{corr} = U_e + U_v + U_r + U_t = E_{ZPE} + C_v T$ (Eq. 8.3)

3. The correction to the *Enthalpy* (*H*) is then calculated from the *thermal correction to Energy* (U_{corr}).

   - *Thermal correction to Enthalpy* $= H_{corr} = U_{corr} + pV = U_{corr} + k_B T$ (Eq. 8.4)

The term *pV* is only valid for molar quantities of an ideal gas, instead, the term $k_B T$ is used for single particles.

4. The correction to the *Gibbs energy* (*G*) is obtained from the thermal correction to the *enthalpy* (H_{corr}) and the *entropy* (*S*)

   - *Thermal correction to Gibbs Free Energy* $= G_{corr} = H_{corr} - TS$ (Eq. 8.5)

   Where: $S = S_e + S_v + S_r + S_t$ (Eq. 8.6)

The Gibbs energy includes ΔpV = ΔnRT, so when it is used for calculating ΔG_r for a reaction, the obtained ΔG_r will be computed correctly if the changes in the number of moles of gas are taken into account during the reaction.

5. Then, the estimated total energies of the molecule are calculated as the sum of the *electronic energy* (*E*) and the corresponding corrections:

   - *Sum of electronic and zero-point Energies* $= U_0 = E + E_{ZPE}$ (Eq. 8.7)
   - *Sum of electronic and thermal Energies* $= U_T = U_0 + C_v T = E + U_{corr}$ (Eq. 8.8)
   - *Sum of electronic and thermal Enthalpies* $= H_T = U_T + k_B T = E + H_{corr}$ (Eq. 8.9)
   - *Sum of electronic and thermal Free Energies* $= G_T = H_T - TS = E + G_{corr}$ (Eq. 8.10)

8.1.3. Computational methods used in this thesis

- Geometries of all stationary points were optimized without symmetry constrains with the Gaussian 16 program[139] using the DFT B3LYP hybrid exchange-correlation functional.[140] The all-electron cc-pVDZ basis set was employed for non-metal atoms,[141] and the cc-pVDZ-PP basis set containing an effective core relativistic *pseudopotential* (PP) was used for Rh. Pseudopotentials are used to describe the

combined repulsion of core electrons on valence electrons in the wavefunction to include, in a cheap way, relativistic effects.[142]

- In Chapter 4, the geometries of **$TS^{os}(2A_{exo})$** and **$TS^{os}(2A_{endo})$** were optimized again using the unrestricted UB3LYP functional. "U" stands for unrestricted open-shell wavefunctions, which allows the possibility for electrons to be unpaired.

- The electronic energies of the previously optimized structures were improved by performing single point energy calculations (SPE) with cc-pVTZ and cc-pVTZ-PP basis sets using either the (U)B3LYP,[139] the M06L[141b] or the ωB97X-D[143] functionals.

- The D3 Grimme energy corrections for dispersion with the original damping function[144] were added in all geometry optimizations and SPE calculations to consider weak inter- and/or intramolecular interactions, except for the ωB97X-D[143] functional, which has integrated a version of D2 dispersion model with a similar damping function to that used by the D3 model.

- Solvent corrections were computed with the *Self-Consistent Reaction Field* (SCRF) using the solvation model based on density (SMD).[145] The SMD model contains solvent descriptors (dielectric constant, index of refraction, Abraham's hydrogen bond acidity and basicity, surface tension, aromaticity and electronegative halogenacity) to mimic the experimental solvent conditions.

- Frequency calculations were performed to characterize stationary points (minimum or saddle points), and to determine the thermal corrections and entropy effects at the designated temperature and 1 atm.

- When required, the ligands employed for the computational modelling were simplified to reduce the computational costs of the calculations.
- All stationary points were unambiguously confirmed by IRC calculations.

As a summary, the reported Gibbs energies contain:

- In Chapter 3: Electronic energies including solvent effects calculated at the M06L-D3/cc-pVTZ-PP/SMD(76 % THF, 24 % CH_2Cl_2) // B3LYP-D3/cc-pVDZ-PP level together with gas phase thermal and entropic contributions computed at 313.15 K and 1 atm obtained with the B3LYP-D3/cc-pVDZ-PP method.

- In Chapter 4: Electronic energies including solvent effects calculated at the (U)B3LYP-D3/cc-pVTZ-PP/SMD(76 % THF, 24 % CH_2Cl_2) // (U)B3LYP-D3/cc-pVDZ-PP level together with gas phase thermal and entropic contributions computed at 313.15 K and 1 atm obtained with the (U)B3LYP-D3/cc-pVDZ-PP method.

- In Chapter 5: Electronic energies including solvent effects calculated at the M06L-D3/cc-pVTZ-PP/SMD(76 % THF, 24 % CH_2Cl_2) // B3LYP-D3/cc-pVDZ-PP level together with gas phase thermal and entropic contributions computed at 298.15 K and 1 atm with the B3LYP-D3/cc-pVDZ-PP method.
- In Chapter 6: Electronic energies including solvent effects calculated at the ωB97X-D/cc-pVTZ-PP/SMD(Toluene) // B3LYP-D3/cc-pVDZ-PP level together with gas phase thermal and entropic contributions computed at 353.15 K and 1 atm obtained with the B3LYP-D3/cc-pVDZ-PP method.

8.2. Materials and instrumentation

8.2.1. General methods

Unless otherwise noted, materials were obtained from commercial suppliers and used without further purification. All reactions requiring anhydrous and oxygen-free conditions were conducted in oven dried glassware under dry nitrogen or hydrogen atmosphere. Dichloromethane and tetrahydrofuran were dried and degassed under nitrogen by passing through solvent purification columns (MBraun, SPS-800). Reaction progress during the preparation of all compounds was monitored using thin layer chromatography. Solvents were removed under reduced pressure with a rotary evaporator. When required, reaction mixtures were chromatographed on silica gel.

8.2.2. Spectroscopy

- **NMR Spectroscopy:** All ^{1}H and ^{13}C NMR spectra were recorded on a Bruker ASCEND 400 spectrometer equipped with a 5 mm BBFO probe using $CDCl_3$ or THF-*d8* as a deuterated solvent. Chemical shifts for ^{1}H and ^{13}C NMR are reported in ppm (δ) relative to residual solvent signals (**$CDCl_3$:** 7.26 ppm for ^{1}H and 77,16 ppm for ^{13}C; **THF-*d8*:** 1.72, 3.58 ppm for ^{1}H and 25.12, 67.21 ppm for ^{13}C). Coupling constants are given in Hertz (Hz). ^{1}H and ^{13}C NMR signals were assigned based on 2D-NMR HSQC, HMBC, COSY and NOESY experiments.
- **Infrared Spectroscopy (IR):** IR spectra were recorded on a benchtop Agilent Cary 630 FT-IR spectrometer equipped with a single reflection ATR (attenuated total reflectance) sampling accessory.

8.2.3. Spectrometry

- **Mass spectrometry (ESI-MS):** Electrospray ionization mass spectra were recorded on an Esquire 6000 ion trap mass spectrometer (Bruker) equipped with an electrospray ion source operated in the positive ESI(+) ion mode.
- **High resolution mass spectrometry (ESI-HRMS):** Electrospray ionisation high-resolution mass spectra were recorded using a Bruker microTOF-Q II instrument with a quadrupole-Time-Of-Flight hybrid analyzer operated in the positive ESI(+) ion mode.

8.2.4. Single crystal X-ray diffraction

The X-ray intensity data were measured on a 'Bruker D8 QUEST ECO' three-circle diffractometer system equipped with a Ceramic x-ray tube (Mo Kα, λ = 0.71076 Å) and a doubly curved silicon crystal Bruker Triumph monochromator.

8.2.5. Chromatography

- **Thin layer chromatography (TLC):** were performed with pre-coated Macherey-Nagel Xtra SIL G/UV254 silica gel plates.
- **Flash chromatography:** were performed on silica gel flash columns (40 μm particle size) using an automated purification instrument Interchim PuriFlash XS 520 Plus equipped with a quaternary gradient pump (up to 300 ml/min, 20 bar) and an UV-Vis 200-800 nm díode array detector.
- **Column chromatography:** were performed using silica gel with a size of 40-63 μm mesh particle size.
- **High performance liquid chromatography (HPLC):** were performed using a CHIRALPAK IA column (4.6 x 250 mm, 5 μm) on an Agilent Technologies 1260 Infinity instrument, equipped with a quaternary pump G1311C, an auto sampler G1329B, a thermostatic column compartment G1316A and a variable wavelength UV-Vis detector G1314F.

8.2.6. Melting points

Melting points were measured in a SMP10 apparatus from Stuart without any correction.

References

1 Van't Hoff, J. H. *La chimie dans L'espace*; P. M. Bazendijk, **1875**.

2 Burton, B. S.; von Pechmann, H. Ueber die einwirkung von chlorphosphor auf acetondicarbonsäureäther. *Ber. Dtsch. Chem. Ges.* **1887**, *20*, 145.

3 Jones, E. R. H.; Mansfield, G. H.; Whiting M. C. Researches on acetylenic compounds. Part XLVII. The prototropic rearrangements of some acetylenic dicarboxylic acids. *J. Chem. Soc.* **1954**, 3208

4 For isolation, see: (a) Willstätter, R.; Page, H. J. Untersuchungen über chlorophyll. XXIV. Über die pigmente der braunalgen. *Justus Liebigs Ann. Chem.* **1914**, *404*, 237. For characterization, see: (b) Bonnett, R.; Spark, A. A.; Tee, J. L.; Weedon, B. C. L. FUCOXANTHIN. *Proc. Chem. Soc. London.* **1964**, 419.

5 For isolation, see: (a) Schütt, F. Beispielaufsatz: ueber peridineenfarbstoffe. *Ber. Dtsch. Bot. Ges.* **1890**, *8*, 9. For characterization, see: (b) Strain, H. H.; Svec, W. A.; Aitzetmüller, K.; Grandolfo, M. C.; Katz, J. J.; Kjøsen, H.; Norgard, S.; Liaaen-Jensen, S.; Haxo, F. T.; Wegfahrt, P.; Rapoport, H. Structure of peridinin, the characteristics dinoflagellate carotenoid. *J. Am. Chem. Soc.* **1971**, *93*, 1823.

6 For a monograph, see: (a) Krause, N.; Hashmi, A. S. K. Modern allene chemistry, Vols. 1 and 2; Wiley-VCH, **2004**. For selected recent reviews, see: (b) Alonso, J. M.; Almendros, P. Deciphering the chameleonic chemistry of allenols: breaking the taboo of a onetime esoteric functionality. *Chem. Rev.* **2021**, *121*, 4193. (c) Santhoshkumar, R; Cheng, C.-H. Fickle Reactivity of Allenes in transition-metal-catalyzed C−H functionalizations. *Asian J. Org. Chem.* **2018**, *7*, 1151. (d) Yu, S.; Ma. S. Allenes in catalytic asymmetric synthesis and natural product syntheses. *Angew. Chem. Int. Ed.* **2012**, *51*, 3074. (e) Ma, S. Electrophilic addition and cyclization reactions of allenes. *Acc. Chem. Res.* **2009**, *42*, 1679.

7 Selected reviews: (a) Hoffmann-Röder, A.; Krause, N. Synthesis and properties of allenic natural products and pharmaceuticals. *Angew. Chem. Int. Ed.* **2004**, *43*, 1196. (b) Dembitsky, V. M.; Maoka, T. Allenic and cumulenic lipids. *Prog Lipid Res.* **2007**, 46, 328.

8 Selected examples: (a) McGrath, M. J.; Fletcher, M. T.; König, W. A.; Moore, C. J.; Cribb, B. W.; Allsopp, P. G.; Kitching, W. A Suite of novel allenes from australian Melolonthine scarab beetles. structure, synthesis, and stereochemistry. *J. Org. Chem.* **2003**, *68*, 3739. (b) Fletcher, M. T.; McGrath, M. J.; König, W. A.; Moore, C. J.; Cribb, B. W.; Allsopp, P. G.; Kitching, W. A novel group of allenic hydrocarbons from five australian (Melolonthine) beetles. *Chem Comm.* **2001**,*10*, 885.

9 Selected examples: (a) Johnson, E. A.; Burdon, K. L. Mycomycin, a new antibiotic produced by a moldlike actinomycete active against the bacilli of human tuberculosis *J. Bacteriol.* **1947**, *54*, 281. (b)

Celmer, W. D.; Solomons, I. A. The structure of the antibiotic Mycomycin. *J. Am. Chem. Soc.* **1952**, *74*, 1870. (c) Bagby, M. O.; Smith Jr., C. R.; Wolff, I. A. Laballenic acid. a new allenic acid from Leonotis Nepetaefolia seed oil. *J. Org. Chem.* **1965**, *30*, 4227. (d) Mikalaijczak, K. L.; Rogers, M. F.; Smith, C. R.; Wolff, I. A. An octadecatrienoic acid from Lamium purpureum L. seed oil containing 5,6-allenic and *trans*-16-olefinic unsaturation. *Biochem. J.* **1967**, *105*, 1245.

10 Selected examples: (a) Chilton, W. S.; Tsou, G.; Kirk, L.; Benedict, R. G. A naturally-occurring allenic amino acid. *Tetrahedron Lett.* **1968**, *9*, 6283. (b) Castelhano, A.L.; Krantz, A. Allenic amino acids. 1. synthesis of γ-allenic GABA by a novel aza-Cope rearrangement. *J. Am. Chem. Soc.* **1984**, *106*, 1877.

11 Selected examples: (a) Meinwald, J.; Erickson, K.; Hartshorn, M.; Meinwald, Y. C.; Eisner, T. Defensive mechanisms of arthropods. XXIII. An allenic sesquiterpenoid from the grasshopper *Romalea microptera*. *Tetrahedron Lett.* **1968**, *9*, 2959. (b) Bohlmann, F.; Gupta, R. K.; Jakupovic, J.; King, R. M.; Robinson, H. Naturally occurring terpene derivatives, 292. Natürlich vorkommende terpen-derivate, 292. über das erste sesquiterpenlacton mit einer allengruppe aus *Vernonia cotoneaster*. *Liebigs Ann. Chem.* **1980**, 1904.

12 Selected examples: (a) Theobald, N.; Shoolery, J. N.; Djerassi, C.; Erdman, T. R.; Scheuer, P. J. Minor and trace sterols in marine invertebrates. 24-Ethyl-$\Delta^{5,24(28),28}$-cholestatrien-3-β-ol - a naturally occurring allenic marine sterol. *J. Am. Chem. Soc.* **1978**, *100*, 5574. (b) Batzold, F. H.; Robinson, C. H. Irreversible inhibition of Δ^5-3-ketosteroid isomerase by 5,10-secosteroids. *J. Am. Chem. Soc.* **1975**, *97*, 2576. (c) Beach, D. H.; Chen, F.; Cushion, M. T.; Macomber, R. S.; Krudy, G. A.; Wyder, M. A.; Kaneshiro, E. S. Effects of steroidal allenic phosphonic acid derivatives on the parasitic protists Leishmania donovani, Leishmania mexicana mexicana, and Pneumocystis carinii carinii. *Antimicrob. Agents. Chemother*. **1997**, *41*, 162.

13 Selected examples: (a) Megati, S.; Goren, Z.; Silverton, J. V.; Orlina, J.; Nishimura, H.; Shirasaki, T. Mitsuya, H.; Zemlicka, J. (*R*)-(-)- and (*S*)-(+)-Adenallene: synthesis, absolute configuration, enantioselectivity of antiretroviral effect, and enzymic deamination. *J. Med. Chem.* **1992**, *35*, 4098. (b) Jones, B. C. N. M.; Silverton, J. V.; Simons, C.; Megati, S.; Nishimura, H.; Maeda, Y.; Mitsuya, H.; Zemlicka, J. Synthesis, absolute configuration, and enantioselectivity of antiretroviral effect of (*R*)-(-)- and (*S*)-(+)-cytallene. Lipase-catalyzed enantioselective acylations of (±)-N^4-acylcytallenes. *J. Med. Chem.* **1995**, *38*, 1397.

14 Wu, J. I.-C.; Wang, C.; McKee, W. C.; Schleyer, P. von R.; Wu W.; Mo, Y. On the large σ-hyperconjugation in alkanes and alkenes. *J. Mol. Model.* **2014**, *20*, 2228.

15 Selected recent reviews: (a) Alonso, J. M.; Quirós, M. T.; Muñoz, M. P. Chirality transfer in metal-catalysed intermolecular addition reactions involving allenes. *Org. Chem. Front.* **2016**, *3*, 1186. (b) Neff, R. K.; Frantz, D. E. Recent applications of chiral allenes in axial-to-central chirality transfer reactions. *Tetrahedron*, **2015**, *71*, 7.

16 For selected reviews, see: (a) Hashmi, A. S. K. New and selective transition metal catalyzed reactions of allenes. *Angew. Chem. Int. Ed.* **2000**, *39*, 3590. (b) Zimmer, R.; Dinesh, C. U.; Nandanan, E.; Khan, F. A. Palladium-catalyzed reactions of allenes. *Chem. Rev.* **2000**, *100*, 3067. (c) Dudnik, A. S.; Sromek, A. W.; Rubina, M.; Kim, J. T.; Kel'in, A. V. Gevorgyan. V. Metal-catalyzed 1,2-Shift of diverse migrating groups in allenyl systems as a new paradigm toward densely functionalized heterocycles. *J. Am. Chem. Soc.* **2008**, *130*, 1440. (d) Alcaide, B.; Almendros, P. Novel cyclization reactions of aminoallenes. *Adv. Synth. Catal.* **2011**, *353*, 2561. (e) Aubert, C.; Fensterbank, L.; Garcia, P.; Malacria, M.; Simonneau, A. Transition metal catalyzed cycloisomerizations of 1,n-allenynes and -allenenes. *Chem. Rev.* **2011**, *111*, 1954. (f) Krause, N.; Winter, C. Gold-catalyzed nucleophilic cyclization of functionalized allenes: a powerful access to carbo- and heterocycles. *Chem. Rev.* **2011**, *111*, 1994. (g) Alonso, J. M.; Muñoz, M. P. When indoles meet allene and its derivatives. *Eur. J. Org. Chem.* **2020**, 7197. (h) Wang, J.-Y.; Hao, W.-J.; Tu, S.-J.; Jiang, B. Engaging yne-allenes in cycloaddition reactions: recent developments. *Chin. J. Chem.* **2022**, *40*, 1224.

17 Makino, T.; Itoh, K. Rhodium complex-catalyzed cycloisomerization of allenenes: exo and endo cyclization depending on the auxiliary ligands. *J. Org. Chem.* **2004**, *69*, 395.

18 Zhou, Y.; Nikbakht, A.; Bauer, F.; Breit, B. A rhodium catalyzed cycloisomerization and tandem Diels–Alder reaction for facile access to diverse bicyclic and tricyclic heterocycles. *Chem. Sci.* **2019**, *10*, 4805.

19 Cadran, N.; Cariou, K.; Hervé, G.; Aubert, C.; Fensterbank, L.; Malaria, M.; Marco-Contelles, J. $PtCl_2$-Catalyzed cycloisomerizations of allenynes. *J. Am. Chem. Soc.* **2004**, *126*, 3408.

20 (a) Trillo, B.; López, F.; Gulías, M.; Castedo, L.; Mascareñas. J. L. Platinum-catalyzed intramolecular [4C+3C] cycloaddition between dienes and allenes. *Angew. Chem. Int. Ed.* **2008**, *47*, 951. (b) Trillo, B.; López, F.; Montserrat, S.; Ujaque, G.; Castedo, L.; Lledós, A.; Mascareñas. J. L. Gold-catalyzed [4C+3C] intramolecular cycloaddition of allenedienes: synthetic potential and mechanistic implications. *Chem. Eur. J.* **2009**, *15*, 3336.

21 Alonso, I.; Trillo, B.; López, F.; Montserrat, S.; Ujaque, G.; Castedo, L.; Lledós, A.; Mascareñas. J. L. Gold-catalyzed [4C+2C] cycloadditions of allenedienes, including an enantioselective version with

new phosphoramidite-based catalysts: mechanistic aspects of the divergence between [4C+3C] and [4C+2C] pathways. *J. Am. Chem. Soc.* **2009**, *131*, 13020.

22 (a) Mauleón, P.; Zeldin, R. M.; González, A. Z.; Toste. F. D. Ligand-controlled access to [4 + 2] and [4 + 3] cycloadditions in gold-catalyzed reactions of allene-dienes. *J. Am. Chem. Soc*. **2009**, *131*, 6348. (b) Benitez, D.; Tkatchouk, E.; Gonzalez, A. Z.; Goddard, W. A.; Toste, F. D. On the impact of steric and electronic properties of ligands on gold(I)-catalyzed cycloaddition reactions. *Org. Lett.* **2009**, *11*, 4798.

23 Christian, A. H.; Niemeyer, Z. L.; Sigman, M. S.; Toste, F. D. Uncovering subtle ligand effects of phosphines using gold(I) catalysis. *ACS Catal.* **2017**, *7*, 3973.

24 Kawaguchi, Y.; Nagata, A.; Kurokawa, K.; Yokosawa, H.; Mukai, C. Rhodium(I)-catalyzed ring-closing reaction of allene–alkene–alkynes: One-step construction of tricyclo[6.4.0.$0^{2,6}$] and bicyclo[6.3.0] skeletons from linear carbon chains. *Chem. Eur. J.* **2018**, *24*, 6538.

25 Noucti, N. N.; Alexanian. E. J. Stereoselective nickel-catalyzed [2+2+2] cycloadditions and alkenylative cyclizations of ene-allenes and alkenes. *Angew. Chem. Int. Ed.* **2013**, *52*, 8424.

26 Berthelot, M. Ueber die einwirkung der hitze auf einige kohlenwasserstoffe. *Justus Liebigs Ann. Chem.* **1866**, *139*, 272.

27 Reppe, W.; Schweckendiek, W. J. Cyclisierende polymerisation von acetylen. III benzol, benzolderivate und hydroaromatische verbindungen. *Justus Liebigs Ann. Chem.* **1948**, *560*, 104.

28 Hill, J. E.; Balaich, G.; Fanwick, P. E.; Rothwell, I. P. The chemistry of titanacyclopentadiene rings supported by 2,6-diphenylphenoxide ligation: stoichiometric and catalytic reactivity. *Organometallics* **1993**, *12*, 2911.

29 Sato, Y.; Nishimata, T.; Mori. M. Asymmetric synthesis of isoindoline and isoquinoline derivatives using nickel(0)-catalyzed [2 + 2 + 2] cocyclization. *J. Org. Chem.* **1994**, *59*, 6133.

30 Stará, I. G.; Starý, I.; Kollárovič, A.; Teplý, F.; Vyskočil, S.; Šaman, D. Transition metal catalysed synthesis of tetrahydro derivatives of [5]-, [6]- and [7]helicene. *Tetrahedron Lett.* **1999**, *40*, 1993.

31 Shibata, T.; Arai, Y.; Tahara, Y.-K. Enantioselective construction of quaternary carbon centers by catalytic [2 + 2 + 2] cycloaddition of 1,6-enynes and alkynes. *Org. Lett.* **2005**, *7*, 4955.

32 For a monograph, see: (a) Tanaka, K. *Transition-metal-mediated aromatic ring construction*; John Wiley & Sons, Inc., **2013**. Selected reviews: (b) Saito, S.; Yamamoto, Y. Recent advances in the transition-metal-catalyzed regioselective approaches to polysubstituted benzene derivatives. *Chem.*

Rev. **2000**, *100*, 2901. (c) Gandon, V.; Aubert, C.; Malacria, M. Recent progress in Co-mediated [2 + 2 + 2] cycloaddition reactions. *Chem. Commun.* **2006**, 2209. (d) Galan, B. R.; Rovis, T. Beyond Reppe: building substituted arenes by [2 + 2 + 2] cycloadditions of alkynes. *Angew. Chem., Int. Ed.* **2009**, *48*, 2830. (e) Pla-Quintana, A.; Roglans, A. [2 + 2 + 2] Cycloaddition reactions of macrocyclic systems catalyzed by transition metals. A review. *Molecules* **2010**, *15*, 9230. (f) Inglesby, P. A.; Evans, P. A. Stereoselective transition metal-catalysed higher-order carbocyclisation reactions. *Chem. Soc. Rev.* **2010**, *39*, 2791. (g) Zhou, L.; Li, S.; Kanno, K.-i.; Takahashi, T. Recent development for Formation of aromatic compounds via metallacyclopentadienes as metal-containing heterocycles. *Heterocycles* **2010**, *80*, 725. (h) Domínguez, G.; Pérez-Castells, J. Recent advances in [2 + 2 + 2] cycloaddition reactions. *Chem. Soc. Rev.* **2011**, *40*, 3430. (i) Weding, N.; Hapke, M. Preparation and synthetic applications of alkene complexes of group 9 transition metals in [2 + 2 + 2] cycloaddition reactions. *Chem. Soc. Rev.* **2011**, *40*, 4525. (j) Broere, D. L. J.; Ruijter, E. Recent advances in transition-metal-catalyzed [2 + 2 + 2]-cyclo(co)trimerization reactions. *Synthesis* **2012**, *44*, 2639. (k) Shibata, Y.; Tanaka, K. Rhodium-catalyzed [2 + 2 + 2] cycloaddition of alkynes for the synthesis of substituted benzenes: catalysts, reaction scope, and synthetic applications. *Synthesis* **2012**, *44*, 323 (l) Babazadeh, M.; Soleimani-Amiri, S.; Vessally, E.; Hosseinian, A.; Edjlali, L. Transition metal-catalyzed [2 + 2 + 2] cycloaddition of nitrogen-linked 1,6-diynes: a straightforward route to fused pyrrolidine systems. *RSC Adv.* **2017**, *7*, 43716. (m) Matton, P.; Huvelle, S.; Haddad M.; Phansavath P.; Vidal, V. R. Recent progress in metal-catalyzed [2+2+2] cycloaddition reactions. *Synthesis* **2022**, *54*, 4.

33 (a) Varela, J. A.; Saá, C. Construction of pyridine rings by metal-mediated [2 + 2 + 2] cycloaddition. *Chem. Rev.* **2003**, *103*, 3787. (b) Nakamura, I.; Yamamoto, Y. Transition-metal-catalyzed reactions in heterocyclic synthesis. *Chem. Rev.* **2004**, *104*, 2127. (c) Heller, B.; Hapke, M. The fascinating construction of pyridine ring systems by transition metal-catalysed [2 + 2 + 2] cycloaddition reactions. *Chem. Soc. Rev.* **2007**, *36*, 1085. (d) Varela, J. A.; Saá, C. Recent advances in the synthesis of pyridines by transition-metal-catalyzed [2 + 2 + 2] cycloaddition. *Synlett* **2008**, *2008*, 2571. (e) Okamoto, S. Synthesis of 2,2′-bipyridines by transition metal-catalyzed alkyne/nitrile [2 + 2 + 2] cycloaddition reactions. *Heterocycles* **2012**, *85*, 1579. (f) Chopade, P. R.; Louie, J. [2 + 2 + 2] cycloaddition reactions catalyzed by transition metal complexes. *Adv. Synth. Catal.* **2006**, *348*, 2307. (g) Hua, R.; Abrenica, M. V. A.; Wang, P. Cycloaddition of alkynes: atom-economic protocols for constructing six-membered cycles. *Curr. Org. Chem.* **2011**, *15*, 712. (h) Tanaka, K. Rhodium-catalyzed [2 + 2 + 2] cycloaddition for the synthesis of substituted pyridines, pyridones, and thiopyranimines. *Heterocycles* **2012**, *85*, 1017. (i) Gulevich, A. V.; Dudnik, A. S.; Chernyak, N.; Gevorgyan, V. Transition metal-mediated synthesis of monocyclic aromatic heterocycles. *Chem. Rev.* **2013**, *113*, 3084. (j) Thakur, A.; Louie, J. Advances in nickel-catalyzed cycloaddition reactions to construct carbocycles and heterocycles. *Acc. Chem. Res.* **2015**, *48*, 2354. (k) Lledó, A.; Pla-Quintana, A.; Roglans, A. Allenes,

versatile unsaturated motifs in transition-metal-catalysed [2 + 2 + 2] cycloaddition reactions. *Chem. Soc. Rev.* **2016**, *45*, 2010. (l) Domínguez, G.; Pérez-Castells, J. Alkenes in [2 + 2 + 2] cycloadditions. *Chem. - Eur. J.* **2016**, *22*, 6720. (m) Cen, K.; Usman, M.; Shen, W.; Liu, M.; Yang, R.; Cai, J. A review on the assembly of multi-substituted pyridines via Co-catalyzed [2 + 2 + 2] cycloaddition with nitriles. *Org. Biomol. Chem.* **2022**, *20*, 7391.

34 (a) Tanaka, K. Cationic rhodium(I)/BINAP-type biphosphine complexes: versatile new catalysts for highly chemo-, regio-, and enantioselective [2 + 2 + 2] cycloadditions. *Synlett* **2007**, 1977. (b) Shibata, T.; Tsuchikama, K. Recent advances in enantioselective [2 + 2 + 2] cycloaddition. *Org. Biomol. Chem.* **2008**, *6*, 1317. (c) Tanaka, K. Transition-metal-catalyzed enantioselective [2 + 2 + 2] cycloadditions for the synthesis of axially chiral biaryls. *Chem. - Asian J.* **2009**, *4*, 508. (d) Li, S.; Zhou, L.; Kanno, K.-I.; Takahashi, T. Recent development for enantioselective synthesis of aromatic compounds from alkynes via metallacyclopentadienes. *J. Heterocyclic Chem.* **2011**, *48*, 517. (e) Amatore, M.; Aubert, C. Recent advances in stereoselective [2 + 2 + 2] cycloadditions. *Eur. J. Org. Chem.* **2015**, *2015*, 265. (f) Pla-Quintana, A.; Roglans, A. Chiral induction in [2 + 2 + 2] cycloaddition reactions. *Asian J. Org. Chem.* **2018**, *7*, 1706.

35 (a) Yamamoto, Y. Recent advances in intramolecular alkyne cyclotrimerization and its applications. *Curr. Org. Chem.* **2005**, *9*, 503. (b) Kotha, S.; Brahmachary, E.; Lahiri, K. Transition metal catalyzed [2 + 2 + 2] cycloaddition and application in organic synthesis. *Eur. J. Org. Chem.* **2005**, 4741. (c) Kotha, S.; Goyal, D.; Chavan, A. S. Diversity-oriented approaches to unusual α-amino acids and peptides: step economy, atom economy, redox economy, and beyond. *J. Org. Chem.* **2013**, *78*, 12288. (d) Albano, G.; Aronica, L. A. Cyclization reactions for the synthesis of phthalans and isoindolines. *Synthesis* **2018**, *50*, 1209. (e) Kotha, S.; Lahiri, K.; Sreevani, G. Design and synthesis of aromatics through [2 + 2 + 2] cyclotrimerization. *Synlett* **2018**, *29*, 2342.

36 Pla-Quintana, A.; Roglans, A. The choice of rhodium catalysts in [2+2+2] cycloaddition reaction: a personal account. *Molecules* **2022**, *27*, 1332.

37 For selected examples, see: (a) Haraburda, E.; Lledó, A.; Roglans, A.; Pla-Quintana, A. Dehydrogenative [2 + 2 + 2] cycloaddition of cyano-yne-allene substrates: convenient access to 2,6-naphthyridine scaffolds. *Org. Lett.* **2015**, *17*, 2882. (b) Miura, T.; Morimoto, M.; Murakami, M. Enantioselective [2 + 2 + 2] cycloaddition reaction of isocyanates and allenes catalyzed by nickel. *J. Am. Chem. Soc.* **2010**, *132*, 15836. (c) Oonishi, Y.; Kitano, Y.; Sato, Y. Construction of tricyclic pyran derivatives through intramolecular [2+2+2] cycloaddition of allenynes with tethered aldehydes. *Tetrahedron* **2013**, *69*, 7713. (d) Oonishi, Y.; Yokoe, T.; Hosotani, A.; Sato, Y. Rhodium(I)-catalyzed

cyclization of allenynes with a carbonyl group through unusual insertion of a C=O bond into a rhodacycle intermediate. *Angew. Chem. Int. Ed.* **2014**, 53, 1135. (e) Oonishi, Y.; Hato, Y.; Sato, Y. Rhodium(I)-catalyzed [2+2+2] cycloaddition between allene, alkyne, and imine via a strained azarhodacycle intermediate. *Adv. Synth. Catal.* **2015**, *357*, 3033. (f) Sakashita, K.; Masutomi, K.; Noguchi, K.; Tanaka, K. Rhodium-catalyzed enantioselective [2 + 2 + 2] cycloaddition of tosylamide-linked 5-allenal and 5-allenone with internal alkynes. *Chem. Lett.* **2014**, *43*, 1260. (g) Oonishi, Y.; Saito, A.; Sato, Y. Rhodium(I)-catalyzed intermolecular [2+2+2] cycloaddition of allenyl aldehydes with alkynes and related cyclization. *Asian J. Org. Chem.* **2015**, *4*, 81.

38 (a) Parera, M.; Dachs, A.; Solà, M.; Pla-Quintana, A.; Roglans, A. Direct detection of key intermediates in rhodium(I)-catalyzed [2+2+2] cycloadditions of alkynes by ESI-MS. *Chem. Eur. J.* **2012**, *18*, 13097. (b) Dachs, A.; Torrent, A.; Pla-Quintana, A.; Roglans, A.; Jutand, A. Rates and mechanism of rhodium-catalyzed [2+2+2] cycloaddition of bisalkynes and a monoalkyne. *Organometallics* **2009**, *28*, 6036. (c) Uchimura, H.; Ito, J. I.; Iwasa, S.; Nishiyama, H. Oxidative addition reactions and stereochemistry on rhodium/4,5-bis(2-oxazolinyl)xanthene complexes. *J. Organomet. Chem.* **2007**, *692*, 481.

39 Dachs, A.; Pla-Quintana, A.; Parella, T.; Solà, M.; Roglans, A. Intramolecular [2+2+2] cycloaddition reactions of yne-ene-yne and yne-yne-ene enediynes catalysed by Rh^{I}: experimental and theoretical mechanistic studies. *Chem. Eur. J.* **2011**, 17, 14493. (b) Dachs, A.; Osuna, S.; Roglans, A.; Solà, M. Density functional study of the [2+2+2] cyclotrimerization of acetylene catalyzed by Wilkinson's catalyst, $RhCl(PPh_3)_3$. *Organometallics* **2010**, *29*, 562. (c) Dachs, A.; Torrent, A.; Roglans, A.; Parella, T.; Osuna, S.; Solà, M. Rhodium(I)-catalysed intramolecular [2+2+2] cyclotrimerisations of 15-, 20- and 25-membered azamacrocycles: experimental and theoretical mechanistic studies. *Chem. Eur. J.* **2009**, *15*, 5289. (d) Orian, L.; van Stralen, J. N. P.; Bickelhaupt, F. M. Cyclotrimerization reactions catalyzed by rhodium(I) half-sandwich complexes: a mechanistic density functional study. *Organometallics* **2007**, *26*, 3816.

40 Schore, N. E. Transition-metal-mediated cycloaddition reactions of alkynes in organic synthesis. *Chem. Rev.* **1988**, *88*, 1081.

41 Torres, Ò.; Roglans, A.; Pla-Quintana, A.; Luis, J. M.; Solà, M. Computational insight into Wilkinson's complex catalyzed [2 + 2 + 2] cycloaddition mechanism leading to pyridine formation. *J. Organomet. Chem.* **2014**, *768*, 15.

42 Roglans, A.; Pla-Quintana, A.; Solà, M. Mechanistic studies of transition-metal-catalyzed [2 + 2 + 2] cycloaddition reactions. *Chem. Rev.* **2021**, *121*, 1894.

43 Benson, R. E.; Lindsey Jr., R.V. Chemistry of allene. I. Cyclopolymerization. Synthesis and chemistry of 1,2,4-and 1,3,5-trimethylenecyclohexane and 1,3,5,7-tetramethylenecyclooctane. *J. Am. Chem. Soc.* **1959**, *81*, 4247.

44 Benson, R. E.; Lindsey Jr., R.V. Chemistry of allene. II. Reaction of allene with acetylenes. *J. Am. Chem. Soc.* **1959**, *81*, 4250.

45 (a) Munz, C.; Stephan, C.; Dieck H. Diazadiene als steuerliganden in der homogenen katalyse XIX[1]. Palladium-katalysierte 2:2-cyclisierung eines alkins mit allenen zu naphthalin-2,3,6,7-tetracarbonsäurederivaten. *J. Organomet. Chem.* **1990**, *395*, C42. (b) Stephan, C.; Munz, C.; Dieck H. Die palladiumkatalysierte cocyclisierung von allenen mit elektronenarmen alkinen. Einige untersuchungen zur kupplung von allenderivaten mit acetylendicarbonsäuredimethylester an palladium und platin. *J. Organomet. Chem.* **1994**, *468*, 273.

46 Takahashi, T.; Tsai, F.-Y.; Li, Y.; Nakajima, K.; Kotora, M. Carbon−carbon bond formation reaction of zirconacyclopentadienes with alkynes in the presence of Ni(II)-complexes. *J. Am. Chem. Soc.* **1999**, *121*, 11093.

47 Hsieh, J.-C.; Rayabarapu, D. K.; Cheng, C.-H. Nickel-catalyzed highly chemoselective cocyclotrimerization of arynes with allenes: a novel method for 10-methylene-9,10-dihydrophenanthrenes. *Chem. Commun.* **2004**, 532.

48 Liu, Y.-L.; Liang, Y.; Pi, S.-F.; Huang, X.-C.; Li, J.-H. Palladium-catalyzed cocyclotrimerization of allenes with arynes: selective synthesis of phenanthrenes. *J. Org. Chem.* **2009**, *74*, 3199.

49 Shanmugasundaram, M.; Wu, M.-S.; Cheng, C.-H. Nickel-catalyzed highly regio- and chemoselective cocyclotrimerization of propiolates with allenes: a novel route to polysubstituted benzene derivatives. *Org. Lett.* **2001**, *3*, 4233.

50 Sakashita, K.; Shibata, Y.; Tanaka, K. Rhodium-catalyzed cross-cyclotrimerization and dimerization of allenes with alkynes. *Angew. Chem. Int. Ed.* **2016**, *55*, 6753.

51 Shanmugasundaram, M.; Wu, M.-S.; Jeganmohan, M.; Huang, C.-W.; Cheng, C.-H. Highly regio- and chemoselective [2 + 2 + 2] cycloaddition of electron-deficient diynes with allenes catalyzed by nickel complexes: a novel entry to polysubstituted benzene derivatives. *J. Org. Chem.* **2002**, *67*, 7724.

52 Yasuda, S.; Kawaguchi, Y.; Okamoto, Y.; Mukai, C. Chemo- and regioselective rhodium(I)-catalyzed [2+2+2] cycloaddition of allenynes with alkynes. *Chem. Eur. J.* **2016**, *22*, 12181.

53 Arai, S.; Izaki, A.; Amako, Y.; Nakajima, M.; Uchiyama, M.; Nishida, A. Regioselective [2+2+2] cycloaddition reaction using allene-ynes with simple allenes under nickel catalysis. *Adv. Synth. Catal.* **2019**, *361*, 4882.

54 Jiang, X.; Ma, S. *Trans*-RhCl(CO)(PPh_3)$_2$-catalyzed monomeric and dimeric cycloisomerization of propargylic 2,3-dienoates. Establishment of α,β-unsaturated δ-lactone rings by cyclometalation. *J. Am. Chem. Soc.* **2007**, *129*, 11600.

55 Brusoe, A. T.; Alexanian. E. J. Rhodium(I)-catalyzed ene–allene–allene [2+2+2] cycloadditions: stereoselective synthesis of complex *trans*-fused carbocycles. *Angew. Chem. Int. Ed.* **2011**, *50*, 6596.

56 Brusoe, A. T.; Edwankar, R. V.; Alexanian, E. J. Enantioselective intermolecular [2 + 2 + 2] cycloadditions of ene–allenes with allenoates. *Org. Lett.* **2012**, *14*, 6096.

57 (a) Chevliakov, M. V.; Montgomery, J. A stereodivergent approach to (-)-*R*-kainic acid and (+)-*R*-allokainic acid utilizing the complementarity of alkyne and allene cyclizations. *J. Am. Chem. Soc.* **1999**, *121*, 11139. (b) Makino, T.; Itoh, K. Rhodium complex-catalyzed cycloisomerization of allenenes: exo and endo cyclization depending on the auxiliary ligands. *J. Org. Chem.* **2004**, *69*, 395.

58 Chang, S.-J.; McNally, D.; Shary-Tehrany, S.; Hickey, M. J., Sr.; Boyd, R. H. The heats of combustion and strain energies of bicyclo[n.m.0]alkanes. *J. Am. Chem. Soc.* **1970**, *92*, 3109.

59 (a) Aubert, C.; Llerena, D.; Malacria, M. Allenes as new partners in intramolecular cobalt-mediated [2+2+2] cycloaddition reactions. *Tetrahedron Lett.* **1994**, *35*, 2341. (b) Llerena, D.; Buisine, O.; Aubert, C.; Malacria, M. Synthesis of variously substituted allenediynes and their cobalt (I)-mediated [2+2+2] cycloaddition reactions. *Tetrahedron* **1998**, *54*, 9373.

60 (a) Buisine, O.; Aubert, C.; Malacria, M. First example of a total axial to centered chirality transfer in the [2 + 2 + 2] cycloadditions of allenediynes. *Synthesis* **2000**, 985. (b) Petit, M.; Aubert, C.; Malacria, M. Cobalt(I)-mediated [2 + 2 + 2] cyclization of allenediynes toward a diastereoselective approach to 11-aryl steroid skeletons. *Org. Lett.* **2004**, *6*, 3937. (c) Petit, M.; Aubert, C.; Malacria, M. Diastereoselective approach to 11-aryl steroid skeletons through a cobalt(I)-mediated [2+2+2] cyclization of allenediynes. *Tetrahedron*, **2006**, *62*, 10582.

61 (a) Bennacer, B.; Fujiwara, M.; Lee, S.-Y.; Ojima, I. Silicon-initiated carbonylative carbotricyclization and [2+2+2+1] cycloaddition of enediynes catalyzed by rhodium complexes. *J. Am. Chem. Soc.* **2005**, *127*, 17756.

62 Ohta, Y.; Yasuda, S.; Yokogawa, Y.; Kurokawa, K.; Mukai, C. Stereospecific and stereoselective rhodium(I)-catalyzed intramolecular [2+2+2] cycloaddition of allene-ene-ynes: construction of bicyclo[4.1.0]heptenes. *Angew. Chem. Int. Ed.* **2015**, *54*, 1240.

63 Saito, N.; Ichimaru, T.; Sato, Y. Ruthenium-catalyzed intramolecular [2+2+2] cyclization of allene–yne–enes: construction of fused-tricyclic skeletons. *Chem. - Asian J.* **2012**, *7*, 1521.

64 Cassú, D.; Parella, T.; Solà, M.; Pla-Quintana, A.; Roglans, A. Rhodium-catalyzed [2+2+2] cycloaddition reactions of linear allene–ene–ynes to afford fused tricyclic scaffolds: insights into the mechanism. *Chem. Eur. J.* **2017**, *23*, 14889.

65 (a) Haraburda, E.; Torres, O.; Parella, T.; Solà, M.; Pla-Quintana, A. Stereoselective rhodium-catalysed [2+2+2] cycloaddition of linear allene–ene/yne–allene substrates: reactivity and theoretical mechanistic studies. *Chem. Eur. J.* **2014**, *20*, 5034. (b) Haraburda, E.; Fernández, M.; Gifreu, A.; Garcia, J.; Parella, T.; Pla-Quintana, A.; Roglans, A. Chiral induction in intramolecular rhodium-catalyzed [2+2+2] cycloadditions of optically active allene–ene/yne–allene substrates. *Adv. Synth. Catal.* **2017**, *359*, 506.

66 Hopf, H.; Markopoulos, G. The chemistry of bisallenes. *Beilstein J. Org. Chem.* **2012**, *8*, 1936.

67 Alcaide, B.; Almendros, P.; Aragoncillo, C. Cyclization reactions of bis(allenes) for the synthesis of polycarbo(hetero)cycles. *Chem. Soc. Rev.* **2014**, *43*, 3106.

68 Guofei, C.; Xuefeng, J.; Chunling, F.; Shengming, M. The diversified reactivities of 1,5-bisallenes. *Chem. Lett.* **2010**, *39*, 78.

69 (a) Bai, T.; Ma, S.; Jia, G. Insertion reactions of allenes with transition metal complexes. *Coord. Chem. Rev.* **2009**, *253*, 423. (b) Jeganmohan, M.; Cheng, C.-H. Transition metal-catalyzed three-component coupling of allenes and the related allylation reactions. *Chem. Commun.* **2008**, 3101.

70 Muñoz, M. P. Transition metal-catalysed intermolecular reaction of allenes with oxygen nucleophiles: a perspective. *Org. Biomol. Chem.* **2012**, *10*, 3584.

71 (a) Kang, S.-K.; Baik, T.-G.; Kulak, A. N.; Ha, Y.-H.; Lim, Y.; Park. J. Palladium-catalyzed carbocyclization/silastannylation and distannylation of bis(allenes). *J. Am. Chem. Soc.* **2000**, *122*, 11529. (b) Hong, Y.-T.; Yoon, S.-K.; Kang, S.-K.; Yu, C.-M. A stereoselective carbocyclization of bis(allenes) with germylstannane catalyzed by palladium complexes. *Eur. J. Org. Chem.* **2004**, 4628. (c) Lian, X.; Ma, S. Palladium(II)-catalyzed highly stereoselective sandwich-type triple cyclization reaction of 1,5-bisallenes and 2,3-allenoic acids. *Chem. Eur. J.* **2010**, 16, 7960.

72 Lim, Y. N.; Kim, H.-T.; Yoon, H.-S.; Jang, H.-Y. Regio- and stereoselective reductive cyclization of 1,5-bisallenes under hydrogenation conditions. *Bull. Korean Chem. Soc.* **2011**, *32*, 3117.

73 Amako, Y.; Hori, H.; Arai, S.; Nishida, A. Regioselective hydronickelation of allenes and its application to the hydrocyanative carbocyclization reaction of allene–ynes and bis-allenes. *J. Org. Chem.* **2013**, *78*, 10763.

74 Deng, Y.; Shi, Y.; Ma, S. An efficient synthesis of 2,5-dihydrofuran-fused bicyclic skeletons via the Pd(II)-catalyzed tandem-cyclization reaction of 1,ω-bisallenols. *Org. Lett.* **2009**, *11*, 1205.

75 Deng, Y.; Fu, C.; Ma, S. Selectivity manipulation of bicyclization reactions of 1,5-bis(1,2-allenylketone)s: Pd versus Rh and electronic effect. *Chem. Eur. J.* **2011**, *17*, 4976.

76 Quirós, M. T.; Hurtado-Rodrigo, C.; Muñoz, M. P. Nucleophile dependent formation of 6- and 7-membered *N*-heterocycles by platinum-catalysed cyclisation of 1,5-bisallenes. *Org. Biomol. Chem.* **2017**, *15*, 6731.

77 Zhu, C.; Yang, B.; Qiu, B.; Bäckvall J.-E. Highly selective construction of seven-membered carbocycles by olefin-assisted palladium-catalyzed oxidative carbocyclization–alkoxycarbonylation of bisallenes. *Angew. Chem. Int. Ed.* **2016**, *55*, 14405.

78 Zhu, C.; Yang, B.; Mai, B. Y.; Palazzotto, S.; Qiu, Y.; Gudmundsson, A.; Ricke, A.; Himo, F.; Bäckvall, J.-E. Highly selective palladium-catalyzed hydroborylative carbocyclization of bisallenes to seven-membered rings. *J. Am. Chem. Soc.* **2018**, *140*, 14324.

79 Shu, W.; Jia, G.; Ma, S. Palladium-catalyzed three-component cascade cyclization reaction of bisallenes with propargylic carbonates and organoboronic acids: efficient construction of cis -fused bicyclo[4.3.0]nonenes. *Angew. Chem. Int. Ed.* **2009**, *48*, 2788.

80 Kang *et al.*[71a] and Yu *et al.*[71b] had already observed the head-to-head adduct although they postulated its formation via carbopalladation process.

81 Jiang, X.; Cheng, X.; Ma, S. Controllable [2+2] cycloadditions of 1,5-bisallenyl-substituted compounds. *Angew. Chem. Int. Ed.* **2006**, *45*, 8009.

82 Arai, S.; Kawata, Y.; Amako, Y.; Nishida, A. Nickel-catalyzed [2 + 2] cycloaddition reaction using bisallenes. *Tetrahedron Lett.* **2019**, *60*, 151168.

83 Kim, S. M.; Park, J. H.; Kang, Y. K.; Chung, Y. K. N-heterocyclic carbene gold(I) catalyzed transformation of *N*-tethered 1,5-bisallenes to 6,7-dimethylene-3-azabicyclo[3.1.1]heptanes. *Angew. Chem. Int. Ed.* **2009**, 48, 4532.

84 Lu, P.; Ma, S. Observation of new cycloisomerization pattern of 1,5-bisallenes. Catalyst and substituent effects. *Org. Lett.* **2007**, *9*, 2095.

85 (a) Inagaki, F.; Narita, S.; Hasegawa, T.; Kitagaki, S.; Mukai, C. Rhodium(I)-catalyzed intramolecular carbonylative [2+2+1] cycloaddition of bis(allene)s: bicyclo[6.3.0]undecadienones and bicyclo[5.3.0]decadienones. *Angew. Chem. Int. Ed.* **2009**, *48*, 2007. (b) Kawamura, T.; Inagaki, F.; Narita, S.; Takahashi, Y.; Hirata, S.; Kitagaki, S.; Mukai, C. Rhodium(I)-catalyzed intramolecular carbonylative [2+2+1] cycloadditions and cycloisomerizations of bis(sulfonylallene)s. *Chem. Eur. J.* **2010**, *16*, 5173.

86 (a) He, M.; Chen, N.; Zhou, T.; Li, Q.; Li, H.; Lang, M.; Wang, J.; Peng, S. Copper-catalyzed tandem cross-coupling/[2 + 2] cycloaddition of 1,6-allenynes with diazo compounds to 3-Azabicyclo[5.2.0] ring systems. *Org. Lett.* **2019**, *21*, 9559. (b) He, M.; Chen, N.; Liu, L.; Zhu, Y.; Li, Q.; Li, H.; Lang, M.; Wang, J; Peng, S. Synthesis of 3-azabicyclo[m.2.0] ring systems via a copper-catalyzed cascade reaction of diazo compounds with 1,n-allenynes. *J. Org. Chem.* **2020**, *85*, 4418.

87 Ma, S.; Lu, P.; Lu, L.; Hou, H.; Wei, J.; He, Q.; Gu, Z.; Jiang, X.; Jin, X. What can a metal catalyst do with allenes? One-step formation of steroid scaffolds from readily available starting materials. *Angew. Chem. Int. Ed.* **2005**, *44*, 527.

88 Lu, L.; Ma, S. Rh^{I}-catalyzed bimolecular cyclization between two different 1,5-bisallenes: a combinatorial one-step approach to heterosteroids and mechanistic implications. *Chem. Asian J.* **2007**, *2*, 199.

89 Lu, P.; Ma, S. Rh-catalyzed triple allene approach to bicyclo[4.4.0]decene derivatives and its application for the stepwise synthesis of steroid-like tetracyclic skeletons. *Org. Lett.* **2007**, *9*, 5319.

90 Park, J. H.; Kim, E.; Kim, H.-M.; Choi, S. Y.; Chung, Y. K. Cobalt/rhodium heterobimetallic nanoparticle-catalyzed carbonylative [2+2+1] cycloaddition of allenes and bisallenes to Pauson–Khand-type reaction products. *Chem. Commun.* **2008**, 2388.

91 For selected reviews, see: (a) Meyer, A. G.; Bissember, A. C.; Hyland, C. J. T.; Williams, C. C.; Szabo, M.; Abel, S.-A. G.; Bird, M. J.; Hyland, I. K.; Pham, H. Seven-membered rings, chapter 7. *Prog. Heterocycl. Chem.* **2018**, *30*, 493. (b) Nguyen, T. V.; Hartmann, J. M.; Enders, D. Recent synthetic strategies to access seven-membered carbocycles in natural product synthesis. *Synthesis* **2013**, *45*, 845. (c) Riley, D. L.; van Otterlo, W. A. L. Oxepines and azepines. In *Heterocycles in natural product synthesis*; Wiley-VCH, **2011**. (d) Kantorowski, E. J.; Kurth, M. J. Expansion to seven-membered rings. *Tetrahedron* **2000**, 56, 4317. (e) Liu, J.-h.; Steigel, A.; Reininger, E.; Bauer, R. Two new prenylated 3-benzoxepin derivatives as cyclooxygenase inhibitors from *Perilla frutescens* var. acuta. *J. Nat. Prod.*

2000, 63, 403. Selected recent studies based on the synthesis of benzo[*d*]azepine derivatives: (f) Jiang, B.; Liu, J.-X.; Wei, Y.; Shi, M. Nickel-catalyzed synthesis of benzo[b]naphthol[*1,2-d*]azepine via intramolecular radical tandem cyclization of alkyl bromide-tethered alkylidenecyclopropanes. *Org. Lett.* **2018**, *20*, 6229. (g) Nayak, M.; Kang, Y. K.; Kim, I. Altering the cyclization modes: temperature-dependent intramolecular 7-*endo-dig* vs 6-*endo-dig* electrophilic ring closures. *Org. Lett.* **2017**, *19*, 1474. (h) Adamovskyi, M. I.; Ryabukhin, S. V.; Sibgatulin, D. A.; Rusanov, E.; Grygorenko, O. O. Beyond the five and six: evaluation of seven-membered cyclic anhydrides in the Castagnoli-Cushman reaction. *Org. Lett.* **2017**, *19*, 130.

92 Trost, B. M.; Zou, Z.; Schultz, J. E. Transition-metal-catalyzed cycloaddition reactions to access seven-membered rings. *Chem. Eur. J.* **2020**, *26*, 15354.

93 (a) Kozuch, S.; Shaik, S. Kinetic-quantum chemical model for catalytic cycles: the Haber−Bosch process and the effect of reagent concentration. *J. Phys. Chem. A* **2008**, *112*, 6032. (b) Kozuch, S.; Shaik, S. How to conceptualize catalytic cycles? The energetic span model. *Acc. Chem. Res.* **2011**, *44*, 101.

94 Artigas, A.; Castanyer, C.; Roig, N.; Lledó, A.; Solà, M.; Pla-Quintana, A.; Roglans, A. Synthesis of fused dihydroazepine derivatives of fullerenes by a Rh-catalyzed cascade process. *Adv. Synth. Catal.* **2021**, *363*, 383.

95 (a) Pradhan, R.; Patra, M.; Behera, A. K.; Mishra, B. K.; Behera, R. K. A synthon approach to spiro compounds. *Tetrahedron* **2006**, *62*, 779. (b) Babar, K.; Zahoor, A. F.; Ahmad, S.; Akhtar, R. Recent synthetic strategies toward the synthesis of spirocyclic compounds comprising six-membered carbocyclic/heterocyclic ring systems. *Mol. Diversity* **2020**, *25*, 2487.

96 Saragi, T. P. I.; Spehr, T.; Siebert, A.; Fuhrmann-Lieker, T.; Salbeck, J. Spiro compounds for organic optoelectronics. *Chem. Rev.* **2007**, *107*, 1011.

97 For selected reviews, see: (a) Abdul, R.; Xufeng, L. Development and application of chiral spirocyclic phosphoric acids in asymmetric catalysis. *Org. Biomol. Chem.* **2018**, *16*, 4753. (b) Xie, J.-H.; Duan, H.-F.; Fan, B.-M.; Cheng, X.; Wang, L.-X.; Zhou, Q.-L. Application of SDP ligands for Pd-catalyzed allylic alkylation. *Adv. Synth. Catal.* **2004**, *346*, 625. (c) Xu, C.; Qi, Y.; Yang, X.; Li, X.; Li, Z.; Bai, L. Development of C2-symmetric chiral spirocyclic phase-transfer catalysts: synthesis and application to asymmetric alkylation of glycinate Schiff base. *Org. Lett.* **2021**, *23*, 2890. (d) Cheng, X.; Zhang, Q.; Xie, J.-H.; Wang, L.-X.; Zhou, Q.-L. Highly rigid diphosphane ligands with a large dihedral angle based on a chiral spirobifluorene backbone. *Angew. Chem. Int. Ed.* **2005**, *44*, 1118.

98 For selected reviews, see: (a) Badillo, J. J.; Hanhan, N. V.; Franz, A. K. Enantioselective synthesis of substituted oxindoles and spirooxindoles with applications in drug discovery. *Curr. Opin. Drug Discovery Dev.* **2010**, *13*, 758. (b) Ding, A.; Meazza, M.; Guo, H.; Yang, J. W.; Rios, R. New development in the enantioselective synthesis of spiro compounds. *Chem. Soc. Rev.* **2018**, *47*, 5946. (c) Xu, P.-W.; Yu, J.-S.; Chen, C.; Cao, Z.-Y.; Zhou, F.; Zhou, J. Catalytic enantioselective construction of spiro quaternary carbon stereocenters. *ACS Catal.* **2019**, *9*, 1820. (d) Boddy, A. J.; Bull, J. A. Stereoselective synthesis and applications of spirocyclic oxindoles. *Org. Chem. Front.* **2021**, *8*, 1026.

99 (a) Sharma, R. L.; Kour, D.; Singh, J.; Kumar, S.; Gupta, P.; Gupta, S.; Kour, B.; Sachar, A. Synthesis of some indole based spiro and condensed heterocycles as potential biologically active agents. *J. Heterocyclic Chem.* **2008**, *45*, 1775. (b) Wang, Y.; Shi, F.; Yao, X.-X.; Sun, M.; Dong, L.; Tu, S.-J. Catalytic asymmetric construction of 3,3′-spirooxindoles fused with seven-membered rings by enantioselective tandem reactions. *Chem. – Eur. J.* **2014**, *20*, 15047.

100 Yeung, B. K. S.; Zou, B.; Rottmann, M.; Lakshminarayana, S. B.; Ang, S. H.; Leong, S. Y.; Tan, J.; Wong, J.; Keller-Maerki, S.; Fischli, C.; Goh, A.; Schmitt, E. K.; Krastel, P.; Francotte, E.; Kuhen, K.; Plouffe, D.; Henson, K.; Wagner, T.; Winzeler, E. A.; Petersen, F.; Brun, R.; Dartois, V.; Diagana, T. T.; Keller, T. H. Spirotetrahydro *β*-carbolines (spiroindolones): a new class of potent and orally efficacious compounds for the treatment of malaria. *J. Med. Chem.* **2010**, *53*, 5155.

101 Pellegrino, S.; Ruscica, M.; Magni, P.; Vistoli, G.; Gelmi, M. L. Antiproliferative activity on human prostate carcinoma cell lines of new peptidomimetics containing the spiroazepinoindolinone scaffold. *Bioorg. Med. Chem.* **2013**, *21*, 5470.

102 Heinrich, M.; Teoh, H. L. Galanthamine from snowdrop – the development of a modern drug against Alzheimer's disease from local Caucasian knowledge. *J. Ethnopharmacol.* **2004**, *92*, 147.

103 (a) Hu, T.; Burton, I. W.; Cembella, A. D.; Curtis, J. M.; Quilliam, M. A.; Walter, J. A.; Wright, J. L. C. Characterization of spirolides a, c, and 13-desmethyl c, new marine toxins isolated from toxic plankton and contaminated shellfish. *J. Nat. Prod.* **2001**, *64*, 308. (b) Uemura, D.; Chou, T.; Haino, T.; Nagatsu, A.; Fukuzawa, S.; Zheng, S.; Chen, H. Pinnatoxin A: a toxic amphoteric macrocycle from the Okinawan bivalve Pinna muricata. *J. Am. Chem. Soc.* **1995**, *117*, 1155. (c) Takada, N.; Umemura, N.; Suenaga, K.; Chou, T.; Nagatsu, A.; Haino, T.; Yamada, K.; Uemura, D. Pinnatoxins B and C, the most toxic components in the pinnatoxin series from the Okinawan bivalve Pinna muricata. *Tetrahedron Lett.* **2001**, *42*, 3491. (d) Takada, N.; Umemura, N.; Suenaga, K.; Uemura, D. Structural determination of pteriatoxins A, B and C, extremely potent toxins from the bivalve Pteria penguin. *Tetrahedron Lett.* **2001**, *42*, 3495. (e) Ishihara, J.; Horie, M.; Shimada, Y.; Tojo, S.; Murai, A.

Asymmetric construction of the azaspiro[5.6]dodec-9-ene system in marine natural toxins. *Synlett* **2002**, 403.

104 (a) Araoz, R.; Servent, D.; Molgó, J.; Iorga, B. I.; Fruchart-Gaillard, C.; Benoit, E.; Gu, Z.; Stivala, C.; Zakarian, A. Total synthesis of pinnatoxins A and G and revision of the mode of action of pinnatoxin A. *J. Am. Chem. Soc.* **2011**, *133*, 10499. (b) Bourne, Y.; Sulzenbacher, G.; Radić, Z.; Aráoz, R.; Reynaud, M.; Benoit, E.; Zakarian, A.; Servent, D.; Molgó, J.; Taylor, P.; Marchot, P. Marine macrocyclic imines, pinnatoxins A and G: structural determinants and functional properties to distinguish neuronal α7 from muscle $\alpha 1_2\beta\gamma\delta$ nAChRs. *Structure* **2015**, *23*, 1106.

105 Artigas, A.; Vila, J.; Lledó, A.; Solà, M.; Pla-Quintana, A.; Roglans, A. A Rh-catalyzed cycloisomerization/Diels–Alder cascade reaction of 1,5-bisallenes for the synthesis of polycyclic heterocycles. *Org. Lett.* **2019**, *21*, 6608.

106 Guo, Y.-G.; Xie, Y.-G.; Wu, G.-J.; Cheng, T.-F.; Zhu, S.-L.; Yan, S.-K.; Jin, H.-Z.; Zhang, W.-D. Xylopidimers A–E, five new guaiane dimers with various carbon skeletons from the roots of Xylopia vielana. *ACS Omega* **2019**, *4*, 2047.

107 (a) Parr, R. G.; Yang, W. Density functional approach to the frontier-electron theory of chemical reactivity. *J. Am. Chem. Soc.* **1984**, *106*, 4049. (b) Fuentalba, P.; Pérez, P.; Contreras, R. On the condensed Fukui function. *J. Chem. Phys.* **2000**, *113*, 2544.

108 Vitaku, E.; Smith, D. T., Njardarson J. T. Analysis of the structural diversity, substitution patterns, and frequency of nitrogen heterocycles among U.S. FDA approved pharmaceuticals. *J. Med. Chem.* **2014**, *57*, 10257.

109 Seeman, J. I. Effect of conformational change on reactivity in organic chemistry. Evaluations, applications, and extensions of Curtin-Hammett Winstein-Holness kinetics. *Chem. Rev.* **1983**, *83*, 83.

110 (a) Sulub-Sulub, R.; Loría-Bastarrachea, M. I.; Santiago-Garcia, J. L.; Aguilar-Vega, M. Synthesis and characterization of new polyimides from diphenylpyrene dianhydride and ortho methyl substituted diamines. *RSC Adv.* **2018**, *8*, 31881. (b) Abdulhamid, M. A.; Ma, X.; Ghanem, B. S.; Pinnau, I. Synthesis and characterization of organo-soluble polyimides derived from alicyclic dianhydrides and a dihydroxyl-functionalized spirobisindane diamine. *ACS Appl. Polym. Mater.* **2019**, *1*, 63.

111 Vila, J.; Solà, M.; Pla-Quintana, A.; Roglans, A. Highly selective synthesis of seven-membered azaspiro compounds by a Rh(I)-catalyzed cycloisomerization/Diels–Alder cascade of 1,5-bisallenes. *J. Org. Chem.* **2022**, *87*, 5279.

112 Vila, J.; Vinardell, R.; Solà, M.; Pla-Quintana, A.; Roglans, A. A Rh(I)-catalyzed cascade cyclization of 1,5-bisallenes and alkynes for the formation of cis-3,4-arylvinyl pyrrolidines and cyclopentanes. *Adv. Synth. Catal.* **2022**, *364*, 206.

113 (a) Horner, L.; Hoffman, H. Neuere methoden der präparativen organischen chemie II. Präparative und analytische bedeutung tertiärer phosphine und verwandter verbindungen. Phosphor-organische verbindungen VI. *Angew. Chem.* **1956**, *68*, 473. (b) Johnson, A. W.; Tebby, J. C. The adducts from triphenylphosphine and dimethyl acetylenedicarboxylate. *J. Chem. Soc.* **1961**, 2126.

114 Selected examples: (a) Gallen, A.; Riera, A.; Verdaguer, X.; Grabulosa, A. Coordination chemistry and catalysis with secondary phosphine oxides. *Catal. Sci. Technol.* **2019**, *9*, 5504. (b) Reek, J. H.; Bruin, B.; Pullen, S.; Mooibroek, T. J.; Kluwer, A. M.; Caumes, X. Transition metal catalysis controlled by hydrogen bonding in the second coordination sphere. *Chem. Rev.* **2022**, *122*, 12308.

115 (a) Christiansen, A.; Selent, D.; Spannenberg, A.; Baumann, W.; Franke, R.; Börner, A. Reaction of secondary phosphine oxides with rhodium(I). *Organometallics* **2010**, *29*, 3139. (b) Christiansen, A.; Selent, D.; Spannenberg, A.; Köcjerling, M.; Reinke, H.; Bauman, W.; Jiao, H.; Franke, R.; Börner, A. Heteroatom-substituted secondary phosphine oxides (HASPOs) as decomposition products and preligands in rhodium-catalysed hydroformylation. *Chem. Eur. J.* **2011**, *17*, 2120.

116 Matsumoto, M.; Tamura, M. Rhodium-catalyzed low pressure hydroformylation of higher α-olefins: New, thermally stable rhodium catalysts by reaction of $RhH(CO)(PPh_3)_3$ with phosphinous acids. *J. Mol. Catal.* **1983**, *19*, 365.

117 (a) Jiang, X.; Van den Berg, M.; Minnaard, A. J.; Feringa, B. L.; De Vries, J. G. The application of monodentate secondary phosphine oxide ligands in rhodium- and iridium-catalyzed asymmetric hydrogenation. *Tetrahedron: Asymmetry* **2004**, *15*, 2223. (b) Landert, H.; Spindler, F.; Wyss, A.; Blaser, H.; Pugin, B.; Ribourdouille, Y.; Gschwend, B.; Ramalingamm, B.; Pfaltz, A. Chiral mixed secondary phosphine-oxide–phosphines: high-performing and easily accessible ligands for asymmetric hydrogenation. *Angew. Chem. Int. Ed.* **2010**, *49*, 6873.

118 (a) Haydl, A. M.; Xu, K.; Breit, B. Regio- and enantioselective synthesis of *N*-substituted pyrazoles by rhodium-catalyzed asymmetric addition to allenes. *Angew.Chem.Int.Ed.* **2015**, *54*, 7149. (b) Xu, K.; Raimondi, W.; Bury, T.; Breit, B. Enantioselective formation of tertiary and quaternary allylic C–N bonds via allylation of tetrazoles. *Chem. Commun.* **2015**, *51*, 10861. (c) Haydl, A. M.; Hilpert, L. J.; Breit, B. Regioconvergent and enantioselective rhodium-catalyzed hydroamination of internal and terminal alkynes: a highly flexible access to chiral pyrazoles. *Chem. Eur. J.* **2016**, 22, 6547. For a non-enantioselective hydroamination, see: (d) Xu, K.; Thieme, N.; Breit, B. Unlocking the N^2 selectivity

of benzotriazoles: regiodivergent and highly selective coupling of benzotriazoles with allenes. *Angew. Chem. Int. Ed.* **2014**, *53*, 7268.

119 Clavier, H.; Buono, G. [2+1] Cycloaddition affording methylene- and vinylidenecyclopropane derivatives: a journey around the reactivity of metal-phosphinito–phosphinous acid complexes. *Chem. Rec*. **2017**, *17*, 399.

120 Achard, T.; Lepronier, A.; Gimbert, Y.; Clavier, H.; Giordano, L.; Tenaglia, A.; Buono, G. A regio- and diastereoselective platinum-catalyzed tandem [2+1]/[3+2] cycloaddition sequence. *Angew. Chem. Int. Ed.* **2011**, 50, 3552.

121 Lee, J.; Hahm, H.; Kwak, J.; Kim, M. New aspects of recently developed rhodium(*N*-heterocyclic carbene)-catalyzed organic transformations. *Adv. Synth. Catal*. **2019,** *361*, 1479.

122 (a) Kuhl, O. The chemistry of functionalised *N*-heterocyclic carbenes. *Chem. Soc. Rev*. **2007**, *36*, 592. (b) Zhang, W. H.; Chien, S. W.; Hor, T. S. A. Recent advances in metal catalysts with hybrid ligands. *Coord. Chem. Rev*. **2011**, *255*, 1991. (c) Hameury, S.; de Fremont, P.; Braunstein, P. Metal complexes with oxygen-functionalized NHC ligands: synthesis and applications. *Chem. Soc. Rev*. **2017**, *46*, 632. (d) Peris, E. Smart *N*-Heterocyclic carbene ligands in catalysis. *Chem. Rev*. **2018**, *118*, 9988. (e) Neshat, A.; Mastrorilli, P.; Mobarakeh, A. M., *Molecules* **2022**, *27*, 95.

123 Fliedel, C.; Braunstein, P. Recent advances in *S*-functionalized *N*-heterocyclic carbene ligands: from the synthesis of azolium salts and metal complexes to applications. *J. Organomet. Chem*. **2014**, *751*, 286.

124 (a) Huynh, H. V.; Yeo, C. H.; Tan, G. K. Hemilabile behavior of a thioether-functionalized *N*-heterocyclic carbeneligand. *Chem. Commun*. **2006**, 3833. (b) Fliedel, C.; Schnee, G.; Braunstein, P. Versatile coordination modes of novel hemilabile *S*-NHC ligands. *Dalton Trans*. **2009**, 2474. (c) Huynh, H. V.; Yeo, C. H.; Chew, Y. X. Syntheses, Structures, and Catalytic Activities of Hemilabile Thioether-Functionalized NHC Complexes. *Organometallics* **2010**, *29*, 1479. (d) Egly, J.; Bouche, M.; Chen, W.; Maisse-Francois, A.; Achard, T.; Bellemin-Laponnaz, S. Synthesis, structural characterization and anti-proliferative activity of (κ^1-C)- and (κ^2-C,S)-Pt^{II} complexes bearing thioether-functionalized *N*-heterocyclic carbenes. *Eur. J. Inorg. Chem*. **2018**, 159. (e) Ulm, F.; Poblador-Bahamonde, A. I.; Choppin, S.; Bellemin-Laponnaz, S.; Chetcuti, M. J.; Achard, T.; Ritleng, V. Synthesis, characterization, and catalytic application in aldehyde hydrosilylation of half-sandwich nickel complexes bearing (κ^1-C)- and hemilabile (κ^2-C,S)-thioether-functionalised NHC ligands. *Dalton Trans*. **2018**, *47*, 17134. (f) De Marco, R.; Dal Grande, M.; Baron, M.; Orian, L.; Graiff, C.; Achard, T.; Bellemin-Laponnaz, S.; Pothig, A.; Tubaro, C., Synthesis, structural characterization and

antiproliferative activity of gold(I) and gold(III) complexes bearing thioether-functionalized *N*-heterocyclic carbenes. *Eur. J. Inorg. Chem.* **2021**, *2021*, 4196-4206.

125 Wolf, J.; Labande, A.; Daran, J. C.; Poli, R.. Nickel(II), palladium(II) and rhodium(I) complexes of new NHC-thioether ligands: efficient ketone hydrosilylation catalysis by a cationic Rh complex. *Eur. J. Inorg. Chem.* **2007**, 5069.

126 Ros, A.; Alcarazo, M.; Monge, D.; Alvarez, E.; Fernández, R.; Lassaletta, J. M. Stereoselective synthesis of cationic heterobidentate C(NHC)/SR rhodium(I) complexes using stereodirecting *N*,*N*-dialkylamino groups. *Tetrahedron: Asymmetry* **2010**, *21*, 1557.

127 (a) Hoshimoto, Y.; Ohata, T.; Ohashi, M.; Ogoshi, S. Nickel-catalyzed Synthesis of *N*-aryl-1,2-dihydropyridines by [2+2+2] cycloaddition of imines with alkynes through T-shaped 14-electron aza-nickelacycle key intermediates. *Chem. Eur. J.* **2014**, *20*, 4105. (b) Zhao, J.-P.; Chan, S.-C.; Ho, C.-Y. Substituted 1,3-cyclohexadiene synthesis by NHC-nickel(0) catalyzed [2+2+2] cycloaddition of 1,n-enyne. *Tetrahedron* **2015**, *71*, 4426. (c) Xue, F.; Loh, Y.K.; Song, X.; Teo, W.J.; Chua, J.Y.D.; Zhao, J.; Hor, T.S.A. Nickel-catalyzed facile [2+2+2] cyclotrimerization of unactivated internal alkynes to polysubstituted benzenes. *Chem. Asian J.* **2017**, *12*, 168. (d) Sánchez, I.G.; Sámal, M.; Nejedlý, J.; Karras, M.; Klívar, J.; Rybácek, J.; Budesínský, M.; Bednárová, L.; Seidlerová, B.; Stará, I.G.; Starý, I. Oxahelicene NHC ligands in the asymmetric synthesis of nonracemic helicenes. *Chem. Commun.* **2017**, *53*, 4370. (e) Thakur, A.; Louie, J. Advances in nickel-catalyzed cycloaddition reactions to construct carbocycles and heterocicles. *Acc. Chem. Res.* **2015**, *48*, 2354.

128 (a) Saino, N.; Kogure, D.; Okamoto, S. Intramolecular cyclotrimerization of triynes catalyzed by *N*-heterocyclic carbene-$CoCl_2$/Zn or $FeCl_3$/Zn. *Org. Lett.* **2005**, *7*, 3065. (b) Geny, A.; Gaudrel, S.; Slowinski, F.; Amatore, M.; Chouraqui, G.; Malacria, M.; Aubert, C.; Gandon, V. A straightforward procedure for the [2+2+2] cycloaddition of enediynes. *Adv. Synth. Catal.* **2009**, *351*, 271.

129 González, I.; Pla-Quintana, A.; Roglans, A. Rhodium *N*-heterocyclic carbene complexes as effective catalysts for [2+2+2] cycloaddition reactions. *Synlett* **2009**, 2844.

130 Fernández, M.; Ferré, M.; Pla-Quintana, A.; Parella, T.; Pleixats, R.; Roglans, A. Rhodium-NHC hybrid silica materials as recyclable catalysts for [2+2+2] cycloaddition reactions of alkynes. *Eur. J. Org. Chem.* **2014**, 6242.

131 Kelly, R. A.; Clavier, H.; Giudice, S.; Scott, N. M.; Stevens, E. D.; Bordner, J.; Samardjiev, I.; Hoff, C. D.; Cavallo, L.; Nolan, S. P. Determination of *N*-Heterocyclic carbene (NHC) steric and electronic parameters using the [(NHC)Ir$(CO)_2$Cl] system. *Organometallics* **2008**, *27*, 202.

132 Cesar, V.; Bellemin-Laponnaz, S.; Wadepohl, H.; Gade, L. H. Designing the "search pathway" in the development of a new class of highly efficient stereoselective hydrosilylation catalysts. *Chem. Eur. J.* **2005**, *11*, 2862.

133 (a) Peñafiel, I.; Pastor, I. M.; Yus, M.; Esteruelas, M. A.; Olivan, M. Preparation, hydrogen bonds, and catalytic activity in metal-promoted addition of arylboronic acids to enones of a rhodium complex containing an NHC ligand with an alcohol function. *Organometallics* **2012**, *31*, 6154. (b) Yu, X. Y.; Patrick, B. O.; James, B. R. New rhodium(I) carbene complexes from carbene transfer reactions. *Organometallics* **2006**, *25*, 2359. (c) Warsink, S.; Venter, J. A.; Roodt, A. NHC-amide donor ligands in rhodium complexes: syntheses and characterization. *J. Organomet. Chem.* **2015**, *775*, 195.

134 (a) Inglesby, P. A.; Bacsa, J.; Negru, D. E.; Evans, P. A. The isolation and characterization of a rhodacycle intermediate implicated in metal-catalyzed reactions of alkylidenecyclopropanes. *Angew. Chem. Int. Ed*. **2014**, *53*, 3952. (b) Teng, Q.; Mao, W.; Chen, D.; Wang, Z.; Tung, C.-H.; Xu, Z. Asymmetric synthesis of a fused tricyclic hydronaphthofuran scaffold by desymmetric [2+2+2] cycloaddition. *Angew. Chem. Int. Ed*. **2019**, *59*, 2220. (c) Hong, X.; Stevens, M. C.; Liu, P.; Wender, P. A.; Houk, K.N. Reactivity and chemoselectivity of allenes in Rh(I)-catalyzed intermolecular (5 + 2) cycloadditions with vinylcyclopropanes: allene-mediated rhodacycle formation can poison Rh(I)-catalyzed cycloadditions. *J. Am. Chem. Soc.* **2014**, *136*, 17273. (d) Casitas, A.; Krause, H.; Lutz, S.; Goddard, R.; Bill, E.; Fürstner, A. Ligand exchange on and allylic C-H activation by iron(0) fragments: π-complexes, allyliron species, and metallacycles. *Organometallics* **2018**, *37*, 729. (e) Schobert, R. Chelated η^2-alkene- and η^3-allyl-carbene complexes of late transition metals: structure-reactivity relations and preparative use. Part 10. The chemistry of metallacyclic alkenylcarbene complexes. *J. Organomet. Chem.* **2001**, *617-618*, 346.

135 Vila, J.; Solà, M.; Achard, T.; Bellemin-Laponnaz, S.; Pla-Quintana, A.; Roglans, A. Rh(I) Complexes with Hemilabile Thioether-Functionalized NHC Ligands as Catalysts for [2 + 2 + 2] Cycloaddition of 1,5-Bisallenes and Alkynes. *ACS Catal.* **2023**, *13*, 3201.

136 (a) Schlegel, H. B. Geometry optimization. *WIRES Comput. Mol. Sci.* **2011**, *1*, 790. (b) Schlegel, H. B. Exploring potential energy surfaces for chemical reactions: An overview of some practical methods. *J. Comput. Chem.* **2003**, *24*, 1514. (c) Schlegel H.B. Geometry optimization on potential energy surfaces. In: Yarkony DR, ed. *Modern electronic structure theory*. Singapore: World Scientific Publishing; **1995**, 459. (d) Schlegel, H. B. Exploring potential energy surfaces for chemical reactions: an overview of some practical methods *Adv. Chem. Phys.* **1987**, *67*, 249.

137 Fukui, K. The path of chemical reactions – the IRC approach. *Acc. Chem. Res.* **1981**, *14*, 363.

138 (a) Atkins, P.; De Paula, J. *Elements of physical chemistry*, 3rd ed.; Oxford University Press, **2006**. (b) Ochterski. J. W. Thermochemistry in Gaussian. https://gaussian.com/thermo (accessed August 29th, 2022).

139 Gaussian 16, Revision A.03, Frisch, M. J.; Trucks, G. W.; Schlegel, H. B.; Scuseria, G. E.; Robb, M. A.; Cheeseman, J. R.; Scalmani, G.; Barone, V.; Petersson, G. A.; Nakatsuji, H.; Li, X.; Caricato, M.; Marenich, A. V.; Bloino, J.; Janesko, B. G.; Gomperts, R.; Mennucci, B.; Hratchian, H. P.; Ortiz, J. V.; Izmaylov, A. F.; Sonnenberg, J. L.; Williams-Young, D.; Ding, F.; Lipparini, F.; Egidi, F.; Goings, J.; Peng, B.; Petrone, A.; Henderson, T.; Ranasinghe, D.; Zakrzewski, V. G.; Gao, J.; Rega, N.; Zheng, G.; Liang, W.; Hada, M.; Ehara, M.; Toyota, K.; Fukuda, R.; Hasegawa, J.; Ishida, M.; Nakajima, T.; Honda, Y.; Kitao, O.; Nakai, H.; Vreven, T.; Throssell, K.; Montgomery, J. A., Jr.; Peralta, J. E.; Ogliaro, F.; Bearpark, M. J.; Heyd, J. J.; Brothers, E. N.; Kudin, K. N.; Staroverov, V. N.; Keith, T. A.; Kobayashi, R.; Normand, J.; Raghavachari, K.; Rendell, A. P.; Burant, J. C.; Iyengar, S. S.; Tomasi, J.; Cossi, M.; Millam, J. M.; Klene, M.; Adamo, C.; Cammi, R.; Ochterski, J. W.; Martin, R. L.; Morokuma, K.; Farkas, O.; Foresman, J. B.; Fox, D. J. Gaussian, Inc., Wallingford CT, 2016.

140 (a) Stephens, P. J.; Devlin, F. J.; Chabalowski, C. F.; Frisch, M. J. Ab initio calculation of vibrational absorption and circular dichroism spectra using density functional force fields. *J. Phys. Chem.* **1994**, *98*, 11623. (b) Becke, A. D. Density-functional thermochemistry. III. The role of exact exchange. *J. Chem. Phys.* **1993**, *98*, 5648. (c) Lee, C.; Yang, W.; Parr, R. G. Development of the Colle-Salvetti correlation-energy formula into a functional of the electron density. *Phys. Rev. B* **1988**, *37*, 785.

141 (a) Dunning, T. H. Gaussian basis sets for use in correlated molecular calculations. I. The atoms boron through neon and hydrogen. *J. Chem. Phys.* **1989**, *90*, 1007. (b) Woon, D. E.; Dunning, T. H. Gaussian basis sets for use in correlated molecular calculations. III. The atoms aluminum through argon. *J. Chem. Phys*. **1993**, *98*, 1358.

142 Cundari, T. R.; Benson, M. T.; Lutz, M. L.; Sommerer, S. O. Effective core potential approaches to the chemistry of the heavier elements. In *Reviews in Computational Chemistry,* Vol. 8.; John Wiley & Sons, Ltd, **1996**; pp 145-202.

143 Chai, J.-D.; Head-Gordon, M. Long-range corrected hybrid density functionals with damped atom–atom dispersion corrections. *Phys. Chem. Chem. Phys.* **2008**,*10*, 6615.

144 Grimme, S.; Antony, J.; Ehrlich, S.; Krieg, H. A Consistent and accurate Ab initio parametrization of density functional dispersion Correction (DFT-D) for the 94 elements H-Pu. *J. Chem. Phys.* **2010**, *132*, 154104.

145 Marenich, A. V.; Cramer, C. J.; Truhlar, D. G. Universal solvation model based on solute electron density and on a continuum model of the solvent defined by the bulk dielectric constant and atomic surface tensions. *J. Phys. Chem. B* **2009**, *113*, 6378.

146 Hashmi, A. S. K.; Häffner, T.; Rudolph, M.; Rominger, F. Gold catalysis: domino reaction of en-diynes to highly substituted phenols. *Chem. - A Eur. J.* **2011**, *17*, 8195.

147 Horiuchi, T.; Nagata, M.; Kitagawa, M.; Akahane, K.; Uoto, K. Discovery of novel thieno[2,3-d]pyrimidin-4-yl hydrazone-based inhibitors of cyclin D1-CDK4: synthesis, biological evaluation and structure-activity relationships. Part 2. *Bioorg. Med. Chem.* **2009**, *17*, 7850.

148 Aleman, J. del Solar, V.; Navarro-Ranninger, C. Anticancer platinum complexes as non-innocent compounds for catalysis in aqueous media. *Chem. Commun*., **2010**, *46*, 454.

149 Wilking, M.; Mück-Lichtenfeld, C.; Hennecke, U.; and Daniliuc G.C. Enantioselective, desymmetrizing bromolactonization of alkynes. *J. Am. Chem. Soc.* **2013**, *135*, 8133.

SUPPLEMENTARY MATERIAL

Supplementary material from digital sources

The material listed below is attached to this thesis as digital supplementary material in *.pdf* format:

- A digital copy of this manuscript: ***tjvv1de5.pdf***
- NMR spectra and X-Ray crystal data of Chapter 3: ***tjvv2de5.pdf***
- NMR spectra of Chapter 4: ***tjvv3de5.pdf***
- NMR spectra and X-Ray crystal data of Chapter 5: ***tjvv4de5.pdf***
- NMR spectra and X-Ray crystal data of Chapter 6: ***tjvv5de5.pdf***

The selected output files from the DFT calculations are provided through the following links to ioChemBD quantum chemistry repository (the structure of all files can be visualized in 3D):

- Chapter 3: https://iochem.udg.edu:8443/browse/handle/100/660
- Chapter 4: http://dx.doi.org/10.19061/iochem-bd-4-37
- Chapter 5: http://dx.doi.org/10.19061/iochem-bd-4-30
- Chapter 6: http://dx.doi.org/10.19061/iochem-bd-4-46

Preparation of starting materials

Figure S1. Sumary of 1,5-bisallenes

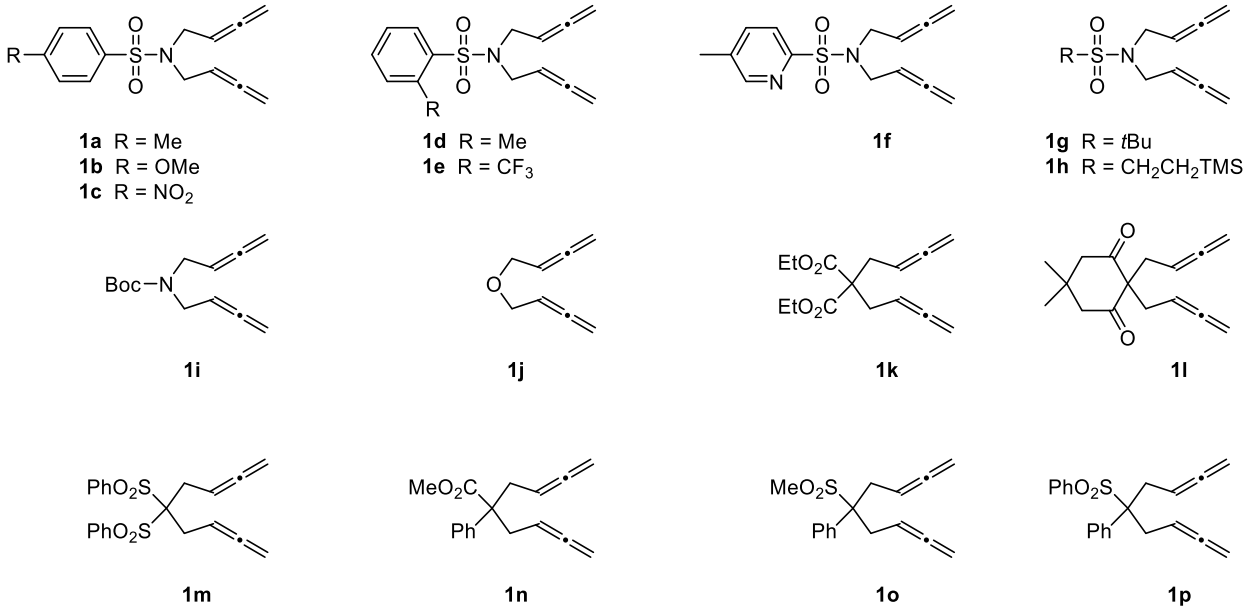

Retrosynthetic analysis of 1,5-bisallenes

1,5-Bisallenes **1(a-p) and 1a-*d*$_4$** can be generated via Crabbe homologation reaction from their corresponding diynes **S1a-p**, which can be easily prepared through double alquilation of the tethers with propargyl bromide, both commercially available. For 1,5-bisallene **1i**, the diyne **S1i** was obtained via carbamation of dipropargylamine with di-*tert*-butyl dicarbonate. Synthesis of diynes **S1d** and **S1j** were not performed since **S1d** was already synthetized by other members of the group and **S1j** is commercially available.

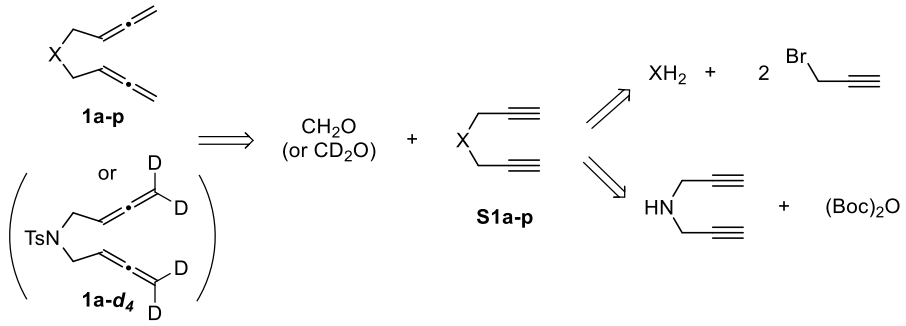

Scheme S1. Retrosynthetic analysis of 1,5-bisallenes **1a-p** and **1a-*d*$_4$**.

General procedure GP1 for the preparation of sulfonamide-tethered diynes S1(a-h)

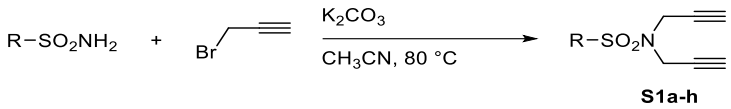

Scheme S2. Synthesis of sulfonamide-tethered diynes **S1a-h**.

In a 100 mL round-bottom flask equipped with a reflux condenser and a magnetic stirrer, a mixture of the corresponding sulfonamide (1 equivalent), K_2CO_3 (6 equivalents) and propargyl bromide 80% in toluene (2.3 equivalents) in acetonitrile was stirred at 80°C until completion (TLC monitoring). The reaction mixture was cooled to room temperature, the solids were filtered off and the filtrate was concentrated under reduced pressure. The resulting crude was purified by column chromatography (SiO_2, 40–60 μm) to afford the corresponding diyne.

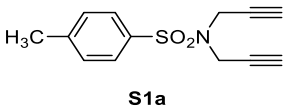

S1a

Diyne S1a was obtained from *p*-toluenesulfonamide (1.27 g, 7.4 mmol) in 60 mL of acetonitrile following the general procedure **GP1**. Purification by column chromatography (Hexanes/CH_2Cl_2, 1:1 v/v) provided **S1a** (1.81 g, 99 % yield) as a colourless solid.

MW ($C_{13}H_{13}NO_2S$): 247.3 g/mol. **Rf**: 0.33 (Hexanes/CH_2Cl_2 1:1). **^{1}H NMR ($CDCl_3$, 400 MHz): δ_H** 2.14 (t, ^4J = 2.4 Hz, 2H), 2.41 (s, 3H), 4.15 (d, ^4J = 2.4 Hz, 4H), 7.28 (d, ^3J = 8.4 Hz, 2H), 7.70 (d, $^3J_{ortho}$ = 8.4 Hz, 2H). **^{13}C{1H} NMR ($CDCl_3$, 101 MHz): δ_C** 21.67, 36.27, 74.17, 76.24, 127.96, 129.67, 135.22, 144.11. **ESI-MS (m/z):** $[M+H]^+$ = 248.0. Spectral data in accordance with literature values.[146]

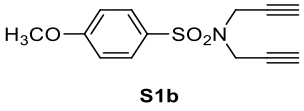

S1b

Diyne S1b was obtained from 4-methoxybenzenesulfonamide (1.39 g, 7.4 mmol) in 60 mL of acetonitrile following the general procedure **GP1**. Purification by column chromatography (Hexanes/EtOAc, 8:2 v/v) provided **S1b** (1.96 g, quant. yield) as a colourless solid.

MW ($C_{13}H_{13}NO_3S$): 263.3 g/mol. **Rf:** 0.18 (Hexanes/CH_2Cl_2 1:1). **M.P:** 53-55 ºC. **IR (ATR) ν (cm^{-1})**: 3275, 1594, 1497, 1340, 1262, 1149, 1092. **^{1}H NMR ($CDCl_3$, 400 MHz): δ_H** 2.16 (t, ^4J = 2.4 Hz, 2H), 3.87 (s, 3H), 4.16 (d, ^4J = 2.4 Hz, 4H), 6.97 (d, $^3J_{ortho}$ = 9.2 Hz, 2H), 7.77 (d, $^3J_{ortho}$ = 9.2 Hz, 2H). **^{13}C{1H} NMR ($CDCl_3$, 101 MHz): δ_C** 36.32, 55.77, 74.16, 76.40, 114.24, 129.83, 130.21, 163.47. **EA:** calculated for [$C_{13}H_{13}NO_3S$]: C, 59.30. H, 4.98. N, 5.32. Found: C, 59.51. H, 4.92. N, 5.70. **ESI-MS (*m/z*)**: $[M+H]^+$ = 264.0

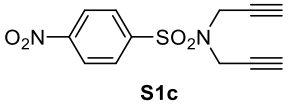

S1c

Diyne S1c was obtained from 4-nitrobenzenesulfonamide (2.31 g, 11.4 mmol) in 60 mL of acetonitrile following the general procedure **GP1**. Purification by

column chromatography (Hexanes/EtOAc, 8:2 v/v) provided **S1c** (2.00 g, 63 %. yield) as a colourless solid.

MW ($C_{12}H_{10}N_2O_4S$): 278.3 g/mol. **Rf**: 0.36 (CH2Cl2/Hexanes 1:1). **M.P**: 121-123 ºC. **IR (ATR) ν (cm^{-1})**: 3262, 1605, 1527, 1347, 1163, 1090. **^{1}H NMR (CDCl$_3$, 400 MHz): δ_H** 2.19 (t, ^3J = 2.4 Hz, 2H), 4.23 (d, ^4J = 2.4 Hz, 4H), 8.04 (d, $^3J_{ortho}$ = 8.8 Hz, 2H), 8.36 (d, $^3J_{ortho}$ = 8.8 Hz, 2H). **^{13}C{1H} NMR (CDCl$_3$, 101 MHz): δ_C** 36.7, 74.9, 75.6, 124.3, 129.2, 144.3, 150.5. **ESI-HRMS (m/z)** calculated for [M+Na] + = 301.0253. Found 301.0259. **ESI-MS (m/z)**: [M+H]+ = 279.0.

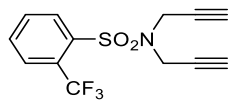

S1e

Diyne S1e was obtained from 2-(trifluoromethyl)benzenesulfonamide (5.63 g, 25 mmol) in 100 ml of acetonitrile following the general procedure **GP1**. Purification by column chromatography (Hexanes/EtOAc, 8:2 v/v) provided **S1e** (6.68 g, 89% yield) as pale orange solid.

MW ($C_{13}H_{10}F_3NO_2S$): 301.3 g/mol. **Rf:** 0.33 (Hexanes/CH_2Cl_2 1:1). **M.P**: 53-55 ºC. **IR (ATR) ν (cm^{-1}):** 3265, 1446, 1309, 1139, 1099. **^{1}H NMR (CDCl$_3$, 400 MHz): δ_H** 2.24 (t, ^4J = 2.4 Hz, 2H). 4.24 (d, ^4J = 2.4 Hz, 4H). 7.67-7.75 (m, 2H), 7.86-7.93 (m, 1H), 8.12-8.20 (m, 1H). **^{13}C{1H} NMR (CDCl$_3$, 101 MHz): δ_C** 36.30, 74.08, 76.53, 122.57 (q, $^1J_{C\text{-}F}$ = 273.7 Hz), 128.32 (q, $^2J_{C\text{-}F}$ = 33.3 Hz), 128.75 (q, $^3J_{C\text{-}F}$ = 6.1), 131.78, 132.45 (q, $^4J_{C\text{-}F}$ = 1.0 Hz), 133.17, 138.26 (q, $^3J_{C\text{-}F}$ = 1.3 Hz). **ESI-HRMS (*m/z*)** calculated for $[M+Na]^+$ = 324.0276. Found 324.0282

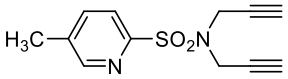

S1f

Diyne S1f was obtained from 5-methyl-2-pyridinesulfonamide (1.27 g, 7.4 mmol) in 60 mL of acetonitrile following the general procedure **GP1**. Purification by column chromatography (Hexanes/EtOAc, 8:2 v/v) provided **S1f** (1.83 g, quant. yield) as a colourless solid.

MW ($C_{12}H_{12}N_2O_2S$): 248.3 g/mol. **Rf:** 0.13 (Hexanes/EtOAc 8:2). **M.P:** 97-99 ºC. **IR (ATR) ν (cm^1):** 3273, 1435, 1338, 1318, 1163, 1103. **^{1}H NMR (CDCl$_3$, 400 MHz): δ_H** 2.08 (t, ^4J = 2.4 Hz, 2H), 2.43 (s, 3H), 4.34 (d, ^4J = 2.4 Hz, 4H), 7.65-7.70 (m, 1H), 7.87 (d, $^3J_{ortho}$ = 8.0 Hz, 1H), 8.49-8.52 (m, 1H). **^{13}C{1H} NMR (CDCl$_3$, 101 MHz): δ_C** 18.70, 37.12, 73.68, 76.62, 122.64, 137.56, 138.01, 150.55, 154.51. **EA:** calculated for [$C_{12}H_{12}N_2O_2S$]: C, 58.05. H, 4.87. N, 11.28. Found: C, 58.25. H, 4.67. N, 11.13 **ESI-MS (*m/z*):** $[M+H]^+$ = 249.0.

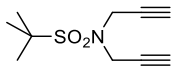

S1g

Diyne S1g was obtained from tert-butylsulfonamide (2.00 g, 14.6 mmol) in 120 mL of acetonitrile following the general procedure **GP1**. Purification by column chromatography (Hexanes/EtOAc, 8:2 v/v) provided **S1g** (2.84 g, 91 % yield) as a colourless solid.

MW ($C_{10}H_{15}NO_2S$): 213.3 g/mol. **Rf:** 0.36 (Hexanes/CH_2Cl_2 1:1). **M.P:** 92-93 ºC . **IR (ATR) ν (cm^{-}1):** 3239, 1436, 1304, 1120, 1083. **^{1}H NMR ($CDCl_3$, 400 MHz): δ_H** 1.41 (s, 9H), 2.34 (t, ^4J = 2.4 Hz, 2H), 4.22 (d, ^4J = 2.4 Hz, 4H). **^{13}C{1H} NMR ($CDCl_3$, 101 MHz): δ_C** 24.44, 37.44, 62.10, 73.63, 77.93. **EA:** calculated for [$C_{10}H_{15}NO_2S$]: C, 56.31. H, 7.09. N, 6.57. Found: C, 56.69. H, 6.69. N, 6.78. **ESI-MS (*m/z*):** $[M+Na]^+$ = 236.0.

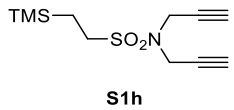

S1h

Diyne S1h was obtained from 2-(trimethylsilyl)ethanesulfonamide (0.67 g, 3.70 mmol), in 40 mL of acetonitrile following the general procedure **GP1**. Purification by column chromatography (Hexanes/EtOAc, 8:2 v/v) provided **S1h** (0.95 g, quant. yield) as a colourless solid.

MW ($C_{11}H_{19}NO_2SSi$): 257.4 g/mol. **Rf:** 0.50 (Hexanes/CH_2Cl_2 1:1). **IR (ATR) ν (cm^{-}1):** 3256, 1377, 1333, 1153, 1078. **^{1}H NMR ($CDCl_3$, 400 MHz): δ_H** 0.05 (s, 9H), 1.02-1.07 (m, 2H), 2.35 (t, ^4J = 2.4 Hz, 2H), 3.02-3.07 (m, 2H), 4.22 (d, ^4J = 2.4 Hz, 4H). **^{13}C{1H} NMR ($CDCl_3$, 101 MHz): δ_C** -1.85, 10.09, 36.72, 49.13, 73.94, 77.50. **ESI-HRMS (*m/z*)** calculated for $[M+Na]^+$ = 280.0798. Found 280.0811.

Preparation of diyne S1i

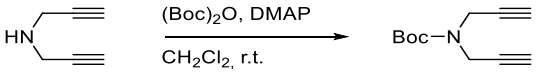

S1i

Scheme S3. Synthesis of diyne **S1i**.

In a 100 mL round-bottom flask equipped with a magnetic stirrer, a mixture of dipropargylamine (0.97 g, 10.41 mmol,1 equiv.) and 4-dimethylaminopyridine (DMAP, 0.13 g, 1.06 mmol, 0.1 equiv.) in CH_2Cl_2 (30 mL) was stirred at 0°C. A solution of $(Boc)_2O$ (3.02 g, 13.84 mmol, 1.3 equiv.) in CH_2Cl_2 was then added at 0ºC for 15 minutes and the resulting mixture was stirred at room temperature overnight. The reaction mixture was concentrated under reduced pressure and the resulting crude was purified by column chromatography on silica gel (silica gel, 40–63 μm) using mixtures of hexane/EtOAc as the eluent (100:0 to 80:20 v/v) to afford diyne **S1i** (2.02 g, quantitative yield) as a yellow oil.

MW ($C_{11}H_{15}NO_2$): 193.25 g/mol. **Rf**: 0.72 (Hexane/EtOAc 8:2). **^{1}H NMR ($CDCl_3$, 400 MHz): δ_H** 1.48 (s, 9H), 2.22 (t, 2H, ^4J = 2.5 Hz), 4.17 (bs, 4H). **^{13}C{1H} NMR ($CDCl_3$, 101 MHz): δ_C** 28.4, 35.3, 72.0, 78.9, 81.3, 154.4. **ESI-MS (m/z):** 216.1 $[M+Na]^+$. Spectral data in accordance with literature values.[147]

Preparation of diyne S1l

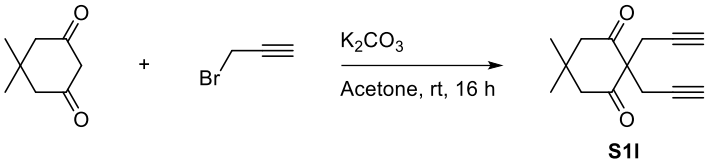

Scheme S4. Synthesis of diyne **S1l**.

In a 100 mL round-bottom flask equipped with a reflux condenser and a magnetic stirrer, a mixture of dimedone (0.30 g, 2.1 mmol), K_2CO_3 (0.89 g, 6.4 mmol) and propargyl bromide 80% in toluene (0.72 mL, 6.5 mmol) in 10 mL of acetone was stirred at room temperature for 16 h. until completion (TLC monitoring). The solids were filtered off and the filtrate was concentrated under reduced pressure. The resulting crude was purified by column chromatography (SiO_2, 40–60 μm, Hexanes/EtOAc, 90:10 to 60:40 v/v) to provide **S1l** (0.31 g, 67% yield) as a colourless solid.

MW ($C_{14}H_{16}O_2$): 216.3 g/mol. **Rf**: 0.33 (Hexanes/EtOAc 8:2). **^{1}H NMR ($CDCl_3$, 400 MHz): δ_H** 1.07 (s, 6H), 2.07 (t, ^4J = 2.7 Hz, 2H), 2.68 (d, ^4J = 2.7 Hz, 4H), 2.69 (s, 4H). **^{13}C{1H} NMR ($CDCl_3$, 101 MHz): δ_C** 24.34, 28.91, 30.80, 52.25, 66.00, 72.56, 79.05, 206.15. **ESI-MS (m/z):** $[M+H]^+$ = 217.1. Spectral data in accordance with literature values.[146]

Preparation of diyne S1m

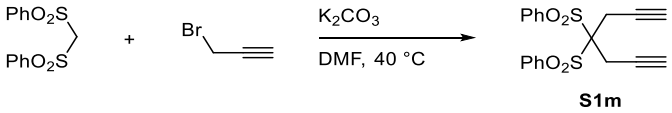

Scheme S5. Synthesis of diyne **S1m**.

In a 100 mL round-bottom flask equipped with a magnetic stirrer, a mixture of bis(phenylsulfonyl)methane (5.01 g, 16.9 mmol) and K_2CO_3 (14.3 g, 103.5 mmol) in 60 mL of anhydrous DMF was stirred at 40 °C for 1 h, and propargyl bromide (5.0 mL, 44.9 mmol) was then added and stirred overnight at 40 ºC. The solids were filtered off and the filtrate was concentrated under reduced pressure. The crude was mixed with water and extracted with CH_2Cl_2. The combined organic layers were washed with brine and dried over anhydrous Na_2SO_4, filtered and solvent was removed *in vacuo*. The resulting crude was purified by column chromatography (SiO_2, 40–60 μm, Hexanes/EtOAc, 90:10 to 60:40 v/v) to afford **S1m** (4,99 g, 79 % yield) as a colourless solid.

MW ($C_{19}H_{16}O_4S_2$): 372.5 g/mol. Rf: 0.25 (Hexanes/EtOAc 8:2). **MP (°C):** 146-147. **IR (ATR) ν (cm^{-1})**: 3296, 1445, 1314, 1143. **^{1}H NMR ($CDCl_3$, 400 MHz): δ_H** 2.23 (t, ^4J = 2.7 Hz, 2H), 3.26 (d, ^4J = 2.7 Hz, 4H), 7.58 – 7.64 (m, 4H), 7.74 (tt, $^3J_{ortho}$ = 7.5 Hz, $^4J_{meta}$ = 1.3 Hz, 2H), 8.19 – 8.24 (m, 4H). **^{13}C{1H} NMR ($CDCl_3$,**

101 MHz): δ_C 20.77, 74.58, 75.59, 87.19, 128.83, 131.81, 135.20, 135.97. **ESI-HRMS (*m/z*)** calculated for $[M+Na]^+$ = 395.0382. Found 395.0376.

General procedure GP2 for the preparation of diynes S1k and S1(n-p)

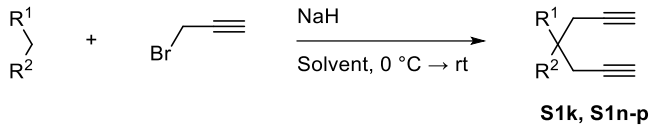

S1k, S1n-p

Scheme S6. General synthesis of diynes **S1k** and **S1n-p**.

In a 100 mL round-bottom flask equipped with a magnetic stirrer, NaH (60 % in mineral oil, 2-3 equivalents) was washed with hexane under inert atmosphere and dry solvent (THF or DMF) was then added. The suspension was cooled down to 0 °C and the corresponding precursor R^1-CH_2-R^2 (1 equivalent) was added. Stirring was continued for 30 minutes while the reaction mixture was allowed to warm up to room temperature. After cooling down to 0 °C, propargyl bromide (2-3 equivalents) was added dropwise. The solution was stirred overnight while warming up to room temperature. The reaction mixture was quenched with NH_4Cl (aq. sat.) and concentrated under reduced pressure. The resulting crude was mixed with water and extracted with CH_2Cl_2. The combined organic layers were washed with brine and dried over anhydrous Na_2SO_4, filtered and the solvent was removed *in vacuo*. The resulting crude was purified by column chromatography (SiO_2, 40–60 μm) to afford the corresponding diyne.

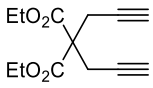

S1k

Diyne S1k was obtained from diethylmalonate (2.0 g, 12.5 mmol), propargyl bromide (3.3 mL, 29.6 mmol) and NaH (0.89 g, 22.2 mmol) in 60 mL of dry THF following the general procedure **GP2**. Purification by column chromatography (Hexanes/EtOAc, 85:15 v/v) provided **S1k** (2.90 g, 98 % yield) as a colourless oil.

MW ($C_{13}H_{16}O_4$): 236.3 g/mol. Rf: 0.54 (Hexanes/EtOAc 8:2). **^{1}H NMR ($CDCl_3$, 400 MHz):** δ_H 1.26 (t, ^3J = 7.2 Hz, 6H), 2.02 (t, ^4J = 2.4 Hz, 2H), 2.99 (d, ^4J = 2.4 Hz, 4H), 4.22 (q, ^3J = 7.2 Hz, 4H). **^{13}C{1H} NMR ($CDCl_3$, 101 MHz):** δ_C 14.14, 22.64, 56.40, 62.21, 71.79, 78.59, 168.74. **ESI-MS (m/z):** $[M+Na]^+$ = 259.1. Spectral data in accordance with literature values.[148]

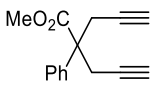

S1n

Diyne S1n was obtained from methyl phenylacetate (0.60 g, 3.99 mmol), propargyl bromide (1.3 mL, 11.7 mmol) and NaH (0.40 g, 10.0 mmol) in 10 mL of dry THF following the general procedure **GP2**. Purification by column chromatography (Hexanes/EtOAc 100:0 to 97:3) provided **S1n** (0.55 g, 61 % yield) as a colourless oil.

MW ($C_{15}H_{14}O_2$): 226.3 g/mol. Rf: 0.39 (Hexanes/EtOAc 9:1). **^{1}H NMR ($CDCl_3$, 400 MHz): δ_H** 1.99 (t, ^4J = 2.6 Hz, 2H), 3.09 (dd, ^2J = 16.7 Hz, ^4J = 2.6 Hz, 2H), 3.19 (dd, ^2J = 16.7 Hz, ^4J = 2.6 Hz, 2H), 3.71 (s, 3H), 7.27 – 7.33 (m, 3H), 7.33 – 7.39 (m, 2H). **^{13}C{1H} NMR ($CDCl_3$, 101 MHz): δ_C** 25.63, 52.87, 53.25, 71.50, 80.07, 126.18, 127.84, 128.70, 139.39, 173.65. **ESI-MS (m/z):** $[M+H]^+$ = 227.1. Spectral data in accordance with literature values.[149]

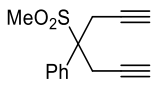

S1o

Diyne S1o was obtained from benzyl methyl sulfone (3.54 g, 20.8 mmol), propargyl bromide (8 mL, 71.8 mmol) and NaH (2.09 g, 52.2 mmol) in 60 mL of anhydrous DMF following the general procedure **GP2**. Purification by column chromatography (Hexanes/EtOAc, 7:3 v/v) provided **S1o** (4.44 g, 87 % yield) as a colourless solid.

MW ($C_{14}H_{14}O_2S$): 246.3 g/mol. Rf: 0.23 (Hexanes/EtOAc 8:2). **MP (°C):** 104 – 105. **IR (ATR) ν (cm^{-1})**: 3284, 1446, 1289, 1126. **^{1}H NMR ($CDCl_3$, 400 MHz): δ_H** 2.13 (t, ^4J = 2.7 Hz, 2H), 2.76 (s, 3H), 3.27 (dd, ^2J = 17.2 Hz, ^4J = 2.7 Hz, 2H), 3.43 (dd, ^2J = 17.2 Hz, ^4J = 2.7 Hz, 2H), 7.40 – 7.48 (m, 3H), 7.75 – 7.80 (m, 2H). **^{13}C{1H} NMR ($CDCl_3$, 101 MHz): δ_C** 24.56, 39.55, 69.61, 73.47, 78.63, 128.58, 128.94, 129.45, 133.63. **ESI-HRMS (*m/z*)** calculated for $[M+Na]^+$ = 269.0607. Found 269.0610.

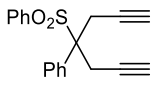

S1p

Diyne S1p was obtained from benzyl phenyl sulfone (0.90 g, 3.87 mmol), propargyl bromide (1.3 mL, 11.7 mmol) and NaH (0.39 g, 9.8 mmol) in 15 mL of anhydrous DMF following the general procedure **GP2**. Purification by column chromatography (Hexanes/EtOAc, 90:10 to 60:40 v/v) provided **S1p** (0.89 g, 74 % yield) as a colourless solid.

MW ($C_{19}H_{16}O_2S$): 308.4 g/mol. Rf: 0.30 (Hexanes/EtOAc 8:2). **MP (°C):** 172 – 173 decomp. **IR (ATR) ν (cm^{-1})**: 3253, 1434, 1295, 1137. **^{1}H NMR ($CDCl_3$, 400 MHz): δ_H** 2.07 (t, ^4J = 2.7 Hz, 2H), 3.27 (dd, ^4J = 17.1 Hz, ^2J = 2.7 Hz, 2H), 3.67 (dd, ^4J = 17.1 Hz, ^2J = 2.7 Hz, 2H), 7.29 – 7.41 (m, 9H), 7.57 (tt, $^3J_{ortho}$ = 6.9 Hz, $^4J_{meta}$ = 1.8 Hz, 1H). **^{13}C{1H} NMR ($CDCl_3$, 101 MHz): δ_C** 23.13, 69.82, 72.71, 78.11, 128.26, 128.57, 129.12, 129.17, 130.48, 133.43, 134.02, 135.10. **ESI-HRMS (*m/z*)** calculated for $[M+Na]^+$ = 331.0763. Found 331.0757.

General procedure GP3 for the preparation of 1,5-bisallenes 1(a-p) and 1a-*d*$_4$

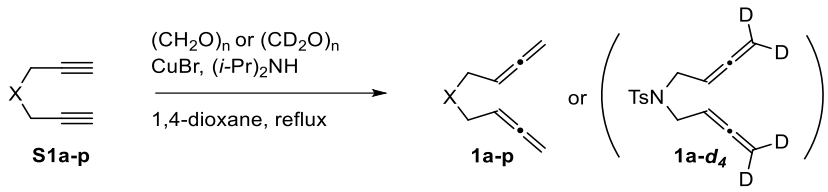

Scheme S7. General synthesis of 1,5-bisallenes **1a-p** and **1a-*d*$_4$**.

In a round-bottom flask equipped with a reflux condenser and a magnetic stirrer, a suspension of the corresponding diyne (1 equiv.), paraformaldehyde (5 equiv.) and CuBr (1 equiv.) in 1,4-dioxane was stirred and heated at reflux. Diisopropylamine (4 equiv.) was then added, and the resulting mixture was stirred at reflux for 16 h. until completion (TLC monitoring). The reaction mixture was allowed to cool to room temperature, filtered through a Celite pad and concentrated under reduced pressure. The resulting brown oil was mixed with Et_2O and water, and the mixture was acidified to pH = 2 with HCl 6M. The Et_2O/water layers were decanted from solid residues, the Et_2O layer was separated, and the water layer was extracted with Et_2O. The combined organic extracts were washed with water until neutral pH, washed with brine, dried over anhydrous Na_2SO_4 and concentrated under reduced pressure. The resulting crude was purified by column chromatography (SiO_2, 40–60 μm) to afford the corresponding bisallene.

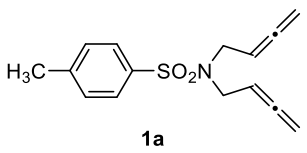

Bisallene 1a was obtained from **diyne S1a** (6.00 g, 24.3 mmol), in 100 mL of 1,4-dioxane following the general procedure **GP3**. Purification by column chromatography (Hexanes/EtOAc, 95:5 v/v) provided **1a** (4.10 g, 61 % yield) as a colourless solid.

MW ($C_{15}H_{17}NO_2S$): 275.4 g/mol. **Rf**: 0.50 (Hexanes/EtOAc 8:2). **^{1}H NMR ($CDCl_3$, 400 MHz): δ_H** 2.41 (s, 3H), 3.89 (dt, ^3J = 6.8 Hz, ^5J = 2.4 Hz, 4H), 4.70 (dt, ^4J = 6.8 Hz, ^5J = 2.4 Hz, 4H), 4.93 (quintet, ^3J = ^4J = 6.8 Hz, 2H), 7.29 (d, $^3J_{ortho}$ = 8.4 Hz, 2H), 7.69 (d, $^3J_{ortho}$ = 8.4 Hz, 2H). **^{13}C{1H} NMR ($CDCl_3$, 101 MHz): δ_C** 21.61, 45.77, 76.27, 85.75, 127.27, 129.79, 137.66, 143.40, 209.78. **ESI-MS (m/z):** $[M+Na]^+$: 298.0. Spectral data in accordance with literature values.[76]

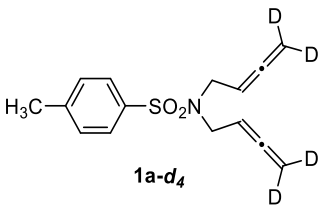

Bisallene 1a-*d*$_4$ was obtained from **diyne S1a** (0.82 g, 3.3 mmol) and paraformaldehyde-d_2 (0.50 g, 15.6 mmol) in 12 mL of 1,4-dioxane following the general procedure **GP3**. Purification by column chromatography (Hexanes/EtOAc, 95:5 v/v) provided **1a-*d*$_4$** (0.383 g, 41 % yield) as a colourless solid.

MW ($C_{15}H_{13}D_4NO_2S$): 279.4 g/mol. **Rf**: 0.50 (Hexanes/EtOAc 8:2). **^{1}H NMR ($CDCl_3$, 400 MHz): δ_H** 2.43 (s, 3H), 3.90 (d, ^3J = 7.0 Hz, 4H), 4.95 (t, ^3J = 7.0 Hz, 2H), 7.29 (d, $^3J_{ortho}$ = 8.2 Hz, 2H), 7.70 (d, $^3J_{ortho}$ = 8.2 Hz, 2H). **^{13}C{1H} NMR ($CDCl_3$, 101 MHz): δ_C** 21.66, 45.82, 85.98, 127.34, 129.83, 137.74, 143.43, 209.92. **ESI-HRMS (*m/z*)** calcd for $[M+Na]^+$ = 302.1123. Found 302.1140.

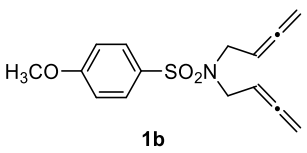

1b

Bisallene 1b was obtained from **diyne S1b** (1.96 g, 7.44 mmol) in 40 mL of 1,4-dioxane following the general procedure **GP3**. Purification by column chromatography (Hexanes/EtOAc, 8:2 v/v) provided **1b** (0.77 g, 35 % yield) as a yellow oil.

MW ($C_{15}H_{17}NO_3S$): 291.4 g/mol. **Rf**: 0.48 (Hexanes/CH_2Cl_2 1:1). **^{1}H NMR ($CDCl_3$, 400 MHz): δ_H** 3.86 (s, 3H), 3.89 (dt, ^3J = 6.8 Hz, ^5J = 2.4 Hz, 4H), 4.71 (dt, ^4J = 6.8 Hz, ^5J = 2.4 Hz, 4H), 4.94 (quintet, $^3J = {}^4J$ = 6.8 Hz, 2H), 6.96 (d, $^3J_{ortho}$ = 8.8 Hz, 2H), 7.75 (d, $^3J_{ortho}$ = 8.8 Hz, 2H). **^{13}C{1H} NMR ($CDCl_3$, 101 MHz): δ_C** 45.76, 55.74, 76.28, 85.79, 114.35, 129.39, 132.28, 162.93, 209.82. **ESI-MS (*m/z*):** $[M+H]^+$ = 292.02. Spectral data in accordance with literature values.[149]

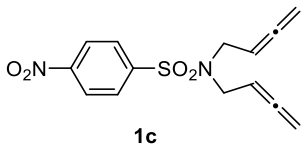

1c

Bisallene **1c** was obtained from diyne **S1c** (1.49 g, 5.36 mmol), following the general procedure **GP3**. Purification by column chromatography (SiO2, 40–63 μm, CH_2Cl_2/Hexanes) provided **1c** (0.35 g, 21% yield) as a yellow solid.

MW ($C_{14}H_{14}N_2O_4S$): 306.3 g/mol. **Rf**: 0.30 (CH2Cl2/Hexanes 1:1). **^{1}H NMR ($CDCl_3$, 400 MHz): δ_H** 3.95 (dt, ^3J = 6.8 Hz, ^5J = 2.5 Hz, 4H), 4.73 (dt, ^4J = 6.8, ^5J = 2.5 Hz, 4H), 4.96 (quint, $^3J = {}^4J$ = 6.8 Hz, 2H), 8.01 (d, $^3J_{ortho}$ = 8.8 Hz, 2H), 8.35 (d, $^3J_{ortho}$ = 8.8 Hz, 2H). **^{13}C{1H} NMR ($CDCl_3$, 101 MHz): δ_C** 45.9, 76.8, 85.4, 124.5, 128.5, 146.7, 150.1, 209.9. **ESI-MS (m/z)**: $[M+H]^+$ = 307.0. Spectral data in accordance with literature values.[73]

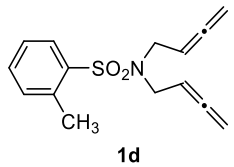

1d

Bisallene 1d was obtained from **diyne S1d** (1.51 g, 6.11 mmol), in 34 mL of 1,4-dioxane following the general procedure **GP3**. Purification by column chromatography (Hexanes/EtOAc, 95:5 v/v) provided **1d** (0.42 g, 25 % yield) as a colourless oil.

MW ($C_{15}H_{17}NO_2S$): 275.37 g/mol. **Rf**: 0.56 (Hexane/EtOAc 8:2). **IR (ATR) ν (cm-1)**: 1951, 1319, 1154. **^{1}H NMR ($CDCl_3$, 400 MHz): δ_H** 2.60 (s, 3H), 3.92 (dt, 4H, ^3J = 6.9 Hz, ^5J = 2.4 Hz), 4.73 (dt, 4H, ^4J = 6.9 Hz, ^5J = 2.4 Hz), 7.33 – 7.28 (m, 2H), 5.00 (p, 2H, $^3J = {}^4J$ = 6.9 Hz), 7.44 (td, 1H $^3J_{ortho}$ = 7.5 Hz, $^4J_{meta}$ = 1.4 Hz),7.95 (dd, 1H, $^3J_{ortho}$ = 8.2 Hz, $^4J_{meta}$ = 1.4 Hz). **^{13}C{1H} NMR ($CDCl_3$, 101 MHz): δ_C** 20.6, 45.2, 76.3,

85.8, 126.2, 130.0, 132.8, 132.9, 137.8, 138.3, 210.0. **HRMS (ESI) m/z:** calcd for $[M+Na]^+$ = 298.0872. Found 298.0878.

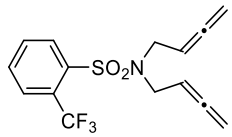

1e

Bisallene 1e was prepared from **diyne S1e** (6.60 g, 21.9 mmol), in 100 mL of 1,4-dioxane following the general procedure **GP3**. Purification by column chromatography (SiO_2, 40–63 μm, CH_2Cl_2/Hexanes) provided **1e** (2.98 g, 41% yield) as an orange oil.

MW ($C_{15}H_{14}F_3NO_2S$): 329.3 g/mol. **Rf**: 0.43 (CH_2Cl_2/Hexanes 1:1). **IR (ATR) ν (cm^{-1}):** 1953, 1437, 1306, 1155, 1113. **^{1}H NMR (CDCl$_3$, 400 MHz): δ_H** 3.96 (dt, ^3J = 6.8 Hz, ^5J = 2.4 Hz, 4H), 4.73 (dt, ^4J = 6.8 Hz, ^5J = 2.4 Hz, 4H), 5.01 (quintet, $^3J = {}^4J$ = 6.8 Hz, 2H), 7.65-7.72 (m, 2H), 7.84-7.90 (m, 1H), 8.12-8.19 (m, 1H). **^{13}C{1H} NMR (CDCl$_3$, 101 MHz): δ_C** 45.59, 76.41, 85.75, 122,69 (q, $^1J_{C\text{-}F}$ = 274.1 Hz), 127.94 (q, $^2J_{C\text{-}F}$ = 33.2 Hz), 128.67 (q, $^3J_{C\text{-}F}$ = 6.5 Hz), 131,76, 132.33 (q, $^4J_{C\text{-}F}$ = 0.9 Hz), 132,71, 139.69 (q, $^3J_{C\text{-}F}$ = 1.3 Hz), 210.05. **ESI-HRMS (*m/z*)** calculated for $[M+Na]^+$ = 352.0590. Found 352.0590. **ESI-MS (*m/z*):** $[M+H]^+$ = 330.0.

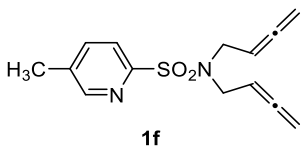

1f

Bisallene 1f was obtained from **diyne S1f** (1.65 g, 6.65 mmol) in 40 mL of 1,4-dioxane following the general procedure **GP3**. Purification by column chromatography (Hexanes/EtOAc, 8:2 v/v) provided **1f** (0.54 g, 29 % yield) as an orange oil.

MW ($C_{14}H_{16}N_2O_2S$): 276.4 g/mol. **Rf**: 0.23 (Hexanes/CH_2Cl_2 1:1). **IR (ATR) ν (cm^{-1}):** 1952, 1335, 1165, 1106. **^{1}H NMR (CDCl$_3$, 400 MHz): δ_H** 2.41 – 2.43 (m, 3H), 4.01 (dt, ^3J = 7.2 Hz, , ^5J = 2.4 HZ, 4H), 4.69 (dt, ^4J = 7.2 Hz, ^5J = 2.4 Hz, 4H), 5.01 (quintet, $^3J = {}^4J$ = 7.2 Hz, 2H), 7.66 (dd, $^3J_{ortho}$ = 8.0 Hz, $^4J_{meta}$ = 2.1 Hz, 1H), 7.84 (d, $^3J_{ortho}$ = 8.0 Hz, 1H), 8.50 (d, $^4J_{meta}$ = 2.1, Hz, 1H). **^{13}C{1H} NMR (CDCl$_3$, 101 MHz): δ_C** 18.62, 46.46, 76.11, 86.10, 122.09, 137.11, 138.08, 150.61, 155.84, 209.77. **ESI-HRMS (*m/z*)** calculated for $[M+Na]^+$ = 299.0825. Found 299.0822. **ESI-MS (*m/z*):** $[M+H]^+$ = 277.0.

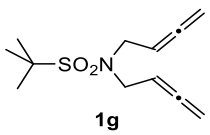

1g

Bisallene 1g was obtained from **diyne S1g** (2.84 g, 13.3 mmol) in 50 mL of 1,4-dioxane following the general procedure **GP3**. Purification by column chromatography (Hexanes/EtOAc, 75:25 v/v) provided **1g** (1.17 g, 36% yield) as a yellow oil.

MW ($C_{12}H_{19}NO_2S$): 241.3 g/mol. **Rf:** 0.25 (Hexanes/CH_2Cl_2 1:1). **IR (ATR) ν (cm^{-1}):** 1952, 1314, 1124, 1074. **^{1}H NMR (CDCl$_3$, 400 MHz): δ_H** 1.38 (s, 9H), 3.94 (dt, ^3J = 6.8 Hz, ^5J = 2.5 Hz, 4H), 4.81 (dt, ^4J = 6.8

Hz, ^5J = 2.5 Hz, 4H), 5.14 (quintet, ^3J = ^4J = 6.8 Hz, 2H). **^{13}C{1H} NMR ($CDCl_3$, 101 MHz): δ_C** 24.58, 46.51, 61.47, 76.49, 86.76, 209.98. **ESI-HRMS (*m/z*)** calculated for $[M+Na]^+$ = 264.1029. Found 264.1033.

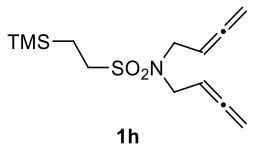

1h

Bisallene 1h was obtained from **diyne S1h** (0.96 g, 3.73 mmol) in 40 mL of 1,4-dioxane following the general procedure **GP3**. Purification by column chromatography (Hexanes/EtOAc, 9:1 v/v) provided **1h** (0.39 g, 37 % yield) as a yellow oil.

MW ($C_{13}H_{23}NO_2SSi$): 285.5 g/mol. **Rf**: 0.28 (Hexanes/CH_2Cl_2 1:1). **IR (ATR) ν (cm^{-1}):** 1953, 1328, 1248, 1137. **^{1}H NMR ($CDCl_3$, 400 MHz): δ_H** 0.04 (s, 9H), 0.96-1.05 (m, 2H), 2.86-2.95 (m, 2H), 3.92 (dt, ^3J = 6.9 Hz, ^5J = 2.4 Hz, 4H), 4.81 (dt, ^4J = 6.9 Hz, ^5J = 2.4 Hz, 4H), 5.12 (quintet, ^3J = ^4J = 6.9 Hz, 2H). **^{13}C{1H} NMR ($CDCl_3$, 101 MHz): δ_C** -1.86, 10.45, 45.67, 49.84, 76.59, 86.43, 209.82. **ESI-HRMS (*m/z*)** calculated for $[M+Na]^+$ = 308.1111. Found 308.1109.

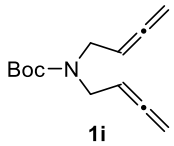

1i

Bisallene 1i was obtained from **diyne S1i** (2.02 g, 10.45 mmol) in 35 mL of 1,4-dioxane following the general procedure **GP3**. Purification by column chromatography (Hexanes/EtOAc, 100:0 to 80:20 v/v) provided **1i** (1.59 g, 69 % yield) as a yellowish oil.

MW ($C_{13}H_{19}NO_2$): 221.30 g/mol. **Rf**: 0.81 (Hexane/EtOAc 8:2). **IR (ATR) *ν* (cm^{-1})**: 2974, 1953, 1691, 1454. **^{1}H NMR ($CDCl_3$, 400 MHz): δ_H** 1.46 (s, 9H), 3.85 (bs, 4H), 4.76 (dt, 4H, ^4J = 6.5 Hz, ^5J = 2.8 Hz), 5.11 (quint, 2H, ^3J = ^4J = 6.5 Hz). **^{13}C{1H} NMR ($CDCl_3$, 101 MHz): δ_C** 28.6, 45.4, 76.2, 79.9, 87.3, 155.3, 209.1. **HRMS (ESI) m/z:** $[M+Na]^+$ Calcd. for $C_{13}H_{19}NO_2Na$ 244.1308. Found 244.1314.

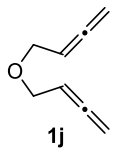

1j

Bisallene 1j was obtained from **diyne S1j** (1.50 g, 15.96 mmol) in 60 mL of 1,4-dioxane following the general procedure **GP3**. Purification by column chromatography (Hexanes/EtOAc, 95:5 v/v) provided **1j** (0.394 g, 20 % yield) as a yellow oil.

MW ($C_8H_{10}O$): 122.2 g/mol. **Rf**: 0.67 (hexanes/EtOAc 8:2). **IR (ATR) *ν* (cm^{-1})**: 2920, 2854, 1953, 1450, 1357, 1318, 1251, 1077. **^{1}H NMR ($CDCl_3$, 400 MHz): δ_H** 4.03 (dt, ^3J = 6.8 Hz, ^5J = 2.4 Hz, 4H), 4.78 (dt, ^4J = 6.8 Hz, ^5J = 2.4 Hz, 4H), 5.23 (quint, ^3J = ^4J = 6.8 Hz, 2H). **^{13}C{1H} NMR ($CDCl_3$, 101 MHz): δ_C** 67.68, 75.78, 87.67, 209.49.

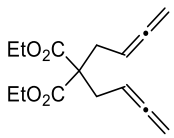

1k

Bisallene 1k was obtained from **diyne S1k** (2.90 g, 12.3 mmol) in 50 mL of 1,4-dioxane following the general procedure **GP3**. Purification by column chromatography (Hexanes/EtOAc, 95:5 v/v) provided **1k** (0.49 g, 15 % yield) as a yellow oil.

MW ($C_{15}H_{20}O_4$): 264.3 g/mol. **Rf**: 0.57 (Hexanes/EtOAc 8:2). **IR (ATR) ν (cm^{-1}):** 1954, 1727, 1275, 1181, 1065. **^{1}H NMR (CDCl$_3$, 400 MHz): δ_H** 1.24 (t, ^3J = 7.1 Hz, 6H), 2.64 (dt, ^3J = 8.0 Hz, ^5J = 2.6 Hz, 4H), 4.18 (q, ^3J = 7.1 Hz, 4H), 4.65 (dt, ^4J = 6.4 Hz, ^5J = 2.6 Hz, 4H), 4.94 (tt, ^3J = 8.0 Hz, ^4J = 6.4 Hz, 2H). **^{13}C{1H} NMR (CDCl$_3$, 101 MHz): δ_C** 14.21, 31.94, 57.81, 61.46, 74.70, 84.29, 170.60, 210.21. **ESI-MS (*m/z*):** $[M+H]^+$ = 265.1. Spectral data in accordance with literature values.[73]

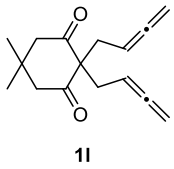

1l

Bisallene 1l was obtained from **diyne S1l** (1.27 g, 5.87 mmol) in 40 mL of 1,4-dioxane following the general procedure **GP3**. Purification by column chromatography (Hexanes/EtOAc, 85:15 v/v) provided **1l** (0.11 g, 7.7% yield) as a yellow-oil.

MW ($C_{16}H_{20}O_2$): 244.3 g/mol. Rf: 0.54 (Hexanes/EtOAc 8:2). **IR (ATR) *ν* (cm^{-1})**: 1952, 1719, 1689. **^{1}H NMR (CDCl$_3$, 400 MHz): δ_H** 1.00 (s, 6H), 2.48 (dt, ^3J = 8.0 Hz, ^5J = 2.3 Hz, 4H), 2.56 (s, 4H), 4.65 (dt, ^4J = 6.6 Hz, ^5J = 2.3 Hz, 4H), 4.93 (tt, ^3J = 8.0 Hz, ^4J = 6.6 Hz, 2H). **^{13}C{1H} NMR (CDCl$_3$, 101 MHz): δ_C** 28.75, 30.87, 33.67, 51.95, 68.34, 74.79, 84.62, 208.30, 210.23. **ESI-HRMS (*m/z*)** calculated for $[M+Na]^+$ = 267.1356. Found 267.1351.

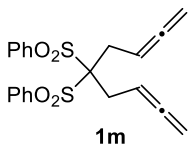

1m

Bisallene 1m was obtained from **diyne S1m** (2.98 g, 8.0 mmol) in 30 mL of 1,4-dioxane following the general procedure **GP3**. Purification by column chromatography (Hexanes/EtOAc, 95:5 to 70:30 v/v) provided **1m** (118.6 mg, 3,7%. yield) as a green oil.

MW ($C_{21}H_{20}O_4S_2$): 400.5 g/mol. Rf: 0.39 (Hexanes/EtOAc 8:2). **IR (ATR) *ν* (cm^{-1})**: 3062, 1952, 1445, 1326, 1308, 1143. **^{1}H NMR (CDCl$_3$, 400 MHz): δ_H** 3.04 (dt, ^3J = 7.4 Hz, ^5J =2.9 Hz, 4H), 4.77 (dt, ^4J = 6.7 Hz, ^5J =2.9 Hz, 4H), 5.36 (tt, ^3J = 7.4 Hz, ^4J =6.7 Hz, 2H), 7.57 – 7.63 (m, 4H), 7.69 – 7.75 (m, 2H), 8.06 – 8.10 (m, 4H). **^{13}C{1H} NMR (CDCl$_3$, 101 MHz): δ_C** 29.36, 76.01, 83.36, 89.96, 128.73, 131.61, 134.81, 136.91, 210.30. **ESI-HRMS (*m/z*)** calculated for $[M+Na]^+$ = 423.0695. Found 423.0699.

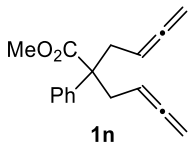

1n

Bisallene 1n was obtained from **diyne S1n** (1.59 g, 7.03 mmol) in 30 mL of 1,4-dioxane following the general procedure **GP3**. Purification by column chromatography (Hexanes/EtOAc, 100:0 to 95:5 v/v) provided **1n** (0.57 g, 32 % yield) as a yellowish oil.

MW ($C_{17}H_{18}O_2$): 254.3 g/mol. Rf: 0.53 (Hexanes/EtOAc 9:1). **IR (ATR) ν (cm^{-1}):** 2948, 1952, 1726. **^{1}H NMR (CDCl$_3$, 400 MHz): δ_H** 2.72 – 2.88 (m, 4H), 3.66 (s, 3H), 4.55 – 4.65 (m, 4H), 4.77 – 4.86 (m, 2H), 7.23 – 7.28 (m, 3H), 7.31 – 7.36 (m, 2H). **^{13}C{1H} NMR (CDCl$_3$, 101 MHz): δ_C** 34.37, 52.19, 54.22, 74.29, 84.94, 126.60, 127.18, 128.56, 141.28, 175.31, 210.18. **ESI-HRMS (*m/z*)** calculated for $[M+Na]^+$ = 277.1199. Found 277.1192

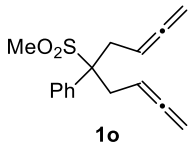

1o

Bisallene 1o was obtained from **diyne S1o** (1.99 g, 8.08 mmol) in 30 mL of 1,4-dioxane following the general procedure **GP3**. Purification by column chromatography (Hexanes/EtOAc, 95:5 to 70:30 v/v) provided **1o** (0.45 g, 20 % yield) as a yellow solid.

MW ($C_{16}H_{18}O_2S$): 274.4 g/mol. Rf: 0.35 (Hexanes/EtOAc 8:2). **MP (°C):** 64 – 65. **IR (ATR) *ν* (cm^{-1})**: 3062, 1950, 1288, 1132. **^{1}H NMR (CDCl$_3$, 400 MHz): δ_H** 2.51 (s, 3H), 3.01 – 3.10 (m, 2H), 3.27 (ddt, ^2J = 14.9 Hz, ^3J = 7.2 Hz, ^5J = 2.8 Hz, 2H), 4.64 – 4.74 (m, 4H), 5.19 (ddt, ^3J = 8.1 Hz, ^3J = 7.2 Hz, ^4J = 6.6 Hz, 2H), 7.34 – 7.44 (m, 3H), 7.58 – 7.63 (m, 2H). **^{13}C{1H} NMR (CDCl$_3$, 101 MHz): δ_C** 31.53, 37.04, 70.62, 75.25, 84.42, 128.77, 128.98, 129.24, 135.01, 210.44. **ESI-HRMS (*m/z*)** calculated for $[M+Na]^+$ = 297.0920. Found 297.0919.

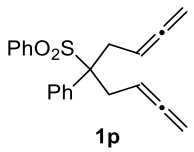

1p

Bisallene 1p was obtained from **diyne S1p** (2.12 g, 6.87 mmol) in 30 mL of 1,4-dioxane following the general procedure **GP3**. Purification by column chromatography (Hexanes/EtOAc, 95:5 to 70:30 v/v) provided **1p** (1.08 g, 47 % yield) as a colourless solid.

MW ($C_{21}H_{20}O_2S$): 336.4 g/mol. Rf: 0.53 (Hexanes/EtOAc 8:2). **MP (°C):** 111 – 112. **IR (ATR) *ν* (cm^{-1})**: 3061, 1951, 1288, 1138. **^{1}H NMR (CDCl$_3$, 400 MHz): δ_H** 2.99 – 3.07 (m, 2H), 3.25 – 3.33 (m, 2H), 4.61 – 4.72 (m, 4H), 5.23 (dq, ^3J = 8.3 Hz, ^3J = ^4J = 6.7 Hz, 2H), 7.17 – 7.25 (m, 6H), 7.26 – 7.32 (m, 3H), 7.48 – 7.53 (m, 1H). **^{13}C{1H} NMR (CDCl$_3$, 101 MHz): δ_C** 30.97, 71.34, 75.07, 84.52, 127.98, 128.29, 128.63, 129.77, 130.42, 133.60, 134.52, 135.25, 210.39. **ESI-HRMS (*m/z*)** calculated for $[M+Na]^+$ = 359.1076. Found 359.1078

Supplementary material for Chapter 3

General procedure GP4 for the synthesis of products 3(aa–nm) and 5a

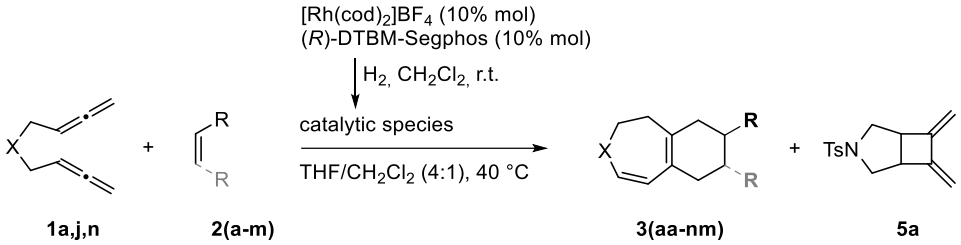

Scheme S8. Rh-catalyzed cascade cycloisomerization/DA reaction of 1,5-bisallenes and alkenes.

In a 10 mL capped vial, a mixture of $[Rh(cod)_2]BF_4$ (7.4 mg, 0.018 mmol) and (*R*)-DTBM-Segphos (23.6 mg, 0.020 mmol) was purged with nitrogen and dissolved in anhydrous CH_2Cl_2 (4 mL). Hydrogen gas was bubbled into the catalyst solution and the mixture was stirred for 30 min. The resulting mixture was concentrated to dryness under a stream of nitrogen, dissolved again in anhydrous CH_2Cl_2 (4 mL) and transferred via syringe into a solution of 1,5-bisallene **1** (0.18 mmol, 1 equiv.) and alkene **2** (9.00 mmol, 50 equiv.) in anhydrous THF (16 mL) preheated to 40 °C and under inert atmosphere. The resulting mixture was stirred at 40 ºC for 16h. The solvent was removed under reduced pressure and the crude reaction mixture was purified by column chromatography on silica gel using hexane/EtOAc mixtures as the eluent to afford compounds **3** and **5a**.

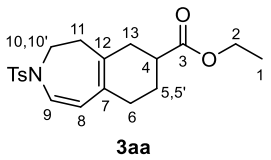

3aa

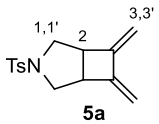

5a

Compound **3aa** was obtained from bisallene **1a** (50 mg, 0.18 mmol) and ethyl acrylate (1.0 mL, 9.0 mmol), following the general procedure **GP4**. Purification by column chromatography (silica gel, 40–63 μm, Hexanes/EtOAc) provided **5a** (7.7 mg, 15% yield) as a colourless solid and **3aa** (40.2 mg, 60 % yield) as a pale-yellow oil.

3aa: **MW** ($C_{20}H_{25}NO_4S$): 375.48 g/mol. **Rf**: 0.49 (Hexane/EtOAc 8:2). **IR (ATR) ν (cm^{-1})**: 2924, 1724, 1344, 1161. **^{1}H NMR (CDCl$_3$, 400 MHz): δ_H** 1.22 (t, ^3J = 7.1, 3H, **H1**), 1.51 – 1.62 (m, 1H, **H5/H5'**), 1.90 – 1.97 (m, 1H, **H5/H5'**), 2.05 – 2.13 (m, 2H, **H11**), 2.10 – 2.17 (m, 2H, **H6**), 2.15 – 2.33 (m, 2H, **H13**), 2.38 – 2.47 (m, 1H, **H4**), 2.42 (s, 3H, **CH$_3$-Ar**), 3.47 (ddd, ^2J = 13.4 Hz, ^3J = 6.1 Hz, ^3J = 3.0 Hz, 1H, **H10/H10'**), 3.64 – 3.71 (m, 1H, **H10/H10'**), 4.11 (q, ^3J = 7.1 Hz, 2H, **H2**), 4.86 (d, $^3J_{cis}$ = 10.3 Hz, 1H, **H8**), 6.66 (d, $^3J_{cis}$ = 10.3 Hz, 1H, **H9**), 7.30 (d, $^3J_{ortho}$ = 8.2 Hz, 2H, **CH-Ar**), 7.66 (d, $^3J_{ortho}$ = 8.2 Hz, 2H, **CH-Ar**). **^{13}C{1H} NMR (CDCl$_3$, 101 MHz): δ_C** 14.35 (**C1**), 21.70 (**CH$_3$-Ar**), 25.41 (**C5**), 30.91 (**C6**), 34.59 (**C13**), 36.32 (**C11**), 39.52 (**C4**), 47.08 (**C10**), 60.49 (**C2**), 110.58 (**C8**), 124.74 (**C9**), 126.11 (**C7**), 127.18 (**CH-Ar**), 130.01 (**CH-**

Ar), 133.54 (**C12**), 135.72 (**C-Ar**), 143.96 (**C-Ar)**, 175.57 (**C3**). **ESI-HRMS (*m/z*)** calcd for $[M+Na]^+$ = 398.1397. Found 398.1405.

5a: **MW** ($C_{15}H_{17}NO_2S$): 275.4 g/mol. **Rf**: 0.35 (Hexane/EtOAc 8:2). **^{1}H NMR (400 MHz, $CDCl_3$) δ(ppm):** 2.43 (s, 3H, **CH_3-Ar**), 2.75 (dd, ^3J = 9.6 Hz, ^2J = 6.0 Hz, 2H, **H1/H1'**), 3.28 – 3.34 (m, 2H, **H1/H1'**), 3.62 (d, ^2J = 9.6 Hz, 2H, **H2**), 4.80 (s, 2H, **H3/H3'**), 5.22 (s, 2H, **H3/H3'**), 7.31 (d, $^3J_{ortho}$ = 8.3 Hz, 2H, **CH-Ar**), 7.68 (d, J = 8.3 Hz, 2H, **CH-Ar**). **^{13}C{1H} NMR ($CDCl_3$, 101 MHz): δ_C** 21.68, 44.81, 53.49, 105.69, 128.24, 129.61, 132.28, 143.68, 149.15. **ESI-MS (*m/z*)** $[M+H]^+$ = 275.1. Spectral data in accordance with literature values.[71a]

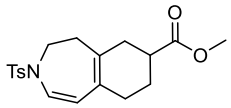

3ab

Compound **3ab** was obtained from bisallene **1a** (52 mg, 0.19 mmol) and methyl acrylate (0.84 mL, 9.3 mmol), following the general procedure **GP4**. Purification by column chromatography (silica gel, 40–63 μm, Hexanes/EtOAc) provided **5a** (7.7 mg, 15% yield) as a colourless solid and **3ab** (36 mg, 53% yield) as a yellow oil.

MW ($C_{19}H_{23}NO_4S$): 361.46 g/mol **Rf**: 0.31 (Hexane/EtOAc 8:2). **IR (ATR) ν (cm^{-1})**: 2924, 1727, 1341, 1158. **^{1}H NMR ($CDCl_3$, 400 MHz): δ_H** 1.51 – 1.63 (m, 1H), 1.91 – 1.98 (m, 1H), 2.06 – 2.33 (m, 6H), 2.40 – 2.50 (m, 1H), 2.42 (s, 3H), 3.48 (ddd, ^2J = 13.4 Hz, ^3J = 6.2 Hz, ^3J = 3.0 Hz, 1H), 3.66 (s, 3H), 3.63 – 3.71 (m, 1H), 4.86 (d, $^3J_{cis}$ = 10.3 Hz, 1H), 6.66 (d, $^3J_{cis}$ = 10.3 Hz, 1H), 7.31 (d, $^3J_{ortho}$ = 8.3 Hz, 2H), 7.66 (d, $^3J_{ortho}$ = 8.3 Hz, 2H). **^{13}C{1H} NMR ($CDCl_3$, 101 MHz): δ_C** 21.70, 25.40, 30.90, 34.58, 36.33, 39.42, 47.08, 51.82, 110.52, 124.82, 126.15, 127.20, 130.02, 133.44, 135.76, 143.97, 176.00. **ESI-HRMS (*m/z*)** calcd for $[M+Na]^+$ = 384.1240. Found 384.1236.

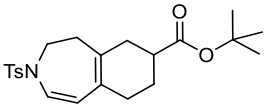

3ac

Compound **3ac** was obtained from bisallene **1a** (49.6 mg, 0.18 mmol) and tert-butyl acrylate (1.36 mL, 98%, 9.1 mmol), following the general procedure **GP4**. Purification by column chromatography (silica gel, 40–63 μm, Hexanes/EtOAc) provided **5a** (7.1 mg, 14 %yield) as a colourless solid and **3ac** (36.6 mg, 50% yield) as a pale yellow oil.

MW ($C_{22}H_{29}NO_4S$): 403.54 g/mol. **Rf**: 0.36 (Hexane/EtOAc 9:1). **IR (ATR) ν (cm^{-1})**: 2924, 1719, 1343, 1149. **^{1}H NMR ($CDCl_3$, 400 MHz): δ_H** 1.41 (s, 9H), 1.48 – 1.59 (m, 1H), 1.85 – 1.94 (m, 1H), 2.08 – 2.27 (m, 6H), 2.29 – 2.38 (m, 1H), 2.42 (s, 3H), 3.48 (ddd, ^2J = 13.4 Hz, ^3J = 6.1 Hz, ^3J = 2.9 Hz, 1H), 3.63 – 3.71 (m, 1H), 4.86 (d, $^3J_{cis}$ = 10.3 Hz, 1H), 6.66 (d, $^3J_{cis}$ = 10.3 Hz, 1H), 7.30 (d, $^3J_{ortho}$ = 8.4, 2H), 7.66 (d, $^3J_{ortho}$ = 8.4 Hz, 2H). **^{13}C{1H} NMR ($CDCl_3$, 101 MHz): δ_C** 21.72, 25.48, 28.20, 30.95, 34.74, 36.35, 40.43, 47.12,

80.24, 110.73, 124.65, 126.09, 127.21, 130.02, 133.82, 135.78, 143.95, 174.99. **ESI-HRMS (*m/z*)** calcd for $[M+Na]^+$ = 426.1710. Found 426.1712.

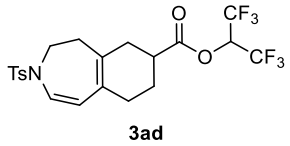

3ad

Compound **3ad** was obtained from bisallene **1a** (51.8 mg, 0.19 mmol) and 1,1,1,3,3,3-hexafluoroisopropyl acrylate (1.55 mL, 99%, 9.2 mmol), following the general procedure **GP4**. Purification by column chromatography (silica gel, 40–63 μm, Hexanes/EtOAc) provided **3ad** (49.3 mg, 53% yield) as a yellowish oil and **5a** (4.3 mg, 8% yield) as a colourless solid.

MW ($C_{21}H_{21}F_6NO_4S$): 497.45 g/mol. **Rf**: 0.40 (Hexane/EtOAc 9:1). **IR (ATR) ν (cm^{-1})**: 2926, 1772, 1349, 1197, 1163. **^{1}H NMR (CDCl$_3$, 400 MHz): δ_H** 1.65 – 1.77 (m, 1H), 1.98 – 2.06 (m, 1H), 2.11 – 2.40 (m, 6H), 2.45 (s, 3H), 2.67 – 2.76 (m, 1H), 3.52 (ddd, ^2J = 13.6 Hz, ^3J = 6.4 Hz, ^3J = 2.9 Hz, 1H), 3.66 – 3.74 (m, 1H), 4.88 (d, $^3J_{cis}$ = 10.3 Hz, 1H), 5.76 (hept, $^3J_{H\text{-}F}$ = 6.1 Hz, 1H), 6.72 (d, $^3J_{cis}$ = 10.3 Hz, 1H), 7.34 (d, $^3J_{ortho}$ = 8.4 Hz, 2H), 7.69 (d, $^3J_{ortho}$ = 8.4 Hz, 2H). **^{13}C{1H} NMR (CDCl$_3$, 101 MHz): δ_C** 21.71, 24.92, 30.28, 33.89, 36.21, 38.89, 47.00, 66.51 (quint, $^2J_{C\text{-}F}$ = 34.7), 110.11, 120.53 (q, $^1J_{C\text{-}F}$ = 283.3), 125.27, 126.37, 127.22, 130.06, 132.29, 135.66, 144.08, 172.16. **ESI-HRMS (*m/z*)** calcd for $[M+Na]^+$ = 520.0988. Found 520.1001.

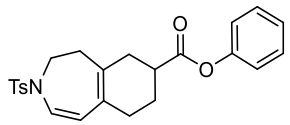

3ae

Compound **3ae** was obtained from bisallene **1a** (50.2 mg, 0.18 mmol) and phenyl acrylate (1.25 mL, 9.1 mmol), following the general procedure **GP4**. Purification by column chromatography (silica gel, 40–63 μm, Hexanes/EtOAc 98:2 to 90:10) provided **3ae** (50.4 mg, 65% yield) as a pale-yellow oil.

MW ($C_{24}H_{25}NO_4S$): 423.53 g/mol. **Rf**: 0.24 (Hexane/EtOAc 9:1). **IR (ATR) ν (cm^{-1})**: 2923, 1748, 1340, 1157. **^{1}H NMR (CDCl$_3$, 400 MHz): δ_H** 1.69 – 1.80 (m, 1H), 2.07 – 2.18 (m, 3H), 2.19 – 2.27 (m, 2H), 2.30 – 2.49 (m, 2H), 2.42 (s, 3H), 2.68 – 2.77 (m, 1H), 3.51 (ddd, ^2J = 13.4 Hz, ^3J = 6.2 Hz, ^3J = 2.9 Hz, 1H), 3.67 – 3.74 (m, 1H), 4.90 (d, $^3J_{cis}$ = 10.3 Hz, 1H), 6.70 (d, $^3J_{cis}$ = 10.3 Hz, 1H), 7.04 (dd, $^3J_{ortho}$ = 8.6 Hz, $^4J_{meta}$ 1.2 Hz, 2H), 7.19 – 7.24 (m, 1H), 7.31 (d, $^3J_{ortho}$ = 8.4 Hz, 2H), 7.32 – 7.41 (m, 2H), 7.67 (d, $^3J_{ortho}$ = 8.4 Hz, 2H). **^{13}C{1H} NMR (CDCl$_3$, 101 MHz): δ_C** 21.72, 25.39, 30.78, 34.45, 36.35, 39.61, 47.09, 110.45, 121.58, 124.97, 125.92, 126.26, 127.21, 129.55, 130.05, 133.21, 135.73, 144.02, 150.86, 174.04. **ESI-HRMS (*m/z*)** calcd for $[M+Na]^+$ = 446.1397. Found 446.1397.

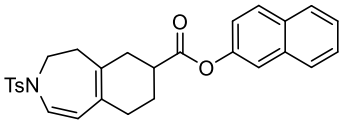

3af

Compound **3af** was obtained from bisallene **1a** (49.9 mg, 0.18 mmol) and naphtyl acrylate (909 mg, 4.6 mmol), following the general procedure **GP4**. Purification by column chromatography (silica gel, 40–63 μm, Hexanes/EtOAc 98:2 to 90:10) provided **3af** (58 mg, 68% yield) as a pale-yellow solid.

MW ($C_{28}H_{27}NO_4S$): 473.59 g/mol. **Rf**: 0.34 (Hexane/EtOAc 8:2). **MP (°C):** 144 - 146 (Hexane/EtOAc 9:1). **IR (ATR) ν (cm^{-1})**: 2921, 1745, 1345, 1161. **^{1}H NMR ($CDCl_3$, 400 MHz): δ_H** 1.73 – 1.86 (m, 1H), 2.12 – 2.30 (m, 5H), 2.34 – 2.54 (m, 2H), 2.42 (s, 3H), 2.74 – 2.82 (m, 1H), 3.53 (ddd, ^2J =13.4 Hz, ^3J = 6.3 Hz, ^3J = 2.9 Hz, 1H), 3.68 – 3.76 (m, 1H), 4.91 (d, $^3J_{cis}$ = 10.3 Hz, 1H), 6.71 (d, $^3J_{cis}$ = 10.3 Hz, 1H), 7.18 (dd, $^3J_{ortho}$ = 8.9, $^4J_{meta}$ = 2.3 Hz, 1H), 7.32 (d, $^3J_{ortho}$ = 8.3 Hz, 2H), 7.43 – 7.53 (m, 3H), 7.68 (d, $^3J_{ortho}$ = 8.3 Hz, 2H), 7.79 (dd, $^3J_{ortho}$ = 7.1 Hz, $^4J_{meta}$ = 2.1 Hz, 1H), 7.82 – 7.86 (m, 2H). **^{13}C{1H} NMR ($CDCl_3$, 101 MHz): δ_C** 21.72, 25.45, 30.83, 34.50, 36.37, 39.70, 47.10, 110.44, 118.53, 121.15, 125.01, 125.83, 126.29, 126.72, 127.21, 127.72, 127.90, 129.53, 130.05, 131.55, 133.20, 133.87, 135.73, 144.02, 148.50, 174.21. **ESI-HRMS (*m/z*)** calcd for $[M+Na]^+$ = 496.1553. Found 496.1547.

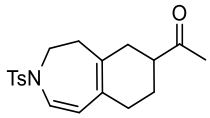

3ag

Compound **3ag** was obtained from bisallene **1a** (49.5 mg, 0.18 mmol) and 3-buten-2-one (0.74 mL, 99%, 9.0 mmol), following the general procedure **GP4**. Purification by column chromatography (silica gel, 40–63 μm, Hexanes/EtOAc 98:2 to 90:10) provided **5a** (5.8 mg, 12% yield) as a colourless solid and **3ag** (45 mg, 72% yield) as a yellowish oil.

MW ($C_{19}H_{23}NO_3S$): 345.46 g/mol. **Rf**: 0.17 (Hexane/EtOAc 8:2). **IR (ATR) ν (cm^{-1})**: 2921, 1703, 1342, 1160. **^{1}H NMR ($CDCl_3$, 400 MHz): δ_H** 1.41 – 1.50 (m, 1H), 1.89 – 1.96 (m, 1H), 2.04 – 2.27 (m, 6H), 2.14 (s, 3H), 2.41 (s, 3H), 2.44 – 2.53 (m, 1H), 3.46 (ddd, ^2J = 13.5 Hz, ^3J = 6.8 Hz, ^3J = 2.3 Hz, 1H), 3.64 – 3.72 (m, 1H), 4.85 (d, $^3J_{cis}$ = 10.3 Hz, 1H), 6.66 (d, $^3J_{cis}$ = 10.3 Hz, 1H), 7.30 (d, $^3J_{ortho}$ = 8.3 Hz, 2H), 7.65 (d, $^3J_{ortho}$ = 8.3 Hz, 2H). **^{13}C{1H} NMR ($CDCl_3$, 101 MHz): δ_C** 21.69, 25.04, 28.16, 31.20, 33.77, 36.40, 47.05, 47.39, 110.46, 124.78, 126.10, 127.17, 130.01, 133.61, 135.70, 143.98, 211.19. **ESI-HRMS (*m/z*)** calcd for $[M+Na]^+$ = 368.1291. Found 368.1294.

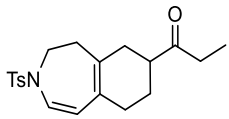

3ah

Compound **3ah** was obtained from bisallene **1a** (50 mg, 0.18 mmol) and 1-penten-3-one (0.93 mL, 97%, 9.1 mmol), following the general procedure **GP4**. Purification by column chromatography (silica gel, 40–63 μm, Hexanes/EtOAc 98:2 to 90:10) provided **3ah** (48.8 mg, 75% yield) as a yellowish oil.

MW ($C_{20}H_{25}NO_3S$): 359.48 g/mol. **Rf**: 0.29 (Hexane/EtOAc 8:2). **IR (ATR) ν (cm^{-1})**: 2924, 1704, 1342, 1160. **^{1}H NMR ($CDCl_3$, 400 MHz): δ_H** 1.03 (t, ^3J = 7.3 Hz, 3H), 1.40 – 1.52 (m, 1H), 1.83 – 1.93 (m, 1H), 2.01 – 2.30 (m, 6H), 2.37 – 2.56 (m, 3H), 2.42 (s, 3H), 3.47 (ddd, ^2J = 13.4, ^3J = 7.1 Hz, ^3J = 2.2 Hz, 1H), 3.65 – 3.74 (m, 1H), 4.86 (d, $^3J_{cis}$ = 10.3 Hz, 1H), 6.66 (d, $^3J_{cis}$ = 10.3 Hz, 1H), 7.31 (d, $^3J_{ortho}$ = 8.4 Hz, 2H), 7.66 (d, $^3J_{ortho}$ = 8.4 Hz, 2H). **^{13}C{1H} NMR ($CDCl_3$, 101 MHz): δ_C** 7.91, 21.72, 25.30, 31.30, 34.08, 34.10, 36.45, 46.47, 47.08, 110.53, 124.78, 126.08, 127.21, 130.03, 133.82, 135.76, 143.99, 213.86. **ESI-HRMS (*m/z*)** calcd for $[M+Na]^+$ = 382.1447. Found 382.1447.

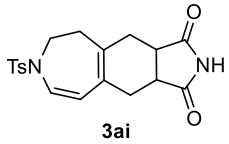

3ai

Compound **3ai** was obtained from bisallene **1a** (50 mg, 0.18 mmol) and maleimide (88 mg, 0.91 mmol), following the general procedure. Purification by column chromatography (silica gel, 40–63 μm, hexanes/EtOAc 8:2 to 1:1) provided **3ai** (51 mg, 76% yield) as a pale-yellow solid.

MW ($C_{19}H_{20}N_2O_4S$): 372.44 g/mol. **Rf**: 0.24 (Hexane/EtOAc 1:1). **MP (°C)**: 221 – 223 (Hexane/EtOAc 1:1). **IR (ATR) ν (cm^{-1})**: 3220, 2924, 1775, 1699, 1331, 1157. **^{1}H NMR ($CDCl_3$, 400 MHz): δ_H** 2.25 – 2.35 (m, 4H), 2.42 (s, 3H), 2.44 – 2.56 (m, 2H), 3.02 – 3.12 (m, 2H), 3.41 – 3.57 (m, 2H), 4.97 (d, $^3J_{cis}$ = 9.9 Hz, 1H), 6.65 (d, $^3J_{cis}$ = 9.9 Hz, 1H), 7.31 (d, $^3J_{ortho}$ = 8.3 Hz, 2H), 7.64 (d, $^3J_{ortho}$ = 8.3 Hz, 2H), 8.06 (s, 1H). **^{13}C{1H} NMR ($CDCl_3$, 101 MHz): δ_C** 21.72, 31.95, 32.17, 38.10, 40.89, 41.00, 46.51, 110.13, 126.84, 127.18, 127.42, 130.10, 135.16, 135.66, 144.22, 179.60, 179.78. **ESI-HRMS (*m/z*)** calcd for $[M+Na]^+$ = 395.1036. Found 395.1043.

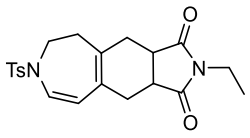

3aj

Compound **3aj** was obtained from bisallene **1a** (49.8 mg, 0.18 mmol) and N-ethylmaleimide (603 mg, 4.8 mmol), following the general procedure **GP4**. Purification by column chromatography (silica gel, 40–63 μm, Hexanes/EtOAc 8:2 to 1:1) provided **3aj** (46.5 mg, 64% yield) as a pale-yellow solid.

MW ($C_{21}H_{24}N_2O_4S$): 400.49 g/mol. **Rf**: 0.37 (Hexane/EtOAc 1:1). **MP (°C):** 140 – 141 (Hexane/EtOAc 1:1). **IR (ATR) ν (cm^{-1})**: 2913, 1764, 1687, 1334, 1160. **^{1}H NMR ($CDCl_3$, 400 MHz): δ_H** 0.90 (t, ^3J = 7.2 Hz, 3H), 2.14 – 2.36 (m, 4H), 2.41 (s, 3H), 2.47 – 2.58 (m, 2H), 2.94 – 3.04 (m, 2H), 3.39 (d, ^3J = 7.2 Hz, 2H), 3.38 – 3.45 (m, 1H), 3.51 (ddd, ^2J = 13.7 Hz, ^3J = 6.9 Hz, ^3J = 1.7 Hz, 1H), 4.96 (d, $^3J_{cis}$ = 10.0 Hz, 1H), 6.63 (d, $^3J_{cis}$ = 10.0 Hz, 1H), 7.28 (d, $^3J_{ortho}$ = 8.3 Hz, 2H), 7.61 (d, $^3J_{ortho}$ = 8.3 Hz, 2H). **^{13}C{1H} NMR ($CDCl_3$, 101 MHz): δ_C** 13.24, 21.69, 32.30, 32.55, 33.81, 37.94, 39.63, 39.71, 46.39, 110.14, 126.55, 127.14, 127.44,

130.04, 135.18, 135.59, 144.11, 179.43, 179.74. **ESI-HRMS (*m/z*)** calcd for $[M+Na]^+$ = 423.1349. Found 423.1348.

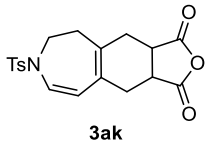

3ak

Compound **3ak** was obtained from bisallene **1a** (49.6 mg, 0.18 mmol) and maleic anhydride (446 mg, 4.5 mmol), following the general procedure **GP4**. Purification by column chromatography (silica gel, 40–63 μm, Hexanes/EtOAc 8:2 to 1:1) provided **3ak** (54.8 mg, 81% yield) as a yellow solid.

MW ($C_{19}H_{19}NO_5S$): 373.42 g/mol. **Rf**: 0.46 (Hexane/EtOAc 1:1). **MP (°C):** 156 – 157 (Hexane/EtOAc 1:1). **IR (ATR) ν (cm^{-1})**: 2919, 1841, 1769, 1348, 1159. **^{1}H NMR ($CDCl_3$, 400 MHz): δ_H** 2.17 – 2.26 (m, 1H), 2.31 – 2.41 (m, 3H), 2.44 (s, 3H), 2.50 – 2.62 (m, 2H), 3.27 – 3.38 (m, 2H), 3.49 – 3.55 (m, 2H), 4.98 (d, $^3J_{cis}$ = 10 Hz, 1H), 6.71 (d, $^3J_{cis}$ = 10 Hz, 1H), 7.32 (d, $^3J_{ortho}$ = 8.4 Hz, 2H), 7.63 (d, $^3J_{ortho}$ = 8.4 Hz, 2H). **^{13}C{1H} NMR ($CDCl_3$, 101 MHz): δ_C** 21.73, 32.07, 32.20, 37.97, 40.26, 40.33, 46.30, 109.70, 127.09, 127.67, 127.76, 130.22, 134.93, 135.51, 144.49, 173.80, 174.09. **ESI-HRMS (*m/z*)** calcd for $[M+Na]^+$ = 396.0876. Found 396.0876.

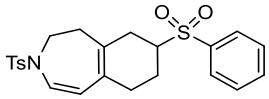

3al

Compound **3al** was obtained from bisallene **1a** (50.1 mg, 0.18 mmol) and phenyl vinyl sulfone (828 mg, 4.9 mmol), following the general procedure **GP4**. Purification by column chromatography (silica gel, 40–63 μm, Hexanes/EtOAc 98:2 to 90:10) provided **3al** (24.7 mg, 31% yield) as a pale-yellow solid.

MW ($C_{23}H_{25}NO_4S_2$): 443.58 g/mol. **Rf**: 0.29 (Hexane/EtOAc 7:3). **MP (°C):** 104 – 109 (dec.), (Hexane/EtOAc 9:1). **IR (ATR) ν (cm^{-1})**: 2923, 1343, 1302, 1160, 1143. **^{1}H NMR ($CDCl_3$, 400 MHz): δ_H** 1.37 – 1.50 (m, 1H), 1.92 – 2.15 (m, 6H), 2.20 – 2.28 (m, 1H), 2.32 (s, 3H), 2.91 – 3.01 (m, 1H), 3.34 (ddd, ^2J = 13.6 Hz, ^3J = 7.0 Hz, ^3J = 2.3 Hz, 1H), 3.50 - 3.57 (m, 1H), 4.71 (d, $^3J_{cis}$ = 10.3 Hz, 1H), 6.57 (d, $^3J_{cis}$ = 10.3 Hz, 1H), 7.20 (d, $^3J_{ortho}$ = 8.4 Hz, 2H), 7.43 – 7.50 (m, 2H), 7.51 – 7.59 (m, 3H), 7.72 – 7.81 (m, 2H). **^{13}C{1H} NMR ($CDCl_3$, 101 MHz): δ_C** 21.73, 22.19, 30.83, 31.29, 36.21, 46.87, 60.18, 109.54, 125.61, 126.45, 127.20, 129.08, 129.32, 130.09, 131.46, 133.93, 135.56, 137.27, 144.16. **ESI-HRMS (*m/z*)** calcd for $[M+Na]^+$ = 466.1117. Found 466.1117.

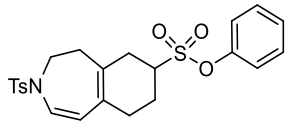

3am

Compound **3am** was obtained from bisallene **1a** (50.3 mg, 0.18 mmol) and phenyl vinyl sulfonate (1,0 g, 5.4 mmol), following the general procedure **GP4**. Purification by column chromatography (silica gel, 40–63 μm,

Hexanes/EtOAc 98:2 to 90:10) provided **3am** (50.2 mg, 60% yield) as a colourless solid.

MW ($C_{23}H_{25}NO_5S_2$): 459.57 g/mol. **Rf**: 0.48 (Hexane/EtOAc 7:3). **MP (°C):** 125 – 126 (Hexane/EtOAc 9:1). **IR (ATR) ν (cm^{-1})**: 2919, 1364, 1341, 1159, 1143. **^{1}H NMR ($CDCl_3$, 400 MHz): δ_H** 1.78 – 1.92 (m, 1H), 2.08 – 2.24 (m, 2H), 2.26 – 2.33 (m, 2H), 2.34 – 2.41 (m, 1H), 2.43 (s, 3H), 2.47 – 2.55 (m, 1H), 2.58 – 2.69 (m, 1H), 3.29 – 3.40 (m, 1H), 3.49 (ddd, ^2J = 13.6 Hz, ^3J = 7.0 Hz, ^3J = 2.3 Hz, 1H), 3.67 – 3.75 (m, 1H), 4.87 (d, $^3J_{cis}$ = 10.3 Hz, 1H), 6.73 (d, $^3J_{cis}$ = 10.3 Hz, 1H), 7.21 – 7.25 (m, 2H), 7.27 – 7.30 (m, 1H), 7.32 (d, $^3J_{ortho}$ = 8.3 Hz, 2H), 7.36 – 7.42 (m, 2H), 7.66 (d, $^3J_{ortho}$ = 8.3 Hz, 2H). **^{13}C{1H} NMR ($CDCl_3$, 101 MHz): δ_C** 21.74, 23.21, 30.59, 32.10, 36.18, 46.89, 56.81, 109.39, 122.09, 125.88, 126.55, 127.22, 127.25, 130.09, 130.12, 131.06, 135.56, 144.21, 149.05. **ESI-HRMS (*m/z*)** calcd for $[M+Na]^+$ = 482.1066. Found 482.1078.

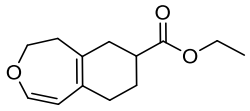

3ja

Compound **3ja** was obtained from bisallene **1j** (23.4 mg, 0.19 mmol) and ethyl acrylate (1.0 mL, 99%, 9.1 mmol), following the general procedure **GP4**. Purification by column chromatography (silica gel, 40–63 μm, Hexanes/EtOAc 99:1) provided **3ja** (7.2 mg, 17% yield) as a pale-yellow oil.

MW ($C_{13}H_{18}O_3$): 222.28 g/mol. **Rf**: 0.61 (Hexane/EtOAc 9:1). **IR (ATR) ν (cm^{-1})**: 2924, 1729. **^{1}H NMR ($CDCl_3$, 400 MHz): δ_H** 1.26 (t, ^3J = 7.1 Hz, 3H), 1.57 – 1.69 (m, 1H), 1.95 – 2.02 (m, 1H), 2.08 – 2.20 (m, 2H), 2.22 – 2.44 (m, 3H), 2.45 – 2.54 (m, 2H), 4.07 – 4.22 (m, 2H), 4.14 (q, ^3J = 7.1 Hz, 2H), 4.57 (d, $^3J_{cis}$ = 7.9 Hz, 1H), 6.26 (d, $^3J_{cis}$ = 7.9 Hz, 1H) . **^{13}C{1H} NMR ($CDCl_3$, 101 MHz): δ_C** 14.40, 25.54, 30.72, 34.27, 38.90, 39.77, 60.49, 70.09, 105.83, 126.20, 131.98, 145.02, 175.86. **ESI-HRMS (*m/z*)** calcd for $[M+Na]^+$ = 245.1148. Found 245.1146.

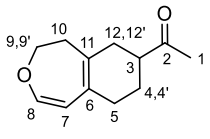

3jg

Compound **3jg** was obtained from bisallene **1j** (23.4 mg, 0.19 mmol) and 3-buten-2-one (0.74, 99%, mL, 9.0 mmol), following the general procedure **GP4**. Purification by column chromatography (silica gel, 40–63 μm, Hexanes/EtOAc 98:2) provided **3jg** (10.0 mg, 27% yield) as a pale-yellow oil.

MW ($C_{12}H_{16}O_2$): 192.26 g/mol. **Rf**: 0.49 (Hexane/EtOAc 8:2). **IR (ATR) ν (cm^{-1})**: 2923, 1704. **^{1}H NMR ($CDCl_3$, 400 MHz): δ_H** 1.44 – 1.57 (m, 1H, **H4/H4'**), 1.92 – 2.01 (m, 1H, **H4/H4'**), 2.09 – 2.22 (m, 3H, H**5**, **H12/H12'**), 2.18 (s, 3H, **H1**), 2.23 – 2.34 (m, 1H, **H12/H12'**), 2.36 – 2.50 (m, 2H, **H10**), 2.50 – 2.60 (m, 1H, **H3**), 4.11 (ddd, ^2J = 10.9 Hz, ^3J = 6.8 Hz, ^3J = 1.6 Hz, 1H, **H9/H9'**), 4.18 (ddd, ^2J = 10.9 Hz, ^3J = 5.9 Hz, ^3J = 2.0 Hz, 1H, **H9/H9'**), 4.57 (d, $^3J_{cis}$ = 7.8 Hz, 1H, **H7**), 6.26 (d, $^3J_{cis}$ = 7.8 Hz, 1H, **H8**) . **^{13}C{1H} NMR**

($CDCl_3$, 101 MHz): δ_C 25.13 (**C4**), 28.21 (**C1**), 31.00 (**C5**), 33.51 (**C12**), 38.96 (**C10**), 47.70 (**C3**), 70.05 (**C9**), 105.73 (**C7**), 126.23 (C**6**), 132.01 (C**11**), 145.08 (C**8**), 211.52 (C**2**). **ESI-HRMS (*m/z*)** calcd for $[M+Na]^+$ = 215.1043. Found 215.1037.

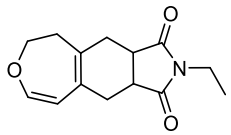

3jj

Compound **3jj** was obtained from bisallene **1j** (23.4 mg, 0.19 mmol) and N-ethylmaleimide (580 mg, 4.6 mmol), following the general procedure **GP4**. Purification by column chromatography (silica gel, 40–63 μm, Hexanes/EtOAc 95:5 to 80:20) provided **3jj** (15.0 mg, 32% yield) as a pale-yellow oil.

MW ($C_{14}H_{17}NO_3$): 247.29 g/mol. **Rf**: 0.21(Hexane/EtOAc 8:2). **IR (ATR) ν (cm^{-1})**: 2922, 1763, 1684. **^{1}H NMR ($CDCl_3$, 400 MHz): δ_H** 1.07 (t, ^3J = 7.2 Hz, 3H), 2.27 – 2.38 (m, 2H), 2.47 – 2.63 (m, 4H), 2.99 – 3.06 (m, 2H), 3.48 (q, ^3J = 7.2 Hz, 2H), 4.00 (ddd, ^2J = 11.2 Hz, ^3J = 6.2 Hz, ^3J = 2.1 Hz, 1H), 4.09 (ddd, ^2J = 11.2 Hz, ^3J = 6.1 Hz, ^3J = 2.2 Hz, 1H), 4.68 (d, $^3J_{cis}$ = 7.6 Hz, 1H), 6.25 (d, $^3J_{cis}$ = 7.6 Hz, 1H). **^{13}C{1H} NMR ($CDCl_3$, 101 MHz): δ_C** 13.34, 31.83, 31.89, 33.90, 39.76, 39.79, 40.00, 69.63, 105.85, 127.48, 133.53, 147.04, 179.71, 180.02. **ESI-HRMS (*m/z*)** calcd for $[M+Na]^+$ = 270.1101. Found 270.1107.

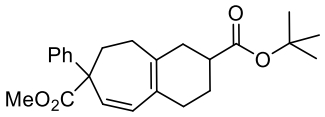

3nc

Compound **3nc** was obtained from bisallene **1n** (45.9 mg, 0.18 mmol) and tert-butyl acrylate (1.36 mL, 98%, 9.1 mmol), following the general procedure **GP4**. Purification by column chromatography (silica gel, 40–63 μm, Hexanes/EtOAc 95:5) provided **3nc** (27.8 mg, 40% yield) as a pale-yellow oil.

MW ($C_{24}H_{30}O_4$): 382.50 g/mol. **^{1}H NMR ($CDCl_3$, 400 MHz)** [a]**: δ_H** 1.46 (s, 9H), 1.59 – 1.68 (m, 1H), 1.89 – 2.19 (m, 5H), 2.19 – 2.26 (m, 2H), 2.27 – 2.45 (m, 2H), 2.50 – 2.66 (m, 1H), 3.72 (s, 3H), 5.94 (d, $^3J_{cis}$ = 12.6 Hz, 1H), 6.04 (d, $^3J_{cis}$ = 12.6 Hz, 1H), 7.19 – 7.29 (m, 3H), 7.30 – 7.36 (m, 2H). Preliminary results, no more characterization done.

[a] Only one diastereoisomer described for simplicity.

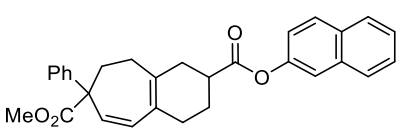

3nf

Compound **3nf** was obtained from bisallene **1n** (46.0 mg, 0.18 mmol) and naphtyl acrylate (909 mg, 4.6 mmol), following the general procedure **GP4**. Purification by column chromatography (silica gel, 40–63 μm, Hexanes/EtOAc 95:5) provided **3nf** (27.2 mg, 33% yield) as a pale-yellow oil.

MW ($C_{30}H_{28}O_4$): 452.55 g/mol. **^{1}H NMR ($CDCl_3$, 400 MHz)** [a]**:** δ_H 1.78 – 1.93 (m, 1H), 1.96 – 2.15 (m, 2H), 2.15 – 2.27 (m, 2H), 2.33 (s, 2H), 2.39 – 2.54 (m, 1H), 2.54 – 2.69 (m, 2H), 2.75 – 2.90 (m, 1H), 3.72 (s, 3H), 5.98 (d, $^3J_{cis}$ = 12.6 Hz, 1H), 6.09 (d, $^3J_{cis}$ = 12.6 Hz, 1H), 7.19 – 7.37 (m, 6H), 7.43 – 7.57 (m, 3H), 7.76 – 7.88 (m, 3H). Preliminary results, no more characterization done.

[a] Only one diastereoisomer described for simplicity.

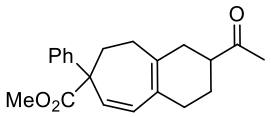

3ng

Compound **3ng** was obtained from bisallene **1n** (46.3 mg, 0.18 mmol) and 3-buten-2-one (0.74 mL, 99%, 9.0 mmol), following the general procedure **GP4**. Purification by column chromatography (silica gel, 40–63 μm, Hexanes/EtOAc 95:5) provided **3ng** (35.2 mg, 60% yield) as a pale-yellow oil.

MW ($C_{21}H_{24}O_3$): 324.42 g/mol. **^{1}H NMR ($CDCl_3$, 400 MHz)** [a]**:** δ_H 1.45 – 1.55 (m, 1H), 1.87 – 2.38 (m, 8H), 2.16 (s, 3H), 2.51 (s, 2H), 3.69 (s, 3H), 5.92 (d, $^3J_{cis}$ = 12.5 Hz, 1H), 6.03 (d, $^3J_{cis}$ = 12.5 Hz, 1H), 7.24 (s, 3H), 7.28 – 7.35 (m, 2H). Preliminary results, no more characterization done.

[a] Only one diastereoisomer described for simplicity.

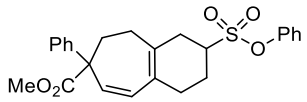

3nm

Compound **3nm** was obtained from bisallene **1n** (23.3 mg, 0.09 mmol) and phenyl vinyl sulfonate (0.31 g, 1.68 mmol), following the general procedure **GP4**. Purification by column chromatography (silica gel, 40–63 μm, Hexanes/EtOAc 95:5 to 80:20) provided **3nm** (16.7 mg, 42% yield) as a pale-yellow oil.

MW ($C_{25}H_{26}O_5S$): 438.54 g/mol. **^{1}H NMR ($CDCl_3$, 400 MHz)** [a]**:** δ_H 1.87 – 2.10 (m, 3H), 2.12 – 2.25 (m, 1H), 2.26 – 2.39 (m, 2H), 2.40 – 2.47 (m, 1H), 2.50 – 2.58 (m, 1H), 2.58 – 2.67 (m, 1H), 2.67 – 2.79 (m, 1H), 3.31 – 3.47 (m, 1H), 3.70 (s, 3H), 5.93 (d, $^3J_{cis}$ = 12.5 Hz, 1H), 6.14 (d, $^3J_{cis}$ = 12.5 Hz, 1H), 7.21 – 7.25 (m, 3H), 7.26 – 7.36 (m, 5H), 7.36 – 7.45 (m, 2H). Preliminary results, no more characterization done.

[a] Only one diastereoisomer described for simplicity.

Characterization of 4a:

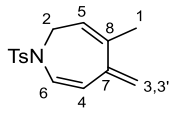

4a

4a: MW ($C_{15}H_{17}NO_2S$): 275.4 g/mol. **Rf**: 0.50 (Hexanes/EtOAc 8:2). **IR (ATR) ν (cm^{-1})**: 2921, 2852, 1456, 1337, 1158, 1090. **^{1}H NMR ($CDCl_3$, 400 MHz): δ_H** 1.76 (s, 3H, **H1**), 2.41 (s, 3H, **CH_3-Ar**), 3.95 (d, ^3J = 7.2 Hz, 2H, **H2**), 5.02 (s, 1H, **H3/H3'**), 5.09 (s, 1H, **H3/H3'**), 5.37 (d, $^3J_{cis}$ = 10.4 Hz, 1H, **H4**), 5.55 (t, ^3J = 7.2 Hz, 1H, **H5**), 6.52 (d, $^3J_{cis}$ = 10.4, 1H, **H6**), 7.28 (d, $^3J_{ortho}$ = 8.4 Hz, 2H, **CH-Ar**), 7.66 (d, $^3J_{ortho}$ = 8.4, 2H, **CH-Ar**). **^{13}C{1H} NMR ($CDCl_3$, 101 MHz): δ_C** 21.64 (**CH_3-Ar**), 23.01 (**C1**), 45.60 (**C2**), 113.72 (**C4**), 117.68 (**C3**), 120.91 (**C5**), 127.01 (**C6**),127.13 (**CH-Ar**), 129.83 (**CH-Ar**), 136.24 (**C-Ar**), 142.06 (**C7**), 143.46 (**C8**), 143.90 (**C-Ar**). **ESI-HRMS (*m/z*)** calcd for $[M+Na]^+$ = 298.0872. Found: 298.0875.

Mechanistic experiments using compound 5a and ethyl acrylate 2a

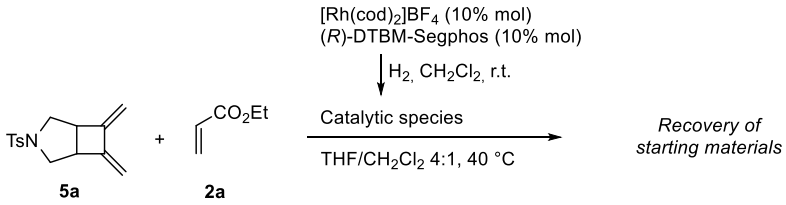

Scheme S9. Diels–Alder attempt between **5a** and **2a** in presence of the catalytic mixture.

In a 10 mL capped vial, a mixture of $[Rh(cod)_2]BF_4$ (4.26 mg, 0.010 mmol) and *(R)*-DTBM-Segphos (12.4 mg, 0.011 mmol) was purged with nitrogen and dissolved in anhydrous CH_2Cl_2 (4 mL). Hydrogen gas was bubbled into the catalyst solution for 30 min. The resulting mixture was concentrated to dryness, dissolved again in anhydrous CH_2Cl_2 (2 mL) and transferred via syringe into a 40 °C preheated solution of **5a** (29 mg, 0.11 mmol) and ethyl acrylate **2a** (0.6 mL, 550 mg, 5.33 mmol) in anhydrous THF (10 mL) and under inert atmosphere. The resulting mixture was stirred at 40 °C for 16h. The solvent and ethyl acrylate **2a** were removed under reduced pressure and the crude reaction mixture was filtered through a short silica gel pad (Hexanes/EtOAc 8:2 v/v). ^{1}H NMR analysis of the crude product revealed the presence of unaltered starting material **5a**.

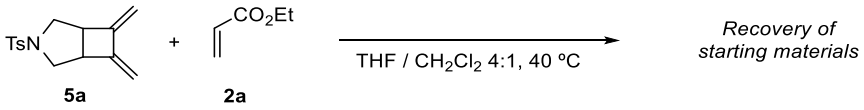

Scheme S10. Diels–Alder attempt between 5a and 2a in absence of the catalytic mixture.

In a 25 mL round-bottom flask equipped with a magnetic stirrer and an inert atmosphere, a solution of **5a** (15 mg, 0.055 mmol) and ethyl acrylate **2a** (0.3 mL, 275 mg, 2.75 mmol) in a 4:1 mixture of THF/CH_2Cl_2 (6 mL) was stirred at 40 °C for 16h. The solvent and ethyl acrylate **2a** were removed under reduced pressure. ^{1}H NMR analysis of the crude product revealed the presence of unaltered starting material **5a**.

Mechanistic experiment using 1,5-bisallene 1a in absence of ethyl acrylate 2a

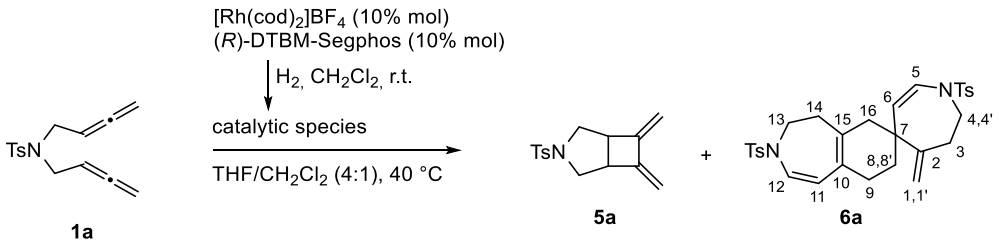

Scheme S11. Isolation attempt of **A5**, leading to **6a** via Diels – Alder homodimerization

In a 10 mL capped vial, a mixture of $[Rh(cod)_2]BF_4$ (7.4 mg, 0.018 mmol) and *(R)*-DTBM-Segphos (23.6 mg, 0.020 mmol) was purged with nitrogen and dissolved in anhydrous CH_2Cl_2 (4 mL). Hydrogen gas was bubbled into the catalyst solution and the mixture was stirred for 30 min. The resulting mixture was concentrated to dryness, dissolved again in anhydrous CH_2Cl_2 (4 mL) and transferred via syringe into a preheated solution to 40 °C of bisallene **1a** (48.4 mg, 0.18 mmol) in anhydrous THF (16 mL) and under inert atmosphere. The resulting mixture was stirred at 40 °C for 16 h. The solvent was removed under reduced pressure and the crude reaction mixture was purified by column chromatography on silica gel using hexane/EtOAc mixtures as the eluent (95:5 to 90:10 v/v), affording first, compound **5a** (5.5 mg, 12% yield) as a colourless solid, and second, **6a** (28.3 mg, 58% yield) as a pale-yellow solid.

6a: **MW** ($C_{30}H_{34}N_2O_4S_2$): 550.73 g/mol. **Rf**: 0.26 (Hexane/EtOAc 8:2). **MP (°C):** 87-92 (dec). **IR (ATR) ν (cm^{-1})**: 2921, 1336, 1156. **^{1}H NMR ($CDCl_3$, 400 MHz): δ_H** 1.46 – 1.55 (m, 1H, **H8/H8'**), 1.56 – 1.66 (m, 1H, **H8/H8'**), 1.93 – 2.20 (m, 6H, H**9**, **H14, H16**), 2.42 (s, 3H, **CH_3-Ar**), 2.42 (s, 3H, **CH_3-Ar**), 2.43 – 2.55 (m, 2H, **H3**), 3.38 – 3.48 (m, 1H, **H4/H4'**), 3.49 – 3.66 (m, 3H, **H4/H4', H13**), 4.52 (s, 1H, **H1/H1'**), 4.63 (s, 1H, **H1/H1'**), 4.71 (d, *J* = 9.5 Hz, 1H, **H6**), 4.84 (d, *J* = 10.3 Hz, 1H, **H11**), 6.27 (d, *J* = 9.5 Hz, 1H, **H5**), 6.64 (d, *J* = 10.3 Hz, 1H, **H12**), 7.28 (d, *J* = 8.2 Hz, 2H, **CH-Ar**), 7.31 (d, *J* = 8.2 Hz, 2H, **CH-Ar**), 7.66 (m, 4H, **CH-Ar**). **^{13}C{1H} NMR ($CDCl_3$, 101 MHz): δ_C** 21.67 (**CH_3-Ar**), 21.71 (**CH_3-Ar**), 29.10 (**C9**), 32.71 (**C8**), 34.74 (**C3**), 36.69 (**C14**), 42.46 (**C7**), 44.58 (**C16**), 47.03 (**C13**), 50.10 (**C4**), 110.59 (**C11**), 111.82 (**C1**), 122.64 (**C6**), 124.72 (**C12**), 125.67 (**C5**), 125.83 (**C10**), 127.18 (**CH-Ar**), 127.19 (**CH-Ar**), 129.78 (**CH-Ar**), 130.01 (**CH-Ar**), 132.95 (**C15**), 135.83 (**C-Ar**), 136.25 (**C-Ar**), 143.72 (**C-Ar**), 143.97(**C-Ar**), 149.30 (**C2**). **ESI-HRMS (*m/z*)** calcd for $[M+Na]^+$ = 573.1852. Found 573.1836.

Figure S2. HPLC chromatogram of **3ng** using *rac*-BINAP

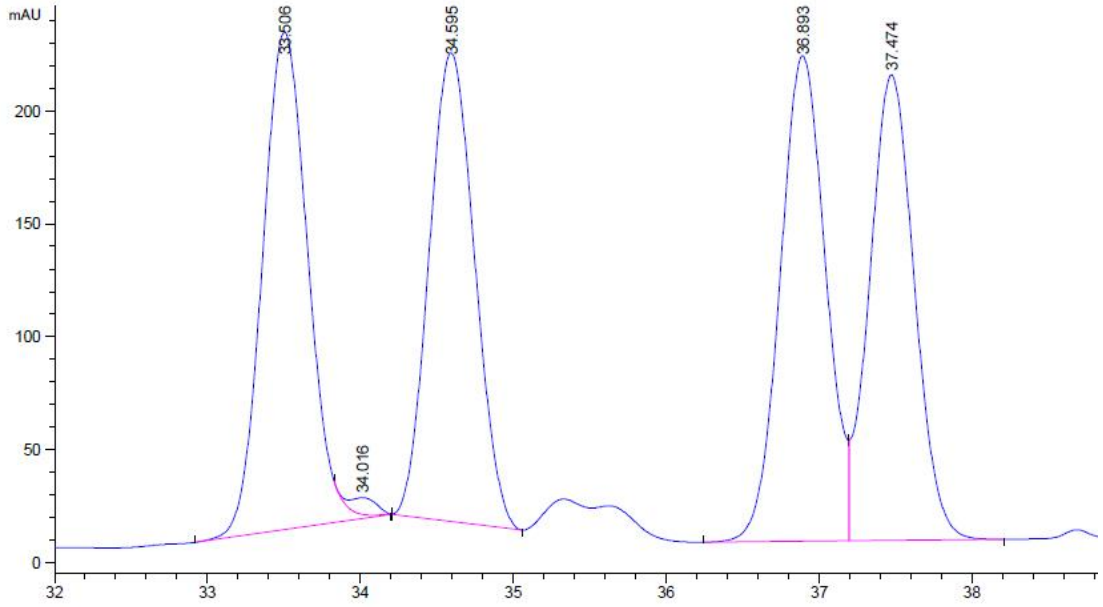

Peak #	RetTime [min]	Type	Width [min]	Area [mAU*s]	Height [mAU]	Area %
1	33.506	BV R	0.3219	4533.66650	220.46706	25.7637
2	34.016	VB E	0.1868	88.03705	7.45377	0.5003
3	34.595	BB	0.3272	4291.13867	207.59969	24.3854
4	36.893	BV	0.3216	4455.71729	215.19081	25.3207
5	37.474	VB	0.3161	4228.56787	206.36345	24.0299

Figure S3. HPLC chromatogram of **3ng** using (*R*)-BINAP

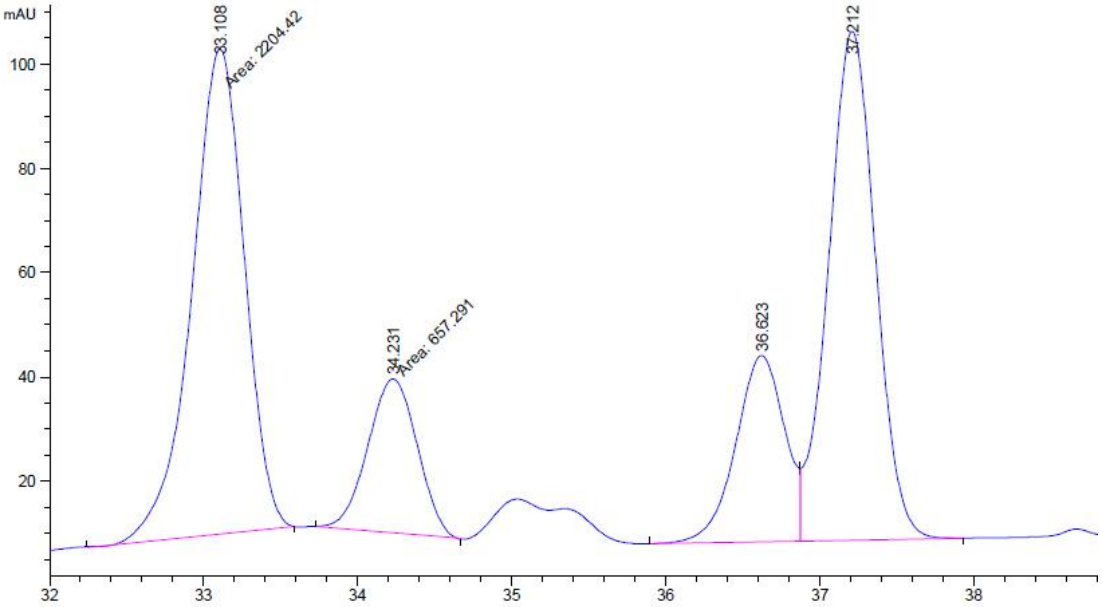

Peak #	RetTime [min]	Type	Width [min]	Area [mAU*s]	Height [mAU]	Area %
1	33.108	MM	0.3951	2204.41992	92.99075	38.4724
2	34.231	MM	0.3715	657.29120	29.48630	11.4713
3	36.623	BV	0.3379	787.89941	35.64592	13.7507
4	37.212	VB	0.3300	2080.26831	97.46037	36.3056

Figure S4. HPLC chromatogram of **3ng** using (*R*)-DTBM-Segphos

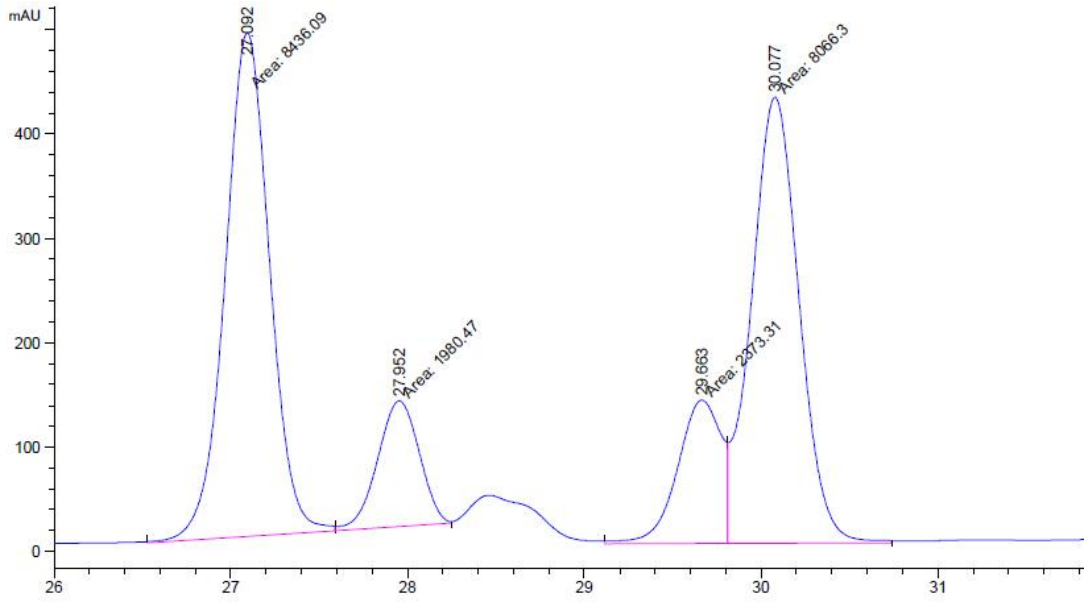

Peak #	RetTime [min]	Type	Width [min]	Area [mAU*s]	Height [mAU]	Area %
1	27.092	MF	0.2910	8436.08887	483.15424	40.4489
2	27.952	FM	0.2738	1980.46521	120.57002	9.4958
3	29.663	MF	0.2876	2373.30542	137.51582	11.3794
4	30.077	FM	0.3143	8066.30029	427.74225	38.6759

Figure S5. HPLC chromatogram of **3nm** using *rac*-Binap

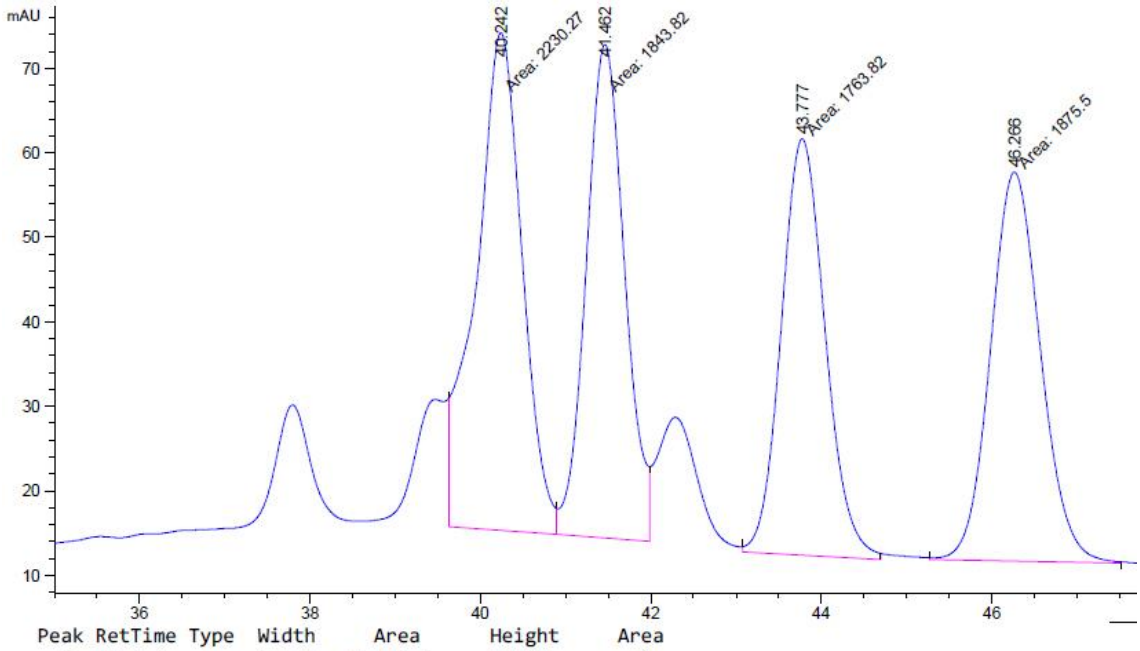

Peak #	RetTime [min]	Type	Width [min]	Area [mAU*s]	Height [mAU]	Area %
1	40.242	FM	0.6314	2230.27051	58.86942	28.9142
2	41.462	FM	0.5266	1843.81714	58.35639	23.9040
3	43.777	MM	0.5971	1763.81909	49.23168	22.8669
4	46.266	MM	0.6793	1875.50452	46.01449	24.3149

Figure S6. HPLC chromatogram of **3nm** using (*R*)-DTBM-Segphos

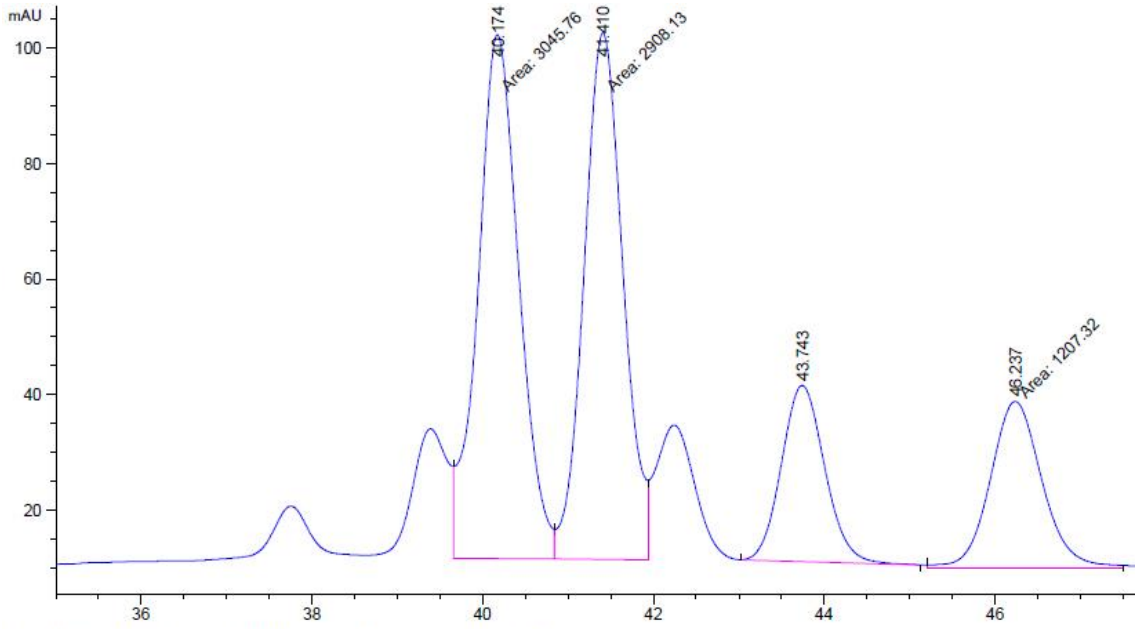

Peak #	RetTime [min]	Type	Width [min]	Area [mAU*s]	Height [mAU]	Area %
1	40.174	MF	0.5593	3045.76392	90.75498	37.0020
2	41.410	MF	0.5316	2908.13013	91.16960	35.3299
3	43.743	BB	0.5448	1070.14600	30.46824	13.0008
4	46.237	MM	0.6995	1207.31592	28.76675	14.6673

Supplementary material for Chapter 4

General procedure GP5 for the synthesis of products 6(a-j)

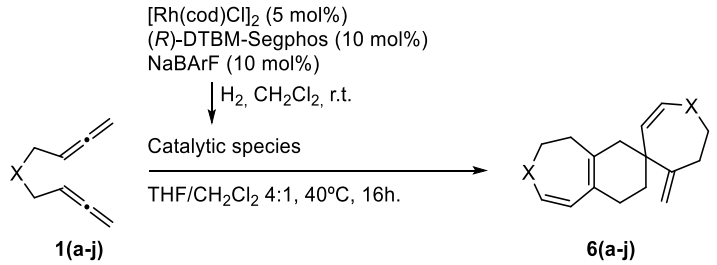

Scheme S12. Rh(I)-catalyzed dimerization of 1,5-bisallenes to produce spiro derivatives.

In a 10 mL capped vial, a mixture of $[Rh(cod)Cl]_2$ (2.2 mg, 0.004 mmol, 0.05 equiv.), (*R*)-DTBM-Segphos (11.3 mg, 0.01 mmol, 0.10 equiv.) and NaBArF (8.5 mg, 0.01 mmol, 0.10 equiv.) was purged with nitrogen and dissolved in anhydrous CH_2Cl_2 (4 mL). Hydrogen gas was bubbled into the catalyst solution and the mixture was stirred for 30 min. The mixture was then concentrated to dryness under a stream of hydrogen, dissolved again in anhydrous CH_2Cl_2 (0.5 mL) and transferred via syringe into a solution of bisallene **1** (0.09 mmol, 1 equiv.) in anhydrous THF (2 mL) under inert atmosphere at 40 °C (aluminium heating block). The resulting mixture was stirred for 16h at 40 °C. The solvent was removed under reduced pressure and the crude reaction mixture was purified by flash chromatography on silica gel using mixtures of hexane/EtOAc as the eluent (90:10 to 60:40 v/v) to afford the spiro compound **6**.

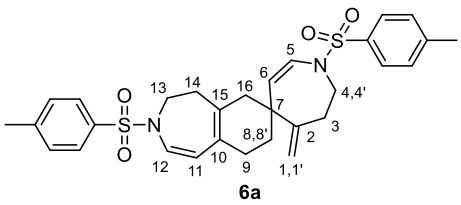

Compound **6a** was obtained from bisallene **1a** (25 mg, 0.09 mmol) following the general procedure **GP5**. Purification by flash chromatography (silica gel, 20 μm, Hexanes/EtOAc 90:10 to 60:40 v/v) provided **6a** (22.3 mg, 89% yield) as a colourless solid.

MW ($C_{30}H_{34}N_2O_4S_2$): 550.73 g/mol. **Rf**: 0.26 (Hexane/EtOAc 8:2). **MP (°C):** 87-92 (dec). **IR (ATR) *ν* (cm^{-1})**: 2921, 1336, 1156. **^{1}H NMR ($CDCl_3$, 400 MHz): δ_H** 1.46 – 1.55 (m, 1H, **H8/H8'**), 1.56 – 1.66 (m, 1H, **H8/H8'**), 1.93 – 2.20 (m, 6H, H**9**, **H14, H16**), 2.42 (s, 3H, **CH_3-Ar**), 2.42 (s, 3H, **CH_3-Ar**), 2.43 – 2.55 (m, 2H, **H3**), 3.38 – 3.48 (m, 1H, **H4/H4'**), 3.49 – 3.66 (m, 3H, **H4/H4', H13**), 4.52 (s, 1H, **H1/H1'**), 4.63 (s, 1H, **H1/H1'**), 4.71 (d, *J* = 9.5 Hz, 1H, **H6**), 4.84 (d, *J* = 10.3 Hz, 1H, **H11**), 6.27 (d, *J* = 9.5 Hz, 1H, **H5**), 6.64 (d, *J* = 10.3 Hz, 1H, **H12**), 7.28 (d, *J* = 8.2 Hz, 2H, **CH-Ar**), 7.31 (d, *J* = 8.2 Hz, 2H, **CH-Ar**), 7.66 (m, 4H, **CH-Ar**). **^{13}C{1H} NMR ($CDCl_3$, 101 MHz): δ_C** 21.67 (**CH_3-Ar**), 21.71 (**CH_3-Ar**), 29.10 (**C9**), 32.71 (**C8**), 34.74 (**C3**), 36.69 (**C14**), 42.46 (**C7**), 44.58 (**C16**), 47.03 (**C13**), 50.10 (**C4**), 110.59 (**C11**), 111.82 (**C1**), 122.64

(**C6**), 124.72 (**C12**), 125.67 (**C5**), 125.83 (**C10**), 127.18 (**CH-Ar**), 127.19 (**CH-Ar**), 129.78 (**CH-Ar**), 130.01 (**CH-Ar**), 132.95 (**C15**), 135.83 (**C-Ar**), 136.25 (**C-Ar**), 143.72 (**C-Ar**), 143.97(**C-Ar**), 149.30 (**C2**). **ESI-HRMS (*m/z*)** calcd for $[M+Na]^+$ = 573.1852. Found 573.1836. **HRMS (ESI) m/z:** calcd for $[M+Na]^+$ = 573.1852. Found 573.1836.

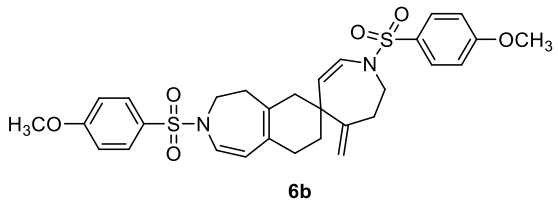

6b

Compound **6b** was obtained from bisallene **1b** (26.5 mg, 0.09 mmol) following the general procedure **GP4**. Purification by flash chromatography (silica gel, 20 μm, Hexanes/EtOAc 90:10 to 60:40 v/v) provided **6b** (23.4 mg, 89% yield) as a colourless oil.

MW ($C_{30}H_{34}N_2O_6S_2$): 582.73 g/mol. **Rf**: 0.28 (Hexane/EtOAc 7:3). **IR (ATR) ν (cm^{-1})**: 2921, 1339, 1153. **^{1}H NMR ($CDCl_3$, 400 MHz): δ_H** 1.49 – 1.55 (m, 1H), 1.58 – 1.66 (m, 1H), 1.94 – 2.20 (m, 6H), 2.38 – 2.55 (m, 2H), 3.39 – 3.47 (m, 1H), 3.49 – 3.66 (m, 3H), 3.86 (s, 3H), 3.87 (s, 3H), 4.53 (s, 1H), 4.64 (s, 1H), 4.70 (d, 1H, $^3J_{cis}$ = 9.5 Hz), 4.83 (d, 1H, $^3J_{cis}$ = 10.3 Hz), 6.27 (d, 1H, $^3J_{cis}$ = 9.5 Hz), 6.64 (d, 1H, $^3J_{cis}$ = 10.3 Hz), 6.91 – 7.02 (m, 4H), 7.68 – 7.74 (m, 4H). **^{13}C{1H} NMR ($CDCl_3$, 101 MHz): δ_C** 29.1, 32.7, 34.8, 36.7, 42.5, 44.6, 47.0, 50.0, 55.8 (2x), 110.5, 111.8, 114.3, 114.5, 122.5, 124.8, 125.7, 125.9, 129.2, 129.3, 130.4, 130.9, 132.9, 163.1, 149.4, 163.2. **HRMS (ESI) m/z:** calcd for $[M+Na]^+$ = 605.1750. Found 605.1767.

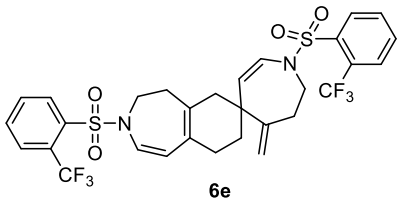

6e

Compound **6e** was obtained from bisallene **1e** (29.8 mg, 0.09 mmol) following the general procedure **GP5**. Purification by flash chromatography (silica gel, 20 μm, Hexanes/EtOAc 90:10 to 60:40 v/v) provided **6e** (26.0 mg, 87% yield) as a colourless oil.

MW ($C_{30}H_{28}F_6N_2O_4S_2$): 658.67 g/mol. **Rf**: 0.32 (Hexane/EtOAc 7:3). **IR (ATR) ν (cm^{-1})**: 2922, 1351, 1305, 1162. **^{1}H NMR ($CDCl_3$, 400 MHz): δ_H** 1.57 – 1.65 (m, 1H),.65 – 1.73 (m, 1H), 2.01 – 2.30 (m, 6H), 2.41 – 2.59 (m, 2H), 3.57 – 3.68 (m, 3H), 3.69 – 3.79(m, 1H), 4.62 (s, 1H), 4.66 (s, 1H), 4.84 (d, 1H, $^3J_{cis}$ = 9.3 Hz), 4.90 (d, 1H, $^3J_{cis}$ = 10.2 Hz), 6.32 (d, 1H, $^3J_{cis}$ = 9.3 Hz), 6.60 (d, 1H, $^3J_{cis}$ = 10.2 Hz), 7.64 – 7.75(m, 4H), 7.86 – 7.94 (m, 2H), 8.00 – 8.06 (m, 2H). **^{13}C{1H} NMR ($CDCl_3$, 101 MHz): δ_C** 29.2, 32.6, 34.7, 37.2, 42.6, 44.5, 47.3, 50.4, 110.8, 112.3, 122.4 (q, $^1J_{C-F}$ = 274.3 Hz), 122.5 (q, $^1J_{C-F}$ = 274.2 Hz), 123.7, 124.5, 125.6, 125.7, 128.1 (q, $^2J_{C-F}$ = 33.4 Hz), 128.3 (q, $^2J_{C-F}$ = 33.4 Hz), 128.6 (q, $^3J_{C-F}$ = 6.3 Hz), 128.8 (q, $^3J_{C-F}$ = 6.4 Hz), 131.3, 131.2, 132.3 (q, $^4J_{C-F}$ = 0.9 Hz), 132.5 (q, $^4J_{C-F}$ = 0.9 Hz), 132.8, 133.0, 133.1, 138.2 (q, $^4J_{C-F}$ = 1.2 Hz), 138.8 (q, $^4J_{C-F}$ = 1.2 Hz), 149.0. **HRMS (ESI) m/z:** calcd for $[M+Na]^+$ = 681.1287. Found 681.1282.

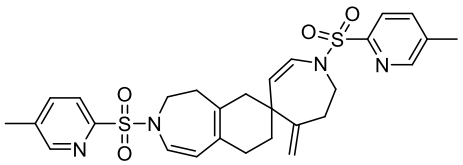

6f

Compound **6f** was obtained from bisallene **1f** (25.3 mg, 0.09 mmol) following the general procedure **GP5**. Purification by flash chromatography (silica gel, 20 μm, Hexanes/EtOAc 90:10 to 60:40 v/v) provided **6f** (19.0 mg, 75% yield) as a colourless oil.

MW ($C_{28}H_{32}N_4O_4S_2$): 552.71 g/mol. **Rf**: 0.15 (Hexane/EtOAc 7:3). **IR (ATR) ν (cm^{-1})**: 2921, 1341, 1168. **^{1}H NMR (CDCl$_3$, 400 MHz): δ_H** 1.52 – 1.62 (m, 1H), 1.65 – 1.74 (m, 1H), 1.93 – 2.15 (m, 3H), 2.20 – 2.30 (m, 3H), 2.43 (s, 6H), 2.48 – 2.64 (m, 2H), 3.54 – 3.64 (m, 1H), 3.64 – 3.82 (m, 3H), 4.60 (s, 1H), 4.69 (s, 1H), 4.76 (d, 1H, $^3J_{cis}$ = 9.4 Hz), 4.83 (d, 1H, $^3J_{cis}$ = 10.3 Hz), 6.34 (d, 1H, $^3J_{cis}$ = 9.4 Hz), 6.59 (d, 1H, $^3J_{cis}$ = 10.3 Hz), 7.64 – 7.72 (m, 2H), 7.79 – 7.88 (m, 2H), 8.48 – 8.55 (m, 2H). **^{13}C{1H} NMR (CDCl$_3$, 101 MHz): δ_C** 18.6, 18.7, 29.2, 32.5, 35.2, 37.4, 42.4, 44.5, 47.8, 50.9, 110.8, 111.9, 122.2, 122.3, 123.1, 124.9, 125.5, 126.6, 133.1, 137.4, 137.6, 138.1, 138.3, 149.2, 150.7, 150.9, 154.0, 154.3. **HRMS (ESI) m/z:** calcd for $[M+Na]^+$ = 575.1757. Found 575.1766.

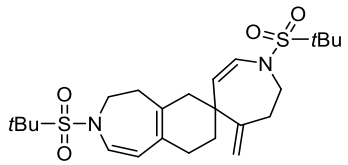

6g

Compound **6g** was obtained from bisallene **1g** (21.8 mg, 0.09 mmol) following the general procedure **GP1**. Purification by flash chromatography (silica gel, 20 μm, Hexanes/EtOAc 90:10 to 60:40 v/v) provided **6g** (14.8 mg, 68% yield) as a colourless oil.

MW ($C_{24}H_{38}N_2O_4S_2$): 482.70 g/mol. **Rf**: 0.32 (Hexane/EtOAc 8:2). **IR (ATR) ν (cm^{-1})**: 2921, 1319, 1128. **^{1}H NMR (CDCl$_3$, 400 MHz): δ_H** 1.39 (s, 9H), 1.41 (s, 9H), 1.66 – 1.82 (m, 2H), 2.06 – 2.25 (m, 3H), 2.32 – 2.41 (m, 1H), 2.43 – 2.50 (m, 2H), 2.54 – 2.69 (m, 2H), 3.72 – 3.85 (m, 4H), 4.63 (d, 1H, $^3J_{cis}$ = 9.7 Hz), 4.76 (d, 1H, $^3J_{cis}$ = 10.3 Hz), 4.80 (s, 1H), 4.91 (s, 1H), 6.41 (d, 1H, $^3J_{cis}$ = 9.7 Hz), 6.49 (d, 1H, $^3J_{cis}$ = 10.3 Hz). **^{13}C{1H} NMR (CDCl$_3$, 101 MHz): δ_C** 24.7, 24.9, 29.1, 33.4, 35.3, 38.4, 42.7, 44.9, 49.1, 51.0, 62.4, 62.9, 108.1, 112.3, 118.9, 125.9, 126.9, 128.4, 132.2, 149.8. **HRMS (ESI) m/z:** calcd for $[M+Na]^+$ = 505.2165. Found 505.2177.

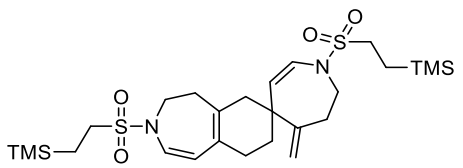

6h

Compound **6h** was obtained from bisallene **1h** (25.9 mg, 0.09 mmol) following the general procedure **GP1**. Purification by flash chromatography (silica gel, 20 μm, Hexanes/EtOAc 90:10 to 60:40 v/v) provided **6h** (14.2 mg, 55% yield) as a colourless oil.

MW ($C_{26}H_{46}N_2O_4S_2Si_2$): 570.95 g/mol. **Rf**: 0.46 (Hexane/EtOAc 8:2). **IR (ATR) ν (cm^{-1})**: 2949, 1335, 1142. **^{1}H NMR (CDCl$_3$, 400 MHz): δ_H** 0.04 (s, 9H), 0.05 (s, 9H), 0.98 – 1.06(m, 4H), 1.67 – 1.85 (m, 2H), 2.07 – 2.27 (m, 3H), 2.33 – 2.49 (m, 3H), 2.54 – 2.70 (m, 2H), 2.89 – 3.01 (m, 4H), 3.63 – 3.80 (m, 4H), 4.75 (d, 1H, $^3J_{cis}$ = 9.4 Hz), 4.79 (s, 1H), 4.83 (d, 1H, $^3J_{cis}$ = 10.2 Hz), 4.91 (s, 1H), 6.29 (d, 1H, $^3J_{cis}$ = 9.4 Hz), 6.49 (d, 1H, $^3J_{cis}$ = 10.2 Hz). **^{13}C{1H} NMR (CDCl$_3$, 101 MHz): δ_C** -1.9, -1.8, 10.4 (x2), 29.2, 33.0, 35.4, 38.1, 42.7, 44.7, 47.2, 49.0, 49.1, 49.9, 109.4, 112.3, 121.4, 125.5, 125.9, 126.6, 132.2, 149.6. **HRMS (ESI) m/z:** calcd for $[M+Na]^+$ = 593.2330. Found 593.2340.

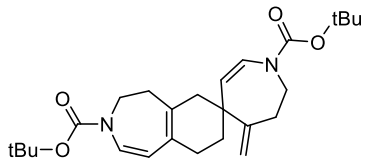

6i

Compound **6i** was obtained from bisallene **1i** (19.7 mg, 0.09 mmol) following the general procedure **GP1**. Purification by flash chromatography (silica gel, 20 μm, Hexanes/EtOAc 90:10 to 60:40 v/v) provided **6i** (8.3 mg, 42% yield) as a colourless oil.

MW ($C_{26}H_{38}N_2O_4$): 442.60 g/mol. **Rf**: 0.63 (Hexane/EtOAc 8:2). **IR (ATR) ν (cm^{-1})**: 2973, 1697, 1649, 1451, 1431. **^{1}H NMR (CDCl$_3$, 400 MHz): δ_H** 1.46 (s, 9H), 1.48 (s, 9H), 1.61 – 1.71 (m, 1H), 1.71 – 1.85 (bs, 1H), 2.05 – 2.25 (m, 3H), 2.29 – 2.42 (m, 3H), 2.55 (bs, 2H), 3.59 – 3.81 (m, 4H), 4.59 – 4.72 (bs, 1H), 4.73 (s, 1H), 4.71 – 4.84 (bs, 1H), 4.86 (s, 1H), 6.24 – 6.55 (bs, 1H), 6.59 – 6.89 (bs, 1H). **^{13}C{1H} NMR (CDCl$_3$, 101 MHz): δ_C** 28.4 (x2), 29.5, 33.0, 34.7, 37.7, 42.5, 44.4, 44.7, 47.6, 80.7, 81.3, 109.6, 111.3, 120.5, 125.4, 126.1, 127.6, 132.9, 150.4, 152.5, 153.7. **HRMS (ESI) m/z:** calcd for $[M+Na]^+$ = 465.2724. Found 465.2718.

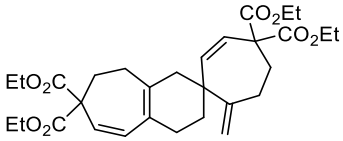

6k

Compound **6k** was obtained from bisallene **1k** (23.8 mg, 0.09 mmol) following the general procedure **GP1**. Purification by flash chromatography (silica gel, 20 μm, Hexanes/EtOAc 90:10 to 60:40 v/v) provided **6k** (19.0 mg, 80% yield) as a colourless oil.

MW ($C_{30}H_{40}O_8$): 528.64 g/mol. **Rf**: 0.44 (Hexane/EtOAc 8:2). **IR (ATR) ν (cm^{-1})**: 2929, 1725, 1224. **^{1}H NMR (CDCl$_3$, 400 MHz): δ_H** 1.20 – 1.30 (m, 12H), 1.59 – 1.77 (m, 2H), 1.98 – 2.25 (m, 5H), 2.25 – 2.44 (m, 5H), 2.44 – 2.62 (m, 2H), 4.11 – 4.23 (m, 8H), 4.69 (s, 1H), 4.81 (s, 1H), 5.57 (d, 1H, $^3J_{cis}$ = 12.1 Hz), 5.70 (d, 1H, $^3J_{cis}$ = 12.1 Hz), 5.80 (d, 1H, $^3J_{cis}$ = 12.4 Hz), 5.85 (d, 1H, $^3J_{cis}$ = 12.4 Hz). **^{13}C{1H} NMR (CDCl$_3$, 101 MHz): δ_C** 14.1 (x2), 14.2 (x2), 28.8, 30.8, 31.7, 32.0, 32.7, 33.5, 43.8, 43.9, 58.6, 61.5, 61.7 (x2), 61.8 (x2), 112.5, 125.5, 125.7, 125.8, 132.8, 138.0, 139.8, 149.9, 171.0, 171.1, 171.2, 171.5. **HRMS (ESI) m/z:** calcd for $[M+Na]^+$ = 551.2615. Found 551.2615.

Table S1. Closed-shell singlet, Open-shell singlet and Open-shell triplet energy comparisson of all reaction pathways computed at 313.15K and 1 atm with the (U)B3LYP-D3/cc-pVTZ/SMD(76% THF, 24% CH_2Cl_2) // (U)B3LYP-D3/cc-pVDZ.

	Closed-shell E (Hartrees)	**Open-shell singlet (oss) E (Hartrees)**	**S^2 (oss)**	**Open-shell triplet (ost) E (Hartrees)**	**S^2 (ost)**	**ΔE_{oss-cs} (kcal/mol)**	**ΔE_{ost-cs} (kcal/mol)**
TS(1A$_{exo}$)	-1769,71922097	-1769,71922097	0,000	-1769,60318767	2,070	0,00	72,8
TS(1A$_{endo}$)	-1769,72084150	-1769,72084150	0,000	-1769,62617458	2,034	0,00	59,4
TS(1B$_{exo}$)	-1769,73199710	-1769,73199710	0,000	-1769,66383335	2,046	0,00	42,8
TS(1B$_{endo}$)	-1769,72526752	-1769,72526752	0,000	-1769,65122395	2,049	0,00	46,5
TS(2A$_{exo}$)	-1769,74405463	-1769,74446238	0,187	-1769,72033707	2,055	-0,26	14,9
TS(2A$_{endo}$)	-1769,74691542	-1769,74703649	0,046	-1769,71978683	2,054	-0,08	17,0
TS(2B$_{exo}$)	-1769,73657120	-1769,73789462	0,399	-1769,71849134	2,058	-0,83	11,3
TS(2B$_{endo}$)	-1769,73915198	-1769,73915198	0,000	-1769,69684649	2,061	0,00	26,5
TS(3A$_{exo}$)	-1769,74014645	-1769,74078180	0,286	-1769,71718532	2,055	-0,40	14,4
TS(3A$_{endo}$)	-1769,73851304	-1769,73851304	0,000	-1769,15419778	2,060	0,00	366,7
TS(3B$_{exo}$)	-1769,73339295	-1769,73339295	0,000	-1769,65003738	2,043	0,00	52,3
TS(3B$_{endo}$)	-1769,73081215	-1769,73081215	0,000	-1769,66846766	2,062	0,00	39,1

Open-shell singlet and Open-shell triplet energy barriers of all reaction paths were also evaluated to confirm that **TS(2A$_{exo}$)** and **TS(2A$_{endo}$)** are the lowest energy barrier transition states.

Supplementary material for Chapter 5

General procedure GP6 for the synthesis of products 7(a-p)n and 7an-d_4

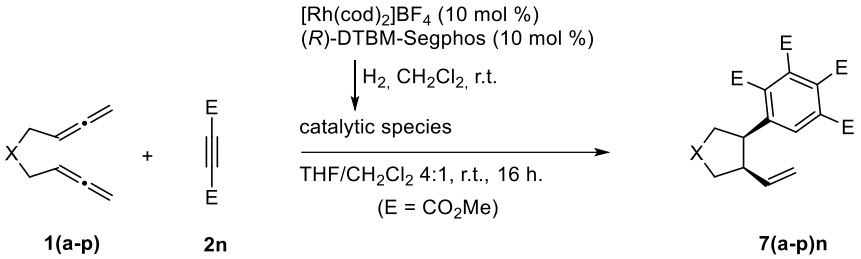

Scheme S13. Rh(I)-catalyzed cascade cyclization of 1,5-bisallenes **1(a-p)** and DMAD **2n** leading to **7(a-p)n**.

In a 10 mL capped vial, a mixture of $[Rh(cod)_2]BF_4$ (3.7 mg, 0.009 mmol) and (*R*)-DTBM-Segphos (11.3 mg, 0.01 mmol) was purged with nitrogen and dissolved in anhydrous CH_2Cl_2 (4 mL). Hydrogen gas was bubbled into the catalyst solution and the mixture was stirred for 30 min. The resulting mixture was concentrated to dryness under a stream of hydrogen, dissolved again in anhydrous CH_2Cl_2 (2 mL) and transferred via syringe into a solution of 1,5-bisallene **1** (0.09 mmol, 1 equiv.) and dimethyl acetylenedicarboxylate **2n** (0.56 mL, 4.54 mmol, 50 equiv.) in anhydrous THF (8 mL) under inert atmosphere at room temperature. The resulting mixture was stirred for 16h. The solvent was removed under reduced pressure and the crude reaction mixture was purified by flash chromatography on silica gel using mixtures of hexane/EtOAc as the eluent (90:10 to 30:70 v/v) to afford compound **7**.

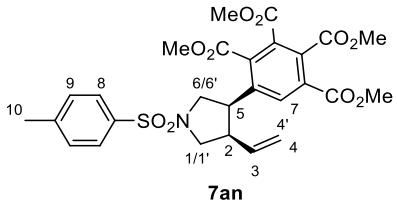

7an

Compound **7an** was obtained from bisallene **1a** (25.0 mg, 0.09 mmol) following the general procedure **GP6**. Purification by flash chromatography (silica gel, 20 μm, Hexanes/EtOAc 90:10 to 30:70 v/v) provided **7an** (28.4 mg, 56% yield) as a colourless solid.

MW ($C_{27}H_{29}NO_{10}S$): 559.59 g/mol. **Rf**: 0.23 (Hexane/EtOAc 6:4). **MP (°C):** 166 – 167. **IR (ATR) ν (cm^{-1})**: 2952, 1742, 1722, 1240, 1215, 1159. **^{1}H NMR ($CDCl_3$, 400 MHz): δ_H** 2.46 (s, 3H, **H10**), 2.91 – 2.99 (m, 1H, **H2**), 3.42 (dd, ^2J = 10.5 Hz, ^3J = 5.3 Hz, 1H, **H1/H1'**), 3.53 (dd, ^2J = 10.5 Hz, ^3J = 7.1 Hz, 1H, **H1/H1'**), 3.61 – 3.67 (m, 3H, **H5, H6, H6'**), 3.81 (s, 3H, **CH_3CO_2**), 3.84 (s, 3H, **CH_3CO_2**), 3.92 (s, 3H, **CH_3CO_2**), 3.93 (s, 3H, **CH_3CO_2**), 4.84 (d, $^3J_{trans}$ = 17.0 Hz, 1H, **H4'**), 4.90 (d, $^3J_{cis}$ = 10.3 Hz, 1H, **H4**), 5.19 – 5.30 (m, 1H, **H3**), 7.36 (d, $^3J_{ortho}$ = 8.2 Hz, 2H, **H9**), 7.77 (d, $^3J_{ortho}$ = 8.2 Hz, 2H, **H8**), 7.94 (s, 1H, **H7**). **^{13}C{1H} NMR ($CDCl_3$, 101 MHz): δ_C** 21.70 (**CH_3-Ar**), 44.04 (**C5**), 46.56 (**C2**), 51.60 (**C6**), 51.87 (**C1**), 52.96 (**$\underline{C}H_3CO_2$**), 53.16 (**$\underline{C}H_3CO_2$**), 53.29 (**$\underline{C}H_3CO_2$**), 53.36 (**$\underline{C}H_3CO_2$**), 118.65 (**C4**), 127.69 (**C8**), 130.01 (**C9**), 130.20, 130.22, 131.92 (**C7**), 133.88 (**C3**), 133.96, 134.17, 137.34, 138.69, 144.01, 164.87 (**$CH_3\underline{C}O_2$**), 165.74 (**$CH_3\underline{C}O_2$**), 167.30 (**$CH_3\underline{C}O_2$**), 167.43 (**$CH_3\underline{C}O_2$**). **ESI-HRMS (*m/z*)** calcd for $[M+Na]^+$ = 582.1404. Found 582.1404.

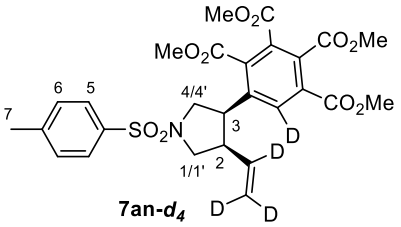

Compound **7an-*d*$_4$** was obtained from bisallene **1a-*d*$_4$** (25.2 mg, 0.09 mmol) following the general procedure **GP6**. Purification by flash chromatography (silica gel, 20 μm, Hexanes/EtOAc 90:10 to 30:70 v/v) provided **7an-*d*$_4$** (13.3 mg, 26% yield) as a colourless oil.

MW ($C_{27}H_{25}D_4NO_{10}S$): 563.61 g/mol. **Rf**: 0.23 (Hexane/EtOAc 6:4). **^{1}H NMR ($CDCl_3$, 400 MHz): δ_H** 2.46 (s, 3H, **H7**), 2.95 (m, 1H, **H2**), 3.42 (dd, ^2J = 10.5, 5.3 Hz, 1H, **H1/H1'**), 3.53 (dd, ^2J = 10.5, 7.1 Hz, 1H, **H1/H1'**), 3.60 – 3.69 (m, 3H, **H3, H4, H4'**), 3.80 (s, 3H, **CH_3CO_2**), 3.84 (s, 3H, **CH_3CO_2**), 3.91 (s, 3H, **CH_3CO_2**), 3.93 (s, 3H, **CH_3CO_2**), 7.36 (d, $^3J_{ortho}$ = 8.2 Hz, 2H, **H6**), 7.77 (d, $^3J_{ortho}$ = 8.2 Hz, 2H, **H5**). **^{13}C{1H} NMR ($CDCl_3$, 101 MHz): δ_C** 21.72 (**CH_3-Ar**), 44.04 (**C3**), 46.38 (**C2**), 51.63 (**C4**), 51.86 (**C1**), 52.97 (**$\underline{C}H_3CO_2$**), 53.17 (**$\underline{C}H_3CO_2$**), 53.30 (**$\underline{C}H_3CO_2$**), 53.38 (**$\underline{C}H_3CO_2$**), 127.72 (**C5**), 130.02 (**C6**), 130.17, 130.22, 134.03, 134.20, 137.37, 138.64, 144.02, 164.87 (**$CH_3\underline{C}O_2$**), 165.76 (**$CH_3\underline{C}O_2$**), 167.32 (**$CH_3\underline{C}O_2$**), 167.45 (**$CH_3\underline{C}O_2$**). **ESI-HRMS (*m/z*)** calcd for $[M+Na]^+$ = 586.1655. Found 586.1647.

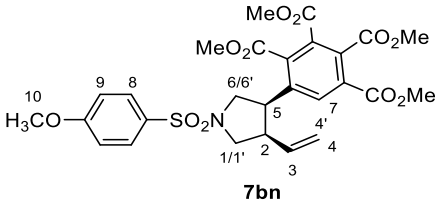

Compound **7bn** was obtained from bisallene **1b** (26.2 mg, 0.09 mmol) following the general procedure **GP4**. Purification by flash chromatography (silica gel, 20 μm, Hexanes/EtOAc 90:10 to 30:70 v/v) provided **7bn** (30.2 mg, 58% yield) as a colourless oil.

MW ($C_{27}H_{29}NO_{11}S$): 575.59 g/mol. **Rf**: 0.19 (Hexanes/EtOAc 6:4). **IR (ATR) ν (cm^{-1})**: 2951, 1728, 1243, 1206, 1155. **^{1}H NMR ($CDCl_3$, 400 MHz): δ_H** 2.92 – 3.02 (m, 1H, **H2**), 3.40 (dd, ^2J = 10.5 Hz, ^3J = 5.4 Hz, 1H, **H1/H1'**), 3.52 (dd, ^2J = 10.5 Hz, ^3J = 7.1 Hz, 1H, **H1/H1'**), 3.59 – 3.70 (m, 3H, **H5, H6, H6'**), 3.81 (s, 3H, **CH_3CO_2**), 3.84 (s, 3H, **CH_3CO_2**), 3.90 (s, 3H, **H10**), 3.91 (s, 3H, **CH_3CO_2**), 3.93 (s, 3H, **CH_3CO_2**), 4.85 (dt, $^3J_{trans}$ = 17.1 Hz, ^4J = ^2J = 1.1 Hz, 1H, **H4'**), 4.91 (dt, $^3J_{cis}$ = 10.5 Hz, ^4J = ^2J = 1.1 Hz, 1H, **H4**), 5.25 (ddd, $^3J_{trans}$ = 17.1 Hz, $^3J_{cis}$ = 10.5 Hz, ^3J = 8.2 Hz, 1H, **H3**), 7.00 – 7.06 (m, 2H, **H9**), 7.80 – 7.85 (m, 2H, **H8**), 7.91 (s, 1H, **H7**). **^{13}C{1H} NMR ($CDCl_3$, 101 MHz): δ_C** 44.04, 46.59, 51.69, 51.88, 52.99, 53.17, 53.30, 53.38, 55.78, 114.55, 118.66, 128.55, 129.80, 130.19, 130.24, 131.92, 133.93, 134.14, 137.36, 138.78, 163.33, 164.89, 165.76, 167.31, 167.45. **ESI-HRMS (*m/z*)** calcd for $[M+Na]^+$ = 598.1353. Found 598.1359.

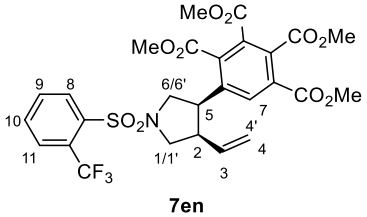

Compound **7en** was obtained from bisallene **1e** (29.9 mg, 0.09 mmol) following the general procedure **GP6**. Purification by flash chromatography (silica gel, 20 μm, Hexanes/EtOAc 90:10 to 30:70 v/v) provided **7en** (28.4 mg, 51% yield) as a pale yellow oil.

MW ($C_{27}H_{26}F_3NO_{10}S$): 613.56 g/mol. **Rf**: 0.26 (Hexanes/EtOAc 6:4). **IR (ATR) ν (cm^{-1})**: 2953, 1726, 1242, 1203, 1143. **^{1}H NMR ($CDCl_3$, 400 MHz): δ_H** 3.12 – 3.21 (m, 1H, **H2**), 3.53 (dd, ^2J = 10.2 Hz, ^3J = 5.2 Hz, 1H, **H1/H1'**), 3.67 (dd, ^2J = 10.2 Hz, ^3J = 6.8 Hz, 1H, **H1/H1'**), 3.71 – 3.79 (m, 2H, **H6, H6'/H5**), 3.79 – 3.89 (m, 1H, **H6'/H5**), 3.86 (s, 3H, **CH_3CO_2**), 3.86 (s, 3H, **CH_3CO_2**), 3.92 (s, 3H, **CH_3CO_2**), 3.92 (s, 3H, **CH_3CO_2**), 4.91 – 5.02 (m, 2H, **H4, H4'**), 5.38 (ddd, $^3J_{trans}$ = 17.0 Hz, $^3J_{cis}$ 10.5 Hz, ^3J = 8.2 Hz, 1H, **H3**), 7.70 – 7.77 (m, 2H, **H9, H10**), 7.93 (m, 2H, **H7, H8/H11**), 8.21 – 8.26 (m, 1H, **H8/H11**). **^{13}C{1H} NMR ($CDCl_3$, 101 MHz): δ_C** 44.32, 46.82, 51.19, 51.63, 53.08, 53.19, 53.27, 53.41, 118.95, 122.73 (q, $^1J_{C-F}$ = 274.0 Hz), 128.03 (q,$^2J_{C-F}$ = 33.2 Hz), 128.72 (q, $^3J_{C-F}$ = 6.4 Hz), 130.22, 130.27, 131.81, 131.92, 132.56 (q, $^4J_{C-F}$ = 1.2 Hz), 133.03, 133.57, 134.31, 137.46, 138.37 (q, $^3J_{C-F}$ = 1.3 Hz), 138.48, 164.84, 165.76, 167.35, 167.46. **ESI-HRMS (*m/z*)** calcd for $[M+Na]^+$ = 636.1122. Found 636.1128.

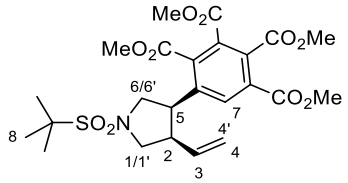

7gn

Compound **7gn** was obtained from bisallene **1g** (21.8 mg, 0.09 mmol) following the general procedure **GP6**. Purification by flash chromatography (silica gel, 20 μm, Hexanes/EtOAc 90:10 to 30:70 v/v) provided **7gn** (24.3 mg, 51% yield) as a colourless oil.

MW ($C_{24}H_{31}NO_{10}S$): 525.57 g/mol. **Rf**: 0.28 (Hexanes/EtOAc 6:4). **IR (ATR) ν (cm^{-1})**: 2952, 1728, 1240, 1201, 1126. **^{1}H NMR ($CDCl_3$, 400 MHz): δ_H** 1.46 (s, 9H, **H8**), 3.12 – 3.22 (m, 1H, **H2**), 3.48 (dd, ^2J = 10.3 Hz, ^3J = 6.0 Hz, 1H, **H1/H1'**), 3.67 – 3.76 (m, 1H, **H6/H6'**), 3.83 (dd, ^2J = 10.3 Hz, ^3J = 6.9 Hz, 1H, **H1/H1'**), 3.86 – 3.97 (m, 2H, **H5, H6/H6'**), 3.86 (s, 3H, **CH_3CO_2**), 3.87 (s, 3H, **CH_3CO_2**), 3.918 (s, 3H, **CH_3CO_2**), 3.924 (s, 3H, **CH_3CO_2**), 4.98 – 5.05 (m, 2H, **H4, H4'**), 5.32 – 5.43 (m, 1H, **H3**), 8.03 (s, 1H, **H7**). **^{13}C{1H} NMR ($CDCl_3$, 101 MHz): δ_C** 24.54, 44.78, 47.18, 53.05, 53.18, 53.21, 53.41, 53.60, 61.51, 118.81, 130.02, 130.32, 131.89, 133.72, 134.30, 137.52, 139.12, 164.82, 165.81, 167.33, 167.51. **ESI-HRMS (*m/z*)** calcd for $[M+Na]^+$ = 548.1561. Found 548.1563.

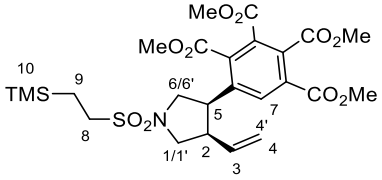

7hn

Compound **7hn** was obtained from bisallene **1h** (25.7 mg, 0.09 mmol) following the general procedure **GP6**. Purification by flash chromatography (silica gel, 20 μm, Hexanes/EtOAc 90:10 to 30:70 v/v) provided **7hn** (11.6 mg, 23 % yield) as a colourless oil.

MW ($C_{25}H_{35}NO_{10}SSi$): 569.70 g/mol. **Rf**: 0.35 (Hexanes/EtOAc 6:4). **IR (ATR) ν (cm^{-1})**: 2951, 1729, 1245, 1204, 1143. **^{1}H NMR ($CDCl_3$, 400 MHz): δ_H** 0.08 (s, 9H, **H10**), 1.06 – 1.13 (m, 2H, **H9**), 2.96 – 3.03 (m, 2H, **H8**), 3.14 – 3.23 (m, 1H, **H2**), 3.48 (dd, ^2J = 10.2 Hz, ^3J = 5.3 Hz, 1H, **H1/H1'**), 3.65 – 3.85 (m, 4H, **H1/H1', H5, H6, H6'**), 3.87 (s, 3H, **CH_3CO_2**), 3.88 (s, 3H, **CH_3CO_2**), 3.92 (s, 3H, **CH_3CO_2**), 3.92 (s, 3H, **CH_3CO_2**), 4.95 – 5.05 (m, 2H, **H4, H4'**), 5.41 (ddd, $^3J_{trans}$ = 16.6 Hz, $^3J_{cis}$ = 10.8 Hz , ^3J = 8.2 Hz, 1H, **H3**), 8.01 (s, 1H, **H7**). **^{13}C{1H} NMR ($CDCl_3$, 101 MHz): δ_C** -1.82, 10.29, 44.48, 46.98, 47.81, 51.45, 51.75, 53.09, 53.19, 53.31, 53.42, 118.89, 130.21, 130.35, 131.97, 133.77, 134.22, 137.43, 138.71, 164.90, 165.82, 167.38, 167.47. **ESI-HRMS (*m/z*)** calcd for $[M+Na]^+$ = 592.1643. Found 592.1645.

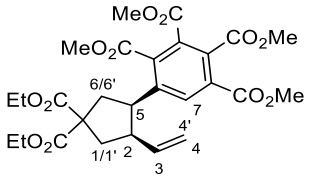

7kn

Compound **7kn** was obtained from bisallene **1k** (24.0 mg, 0.09 mmol) following the general procedure **GP6**. Purification by flash chromatography (silica gel, 20 μm, Hexanes/EtOAc 90:10 to 30:70 v/v) provided **7kn** (18.4 mg, 37 % yield) as a colourless oil.

MW ($C_{27}H_{32}NO_{12}$): 548.54 g/mol. **Rf**: 0.37 (Hexanes/EtOAc 6:4). **IR (ATR) ν (cm^{-1})**: 2952, 1725, 1241, 1201, 1159. **^{1}H NMR ($CDCl_3$, 400 MHz): δ_H** 1.23 – 1.31 (m, 6H, **CH_3-Et**), 2.32 (dd, ^2J = 14.2 Hz, ^3J = 5.2 Hz, 1H, **H1/H1'**), 2.60 (d, ^3J = 8.0 Hz, 1H, **H6/H6'**), 2.61 (d, ^3J = 10.5 Hz, 1H, **H6/H6'**), 2.69 (dd, ^2J = 14.2 Hz, ^3J = 7.5 Hz 1H, **H1/H1'**), 2.97 – 3.05 (m, 1H, **H2**), 3.59 (dt, ^3J = 10.5 Hz, ^3J = 8.0 Hz, 1H, **H5**), 3.85 (s, 3H, **CH_3CO_2**), 3.89 (s, 3H, **CH_3CO_2**), 3.91 (s, 3H, **CH_3CO_2**), 3.92 (s, 3H, **CH_3CO_2**), 4.18 – 4.28 (m, 4H, **CH_2-Et**), 4.80 – 4.85 (m, 2H, **H4, H4'**), 5.39 (ddd, $^3J_{trans}$ = 17.8 Hz, $^3J_{cis}$ = 9.7 Hz, ^3J = 8.2 Hz, 1H, **H3**), 7.93 (s, 1H, **H7**). **^{13}C{1H} NMR ($CDCl_3$, 101 MHz): δ_C** 14.16, 14.18, 38.22, 38.88, 44.80, 46.70, 52.96, 53.08, 53.16, 53.29, 58.93, 61.93, 61.95, 116.93, 129.64, 129.65, 132.31, 133.73, 137.01, 137.74, 140.94, 165.23, 165.87, 167.69, 167.75, 172.03, 172.12. **ESI-HRMS (*m/z*)** calcd for $[M+Na]^+$ = 571.1786. Found 571.1785.

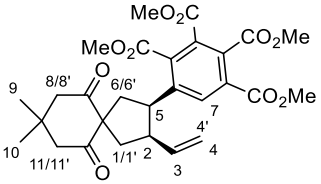

7ln

Compound **7ln** was obtained from bisallene **1l** (22.4 mg, 0.09 mmol) following the general procedure **GP6**. Purification by flash chromatography (silica gel, 20 μm, Hexanes/EtOAc 90:10 to 30:70 v/v) provided **7ln** (13.7 mg, 28 % yield) as a colourless oil.

MW ($C_{28}H_{32}NO_{10}S$): 528.55 g/mol. **Rf**: 0.30 (Hexanes/EtOAc 6:4). **IR (ATR) ν (cm^{-1})**: 2952, 1724, 1690, 1236, 1201, 1157. **^{1}H NMR ($CDCl_3$, 400 MHz): δ_H** 0.95 (s, 3H, **H9/H10**), 1.08 (s, 3H, **H9/H10**), 2.21 (dd, ^2J = 13.6 Hz, ^3J = 4.2 Hz, 1H, **H1/H1'**), 2.33 – 2.42 (m, 2H, **H1/H1', H6/H6'**), 2.57 (dd, ^2J = 10.1 Hz, ^4J = 1.7 Hz, 1H, **H8/H8'/H11/H11'**), 2.60 (dd, ^2J = 10.0 Hz, ^4J = 1.7 Hz, 1H, **H8/H8'/H11/H11'**), 2.65-2.77 (m, 3H, **H6/H6', H8/H8', H11/H11'**), 2.95 – 3.04 (m, 1H, **H2**), 3.56 (dt, ^3J = 11.7 Hz, ^3J = 7.1 Hz, 1H, **H5**), 3.85

(s, 3H, **CH_3CO_2**), 3.90 (s, 3H, **CH_3CO_2**), 3.92 (s, 3H, **CH_3CO_2**), 3.93 (s, 3H, **CH_3CO_2**), 4.76 (d, $^3J_{trans}$ = 17.0 Hz, 1H, **H4'**), 4.81 (d, $^3J_{cis}$ = 10.3 Hz, 1H, **H4**), 5.44 (ddd, $^3J_{trans}$ = 17.0 Hz, $^3J_{cis}$ = 10.3 Hz, ^3J = 8.8 Hz, 1H, **H3**), 7.99 (s, 1H, **H7**). **^{13}C{1H} NMR ($CDCl_3$, 101 MHz): δ_C** 27.70, 29.35, 30.73, 34.09, 39.78, 45.35, 47.99, 51.37, 52.40, 53.00, 53.09, 53.18, 53.29, 69.81, 117.34, 129.55, 129.59, 132.50, 133.78, 136.77, 137.80, 140.97, 165.27, 165.89, 167.75, 167.83, 207.35, 207.68. **ESI-HRMS (*m/z*)** calcd for $[M+Na]^+$ = 551.1888. Found 551.1884.

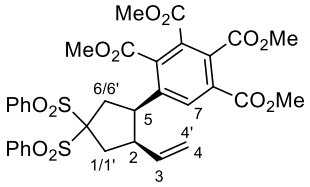

7mn

Compound **7mn** was obtained from bisallene **1m** (29.6 mg, 0.07 mmol) following the general procedure **GP4**. Purification by flash chromatography (silica gel, 20 μm, Hexanes/EtOAc 90:10 to 30:70 v/v) provided **7mn** (30.9 mg, 61 % yield) as a colourless solid.

MW ($C_{33}H_{32}O_{12}S_2$): 684.7 g/mol. **Rf**: 0.35 (Hexanes/EtOAc 6:4). **MP (°C):** 74 – 75. **IR (ATR) ν (cm^{-1})**: 2951, 1726, 1240, 1202, 1140. **^{1}H NMR ($CDCl_3$, 400 MHz): δ_H** 2.61 (dd, ^2J = 14.9 Hz, ^3J = 6.8 Hz, 1H, **H6/H6'**), 2.69 (dd, ^2J = 15.9 Hz, ^3J = 4.9 Hz, 1H, **H1/H1'**), 2.93 (dd, ^2J = 15.9 Hz, ^3J = 7.9 Hz, 1H **H1/H1'**), 3.19 (dd, ^2J = 14.9 Hz, ^3J = 12.0 Hz, 1H, **H6/H6'**), 3.25 – 3.35 (m, 1H, **H2**), 3.87 (s, 3H, **CH_3CO_2**), 3.93 (s, 6H, **2xCH_3CO_2**), 3.96 (s, 3H, **CH_3CO_2**), 4.08 (ddd, ^3J = 12.0 Hz, ^3J = 8.0 Hz, ^3J = 6.8 Hz, 1H, **H5**), 4.79 – 4.88 (m, 2H, **H4, H4'**), 5.61 (dt, $^3J_{trans}$ = 16.9 Hz, $^3J_{cis}$ = ^3J = 9.8 Hz, 1H, **H3**), 7.58 – 7.66 (m, 4H, **H-Ph**), 7.70 – 7.77 (m, 2H, **H-Ph**), 7.97 (s, 1H, **H7**), 8.02 – 8.13 (m, 4H, **H-Ph**). **^{13}C{1H} NMR ($CDCl_3$, 101 MHz): δ_C** 36.57, 36.62, 44.68, 47.46, 53.15, 53.23, 53.26, 53.39, 93.35, 118.08, 128.96, 129.09, 129.34, 129.72, 131.37, 131.46, 132.44, 134.37, 134.91, 135.02, 135.46, 136.38, 136.86, 138.40, 139.49, 164.97, 165.57, 167.66, 167.74. **ESI-HRMS (*m/z*)** calcd for $[M+Na]^+$ = 707.1227. Found 707.1220.

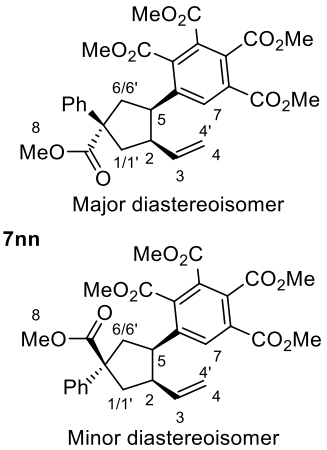

7nn

Compound **7nn** was obtained from bisallene **1n** (23.1 mg, 0.09 mmol) following the general procedure **GP6**. Purification by flash chromatography (silica gel, 20 μm, Hexanes/EtOAc 90:10 to 30:70 v/v) provided an inseparable diastereoisomeric mixture 4:1 of **7nn** (17.2 mg, 35 % yield) as a colourless oil.

MW ($C_{29}H_{30}O_{10}$): 538.5 g/mol. **Rf**: 0.42 (Hexanes/EtOAc 6:4). **IR (ATR) ν (cm^{-1})**: 2950, 1722, 1234, 1196, 1155. **^{1}H NMR ($CDCl_3$, 400 MHz)[a]: δ_H** 2.04 – 2.14 (m, 1H^M, **H1/H1'**), 2.27 (t, ^2J = ^3J = 12.0 Hz, 1H^M, **H6/H6'**), 2.48 (dd, ^2J = 14.0 Hz, ^3J = 7.4 Hz, 1H^m, **H1/H1'**), 2.60 – 2.68 (m, 1H^m, **H6/H6'**), 2.70 – 2.82 (m, 2H^m, **H1/H1', H6/H6'**), 2.92 – 3.02 (m, 1H^m, **H2**), 3.05 – 3.21 (m, 3H^M, **H1/H1', H2, H6/H6'**), 3.45 (ddd, ^3J = 12.1 Hz, ^3J = 9.4 Hz, ^3J = 6.4 Hz, 1H^m, **H5**), 3.65 (s, 3H^M, **CH_3CO_2**), 3.67 (s, 3H^m, **CH_3CO_2**), 3.62 – 3.72 (m, 1H^M, **H5**), 3.74 (s, 3H^m, **CH_3CO_2**), 3.83 (s, 3H^m, **CH_3CO_2**), 3.86 (s, 3H^M, **CH_3CO_2**), 3.86 (s, 3H^M, **CH_3CO_2**), 3.91 (s, 6H^M, **2xCH_3CO_2**. 3H^m, **CH_3CO_2**), 3.94 (s, 3H^m, **CH_3CO_2**), 4.75 – 4.90 (m, 2H^M, 2H^m, **H4, H4'**), 5.23 – 5.41 (m, 1H^M, 1H^m, **H3**), 7.27 – 7.46 (m, 5H^M, 5H^m, **H-Ph**), 7.83 (s, 1H^M, **H7**), 8.01 (s, 1H^m, **H7**). **^{13}C{1H} NMR ($CDCl_3$, 101 MHz)[b]: δ_C** 41.51 (**C1**), 42.13 (**C6**), 43.84 (**C5**), 45.40 (**C2**), 52.92 (**2x$\underline{C}H_3CO_2$**), 53.09 (**$\underline{C}H_3CO_2$**), 53.12 (**$\underline{C}H_3CO_2$**), 53.30 (**$\underline{C}H_3CO_2$**), 57.72, 115.95 (**C4**), 126.33, 126.97, 127.46, 128.70, 129.60, 132.59 (**C7**), 133.54, 137.79, 138.43 (**C3**), 142.29, 142.53, 165.24 (**$CH_3\underline{C}O_2$**), 165.90 (**$CH_3\underline{C}O_2$**), 167.75 (**$CH_3\underline{C}O_2$**), 167.79 (**$CH_3\underline{C}O_2$**), 175.65 (**$CH_3\underline{C}O_2$**). **ESI-HRMS (*m/z*)** calcd for $[M+Na]^+$ = 561.1731. Found 561.1732.

[a] H^M for major diastereoisomer, H^m for minor diastereoisomer. [b] Minor diastereoisomer not described due to ^{13}C sensitivity limitations.

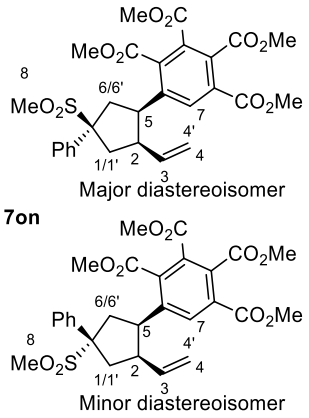

Compound **7on** was obtained from bisallene **1o** (24.9 mg, 0.09 mmol) following the general procedure **GP6**. Purification by flash chromatography (silica gel, 20 μm, Hexanes/EtOAc 90:10 to 30:70 v/v) provided an inseparable diastereoisomeric mixture 5:1 of **7on** (32.6 mg, 64 % yield) as a colourless solid.

MW ($C_{28}H_{30}O_{10}S$): 558.9 g/mol. **Rf**: 0.33 (Hexanes/EtOAc 5:5). **MP (°C):** 77 – 78. **IR (ATR) ν (cm^{-1})**: 2951, 1724, 1241, 1201, 1131. **^{1}H NMR ($CDCl_3$, 400 MHz)[a]: δ_H** 2.52 (s, 3H^m, **H8**), 2.53 (s, 3H^M, **H8**), 2.54 – 2.82 (m, 2H^m, **H1/H1'**, **H6/H6'**), 2.79 – 2.91 (m, 3H^M, **H1, H1', H6/H6'**), 2.91 – 3.01 (m, 1H^M, **H2**), 3.06 (t, ^2J = ^3J = 12.4 Hz, 1H^M, **H6/H6'**), 3.13 – 3.27 (m, 2H^m, **H1/H1'**, **H6/H6'**), 3.38 – 3.51 (m, 1H^M, **H5**. 1H^m, **H2**), 3.69 (s, 3H^M, **CH_3CO_2**), 3.78 (s, 3H^m, **CH_3CO_2**), 3.83 (s, 3H^M, **CH_3CO_2**), 3.86 (s, 3H^m, **CH_3CO_2**), 3.90 (s, 3H^m, **CH_3CO_2**), 3.92 (s, 3H^M, 3H^m, **CH_3CO_2**), 3.96 (s, 3H^M, **CH_3CO_2**), 4.10 – 4.20 (m, 1H^m, **H5**), 4.76 – 4.95 (m, 2H^M, 2H^m, **H4, H4'**), 5.27 (ddd, $^3J_{trans}$ = 17.0 Hz, $^3J_{cis}$ = 10.4 Hz, ^3J = 8.1 Hz, 1H^m, **H3**), 5.45 (ddd, $^3J_{trans}$ = 17.2 Hz, $^3J_{cis}$ = 10.2 Hz, ^3J = 8.1 Hz, 1H^M, **H3**), 7.38 – 7.54 (m, 3H^M, 3H^m, **H-Ph**), 7.56 – 7.63 (m, 2H^m, **H-Ph**), 7.64 – 7.76 (m, 2H^M, **H-Ph**. 1H^m, **H7**), 8.08 (s, 1H^M, **H7**). **^{13}C{1H} NMR ($CDCl_3$, 101 MHz)[b]: δ_C** 36.91 (**C8**), 37.65 (**C6**), 37.78 (**C1**), 43.05 (**C5**), 44.69 (**C2**), 52.79 (**$\underline{C}H_3CO_2$**), 53.14 (**$\underline{C}H_3CO_2$**), 53.28 (**$\underline{C}H_3CO_2$**), 53.31 (**$\underline{C}H_3CO_2$**), 73.79, 117.00 (**C4**), 128.40, 129.29, 129.39, 129.52, 129.95, 132.65 (**C7**), 134.10, 134.87, 137.11, 137.69, 140.70, 165.05 (**$CH_3\underline{C}O_2$**), 165.70 (**$CH_3\underline{C}O_2$**), 167.61(**$CH_3\underline{C}O_2$**), 167.70 (**$CH_3\underline{C}O_2$**). **ESI-HRMS (*m/z*)** calcd for $[M+Na]^+$ = 581.1452. Found 581.1443.

[a] H^M for major diastereoisomer, H^m for minor diastereoisomer. [b] Minor diastereoisomer not reported due to ^{13}C sensitivity limitations.

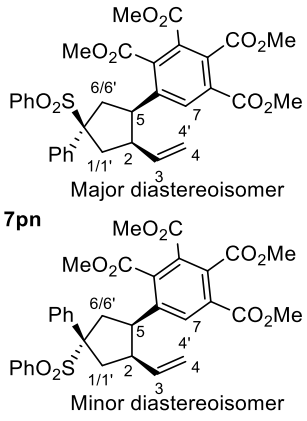

Compound **7pn** was obtained from bisallene **1p** (30.0 mg, 0.09 mmol) following the general procedure **GP6**. Purification by flash chromatography (silica gel, 20 μm, Hexanes/EtOAc 90:10 to 30:70 v/v) provided an inseparable diastereoisomeric mixture 8:1 of **7pn** (31.4 mg, 57 % yield) as a colourless solid.

MW ($C_{33}H_{32}O_{10}S$): 620.7 g/mol. **Rf**: 0.28 (Hexanes/EtOAc 6:4). **MP (°C):** 194 – 195. **IR (ATR) ν (cm^{-1})**: 2953, 1728, 1246, 1200, 1140. **^{1}H NMR ($CDCl_3$, 400 MHz)[a]: δ_H** 2.49 (dd, ^2J = 14.6 Hz, ^3J = 6.1 Hz, 1H^m, **H1/H1'**), 2.64 (dd, ^2J = 14.6 Hz, ^3J = 10.1 Hz, 1H^m, **H6/H6'**), 2.71 – 2.95 (m, 4H^M, **H1, H1', H2, H6/H6'**), 3.12 (t, ^2J = ^3J = 12.4 Hz, 1H^M, **H6/H6'**), 3.19 – 3.30 (m, 2H^m, **H1/H1', H6/H6'**), 3.30 – 3.40 (m, 1H^M, **H5**), 3.45 – 3.53 (m, 1H^m, **H2**), 3.63 (s, 3H^M, **CH_3CO_2**), 3.74 (s, 3H^m, **CH_3CO_2**), 3.81 (s, 3H^M, **CH_3CO_2**), 3.87 (s, 3H^m, **CH_3CO_2**), 3.88 (s, 3H^m, **CH_3CO_2**), 3.90 (s, 3H^m, **CH_3CO_2**), 3.92 (s, 3H^M, **CH_3CO_2**), 3.99 (s, 3H^M, **CH_3CO_2**), 4.26 – 4.34 (m, 1H^m, **H5**), 4.76 – 4.95 (m, 2H^M, 2H^m, **H4, H4'**), 5.27 (ddd, $^3J_{trans}$ = 16.5 Hz, $^3J_{cis}$ = 11.0 Hz, ^3J = 8.3 Hz, 1H^m, **H3**), 5.45 (ddd, $^3J_{trans}$ = 17.3 Hz, $^3J_{cis}$ = 10.2 Hz, ^3J = 7.4 Hz, 1H^M, **H3**), 7.13 – 7.17 (m, 2H^m, **H-Ph**), 7.21 – 7.36 (m, 9H^M, 7H^m, **H-Ph**), 7.48 – 7.55 (m, 1H^M, 1H^m, **H-Ph**), 7.66 (s, 1H^m, **H7**), 8.12

(s, 1H^{M}, **H7**). **^{13}C{1H} NMR ($CDCl_3$, 101 MHz)[b]: δ_C** 38.00, 38.28, 42.80, 44.45, 52.71, 53.13, 53.28, 53.30, 75.09, 116.80, 128.50, 128.50, 128.71, 128.97, 129.38, 129.68, 129.93, 132.86, 133.69, 134.01, 134.08, 136.27, 137.40, 137.75, 140.95, 165.11, 165.67, 167.58, 167.71. **ESI-HRMS (*m/z*)** calcd for $[M+Na]^+$ = 643.1608. Found 643.1603.

[a] H^M for major diastereoisomer, H^m for minor diastereoisomer. [b] Minor diastereoisomer not described due to ^{13}C sensitivity limitations.

General procedure GP7 for the synthesis of products 7o and 7p

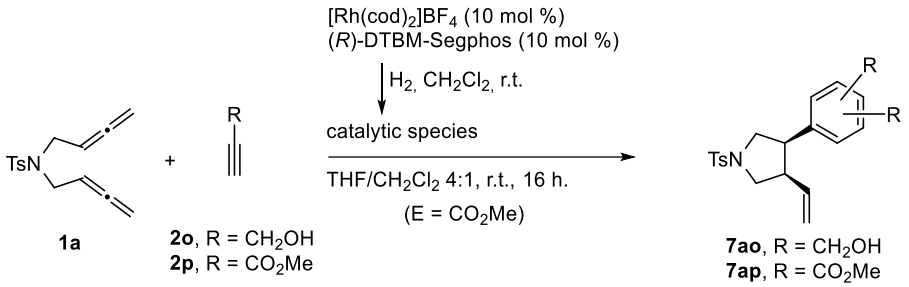

Scheme S14. Rh(I)-catalyzed cascade cyclization of 1,5-bisallene **1a** and alkynes **2(o,p)** leading to **7ao** and **7ap**.

In a 10 mL capped vial, a mixture of $[Rh(cod)_2]BF_4$ (3.7 mg, 0.009 mmol) and (*R*)-DTBM-Segphos (11.3 mg, 0.01 mmol) was purged with nitrogen and dissolved in anhydrous CH_2Cl_2 (4 mL). Hydrogen gas was bubbled into the catalyst solution and the mixture was stirred for 30 min. The resulting mixture was concentrated to dryness under a stream of hydrogen, dissolved again in anhydrous CH_2Cl_2 (2 mL) and transferred via syringe into a solution of bisallene **1a** (25 mg, 0.09 mmol, 1 equiv.) and the corresponding alkyne (50 equiv.) in anhydrous THF (8 mL) under inert atmosphere at room temperature. The resulting mixture was stirred for 16h. The solvent was removed under reduced pressure and the crude reaction mixture was purified by column chromatography on silica gel using mixtures of hexanes/EtOAc as the eluent (95:5 to 30:70 v/v) to afford the desired compound **7**.

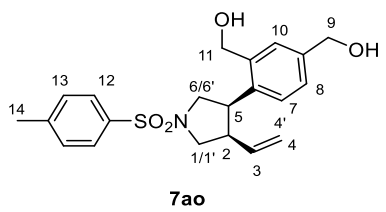

7ao

Compound **7ao** was obtained from bisallene **1a** (25 mg, 0.09 mmol) and propargyl alcohol **2o** (0.26 mL, 4.47 mmol) following the general procedure **GP7**. Purification by flash chromatography (silica gel, 20 μm, Hexanes/EtOAc 95:5 to 30:70 v/v) **7ao** (19.6 mg, 56 % yield) as a colourless solid

MW ($C_{21}H_{25}NO_4S$): 387.5 g/mol. **Rf**: 0.53 (EtOAc). **IR (ATR) ν (cm^{-1})**: 3344 (br band), 2874, 1330, 1155. **^{1}H NMR ($CDCl_3$, 400 MHz): δ_H** 2.48 (s, 3H, **H14**), 2.88 – 3.00 (m, 1H, **H2**), 3.27 (dd, ^2J = 10.0 Hz, ^3J = 8.2

Hz, 1H, **H1/H1'**), 3.54 (dd, ^{2}J = 10.0 Hz, ^{3}J = 8.2 Hz, 1H, **H1/H1'**), 3.57 – 3.68 (m, 2H, **H6, H6'**), 3.74 – 3.83 (m, 1H, **H5**), 4.48 – 4.72 (m, 4H, **H9, H11**), 4.84 (d, $^{3}J_{cis}$ = 10.0 Hz, 1H, **H4**), 4.91 (d, $^{3}J_{trans}$ = 17.0 Hz, 1H, **H4'**), 4.98 – 5.09 (m, 1H, **H3**), 7.02 (d, $^{3}J_{ortho}$ = 8.0 Hz, 1H, **H7**), 7.14 (d, $^{3}J_{ortho}$ = 8.0 Hz, 1H, **H8**), 7.31 (s, 1H, **H10**), 7.38 (d, $^{3}J_{ortho}$ = 8.2 Hz, 2H, **H13**), 7.78 (d, $^{3}J_{ortho}$ = 8.2 Hz, 2H, **H12**). **^{13}C{1H} NMR (CDCl$_3$, 101 MHz): δ_C** 21.73 (**C14**), 42.33 (**C5**), 47.09 (**C2**), 51.59 (**C1**), 53.29 (**C6**), 63.56 (**C11**), 64.89 (**C9**), 117.95 (**C4**), 126.99 (**C8**), 127.45 (**C7**), 127.54 (**C10**), 127.67 (**C12**), 129.98 (**C13**), 134.06, 135.21 (**C3**), 136.98, 138.98, 139.78, 143.84. **ESI-HRMS (*m/z*)** calcd for $[M+Na]^+$ = 410.1397. Found 410.1399.

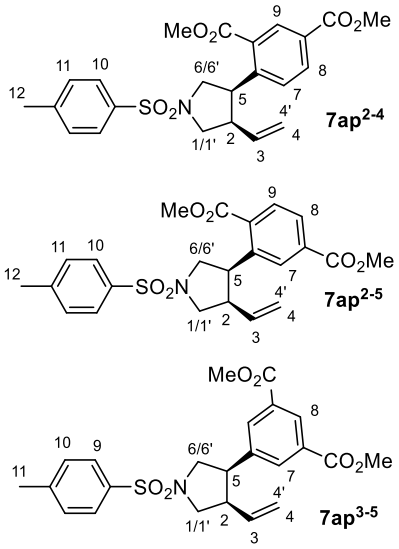

Compound **7ap** was obtained from bisallene **1a** (24.9 mg, 0.09 mmol) and methyl propiolate **2p** (0.40 mL, 4.73 mmol) following the general procedure **GP7**. Purification by flash cromatography (silica gel, 20 μm, Hexanes/EtOAc 95:5 to 30:70 v/v) provided a regioisomeric mixture of **7ap$^{2-4}$**, **7ap$^{2-5}$** and **7ap$^{3-5}$** as a yellow oil. A second flash chromatography (silica gel, 20 μm, Hexanes/EtOAc 95:5 to 30:70 v/v) was carried out to separate regioisomer **7ap$^{3-5}$** (5.3 mg, 13% yield) from an inseparable 3:1 mixture of **7ap$^{2-4}$** and **7ap$^{2-5}$** (8.7 mg, 22 % yield).

MW ($C_{23}H_{25}NO_6S$): 443.5 g/mol. **Rf**: 0.63 (Hexane/EtOAc 6:4). **IR (ATR) ν (cm^{-1}) (3n$^{2-4}$ + 3n$^{2-5}$):** 950, 1719, 1239, 1157. Although the 1H and ^{13}C-NMR spectra are recorded for the inseparable mixture of **3n$^{2-4}$** and **3n$^{2-5}$**, the two spectra are described separately for clarity: **^{1}H NMR (CDCl$_3$, 400 MHz) 7ap$^{2-4}$: δ_H** 2.48 (s, 3H, **H12**), 3.00 – 3.10 (m, 1H, **H2**), 3.30 (dd, ^{2}J = 10.4 Hz, ^{3}J = 7.2 Hz, 1H, **H1/H1'**), 3.54 (dd, ^{2}J = 10.4 Hz, ^{3}J = 7.4 Hz, 1H, **H1/H1'**), 3.60 (dd, ^{2}J = 10.2 Hz, ^{3}J = 7.1 Hz, 1H, **H6/H6'**), 3.68 (dd, ^{2}J = 10.2 Hz, ^{3}J = 5.1 Hz, 1H, **H6/H6'**), 3.85 (s, 3H, **CH$_3$CO$_2$**), 3.93 (s, 3H, **CH$_3$CO$_2$**), 4.56 (dt, ^{3}J = 7.1 Hz, ^{3}J = 5.1 Hz, 1H, **H5**), 4.73 – 4.84 (m, 2H, **H4, H4'**), 5.09 (ddd, $^{3}J_{trans}$ = 17.9 Hz , $^{3}J_{cis}$ = 9.9 Hz, ^{3}J = 8.2 Hz, 1H, **H3**), 7.27 (d, $^{3}J_{ortho}$ = 8.3 Hz, 1H, **H7**), 7.38 (d, $^{3}J_{ortho}$ = 8.3 Hz, 2H, **H11**), 7.79 (d, $^{3}J_{ortho}$ = 8.3 Hz, 2H, **H10**), 8.01 (dd, $^{3}J_{ortho}$ = 8.3 Hz, $^{4}J_{meta}$ = 1.9 Hz, 1H, **H8**), 8.47 (d, $^{4}J_{meta}$ = 1.9 Hz, 1H, **H9**). **^{1}H NMR (CDCl$_3$, 400 MHz) 7ap$^{2-5}$: δ_H** 2.46 (s, 3H, **H12**), 3.00 – 3.11 (m, 1H, **H2**), 3.37 (dd, ^{2}J = 10.4 Hz, ^{3}J = 5.4 Hz, 1H, **H1/H1'**), 3.50 – 3.74 (m, 3H, **H1/H1', H6, H6'**), 3.85 (s, 3H, **CH$_3$CO$_2$**), 3.95 (s, 3H, **CH$_3$CO$_2$**), 4.36 (q, ^{3}J = 7.2 Hz, 1H, **H5**), 4.73 – 4.83 (m, 2H, **H4, H4'**), 5.13 – 5.24 (m, 1H, **H3**), 7.34 – 7.39 (m, 2H, **H11**), 7.79 (d, $^{3}J_{ortho}$ = 8.3 Hz, 2H, **H10**), 7.85 (d, $^{3}J_{ortho}$ = 8.5 Hz, 1H, **H9**), 7.89 – 7.96 (m, 2H, **H7, H8**). **^{1}H NMR (CDCl$_3$, 400 MHz) 7ap$^{3-5}$: δ_H** 2.46 (s, 3H, **H11**), 2.96 – 3.08 (m, 1H, **H2**), 3.41 (dd, ^{2}J = 10.2 Hz, ^{3}J = 5.1 Hz, 1H, **H1/H1'**), 3.49 (q, ^{3}J = 7.1 Hz, 1H, **H5**), 3.61 (m, 2H, **H1/H1', H6/H6'**), 3.77 (dd, ^{2}J = 9.9 Hz, ^{3}J = 7.1 Hz, 1H, **H6/H6'**), 3.94 (s, 6H, **2xCH$_3$CO$_2$**), 4.86 (d, $^{3}J_{trans}$ = 16.9 Hz, 1H, **H4'**), 4.88 (d, $^{3}J_{cis}$ = 10.0 Hz, 1H, **H4**), 5.15 (ddd, $^{3}J_{trans}$ = 16.9 Hz,

$^{3}J_{cis}$ = 10.0 Hz, ^{3}J = 8.3 Hz, 1H, **H3**), 7.37 (d, $^{3}J_{ortho}$ = 8.2 Hz, 2H, **H10**), 7.80 (d, $^{3}J_{ortho}$ = 8.2 Hz, 2H, **H9**), 7.94 (d, $^{4}J_{meta}$ = 1.6 Hz, 2H, **H7**), 8.53 (t, $^{4}J_{meta}$ = 1.6 Hz, 1H, **H8**). **^{13}C{1H} NMR (CDCl$_3$, 101 MHz) 7ap$^{2-4}$:** δ_C 21.72 (**C12**) , 43.11 (**C5**), 46.64 (**C2**), 51.44 (**C1**), 52.44 (**C6**, **C**H$_3$CO$_2$), 52.50 (**C**H$_3$CO$_2$), 117.71 (**C4**), 127.70 (**C10**), 128.29 (**C7**), 128.83, 130.01 (**C11**), 130.85, 131.80 (**C9**), 132.79 (**C8**), 133.95, 134.58 (**C3**), 143.90, 145.38, 166.11 (**CH$_3$C**O$_2$), 167.39 (**CH$_3$C**O$_2$). **^{13}C{1H} NMR (CDCl$_3$, 101 MHz)**[a] **7ap$^{2-5}$:** δ_C 21.72 (**C12**), 43.46 (**C5**), 46.41 (**C2**), 51.53 (**C6**), 51.95 (**C1**), 52.55 (**C**H$_3$CO$_2$), 52.69 (**C**H$_3$CO$_2$), 117.66 (**C4**), 127.73 (**C11**), 127.93 (**C7/C8**), 129.02 (**C7/C8**), 129.96 (**C10**), 130.63 (**C9**), 133.02, 134.24, 134.86 (**C3**), 139.73, 143.78, 166.22 (**CH$_3$C**O$_2$), 167.65 (**CH$_3$C**O$_2$). **^{13}C{1H} NMR (CDCl$_3$, 101 MHz) 7ap$^{3-5}$:** δ_C 21.73, 46.89, 47.39, 51.15, 51.98, 52.61, 118.35, 127.69, 129.48, 130.02, 130.91, 133.53, 134.34, 136.68, 138.66, 139.35, 166.21. **ESI-HRMS (*m/z*) (3n$^{2-4}$ + 3n$^{2-5}$):** calcd for $[M+Na]^+$ = 466.1295. Found 466.1289

[a] One quaternary aromatic carbon atom overlapped with one carbon atom of **7ap$^{2-4}$**.

General observation for all the reactions of synthesized derivatives **7**. Neither by-products nor unreacted starting 1,5-bisallenes were Found in the reaction crude. Therefore, the moderate yields are due to the formation of decomposition products.

Further functionalization of 7an: double bond hydrogenation

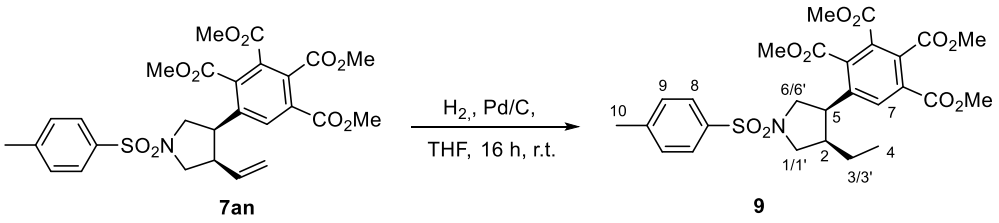

Scheme S15. Double bond hydrogenation of **7an** to produce **9**.

In a 10 mL capped vial, a mixture of **7an** (8.0 mg, 0.014 mmol) and Pd/C (10% wt, 2.0 mg, 0.002 mmol) was dissolved in THF (2 mL). Hydrogen gas was bubbled into the mixture for 20 min and THF was constantly added to avoid dryness. After stirring for 16h under hydrogen atmosphere, the mixture was filtered through celite to remove the Pd/C. Concentration of the resulting solution under reduced pressure afforded compound **9** (8 mg, quant. yield) as a colourless solid.

MW ($C_{27}H_{31}NO_{10}S$): 561.60 g/mol. **Rf**: 0.26 (Hexane/EtOAc 6:4). **MP (°C):** 166 – 167. **IR (ATR) ν (cm^{-1})**: 2953, 1739, 1724, 1241, 1216, 1159. **^{1}H NMR (CDCl$_3$, 400 MHz):** δ_H 0.66 – 0.78 (m, 4H, **H3/H3', H4**), 0.93 – 1.12 (m, 1H, **H3/H3'**), 2.12 – 2.24 (m, 1H, **H2**), 2.46 (s, 3H, **H10**), 3.24 (dd, ^{2}J = 10.4 Hz, ^{3}J = 6.5 Hz, 1H, **H1/H1'**), 3.49 – 3.60 (m, 4H, **H1/H1', H5, H6, H6'**), 3.84 (s, 3H, **CH$_3$CO$_2$**), 3.85 (s, 3H, **CH$_3$CO$_2$**), 3.92 (s, 3H, **CH$_3$CO$_2$**), 3.93 (s, 3H, **CH$_3$CO$_2$**), 7.35 (d, $^{3}J_{ortho}$ = 8.2 Hz, 2H, **H9**), 7.77 (d, $^{3}J_{ortho}$ = 8.2 Hz, 2H, **H8**), 7.97 (s, 1H, **H7**). **^{13}C{1H} NMR (CDCl$_3$, 101 MHz):** δ_C 12.59 (**C4**), 21.73 (**C10**), 21.94 (**C3**), 43.57 (**C5**),

44.53 (**C2**), 51.81 (**C1**), 52.46 (**C6**), 53.13 (**C**H_3CO_2), 53.19 (**C**H_3CO_2), 53.33 (**C**H_3CO_2), 53.41 (**C**H_3CO_2), 127.73 (**C8**), 129.96 (**C9**), 130.00, 130.42, 131.91 (**C7**), 133.94, 134.16, 137.49, 139.81, 143.94, 164.91 (CH_3**C**O_2), 165.72 (CH_3**C**O_2), 167.47 (CH_3**C**O_2), 167.50 (CH_3**C**O_2). **ESI-HRMS (*m/z*)** calcd for $[M+Na]^+$ = 584.1561. Found 584.1557.

Further functionalization of 7an: ester hydrolysis

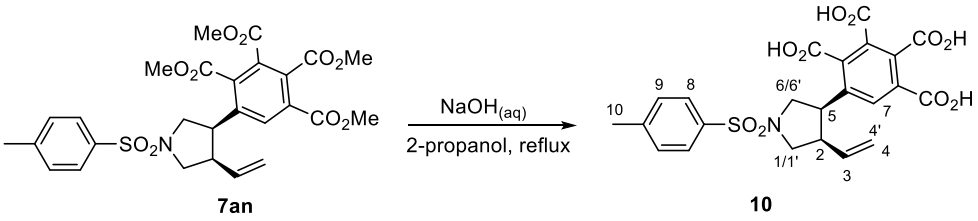

Scheme S16. Ester hydrolysis of **7an** to produce the tetraacid **10**.

To a solution of sodium hydroxide (36 mg, 0.9 mmol) in H_2O (15 mL), a suspension of **7an** (30 mg, 0.054 mmol) in 2-propanol (30 mL) was added at room temperature. The mixture was heated to reflux and stirred for 48 h. The solution was allowed to cool down to room temperature and the 2-propanol was evaporated under reduced pressure. HCl 1M was then added and the aqueous mixture was washed with CH_2Cl_2 (15 mL) and extracted with diethyl ether (3 x 15 mL). The combined ether fractions were dried over anhydrous Na_2SO_4, filtered, and concentrated under reduced pressure to afford **10** (24.8 mg, 92 % yield) as a colourless paste.

MW ($C_{23}H_{21}NO_{10}S$): 503.48 g/mol. **IR (ATR) ν (cm^{-1})**: 3468, 3063, 2918, 2628, 1706. **^{1}H NMR (THF-d_8, 400 MHz):** δ_H 2.42 (s, 3H, **H10**), 3.03 – 3.11 (m, 1H, **H2**), 3.36 (dd, ^2J = 10.4 Hz, ^3J = 4.7 Hz, 1H, **H1/H1'**), 3.52 (dd, ^2J = 10.4 Hz, ^3J = 7.0 Hz, 1H, **H1/H1'**), 3.55 – 3.62 (m, 1H, **H6/H6'**), 3.66 (dd, ^2J = 9.9 Hz, ^3J = 7.3 Hz, 1H, **H6/H6'**), 3.75 (q, ^3J = 7.3 Hz, 1H, **H5**), 4.75 – 4.87 (m, 2H, **H4, H4'**), 5.35 (ddd, $^3J_{trans}$ = 17.1 Hz, $^3J_{cis}$ = 10.5 Hz, ^3J = 8.0 Hz, 1H, **H3**), 7.38 (d, $^3J_{ortho}$ = 8.1 Hz, 2H, **H9**), 7.76 (s, 1H, **H7**), 7.77 (d, $^3J_{ortho}$ = 8.1 Hz, 2H, **H8**). **^{13}C{1H} NMR ($CDCl_3$, 101 MHz):** δ_C 21.26 (**C10**), 44.88 (**C5**), 47.03 (**C2**), 51.84 (**C6**), 52.54 (**C1**), 117.50 (**C4**), 128.31 (**C8**), 130.25 (**C9**), 131.03 (**C7**), 131.31, 132.31, 135.11, 135.59, 135.69 (**C3**), 137.56, 138.34, 144.00, 166.54 (**CO_2H**), 167.51 (**CO_2H**), 168.03 (**CO_2H**), 168.71 (**CO_2H**). **ESI-HRMS (*m/z*)** calcd for $[M+Na]^+$ = 526.0778. Found 526.0787.

Further functionalization of 7an: double bond epoxidation

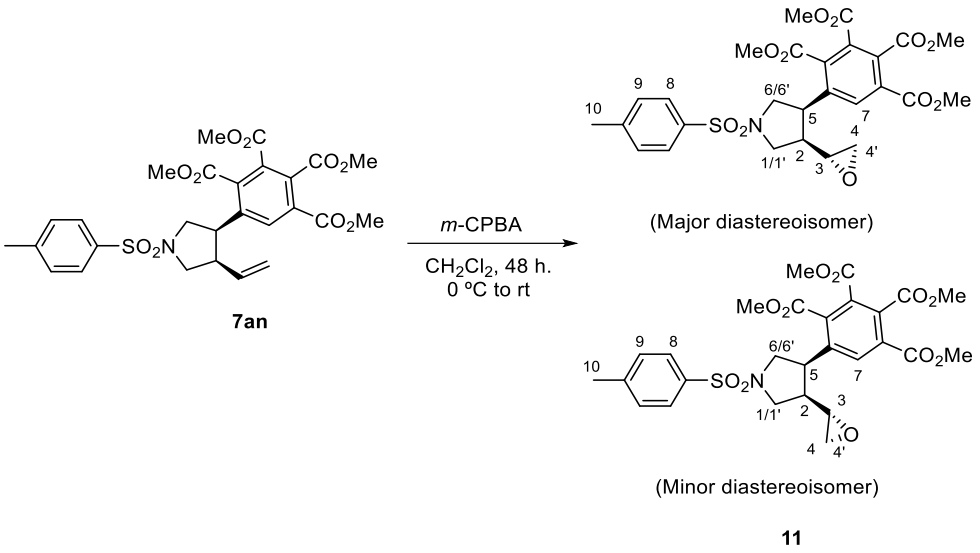

Scheme S17. Double bond epoxidation of **7an** to produce **11**.

In a 10 mL capped vial, **7an** (20.0 mg, 0.036 mmol) was dissolved in CH_2Cl_2 (5 mL) and 3-chloroperbenzoic acid (10 mg, 77% purity, 0.045 mmol) was added in portions at 0 ºC. The solution was allowed to warm to room temperature and was stirred for 48 h. The solvent was removed under reduced pressure and the crude reaction mixture was purified by column chromatography on silica gel using hexanes/EtOAc mixtures as eluent (90:10 to 30:70 v/v) to obtain an inseparable diastereoisomeric mixture 3:1 of **11** (15.7 mg, 75 % yield) as a colourless solid.

MW ($C_{27}H_{29}NO_{11}S$): 575.58 g/mol. **Rf**: 0.28 (Hexanes/EtOAc 5:5). **MP (°C):** 156 – 157. **IR (ATR) ν (cm^{-1})**: 2953, 1743, 1725, 1238, 1216, 1160. **^{1}H NMR ($CDCl_3$, 400 MHz): δ_H** 2.16 – 2.27 (m, 2H^M, **H4/H4', H2**), 2.32 – 2.36 (m, 1H^m, **H4/H4'**), 2.36 (m, 1H^m, **H2**), 2.41 (t, $^2J = {}^3J$ = 4.3 Hz, 1H^M, **H4/H4'**), 2.46 (s, 3H^M, **H10**), 2.44 – 2.51 (m, 1H^M, **H3**. 5H^m, **H10**, **H3, H4/H4'**), 3.28 – 3.33 (m, 2H^m, **H1, H1'**), 3.47 (d, ^3J = 6.2 Hz, 2H^M, **H1, H1'**), 3.54 – 3.80 (m, 3H^M, 3H^m, **H5, H6, H6'**), 3.84 (s, 3H^M, 3H^m, **CH_3CO_2**), 3.85 (s, 3H^m, **CH_3CO_2**), 3.86 (s, 3H^M, **CH_3CO_2**), 3.92 (s, 3H^m, **CH_3CO_2**), 3.92 (s, 3H^M, **CH_3CO_2**), 3.94 (s, 3H^M, 3H^m, **CH_3CO_2**), 7.37 (d, $^3J_{ortho}$ = 8.0 Hz, 2H^M, 2H^m, **H9**), 7.74 – 7.81 (m, 2H^M, 2H^m, **H8**), 8.11 (s, 1H^M, **H7**), 8.13 (s, 1H^m, **H7**). **^{13}C{1H} NMR ($CDCl_3$, 101 MHz) major diastereoisomer: δ_C** 21.74 (**C10**), 42.66 (**C5**), 45.20 (**C2**), 46.46 (**C4**), 49.82 (**C1**), 50.82 (**C3**), 52.20 (**C6**), 53.23 (**$\underline{C}H_3CO_2$**), 53.26 (**$\underline{C}H_3CO_2$**), 53.41 (**$\underline{C}H_3CO_2$**), 53.47 (**$\underline{C}H_3CO_2$**), 127.87 (**C8**), 130.05 (**C9**), 130.18, 130.64, 131.69 (**C7**), 133.42, 134.62, 137.51, 138.37, 144.18, 164.72 (**$CH_3\underline{C}O_2$**), 165.50 (**$CH_3\underline{C}O_2$**), 167.30 (**$CH_3\underline{C}O_2$**), 167.31 (**$CH_3\underline{C}O_2$**). **ESI-HRMS (*m/z*)** calcd for $[M+Na]^+$ = 598.1354. Found 598.1357.

Supplementary material for Chapter 6

General procedure GP8 for the synthesis of 13(a-p)n, 13aq and 13ar

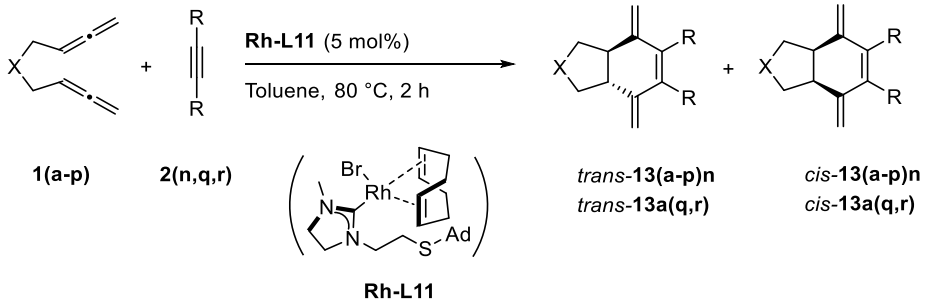

Scheme S18. Rh(I)-catalyzed [2+2+2] cycloaddition reaction of 1,5-bisallenes and alkynes.

In a 10 mL capped vial, rhodium complex **Rh-L11** (5 mol%) was dissolved in anhydrous toluene (1 mL) and transferred via syringe into a solution of the corresponding 1,5-bisallene **1** (1 equiv.) and the alkyne **2** (5 equiv.) in anhydrous toluene (1.5 mL) under inert atmosphere. The resulting mixture was heated and stirred for 2 h. at 80 °C. The solvent was then removed under reduced pressure and the resulting reaction crude was purified by flash chromatography on silica gel (silica gel, 20 μm) using mixtures of hexane/EtOAc as the eluent (90:10 to 40:60 v/v). The *trans:cis* ratio was calculated by NMR spectroscopy on the crude reaction mixture.

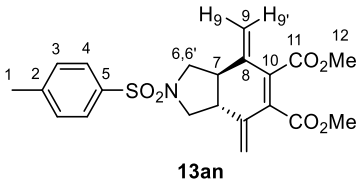

Compound **13an** (dr 92:8) was obtained from bisallene **1a** (24.9 mg, 0.09 mmol) following the general procedure **GP8**. Purification by flash chromatography (silica gel, 20 μm, Hexanes/EtOAc 90:10 to 60:40 v/v) provided **13an** (30.3 mg, 80% yield) as a colourless solid.

MW ($C_{21}H_{23}NO_6S$): 417.48 g/mol. **Rf**: 0.32 (Hexane/EtOAc 6:4). **MP (°C):** 168 – 170 (dec.). **IR (ATR) ν (cm^{-1})**: 2922, 1720, 1333, 1156. **^{1}H NMR ($CDCl_3$, 400 MHz): δ_H** 2.43 (s, 3H, **H1**), 2.39 – 2.50 (m, 2H, **H7**), 3.28 (t, 2H, ^2J = ^3J = 9.6 Hz, **H6/H6'**), 3.77 (s, 6H, **H12**), 3.81 (dd, 2H, ^2J = 9.6 Hz, ^3J = 6.5 Hz, **H6/H6'**), 5.06 (s, 2H, **H9**), 5.38 (s, 2H, **H9'**), 7.32 (d, 2H, $^3J_{ortho}$ = 8.2 Hz, **H3**), 7.73 (d, 2H, $^3J_{ortho}$ = 8.2 Hz, **H4**). **^{13}C{1H} NMR ($CDCl_3$, 101 MHz): δ_C** 21.7 (**C1**), 45.1 (**C7**), 50.4 (**C6**), 52.6 (**C12**), 116.6 (**C9**), 127.4 (**C4**), 130.1 (**C3**), 134.1 (**C5**), 134.5 (**C10**), 137.9 (**C8**), 143.9 (**C2**), 166.9 (**C11**). **HRMS (ESI) m/z:** calcd for $[M+Na]^+$ = 440.1138. Found 440.1136.

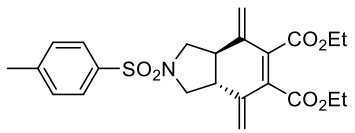

13aq

Compound **13aq** (dr 93:7) was obtained from bisallene **1a** (24.8 mg, 0.09 mmol) following the general procedure **GP8**. Purification by flash chromatography (silica gel, 20 μm, Hexanes/EtOAc 90:10 to 60:40 v/v) provided a non-separable mixture of **13aq** and the cyclotrimerization of the alkyne. Yield of **13aq** was obtained through the NMR of the crude using mesitylene as internal standard (84 % yield).

MW ($C_{23}H_{27}NO_6S$): 445.53 g/mol. **Rf**: 0.41 (Hexane/EtOAc 6:4). **IR (ATR) ν (cm^{-1})**: 2919, 1720, 1338, 1158. **^{1}H NMR (CDCl$_3$, 400MHz): δ_H** 1.29 (t, 6H, ^3J = 7.1 Hz), 2.44 (s, 3H), 2.40 – 2.52 (m, 2H), 3.28 (t, 2H, ^2J = ^3J = 9.7 Hz), 3.82 (dd, 2H, ^2J = 9.7 Hz, ^3J = 6.5 Hz), 4.19 – 4.28 (m, 4H), 5.05 (s, 2H), 5.38 (s, 2H), 7.33 (d, 2H, $^3J_{ortho}$ = 8.2 Hz), 7.73 (d, 2H, $^3J_{ortho}$ = 8.2 Hz). **^{13}C{1H} NMR (CDCl$_3$, 101MHz): δ_C** 14.1, 21.7, 45.1, 50.5, 61.8, 116.3, 127.4, 130.1, 134.2, 134.5, 138.1, 144.0, 166.5. **HRMS (ESI) m/z:** calcd for $[M+Na]^+$ = 468.1451. Found 468.1448.

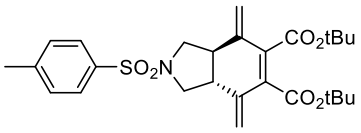

13ar

Compound **13ar** (dr 92:8) was obtained from bisallene **1a** (24.8 mg, 0.09 mmol) following the general procedure **GP8**. Purification by flash chromatography (silica gel, 20 μm, Hexanes/EtOAc 90:10 to 60:40 v/v) provided **13ar** (35.8 mg, 79 % yield) as a colourless oil.

MW ($C_{27}H_{35}NO_6S$): 501.64 g/mol. **Rf**: 0.56 (Hexane/EtOAc 6:4). **IR (ATR) ν (cm^{-1})**: 2929, 1715, 1336, 1151. **^{1}H NMR (CDCl$_3$, 400MHz): δ_H** 1.51 (s, 18H), 2.44 (s, 3H), 2.38 – 2.49 (m, 2H), 3.26 (t, 2H, ^2J = ^3J = 9.7 Hz), 3.79 (dd, 2H, ^2J = 9.7 Hz, ^3J = 6.4 Hz), 5.31 (s, 2H), 4.97 (s, 2H), 7.32 (d, 2H, $^3J_{ortho}$ = 8.2 Hz), 7.73 (d, 2H, $^3J_{ortho}$ = 8.2 Hz). **^{13}C{1H} NMR (CDCl$_3$, 101 MHz): δ_C** 21.7, 28.1, 45.1, 50.5, 83.0, 115.1, 127.4, 130.0, 134.1, 134.8, 138.6, 143.9, 166.1. **HRMS (ESI) m/z:** calcd for $[M+Na]^+$ = 524.2077. Found 524.2079.

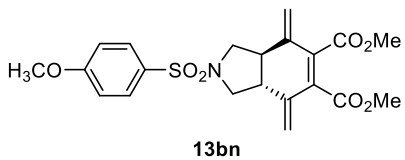

13bn

Compound **13bn** (dr 91:9) was obtained from bisallene **1b** (26.2 mg, 0.09 mmol) following the general procedure **GP8**. Purification by flash chromatography (silica gel, 20 μm, Hexanes/EtOAc 90:10 to 60:40 v/v) provided **13bn** (30.4 mg, 78% yield) as a colourless solid.

MW ($C_{21}H_{23}NO_7S$): 433.47 g/mol. **Rf**: 0.28 (Hexane/EtOAc 6:4). **MP (°C):** 138 – 140 (dec.). **IR (ATR) ν (cm^{-1})**: 2950, 1721, 1338, 1155. **^{1}H NMR (400 MHz, CDCl$_3$): δ_H** 2.39 – 2.52 (m, 2H), 3.27 (t, 2H, ^2J = ^3J = 9.7 Hz), 3.77 (s, 6H), 3.74 – 3.85 (m, 2H), 3.87 (s, 3H), 5.06 (s, 2H), 5.38 (s, 2H), 6.99 (d, 2H, $^3J_{ortho}$ = 8.8

Hz), 7.78 (d, 2H, $^{3}J_{ortho}$ = 8.8 Hz). **^{13}C{1H} NMR (101 MHz, CDCl$_3$): δ_C** 45.1, 50.4, 52.6, 55.7, 114.6, 116.6, 128.8, 129.5, 134.5, 137.9, 163.2, 166.9. **HRMS (ESI) m/z:** calcd for $[M+Na]^+$ = 456.1087. Found 456.1089.

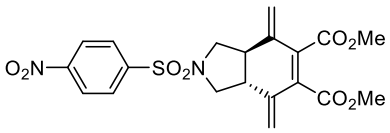

13cn

Compound **13cn** was obtained from bisallene **1c** (27.6 mg, 0.09 mmol) following the general procedure **GP8**. Purification by filtration of the crude provided **13cn** (26.1 mg, 65 % yield, dr 100:nd) as a colourless solid.

MW ($C_{20}H_{20}N_2O_8S$): 448.45 g/mol. **Rf**: 0.32 (Hexane/EtOAc 6:4). **MP (°C):** 258 – 259 (dec.). **IR (ATR) ν (cm^{-1})**: 2953, 1717, 1535, 1343, 1161. **^{1}H NMR (CDCl$_3$, 400MHz): δ_H** 2.49 – 2.61 (m, 2H), 3.34 (t, 2H, ^{2}J = ^{3}J = 9.4 Hz), 3.79 (s, 6H), 3.87 (dd, 2H, ^{2}J = 9.4 Hz, ^{3}J = 6.2 Hz), 5.08 (s, 2H), 5.43 (s, 2H), 8.05 (d, 2H, $^{3}J_{ortho}$ = 8.7 Hz), 8.40 (d, 2H, $^{3}J_{ortho}$ = 8.7 Hz). **^{13}C{1H} NMR (101 MHz, CDCl$_3$): δ_C** 45.3, 50.5, 52.7, 116.9, 124.8, 128.5, 134.5, 137.5, 143.5, 150.4, 166.8. **HRMS (ESI) m/z:** calcd for $[M+Na]^+$ = 471.0833. Found 471.0837.

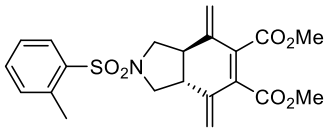

13dn

Compound **13dn** (dr 90:10) was obtained from bisallene **1d** (25.0 mg, 0.09 mmol) following the general procedure **GP8**. Purification by flash chromatography (silica gel, 20 μm, Hexanes/EtOAc 90:10 to 60:40 v/v) provided **13dn** (30.1 mg, 79 % yield) as a colourless oil.

MW ($C_{21}H_{23}NO_6S$): 417.48 g/mol. **Rf**: 0.40 (Hexane/EtOAc 6:4). **IR (ATR) ν (cm^{-1})**: 2948, 1719, 1317, 1156. **^{1}H NMR (CDCl$_3$, 400 MHz): δ_H** 2.65 (s, 3H), 2.68 – 2.75 (m, 2H), 3.37 (dd, 2H, ^{2}J = 9.1 Hz, ^{3}J = 10.0 Hz), 3.80 (s, 6H), 3.82 – 3.88 (m, 2H), 5.08 (s, 2H), 5.42 (s, 2H), 7.31 – 7.35 (m, 2H), 7.47 (td, 1H, $^{3}J_{ortho}$ = 7.5 Hz, $^{4}J_{meta}$ = 1.4 Hz), 7.93 (dd, 1H, $^{3}J_{ortho}$ = 8.2 Hz, $^{4}J_{meta}$ = 1.4 Hz). **^{13}C{1H} NMR (CDCl$_3$, 101 MHz): δ_C** 20.7, 45.5, 49.7, 52.7, 116.7, 126.4, 129.6, 133.0, 133.1, 134.6, 137.3, 137.9, 138.0, 167.0. **HRMS (ESI) m/z:** calcd for $[M+Na]^+$ = 440.1138. Found 440.1139.

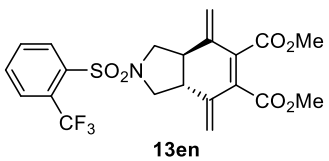

13en

Compound **13en** (dr 92:8) was obtained from bisallene **1e** (29.4 mg, 0.09 mmol) following the general procedure **GP8**. Purification by flash chromatography (silica gel, 20 μm, Hexanes/EtOAc 90:10 to 60:40 v/v) provided **13en** (34.0 mg, 81 % yield) as a colourless oil.

MW ($C_{21}H_{20}F_3NO_6S$): 471.45 g/mol. **Rf**: 0.30 (Hexane/EtOAc 6:4). **IR (ATR) ν (cm^{-1})**: 2952, 1716, 1266, 1138 **^{1}H NMR (CDCl$_3$, 400 MHz): δ_H** 2.66 – 2.80 (m, 2H), 3.42 (t, 2H, ^{2}J = ^{3}J = 9.4 Hz), 3.80 (s, 6H), 3.91 (dd, 2H, ^{2}J = 9.4 Hz, ^{3}J = 6.5 Hz), 5.08 (s, 2H), 5.43 (s, 2H), 7.65 – 7.76 (m, 2H), 7.87 – 7.94 (m, 1H), 8.13 – 8.20 (m, 1H). **^{13}C{1H} NMR (CDCl$_3$, 101 MHz): δ_C** 45.4, 50.1, 52.7, 116.7, 122.7 (q, $^{1}J_{C-F}$ = 275.1 Hz)

128.0 (q, $^{2}J_{C\text{-}F}$ = 33.3 Hz), 128.8 (q, $^{3}J_{C\text{-}F}$ = 6.5 Hz), 132.5 (q, $^{4}J_{C\text{-}F}$ = 1.0 Hz), 131.4, 132.9, 134.6, 137.8, 138.6 (q, $^{4}J_{C\text{-}F}$ = 1.5 Hz), 167.0. **HRMS (ESI) m/z:** calcd for $[M+Na]^+$ = 494.0856. Found 494.0857.

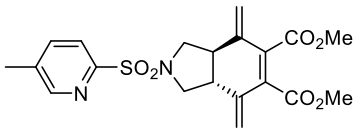

13fn

Compound **13fn** (dr 87:13) was obtained from bisallene **1f** (25.0 mg, 0.09 mmol) following the general procedure **GP8**. Purification by flash chromatography (silica gel, 20 μm, Hexanes/EtOAc 90:10 to 60:40 v/v) provided **13fn** (22.7 mg, 60 % yield) as a colourless solid.

MW ($C_{20}H_{22}N_2O_6S$): 418.46 g/mol. **Rf**: 0.23 (Hexane/EtOAc 6:4). **MP (°C):** 170 – 171 (dec.). **IR (ATR) ν (cm^{-1}):** 2952, 1720, 1340, 1165. **^{1}H NMR (CDCl$_3$, 400 MHz): δ_H** 2.42 (s, 3H), 2.59 – 2.71 (m, 2H), 3.46 (t, 2H, ^{2}J = ^{3}J = 9.7 Hz), 3.79 (s, 6H), 4.04 (dd, 2H, ^{2}J = 9.7 Hz, ^{3}J = 6.5 Hz), 5.06 (s, 2H), 5.39 (s, 2H), 7.68 (dd, 1H, $^{3}J_{ortho}$ = 8.0 Hz, $^{4}J_{meta}$ = 1.6 Hz), 7.86 (d, 1H, $^{3}J_{ortho}$ = 8.0 Hz), 8.46 – 8.47 (m, 1H). **^{13}C{1H} NMR (CDCl$_3$, 101 MHz): δ_C** 18.7, 45.2, 51.3, 52.7, 116.6, 122.8, 134.6, 137.5, 138.0, 138.1, 150.8, 154.1, 167.0. **HRMS (ESI) m/z:** calcd for $[M+Na]^+$ = 441.1091. Found 441.1084.

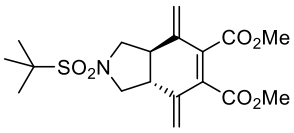

13gn

Compound **13gn** (dr 83:17) was obtained from bisallene **1g** (21.5 mg, 0.09 mmol) following the general procedure **GP8**. Purification by flash chromatography (silica gel, 20 μm, Hexanes/EtOAc 90:10 to 60:40 v/v) provided **13gn** (27.0 mg, 79 % yield, dr 83:17) as a colourless solid.

MW ($C_{18}H_{25}NO_6S$): 383.46 g/mol. **Rf**: 0.39 (Hexane/EtOAc 6:4). **MP (°C):** 197 – 198 (dec.). **IR (ATR) ν (cm^{-1}):** 2952, 1728, 1305, 1113. **^{1}H NMR (CDCl$_3$, 400 MHz): δ_H** 1.41 (s, 9H), 2.65 – 2.79 (m, 2H), 3.50 (t, 2H, ^{2}J = ^{3}J = 9.4 Hz), 3.80 (s, 6H), 3.90 – 3.97 (m, 2H), 5.09 (s, 2H), 5.42 (s, 2H). **^{13}C{1H} NMR (CDCl$_3$, 101 MHz): δ_C** 24.7, 45.7, 52.1, 52.6, 61.6, 116.6, 134.6, 138.1, 167.0. **HRMS (ESI) m/z:** calcd for $[M+Na]^+$ = 406.1295. Found 406.1301.

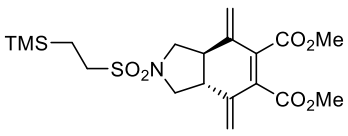

13hn

Compound **13hn** (dr 89:11) was obtained from bisallene **1h** (26.0 mg, 0.09 mmol) following the general procedure **GP8**. Purification by flash chromatography (silica gel, 20 μm, Hexanes/EtOAc 90:10 to 60:40 v/v) provided **13hn** (22.7 mg, 58 % yield) as a colourless solid.

MW ($C_{19}H_{29}NO_6SSi$): 427.59 g/mol. **Rf**: 0.44 (Hexane/EtOAc 6:4). **MP (°C):** 109 – 111 (dec.). **IR (ATR) ν (cm^{-1}):** 2950, 1723, 1332, 1270, 1148. **^{1}H NMR (CDCl$_3$, 400 MHz): δ_H** 0.05 (s, 9H), 0.90 – 1.07(m, 2H), 2.69 – 2.80 (m, 2H), 2.91 – 2.97 (m, 2H), 3.42 (t, 2H, ^{2}J = ^{3}J = 9.4 Hz), 3.81 (s, 6H), 3.88 (dd, 2H, ^{2}J = 9.4 Hz, ^{3}J = 6.2 Hz), 5.11 (s, 2H), 5.45 (s, 2H). **^{13}C{1H} NMR (CDCl$_3$, 101 MHz): δ_C** -1.8, 10.3, 45.7, 47.0, 50.3, 52.7, 116.7, 134.6, 138.0, 167.0. **HRMS (ESI) m/z:** calcd for $[M+Na]^+$ = 450.1377. Found 450.1374.

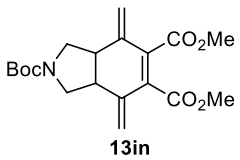

13in

Compound **13in** (dr 50:50) was obtained from bisallene **1i** (19.5 mg, 0.09 mmol) following the general procedure **GP8**. Purification by flash chromatography (silica gel, 20 μm, Hexanes/EtOAc 90:10 to 60:40 v/v) provided **13in** (16.8 mg, 53 % yield, dr 50:50) as a colourless solid.

MW ($C_{19}H_{25}NO_6$): 363.41 g/mol. **Rf**: 0.42 (Hexane/EtOAc 6:4). **MP (°C):** 153 – 155 (dec.). **IR (ATR) ν (cm^{-1}):** 2951, 1724, 1675, 1229. **^{1}H NMR ($CDCl_3$, 400 MHz): δ_H*** 1.48 (s, 9H$^{a/b}$), 1.49 (s, 9H$^{a/b}$), 2.57 – 2.72 (m, 2H^a, 2H^b), 3.31 (t, 2H^b, $^2J = {}^3J$ = 10.1 Hz), 3.34 (t, 2H^a, $^2J = {}^3J$ = 10.2 Hz), 3.76 – 3.81 (m, 2H^b), 3.81 (s, 6H$^{a/b}$), 3.81 (s, 6H$^{a/b}$), 3.88 (dd, 2H^a, ^2J = 10.2 Hz, ^3J = 6.0 Hz), 5.13 (s, 2H^b), 5.15 (s, 2H^a), 5.42 (s, 2H^a, 2H^b). **^{13}C{1H} NMR ($CDCl_3$, 101 MHz): δ_C*** 28.7, 44.7 (a), 45.4 (b), 48.2 (a), 48.6 (b), 52.6, 79.9, 116.1 (b), 116.4 (a), 134.6 (a/b), 134.8 (a/b), 138.6 (a/b), 138.8 (a/b), 154.6, 167.3. **HRMS (ESI) m/z:** calcd for $[M+Na]^+$ = 386.1574. Found 386.1581.

*Some NMR signals can be assigned to a particular diastereoisomer, but since we cannot discern between *trans* and *cis*, they are named as 'a' or 'b' (a/b = 'a' or 'b'). In ^{13}C NMR, nonlabelled signals have the same shift for both diastereoisomers.

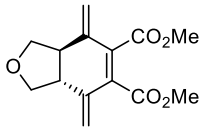

13jn

Compound **13jn** was obtained from bisallene **1j** (11.0 mg, 0.09 mmol) following the general procedure **GP8**. Purification by flash chromatography (silica gel, 20 μm, Hexanes/EtOAc 90:10 to 60:40 v/v) provided **13jn** (14.4 mg, 61 % yield, dr 96:4) as a colourless solid.

MW ($C_{14}H_{16}O_5$): 264.28 g/mol. **Rf**: 0.42 (Hexane/EtOAc 6:4). **MP (°C):** 222 – 223 (dec.). **IR (ATR) ν (cm^{-1}):** 2951, 1718, 1245, 1134. **^{1}H NMR ($CDCl_3$, 400 MHz): δ_H** 2.67 – 2.79 (m, 2H), 3.78 – 3.83 (m, 2H), 3.81 (s, 6H), 4.23 (t, 2H, $^2J = {}^3J$ = 7.2 Hz), 5.03 (d, 2H, ^4J = 1.1 Hz), 5.40 (d, 2H, ^4J = 1.2 Hz). **^{13}C{1H} NMR ($CDCl_3$, 101 MHz): δ_C** 46.7, 52.6, 69.7, 116.0, 135.2, 138.4, 167.3. **HRMS (ESI) m/z:** calcd for $[M+Na]^+$ =. Found 287.0897.

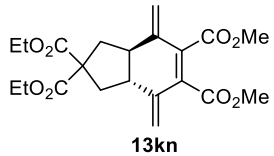

13kn

Compound **13kn** was obtained from bisallene **1k** (23.6 mg, 0.09 mmol) following the general procedure **GP8**. Purification by flash chromatography (silica gel, 20 μm, Hexanes/EtOAc 90:10 to 83:17 v/v) provided **13kn** (22.1 mg, 61 % yield, dr 80:20) as a colourless oil.

MW ($C_{21}H_{26}O_8$): 406.43 g/mol. **Rf**: 0.51 (Hexane/EtOAc 6:4). **IR (ATR) ν (cm^{-1}):** 2950, 1719, 1245. **^{1}H NMR ($CDCl_3$, 400 MHz): δ_H** 1.26 (t, 6H, ^3J = 7.1 Hz), 2.12 (dd, 2H, ^2J = 13.0 Hz, ^3J = 11.2 Hz), 2.37 – 2.42 (m, 2H), 2.81 (dd, 2H, ^2J = 13.0 Hz, ^3J = 6.0 Hz), 3.80 (s, 6H), 4.16 – 4.25 (m, 4H), 5.22 (s, 2H), 5.38 (s, 2H).

^{13}C{1H} NMR ($CDCl_3$, 101 MHz): δ_C 14.2, 37.0, 46.2, 52.5, 58.4, 61.9, 115.9, 134.9, 141.0, 167.6, 172.3, **HRMS (ESI) m/z:** calcd for $[M+Na]^+$ = 429.1520. Found 429.1523.

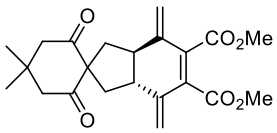

13ln

Compound **13ln** was obtained from bisallene **1l** (16.9 mg, 0.07 mmol) following the general procedure **GP8**. Purification by flash chromatography (silica gel, 20 μm, Hexanes/EtOAc 90:10 to 60:40 v/v) provided **13ln** (21.6 mg, 81 % yield, dr 61:39) as a colourless oil.

MW ($C_{22}H_{26}O_6$): 386.44 g/mol. **Rf**: 0.37 (Hexane/EtOAc 6:4).. **IR (ATR) ν (cm^{-1}):** 2951, 1719, 1690. **^{1}H NMR ($CDCl_3$, 400 MHz):** δ_H **(*trans*)** 1.01 (s, 6H), 2.16 (t, 2H, ^2J = ^3J = 11.5 Hz), 2.33 – 2.40 (m, 2H), 2.45 (dd, 2H, ^2J = 11.5 Hz, ^3J = 5.8 Hz), 2.63 – 2.67 (m, 4H), 3.79 (s, 6H), 5.19 (s, 2H), 5.37 (s, 2H), **^{1}H NMR ($CDCl_3$, 400 MHz):** δ_H **(*cis*)** 0.97 (s, 6H), 2.33 (d, 4H, ^3J = 6.8 Hz), 2.88 – 2.96 (m, 2H), 2.56 (s, 4H), 3.78 (s, 6H), 5.42 (s, 2H), 5.44 (s, 2H). **^{13}C{1H} NMR ($CDCl_3$, 101 MHz):** δ_C **(*trans*)** 28.5, 34.3, 36.5, 43.1, 51.7, 52.5, 69.0, 115.9, 134.8, 140.9, 167.5, 207.3. **^{13}C{1H} NMR ($CDCl_3$, 101 MHz):** δ_C **(*cis*)** 28.5, 30.6, 35.0, 46.0, 52.0, 52.5, 70.6, 119.8, 132.6, 137.4, 167.7, 205.5. **HRMS (ESI) m/z:** calcd for $[M+Na]^+$ = 409.1622. Found 409.1623.

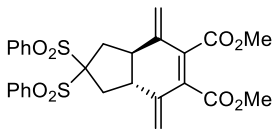

13mn

Compound **13mn** was obtained from bisallene **1m** (25.9 mg, 0.06 mmol) following the general procedure **GP8**. Purification by flash chromatography (silica gel, 20 μm, Hexanes/EtOAc 90:10 to 60:40 v/v) provided **13mn** (18.9 mg, 54 % yield, dr 91:9) as a colourless oil.

MW ($C_{27}H_{26}O_8S_2$): 542.62 g/mol. **Rf**: 0.26 (Hexane/EtOAc 6:4). **IR (ATR) ν (cm^{-1}):** 2949, 1719, 1232, 1137. **^{1}H NMR ($CDCl_3$, 400 MHz):** δ_H 2.43 – 2.48 (m, 2H), 2.52 – 2.60 (m, 2H), 2.88 (dd, 2H, ^2J = 14.2, ^3J = 5.8 Hz), 3.80 (s, 6H), 5.14 (s, 2H), 5.41 (s, 2H), 7.63 (t, 4H, ^3J = 7.6 Hz), 7.75 (t, 2H, ^3J = 7.6 Hz), 8.07 (d, 4H, ^3J = 7.6 Hz). **^{13}C{1H} NMR (, $CDCl_3$, 101 MHz):** δ_C 35.2, 45.7, 52.6, 91.7, 116.1, 129.1, 131.6, 134.6, 135.1, 136.1, 140.1, 167.2. **HRMS (ESI) m/z:** calcd for $[M+Na]^+$ = 565.0961. Found 565.0960.

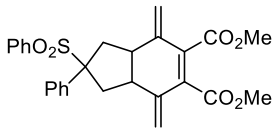

13pn

Compound **13pn** was obtained from bisallene **1p** (30.5 mg, 0.09 mmol) following the general procedure **GP8**. Purification by flash chromatography (silica gel, 20 μm, Hexanes/EtOAc 90:10 to 60:40 v/v) provided **13pn** (24.8 mg, 57 % yield, mixture of diastereoisomers) as a colourless oil.

MW ($C_{27}H_{26}O_6S$): 478.56 g/mol. **Rf**: 0.30 (Hexane/EtOAc 6:4). **IR (ATR) ν (cm^{-1}):** 2949, 1719, 1232, 1137.

HRMS (ESI) m/z: calcd for $[M+Na]^+$ = 501.1342. Found 501.1351.

^1H and ^{13}C NMR signals not described due to the complexity of the spectra.

Figure S7. Gibbs energy formation of the complexes evaluated, resulting from the coordination of 1,5-bisallene **1a** and DMAD **2n** into **Rh-L11**. Carboxylates of DMAD are omitted for clarity.

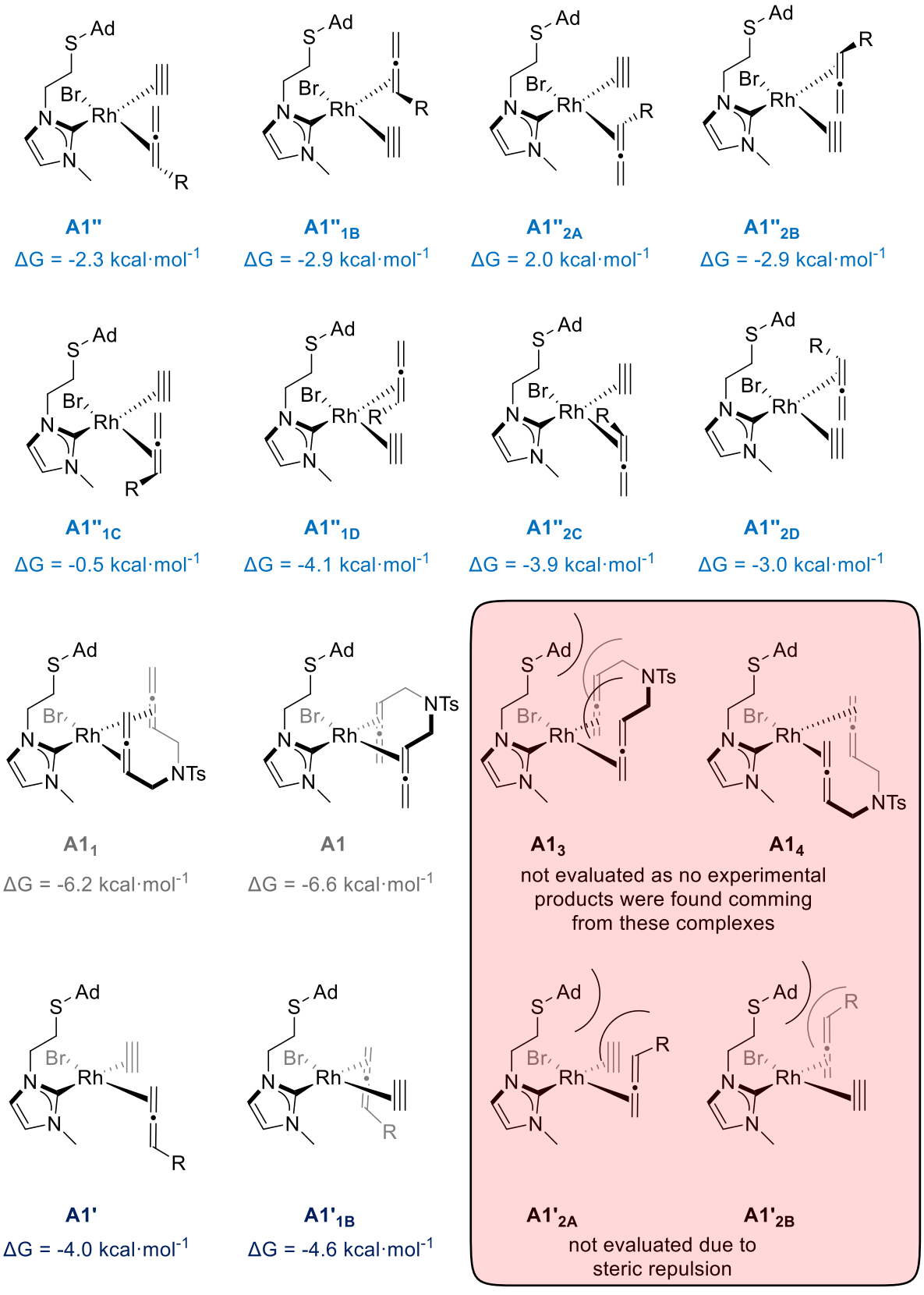

Figure S8. Gibbs energy barriers of the paths evaluated for the oxidative cyclometalation in the formation of **13an** without the sulfur chelating the rhodium.

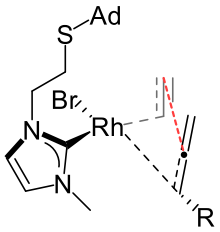

TS(A1"A2)
$\Delta G^{\ddagger}$ = 31.6 kcal·mol^{-1}

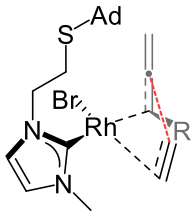

TS(A1"$_{1B}$A2)
$\Delta G^{\ddagger}$ = 29.5 kcal·mol^{-1}

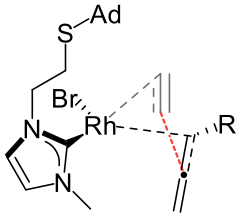

TS(A1"$_{2A}$A2)
$\Delta G^{\ddagger}$ = 29.1 kcal·mol^{-1}

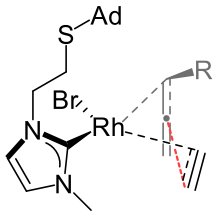

TS(A1"$_{2B}$A2)
$\Delta G^{\ddagger}$ = 35.9 kcal·mol^{-1}

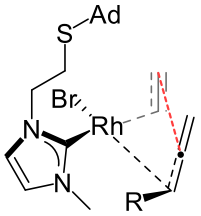

TS(A1"$_{1C}$A2)
$\Delta G^{\ddagger}$ = 26.8 kcal·mol^{-1}

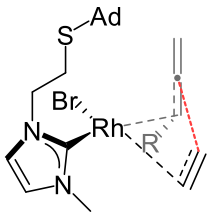

TS(A1"$_{1D}$A2)
$\Delta G^{\ddagger}$ = 34.8 kcal·mol^{-1}

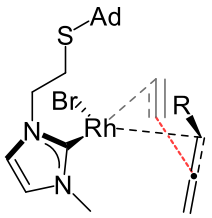

TS(A1"$_{2C}$A2)
$\Delta G^{\ddagger}$ = 25.0 kcal·mol^{-1}

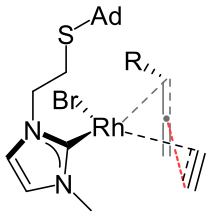

TS(A1"$_{2D}$A2)
$\Delta G^{\ddagger}$ = 25.7 kcal·mol^{-1}

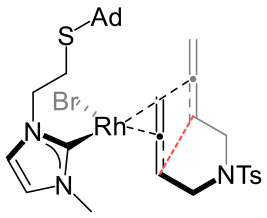

TS(A1$_1$A2)
$\Delta G^{\ddagger}$ = 35.3 kcal·mol^{-1}

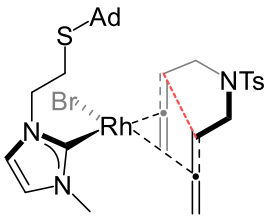

TS(A1A2)
$\Delta G^{\ddagger}$ = 33.7 kcal·mol^{-1}

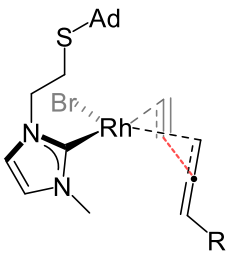

TS(A1'A2)
$\Delta G^{\ddagger}$ = 24.3 kcal·mol^{-1}

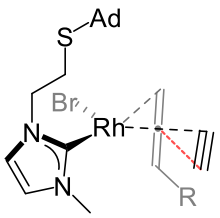

TS(A1'$_{1B}$A2)
$\Delta G^{\ddagger}$ = 23.0 kcal·mol^{-1}

Figure S9. Gibbs energy barriers of the paths evaluated for the oxidative cyclometalation in the formation of **13an** with the sulfur chelating the rhodium.

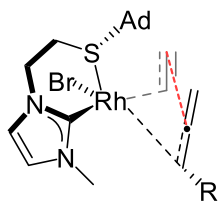

TS^{S}(A1"A2)
$\Delta G^{\ddagger}$ = 19.6 kcal·mol^{-1}

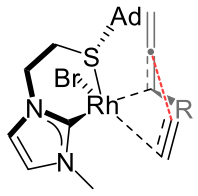

TS^{S}(A1"$_{1B}$A2)
$\Delta G^{\ddagger}$ = 24.8 kcal·mol^{-1}

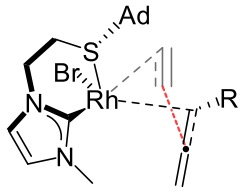

TS^{S}(A1"$_{2A}$A2)
$\Delta G^{\ddagger}$ = 25.4 kcal·mol^{-1}

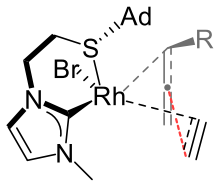

TS^{S}(A1"$_{2B}$A2)
$\Delta G^{\ddagger}$ = 27.2 kcal·mol^{-1}

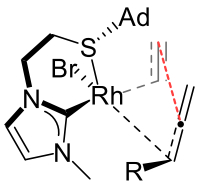

TS^{S}(A1"$_{1C}$A2)
$\Delta G^{\ddagger}$ = 24.6 kcal·mol^{-1}

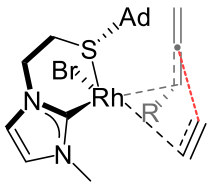

TS^{S}(A1"$_{1D}$A2)
$\Delta G^{\ddagger}$ = 22.2 kcal·mol^{-1}

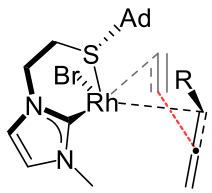

TS^{S}(A1"$_{2C}$A2)
$\Delta G^{\ddagger}$ = 22.9 kcal·mol^{-1}

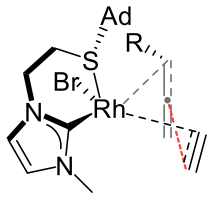

TS^{S}(A1"$_{2D}$A2)
$\Delta G^{\ddagger}$ = 23.8 kcal·mol^{-1}

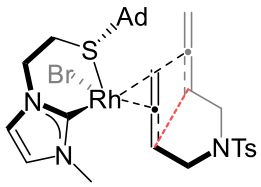

TS^{S}(A1$_1$A2)
$\Delta G^{\ddagger}$ = 37.2 kcal·mol^{-1}

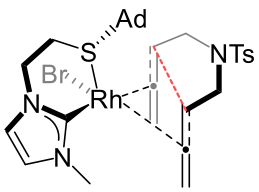

TS^{S}(A1$_1$A2)
$\Delta G^{\ddagger}$ = 39 kcal·mol^{-1}

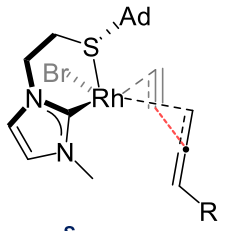

TS^{S}(A1'A2)
$\Delta G^{\ddagger}$ = 16.7 kcal·mol^{-1}

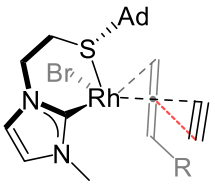

TS^{S}(A1'$_{1B}$A2)
$\Delta G^{\ddagger}$ = 19.1 kcal·mol^{-1}